The pseudokinase Madm and protein phosphatase PP4 control distinct aspects of synaptic plasticity at the Drosophila neuromuscular junction

vom Fachbereich Biologie der Universität Kaiserslautern
zur Erlangung des akademischen Grades
„Doktor der Naturwissenschaften“
eingereichte Dissertation

vorgelegt von

Kumar Aavula

Promotionskommission: Prof. Dr. Stefan Kins

Betreuer: Prof. Dr. Jan Pielage

Korreferent: Prof. Dr. Martin Müller

Kaiserslautern, 14. 08. 2018

D386

Eidesstattliche Erklärung

Ich versichere hiermit, dass diese Dissertation

“The pseudokinase Madm and protein phosphatase PP4 control distinct aspects of synaptic plasticity at the Drosophila neuromuscular junction”

von mir selbstständig und unter ausschließlicher Verwendung der angegebenen Hilfsmittel und Quellen angefertigt wurde.

Die vorliegende Dissertation oder Teile daraus wurden in der jetzigen oder in einer ähnlichen Form bei keiner anderen Hochschule eingereicht und haben somit keinen sonstigen Prüfungszwecken

Kumar Aavula Kaiserslautern

"...the thing with brothers is, you're supposed to take turns being the keeper. Sometimes you get to sit down and be the brother who is kept."

—Orson Scott Card

Table of Contents

1 Summary

Synapses are the fundamental structures that mediate the functionality of neural circuits. The ability of the synapse to modulate its structure and function at a fast rate in response to various sensory inputs enables the nervous system to incorporate new adaptations and behaviors. Synapses are very dynamic throughout the life of the animal especially during early development of the animal. Continuous events of formation and elimination of synapses, as well as activation and inhibition of synaptic function are observed in almost all neurons. These processes require cellular mechanisms that precisely control the balance between synaptic function and plasticity. Imbalance of these processes can result in defective nervous systems and has been reported in many neurological disorders. Thus, it is important to understand the mechanisms that regulate the processes of synapse development, maintenance and function.

Kinases and phosphatases are the key posttranslational regulators of cellular mechanisms. Understanding the function of these molecules in the neuron will shed light on the molecular mechanisms of synaptic plasticity. Using the Drosophila melanogaster larval neuromuscular junction as a model system, Bulat et al. (2014) performed a large RNAi based screen targeting the kinome and phosphatome of Drosophila to identify the essential kinases and phosphatases controlling synapse plasticity. Among others, they identified Myeloid leukemia factor-1 adaptor molecule (Madm) and Protein phosphatase 4 (PP4) as novel regulators of synapse development and maintenance. A function of these molecules in the nervous system has not been reported to date and hence I investigated on the role of Madm and PP4 in the regulation of synapse development, maintenance and function.

In this work, I show that Myeloid leukemia factor-1 adaptor molecule (Madm), is a ubiquitously expressing pseudo-kinase that regulates synaptic growth, stability and function. Using a combination of genetic and imaging assays, I could demonstrate that presynaptic Madm regulates synaptic growth and stability while postsynaptic Madm is involved in organization of the synaptic nerve terminal. In addition, I could demonstrate that Madm functions in association with the mTOR pathway to regulate synapse growth, likely acting downstream of 4E-BP. Using electrophysiological assays, we demonstrated that Madm is essential for basic synaptic transmission and is sufficient to induce retrograde synaptic potentiation.

In the second part, I could demonstrate that protein phosphatase 4 (PP4), a ubiquitously expressed protein phosphatase, is involved in the regulation of multiple aspects of nervous system development. I could show that PP4 is required for the development of the presynaptic nerve terminal and for the control of metamorphosis of the animal. Using genetic and imaging analyses, I demonstrated that loss of PP4 results in an abnormal morphology of cell organelles like the ER and mitochondria. Finally, I provide evidence that loss of PP4 results in defective brain development with poorly developed central nervous system (CNS) structures.

Together, I could demonstrate the importance of novel molecules, the pseudo-kinase Madm and protein phosphatases PP4 in the nervous system to regulate distinct aspects of the neuronal and synaptic development and function.

2 Introduction

Synapses are the key structures of a neuronal circuit that determine the function and complexity of neuronal circuits. Synapses mediate the transfer of information from one nerve cell to the other through chemical or electrical signals. Chemical synapses are the major type that is present in the nervous system, and mediate signal transmission through the release of neurotransmitters at specialized structures called active zones. Even though all synapses of a particular type contain similar components at the synapse, their release strength is not the same. Variable release at different synapses is achieved by different factors including the quantitative availability of release machinery elements like active zones, receptors, ion channels, endoplasmic reticulum, mitochondria, or the size of the synaptic vesicle pool. These components in turn influence the geometry of the synapse and the activity of the circuit (Rollenhagen and Lubke, 2006). The number and functionality of synapses in a circuit are dynamic and undergo constant remodeling in order to facilitate the adaptations of animals to new extrinsic and intrinsic stimuli. Synaptic remodeling is an essential process that is evident in all stages of nervous system development and function. Thus, synapses are plastic in nature and the phenomenon is named synaptic plasticity. Synaptic remodeling is reported to happen naturally in various situations such as in the developing nervous system, in response to experience or activity (learning and memory), in the mature brain or in the process of repair after injury or stroke induced damage (Butz et al., 2009). Failures in synaptic plasticity are the potential cause of many neurological disorders.

2.1 Structural synaptic plasticity

Synapses are highly dynamic. During development, the migrating axon establishes multiple contacts with the target to form synapses, but only few of them develop into functional synapses while the rest are eliminated. During the formation of new synapses, first large numbers of filopodia-like structures are formed, out of which only about 30% develop into new synapses. In vivo, two-photon time-lapse studies on developing mice brain demonstrated dynamic changes in the number of synapses and axonal branches mediated by formation and elimination of axons and synapses during thalamocortical synaptogenesis (Portera-Cailliau et al., 2005). In an activity dependent manner weaker synapses were eliminated (Le Be and Markram, 2006). Multiple independent studies demonstrated similar findings and proposed that synapses exhibit variable lifetimes. Newly formed synapses are

likely to be eliminated in a short time ranging from hours to months. It has been shown that more than 50% of newly formed synapses are eliminated within the next few days (Arellano et al., 2007; Holtmaat et al., 2005). The synapses that are very likely to be eliminate are called transient synapses and those that stay longer are called persistent. Activity is the key to determine whether a synapse becomes transient or persistent (Figure 1). Some synapses are persistent from early developmental stages on even if they are inactive for most of their life time. It has been demonstrated that spontaneous release events at silent synapses contribute to synaptic maintenance (McKinney et al., 1999). An example for such a case is the development and maturation of the visual cortex. In the cortex, visual circuits are established well before the establishment of connections with the retinal ganglion cells through molecular cues and spontaneous activity. During the final stage of maturation, visual cortical connectivity is rearranged to establish orientation preferences for the eyes based on the visual inputs from both the eyes (Espinosa and Stryker, 2012). Synaptic plasticity is also evident in the formation of neuromuscular junctions in vertebrates (Bishop et al., 2004; Lichtman and Sanes, 2003) and invertebrates (Zito et al., 1999). In the mature nervous system, synaptic plasticity occurs in an activity dependent manner. Increase in synaptic activity enhances synaptic strength and induces structural changes at synapses.

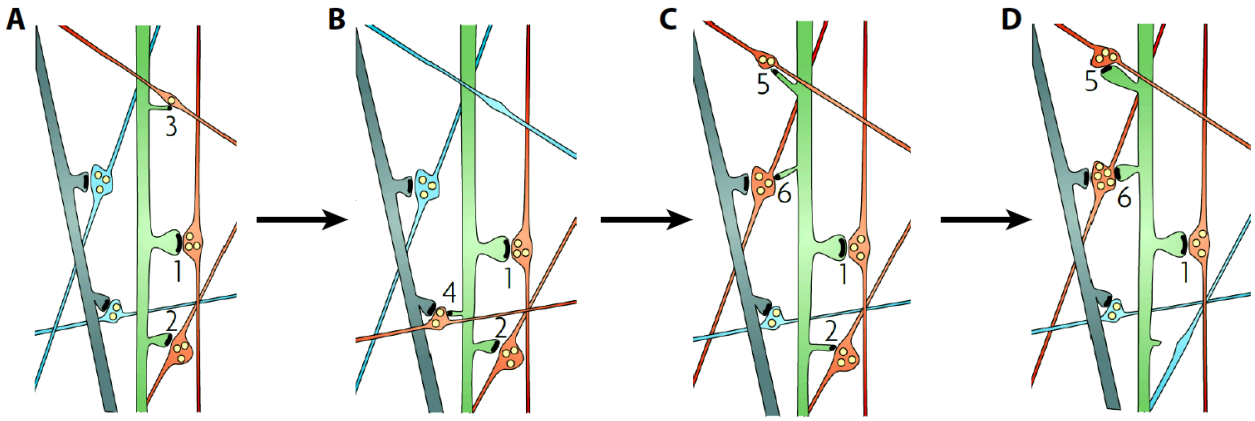

Figure 1: A model of synaptic plasticity. (A) Schematic representation of synaptic plasticity in a circuit with spiny dendrite (green) and the neighboring axons (red – connected, blue-unconnected) forming mature stable synapses (1 and 2) and premature synaptic connection (3). (B) All premature synapses will not develop into mature synapse (3 and 4), as frequent formation and elimination of premature connections takes place in the circuit all along. (C) Upon change in the activity, synaptic remodeling takes place by establishing new contacts (5 and 6) and/or by weakening of existing synapse (2). (D) According to the activity, new contacts are stabilized and develop into a mature synapse; whereas the existing weak synapse is eliminated (2). (*Adopted from Holtmaat and Svoboda (2009), Figure* 5)

It has been reported that repetitive increase in the postsynaptic intracellular calcium concentration due to presynaptic release events can trigger Ca^{2+}/Calmodulin-dependent protein Kinase II (CaMKII) mediated spinogenesis and neurite outgrowth (Jourdain et al., 2003) thereby leading to the formation of new synapses and axon branches but also to synapse elimination depending on the frequency of events (Hutchins and Kalil, 2008; Lang et al., 2006). During long-term potentiation (LTP), the growth of dendritic spines and formation of new synapses is frequently observed. In contrast during long term depression (LTD), spine shrinkage and synapse elimination can occur (Nagerl et al., 2004; Okamoto et al., 2004; Zhou et al., 2004). Activity in the circuit also leads to changes in the type, number and functionality of the ion channels required for the induction of LTP/LTD (Campanac and Debanne, 2008; Kim et al., 2007; Xu et al., 2005). Changes in N-Methyl-D-aspartate(NMDA) receptors, activity of CaMKII and of neurotropic factors like Brain derived neurotrophic factor (BDNF) are then associated with the expression of LTP/LTD (Hubener and Bonhoeffer, 2010) and potentially contribute to the induction of structural plasticity. Such coordinated structural and functional relationship was observed in the process of maturation and experience-dependent cortical rewiring (Espinosa and Stryker, 2012). Behavioral studies in mice demonstrated the formation of new spines in the cortex as a result of visual experience (Hofer et al., 2009) and motor learning (Xu et al., 2009). As newly formed synapses are maintained over the long term, this supports the idea that learning and memory requires structural remodeling of synaptic connectivity in the circuit (Caroni et al., 2012). Another interesting activity dependent plasticity event has been observed during the process of synaptic homeostasis. Here, an increase in spine density was observed upon the blockage of synaptic transmission in Cornu ammonis-1(CA1) pyramidal neurons and lateral geniculate nucleus (LGN) neurons of mice, likely as a result of a homeostatic response (Kirov and Harris, 2000; Rocha and Sur, 1995).

Synaptic dysfunction and spine pathology are the major defects observed in many neurological disorders including Alzheimer's disease, Parkinson's disease, Schizophrenia, Autism spectrum disorder (ASD), and epilepsy (Day et al., 2006; Jiang et al., 1998; Knafo et al., 2009; Uylings and de Brabander, 2002). Aggregated amyloid β protein (Aβ) was shown to inhibit memory consolidation through a progressive loss of synapses and altered synaptic structure in dentate gyrus and CA1 regions (Borlikova et al., 2013). Impaired synaptic plasticity was also reported in many neurodevelopmental and psychiatric disorders. Hypofunctional NMDA receptors were assumed to be one of the causes for schizophrenia and mood disorders (Stephan et al., 2006) and modulation of NMDA receptor activity through agonist application

is used as a treatment (Coyle et al., 2003). Excess of synaptic plasticity is associated with a few conditions including focal dystonia and chronic pain. Non-invasive physiological and imaging studies revealed an increased sensory receptive field beyond the normal topographical boundaries in both the cases, thereby leading to an increase in symptoms of dystonia (Lin and Hallett, 2009) and increased sensitivity to pain (Baliki et al., 2012; Saab, 2012). Modulation of synaptic plasticity may represent therapeutic strategies for many neurological disorders. For example, recovery from the brain injury or lesions requires the induction of mechanism of synaptic rewiring. Task specific activation of the circuit in the region of lesions can lead to changes in axon sprouting, dendritic morphology and can thereby establish appropriate synaptic connectivity (Cramer, 2008; Grefkes and Fink, 2012).

2.2 Homeostatic synaptic plasticity

Synapses undergo continuous changes in their activity and membrane potentials. For a particular synapse, the activity levels must be within a certain range and are maintained by an endogenous feedback mechanism called homeostatic synaptic plasticity (HSP) (Figure2). When the synapse is less active, homeostatic mechanisms can increase synaptic strength by increasing the release probability. If the synapse is hyperactive, it decreases synaptic activity by reducing membrane excitability (Thiagarajan et al., 2007). These mechanisms of balancing synaptic activity have been extensively studied in both vertebrates and invertebrates. For example, in mammalian neurons *in vitro* (Henry et al., 2012; Turrigiano et al., 1998; Wierenga et al., 2006) and *in vivo* (Barnes et al., 2015; Goel and Lee, 2007; Mendez et al., 2018; Teichert et al., 2017), at the la neuromuscular junction of Drosophila (Schulz and Lane, 2017). Apart from balancing synaptic activity, HSP plays an important role in the development of neural circuits (Ranson et al., 2012; Turrigiano and Nelson, 2004), cell-type specific synapse formation and rewiring (Johnson et al., 2017; Sutton, 2010; Tien et al., 2017) and many neurological disease states.

Homeostatic modulation of synaptic activity occurs both at pre- and postsynaptic compartments. Presynaptically, modulation takes place by regulating the release probability of synaptic vesicles, in association with long lasting structural and functional changes at the synapses. Changes includes the size and number of synapses (Mendez et al., 2018), size of active zones (Goel et al., 2017) and reversible changes in the size of the ready releasable pool (Muller et al., 2012; Wang et al., 2011). Increase in presynaptic calcium due to a retrograde

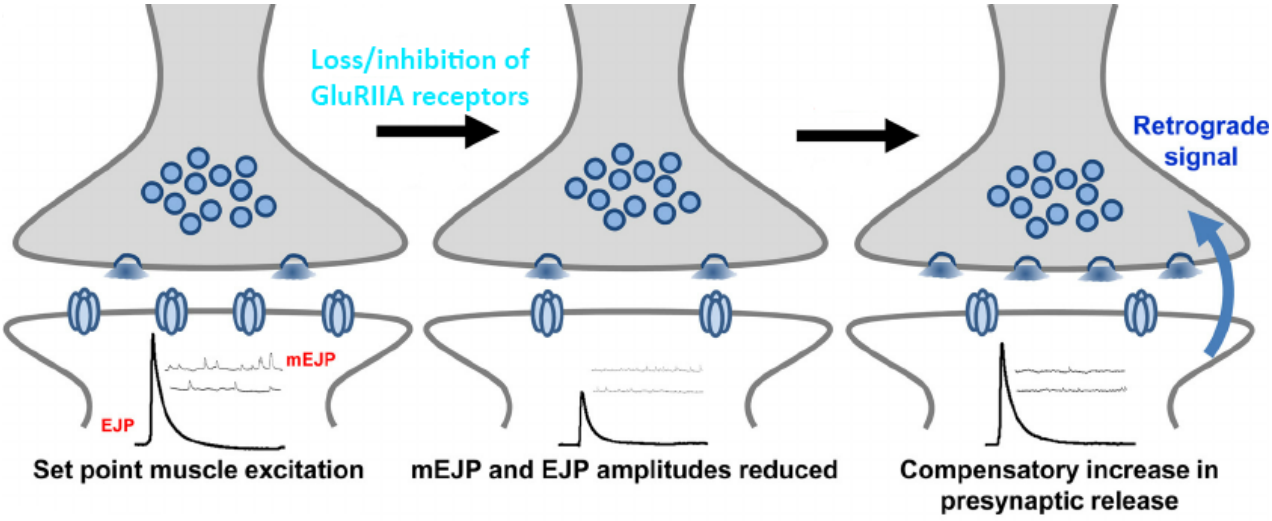

Figure2: Homeostatic plasticity in Drosophila Neuromuscular junction (NMJ). Schematic representation of homeostatic synaptic plasticity in Drosophila NMJ. Healthy synapses maintain the activity within a certain range (left). Pharmacological or genetic loss of Glutamate receptor subunit IIA (GluRIIA) leads to an intermediate situation where the synaptic transmission is reduced (middle). In order to maintain the set point muscle excitation, retrograde signaling mechanism is triggered and influences the presynapse to enhance the release. (*Adopted from (Frank, 2014a), Figure* 2).

signal is the first step in the induction of presynaptic HSP (PHP). Calcium imaging of cultured hippocampal neurons revealed that a decrease in activity induces an increase in the entry of calcium into the presynapse, which in turn increases presynaptic release probability (Zhao et al., 2011). The process of retrograde synaptic potentiation has been studied using the larval Drosophila neuromuscular junction (NMJ) as a model system. In Drosophila, PHP can be induced by genetic ablation of the Glutamate receptor subunit IIA (GluRIIA) receptor subunit or by inhibiting postsynaptic glutamate receptors using a pharmacological antagonist. Using the Drosophila NMJ and vertebrate cell culture systems the role of multiple genes regulating the activity of the presynaptic calcium channels and the involvement of cell organelles including mitochondria and the endoplasmic reticulum have been established (Frank, 2014b; Jeans et al., 2017; Jensen et al., 2009). Also, mechanisms like proteasome dependent regulation of synaptic vesicle release has been found to play an important role during the induction of PHP (Wentzel et al., 2018).

It is now well established that various genes respond to the retrograde signal and induce the PHP by modulating presynaptic calcium dynamics, which in turn alters presynaptic release probability. However, the signals or the molecules that induce the trans-synaptic changes are not very well understood. Wang et al. (2014) demonstrated that endostatin

functions as a trans-synaptic signaling molecule that activates the presynaptic calcium channels in response to the signal from the postsynapse. But the retrograde signal that activates endostatin has not yet been identified. At the Drosophila NMJ, the retrograde stimulus is initiated in the muscle after either genetic loss (chronic) or pharmacological inhibition (acute) of glutamate receptors. One of the identified mechanisms involved in retrograde signaling after chronic perturbation is the activation of mTOR mediated translation. Blocking the translation mechanism in the postsynapse leads to the inhibition of retrograde synaptic potentiation (Penney et al., 2012; Penney et al., 2016). Acute loss of GluRIIA induces a CaMKII-mediated retrograde signal acting locally at the sub synaptic reticulum (SSR) of the type 1b boutons and this is independent of mTOR (Frank et al., 2006; Lu et al., 2003; Newman et al., 2017). However, there is first evidence that the two mechanisms act on common components like dysbindin in the presynapse to induce functional synaptic modulation (Dickman and Davis, 2009; Goel et al., 2017).

Homeostatic plasticity in the postsynapse is also well studied in a vertebrate neuronal cell culture system and is termed synaptic scaling (Turrigiano et al., 1998). Partial inhibition of synaptic release triggers a homeostatic modulation in the postsynapse by increasing the glutamate receptor subunit 1 (GluR1) and GluR2 (Wierenga et al., 2005). Similar to presynaptic homeostatic modulation, postsynaptic mechanisms also depends on alterations of calcium concentrations to induce synaptic scaling. Increase or decrease of calcium entry into the postsynaptic dendrite triggers the postsynaptic response by regulating expression of α-amino-3-hydroxy-5-methyl-4-isoxazolepropionic acid (AMPA) receptors (Hou et al., 2015; Soares et al., 2013; Wierenga et al., 2005) or by modulation of activity of existing calcium permeable AMPA receptors (Fu et al., 2011; Gilbert et al., 2016; Sanderson et al., 2018). During hyperactivity states, AMPA receptors can be internalized in response to phosphorylation and degraded after the activation of the ubiquitin proteasome pathway (Fu et al., 2011; Jakawich et al., 2010; Jang et al., 2015). Induction of such homeostatic mechanisms (at the pre- or postsynapse) might be the initial step in any neuron that deviates from its normal function. The deviation beyond the homeostatic repair threshold results in a malfunction of the circuit (Heinemann, 2009; Houweling et al., 2005; Seeburg et al., 2008; Seeburg and Sheng, 2008; Swann and Rho, 2014; Wondolowski and Dickman, 2013). Activating homeostatic mechanisms represent a potential therapeutic strategy against a number of neurological disorders including neurodegeneration-associated disorders (Perry et al., 2017).

2.3 Insight on the molecules involved in synaptic plasticity and stabilization

Synaptic plasticity and synapse stabilization work in hand-in-hand, and likely share common molecular mechanisms. Recent studies provided better knowledge regarding morphological and functional aspects of plasticity, whereas the molecular knowledge of synaptic maintenance remains very limited. Regulation of the cytoskeleton is a key mechanism for the induction of structural changes at the synapses. Many studies have demonstrated that pre- and postsynapse is enriched with actin and actin regulation can mediate changes in the synaptic structures. Activity-dependent spine growth and remodeling has been demonstrated to be dependent on signal transduction pathways that modulate actin dynamics (Chen et al., 2007; Cingolani and Goda, 2008). Rho-GTPase family proteins have been well studies in the regulation of actin cytoskeleton. Rac1 promotes spine growth by the activation of protein kinases like PKA1 and LIMK1, which in turn inhibit the actin depolymerization factor cofilin (Bamburg, 1999) and influences the synapse stabilization. Formation of spines during LTP and shrinkage of spine during LTD depends on cofilin-mediated actin regulation (Zhou et al., 2004). Similarly, mechanism of LIMK1 mediated actin regulation in the presynapse have been demonstrated to regulate the growth of the NMJ in Drosophila (Piccioli and Littleton, 2014b). Multiple other molecules are involved in actin regulation, including molecules like Wasp, Arp2/3 and Nervous wreck as modulators of synaptic growth (Coyle et al., 2004). Phosphorylation of the actin capping molecule adducin by PKC is essential for the stabilization of synapses and its capping activity controls the synapse formation (Bednarek and Caroni, 2011; Pielage et al., 2011). The adaptor molecule ankyrin2 mediates the interaction of cell adhesion molecules and the cytoskeleton (microtubules) through spectrin and regulates synapse growth and stability (Enneking et al., 2013; Pielage et al., 2008; Pielage et al., 2005). CaMKII and PKC have been demonstrated to be involved in the activity induced LTP maintenance and spine stability during learning (Lisman et al., 2012; Sacktor, 2011; Yamagata et al., 2009). Also the organization of postsynaptic density proteins like PSD95 contributes to synapse stability (Ehrlich et al., 2007) and alterations in AMPA receptor abundancy (Ripley et al., 2011) enhance synaptic strength and stability. In addition, molecules involved in growth regulation and protein synthesis also control synapse plasticity, as growth and protein synthesis are inter-dependent and have been shown essential for synapse stabilization (Bramham, 2008; Costa-Mattioli et al., 2009;

Tanaka et al., 2008). Further studies to understand these mechanisms are needed to gain insights on the molecular control of synaptic remodeling, learning and memory, and neuronal disease and disorders.

2.4 Signaling mechanisms involved in synaptic plasticity

Many signaling mechanisms are involved both in the synapse development and plasticity throughout the life of an animal. For example, the growth regulating BMP and mTOR pathway play a prominent role during development of the nervous system and are later linked to other signaling systems in the regulation of cell homeostasis.

2.4.1 BMP signaling in synaptic plasticity

The bone morphogenetic protein (BMP) signaling pathway is well characterized for its regulation of cell growth and differentiation in almost all organ systems from embryonic development to adult tissues. BMP is expressed with similar basic functionality in the nervous system. In addition to that, the BMP pathway plays an essential role in synaptic function and plasticity and has been well-studied at the Drosophila larval neuromuscular junction. Decapentaplegic (dpp) and Glass bottom boat (gbb) are the Drosophila BMP2/4 type and BMP-7 type ligands, respectively. Multiple types of BMP ligands participate in organ systems differentiation in vertebrates. Secreted gbb binds to the BMP type I receptors saxophone (sax), thick vein (tkv) or the type II receptor wishful thinking (wit) receptors and induce the phosphorylation of the cytoplasmic Mad. pMad is then transported into the nucleus to induce translation by activating the smad family of transcription factors (Rawson et al., 2003). The localization and distribution of pMad is well controlled during the regulation of synapse growth (Merino et al., 2009). BMP also regulates growth of postmitotic neurons, an essential process for synaptic plasticity. It has been demonstrated that rate of dendritic growth and synapse formation can be enhanced by the treatment of cultured neurons with BMP-7 (Ghogha et al., 2012; Withers et al., 2000). Loss of function studies using components of BMP pathway revealed that regulation of synaptic growth and maintenance is achieved through the modulation of cytoskeleton dynamics and the expression of cell adhesion molecules (Aberle et al., 2002; Berke et al., 2013a; Marques et al., 2002; Piccioli and Littleton, 2014b; Zhang et al., 2017). At the NMJ, the trigger for the activation of BMP pathways is released from the postsynaptic muscle. The secretion of gbb and the activation of BMP pathway depends on the activity stimulus received by the muscle. Along with neurotransmitter

release, the stimulus from the surrounding glia also regulates muscle secretion of gbb. Secretion of Maverick (Mav) from the glia was reported to stimulate the secretion of gbb from the muscle to induce retrogradely-controlled synaptic growth at the NMJ (Fuentes-Medel et al., 2012). Retrograde signaling induced by BMP pathway has also been reported to regulate the synaptic release machinery including T-bar integrity, synaptic vesicle organization, size of multivesicular bodies, endosomal to lysosomal trafficking of vesicles and release probability of synaptic vesicles (Laugks et al., 2017; Lee et al., 2016). In addition, there is evidence that components of BMP are essential for the induction of retrograde synaptic potentiation. (Baines, 2004; Goold and Davis, 2007b; Haghighi et al., 2003). Altogether, the BMP pathway is involved in multiple processes to keep the neurons healthy and active, but this mechanism is under constant surveillance by an endocytosis-mediated mechanism to control for unnecessary synaptic growth (O'Connor-Giles et al., 2008; Shi et al., 2013). Thus, BMP signaling is a controlled regulatory mechanism controls synaptic development and function by coordinating with various other signaling mechanism.

2.4.2 mTOR signaling in synaptic plasticity

Mammalian/mechanistic Target of Rapamycin (mTOR), is a key signaling mechanism that regulates the translation machinery in the cell. The mTOR pathway regulates various aspects of the nervous system from early development to the function of the adult nervous system (Garza-Lombo and Gonsebatt, 2016) by activation and inactivation of translation. During development, mTOR regulates the differentiation of pluripotent stem cells via activation of s6k (Easley et al., 2010), initiates neuronal differentiation in the vertebrate neural tube (Fishwick et al., 2010) and temporally controls the neurogenesis in vertebrates and Drosophila (Malagelada et al., 2011; McNeill et al., 2008). The temporal differentiation of photoreceptors and chordotonal organs in Drosophila are under the control of mTOR through regulation of the expression of neural differentiation genes like elav, prospero, and bar proteins (Bateman and McNeill, 2004). TSC2-Rheb-mTOR signaling cooperates with the ephrin-Eph receptor system to control axon guidance in the visual system (Nie et al., 2010). Also, netrin-1 and sema3A gradient induced chemotrophic growth cone migration is dependent on the mTOR-mediated translation (Campbell and Holt, 2001). In mature neurons, mTOR regulates the long-term and short-term synaptic plasticity (Banko et al., 2006; Banko et al., 2005; Kelleher et al., 2004; Tang et al., 2002), mediates changes in the growth of presynaptic nerve terminal and dendrites and regulates the organization of active zones (Cheng et al., 2011; Costa-Mattioli et

al., 2009; Menon et al., 2004; Takei et al., 2004; Tavazoie et al., 2005). mTOR pathway in association with Ras-MAPK pathway regulates the size of the soma and dendrites and can increase dendritic complexity (Kumar et al., 2005). Hyperactivation of mTOR signaling can enhance the activity of the circuit leading to the enhanced repetitive behavior and seizures (Hoeffer et al., 2008; LaSarge and Danzer, 2014). mTOR also acts as an on and off switch to regulate synaptic activity by modulating expression of potassium channel subunits and ionotropic glutamate receptor subunits (Niere and Raab-Graham, 2017). Activity induced activation of mTOR induces synaptic plasticity. The stimulation of NMDARs and mGluRs activates mTOR and increases dendritic protein synthesis (Gong and De Camilli, 2008; Hou and Klann, 2004) and contributes to synaptic plasticity (Jaworski and Sheng, 2006; Swiech et al., 2008). Glutamatergic activation induces the s6k-mediated translation through the activation of Ca^{2+}/calmodulin and induces LTP (Lenz and Avruch, 2005).

Another interesting aspect of mTOR is the local translation. mTOR controls the translation of several synaptic proteins like CaMKIIa, NR1, Homer2, LIMK2, GluA1, and GluA2 that regulates synaptic shape and function locally to gain control over the synapse at the level of individual synapses (Liao et al., 2007). Local translation via mTOR was first observed by Kang & Schuman (1996) in the CA1 neurons and demonstrated a role of local translation in synaptic plasticity. Another interesting aspect of the mTOR pathway is the regulation of retrograde synaptic potentiation. During impaired AMPAR function, retrograde modulation of synaptic transmission depends on mTOR-mediated translation in the postsynapse both in vertebrates and invertebrates (Goel et al., 2017; Henry et al., 2012; Penney et al., 2012). It has been shown that BDNF is synthesized locally by mTOR and released as a signal for the induction of retrograde presynaptic potentiation (Jakawich et al., 2010).

Impaired mTOR function was reported in many neurological diseases. Loss of TSC activity is observed in association with epilepsy, intellectual disability and autism spectral disorder (Crino, 2009, 2010, 2011; Crino et al., 2006). Suppression of polysomal mRNA translation due to an increase in the phosphorylation of eIF2a is observed in clinical and laboratory Alzheimer's disease brains (Chang et al., 2002; Ma et al., 2010; O'Connor et al., 2008; Page et al., 2006). Mutations that cause an inhibition of the mTOR pathway like *pten* or *TSC1/2* induce ASD in humans (O'Roak et al. 2012, Sahin 2012). Loss of FMRP, an RNA binding protein that is involved in the inhibition of translation induces uncontrolled local translation of several genes like GluA2, PSD95, RhoA, Rac1, and matrix metalloproteinase 9 in the postsynapse, leading to severe morphological abnormalities in Fragile X-syndrome (Fernandez et al., 2013; Irwin et

al., 2001). Therefore, the mTOR pathway represents an effective therapeutic target for the treatment of Fragile X-syndrome.

2.4.3 Other signaling mechanisms in synaptic plasticity

Many other signaling pathways have been identified to regulate aspects of synaptic plasticity. JNK is an important signaling enzyme that is involved in many aspects of cellular regulation including gene expression, cell proliferation and programmed cell death. Regulation of JNK signaling is essential for the synapse growth. Proteins like Highwire and Wallenda has been identified as upstream regulators by inducing JNK-Fos mediated transcription (Collins et al., 2006). Neurotrophin Spatzle3 (SPz3) mediated activation of the Tollo- like receptors (TLRs) functions through the JNK pathway to induce synaptic growth (Ballard et al., 2014). JNK has also been shown to interact with SNARE proteins like Syntaxin-1, Syntaxin-2 and Snap-25 and regulates synaptic vesicle release (Biggi et al., 2017). Another major translation regulating pathway is the JAK-STAT pathway, which is activated by various cytokines and growth factors and has a prominent role in the regulation of synaptic plasticity. JAK-STAT signaling regulates the transcription of GABAergic receptors upon the activation by neurotrophic factors like BDNF and regulates the efficacy of GABAergic synaptic activity (Lund et al., 2008; Riffault et al., 2014). Also, the Wnt/β-catenin pathway has been well studied for its functional importance in the nervous system. Wnt signaling regulates the differentiation of pre- and postsynapse during the development of Drosophila larval NMJs (Packard et al., 2002). It also regulates the Glutamate receptor clustering and the active zone remodeling in Drosophila (Kerr et al., 2014; Sugie et al., 2015; Thomas and Sigrist, 2012). Rapid activity induced structural changes are mediated by Wnt signaling in Drosophila (Ataman et al., 2008) and Wnt7a rapidly activates the CaMKII activity and induces increase in spine density and synaptic strength in vertebrates (Ciani et al., 2011). Defective Wnt signaling has been associated with many neurological diseases including neurodegeneration, cognitive deficits and schizophrenia (Inestrosa and Varela-Nallar, 2014; Sadigh-Eteghad et al., 2016; Tiwari et al., 2015).

Although, appreciable understanding on synaptic cellular mechanism has been attained, the knowledge of the mechanisms that regulate synapse stability remains preliminary. To gain insights into potential signaling pathways involved in synapse maintenance targeting of key

regulatory molecules may be promising. Kinases and phosphatases are central regulators of almost all signaling pathway.

2.5 Role of kinases and phosphatases in synapse development and function

Regulation of synaptic structural and functional plasticity involves almost all major cell-signaling pathways, including BMP, MAPK, mTOR, JAK/STAT signaling pathways. Regulation of these pathways involves series of kinases and phosphatases that control the activation and inactivation of critical components of the pathways. In addition, protein phosphorylation is essential for protein folding, protein-protein interactions, protein distribution and for the control of protein stability and degradation. Kinases mediate the phosphorylation and the phosphatases mediate the dephosphorylation of targets. The Drosophila genome encodes most of the kinase and phosphatase family proteins with close structural and functional similarities to vertebrate kinases and phosphatases. In Drosophila 251 kinases and 89 phosphatases have been identified that are homologous to kinases and phosphatases in vertebrates (Morrison et al., 2000).

A number of kinases and phosphatases have been identified that control synapse development. For instance, kinases like CK2 and LIM kinase 1 regulates synapse growth by modulating cytoskeletal dynamics (Bulat et al., 2014; Eaton and Davis, 2005; Piccioli and Littleton, 2014b; Pielage et al., 2011), c terminal Src kinase regulates the expression of cell adhesion molecules during homeostatic synaptic plasticity (Spring et al., 2016) and axonal transport (Horiuchi et al., 2005; Vagnoni and Bullock, 2018), ribosomal S6k and SRPK79D control the size and organization of active zones, (Cheng et al., 2011; Johnson et al., 2009), the phosphorylation controlled postsynaptic translation machinery controls the expression of glutamate receptors and cell adhesion molecules (Sigrist et al., 2000; Sigrist et al., 2002), the regulation of ion channels (Davis et al., 2001), PKA mediates activity dependent regulation of vesicle release (Cho et al., 2015) and synaptojanin (Synj) mediates endocytosis and synaptic vesicle recycling (Chen et al., 2014; Geng et al., 2016; Matta et al., 2012). All these mechanisms are necessary for the normal function of the nervous system and for the induction of LTP, LTD and homeostasis.

In addition, kinases and phosphatases also play an essential role during retrograde control of synaptic development and function. The TOR complex, LRRK2, and CaMKII activity is required postsynaptically to regulate synaptic transmission (Haghighi et al., 2003; Penney

et al., 2012; Penney et al., 2016). CaMKIV regulates the expression and activity of postsynaptic receptors to regulate synaptic homeostasis during scaling (Bleier and Toliver, 2017). PKA has been implicated in many processes in the nervous system and its role in the regulation of GluA1 during homeostatic plasticity (synaptic scaling) has been demonstrated in vertebrates (Diering et al., 2014). Despite these identified roles, more than half of the kinases and phosphatases have not been evaluated for their importance in the nervous system. Understanding the importance and the regulatory function of these molecules will enable a better understanding of the mechanisms of synapse development and plasticity. Bulat et al. (2014) performed an RNAi based screen targeting the kinome and phosphatome of Drosophila to identify novel regulators of synapse development. Here, I investigated the role of the pseudo kinase Madm and the protein phosphatase 4 for the development, maintenance and function of synapses using the Drosophila larval neuromuscular junction as a model system.

2.6 Drosophila larval neuromuscular junction as a model to study synaptic plasticity

Drosophila melanogaster has been established as a model organism for neuroscience research since 1960s. Seymour Benzer was the first to use Drosophila to demonstrate the relationship between genes and behaviors (Benzer, 1967). Since then, Drosophila has been used to study various aspects of the nervous system including neuronal cell fate determination, axonal guidance, synaptogenesis, neural function, behavior, neurodegeneration and disease. Development of advanced genetic tools to access the nervous system and control the gene expression and neuronal function makes it a powerful model system to study the properties of the neuron.

The Drosophila larval neuromuscular junction is used to study the development and function of synapses. Motor neurons project into each hemisegment, and form varicosities like structures called synaptic boutons on the surface of the muscle thereby forming the NMJ. NMJs are stereotypically organized in each hemi-segment and are very well accessible for detailed observations. Boutons are relatively large in size (2–5 µm diameter) and contain the synaptic release machinery including synaptic vesicles and active zone components. Active zones are in direct opposition of the postsynaptic receptors clusters that are embedded in the muscle tissue. The large size of synaptic boutons enables good accessibility to microscopy.

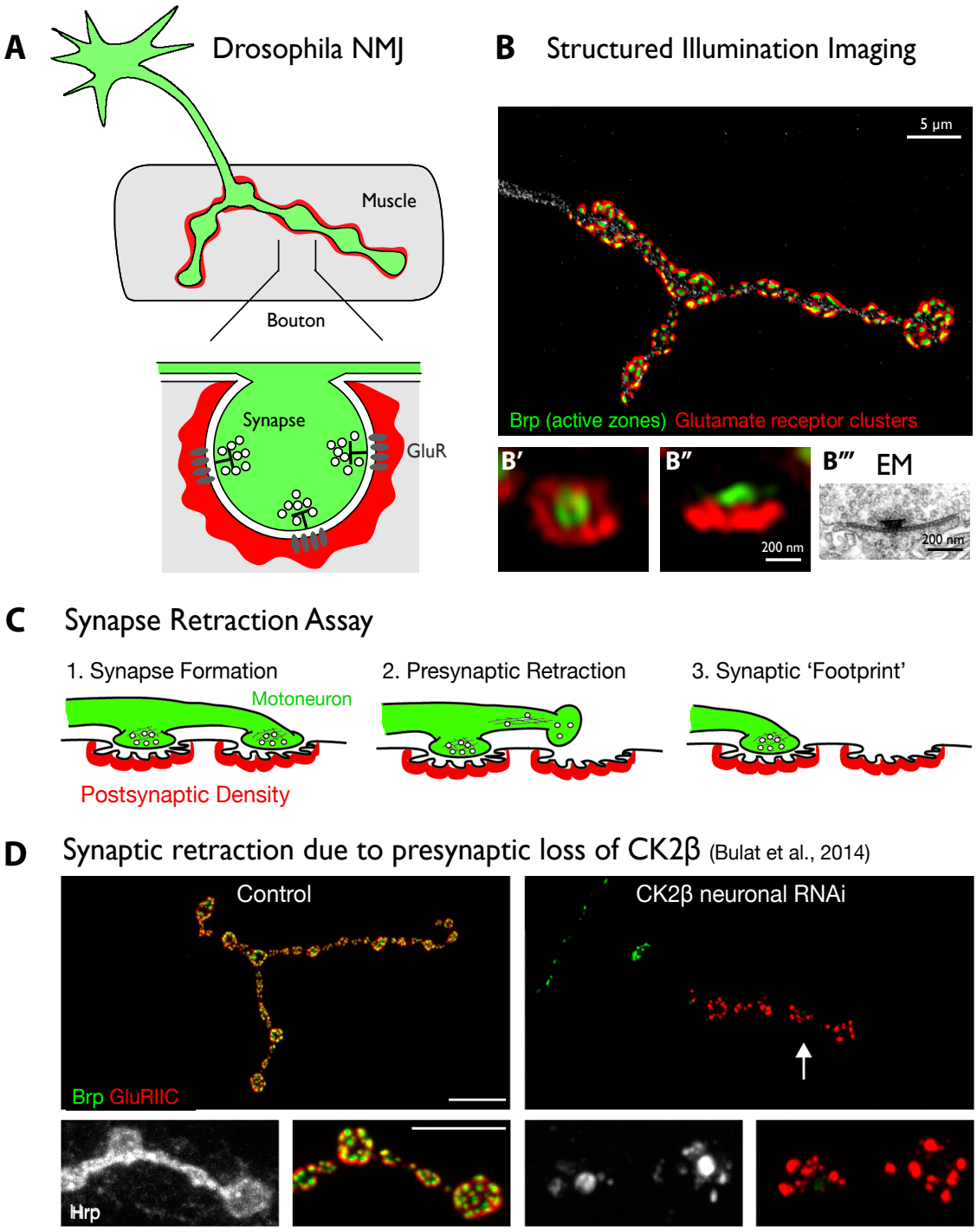

Figure 3: The Drosophila NMJ as a model system to study synaptic plasticity. (A) Schematic representation of a motor neuron projecting onto the muscle forming a neuromuscular junction. The presynaptic nerve terminal forms varicosity-like structures called synaptic boutons at the contact point with the muscle. The NMJ is spread like beads-on-a-string, with well-organized pre- (green) and postsynaptic (red) components. (B) Immunostaining of an NMJ labeling the presynaptic active zone molecule Bruchpilot (Brp) in green and postsynaptic glutamate receptors (GluRIIC) in red. (B', B'') Visualization of a single synapse at a higher resolution; (B''') electron microscopic view of an active zone showing electron dense regions surrounded by synaptic vesicles. (C) Schematic representation of the synaptic retraction assay. 1. A stable synapse with a well-

organized presynaptic nerve terminal and postsynaptic receptors, 2. The presynaptic nerve terminal retracts, 3. a postsynaptic receptor footprint representing a retracted synaptic bouton leaving the neighboring synapses undisturbed (*image Pielage lab*). (D) Example of synaptic retraction observed due to the presynaptic loss of CK2β (*adopted from Bulat et al. (2014), Figure 2*).

The Drosophila larval NMJs are glutamatergic in nature, resembling vertebrate central synapses. On average, >70% of the synaptic proteins in Drosophila are conserved to mammalian counterparts. Availability of specific antibodies for most of the synaptic components facilitates the analysis of synaptic components at high resolution (Figure 3). Recent advances in super resolution imaging have enabled the visualization of synaptic structures, yielding molecular insight into the organization, structure, and function of synaptic vesicle release sites (Liu et al., 2011b; Liu et al., 2011c; Miskiewicz et al., 2011; Owald et al., 2010; Owald et al., 2012). In addition, the Drosophila larval NMJ allows access for functional studies using electrophysiology and functional imaging. Taking advantage of these techniques and implementing them in combinations with the powerful genetic manipulation systems in Drosophila makes it a highly suitable model to study the molecular mechanism of synapse development, function and plasticity. Synaptic remodeling can be easily studied in this system, as a presynaptic retraction is marked by a postsynaptic footprint of the pre-existed synapse for a notable period (Figure 3C, D). Using this system, a wide range of molecules was identified that are involved in synaptogenesis, cytoskeletal molecules and their regulators, cell adhesion molecules, cell signaling molecules that control synapse growth and function, motor proteins, endocytosis and synaptic vesicle recycle regulators (Bulat et al., 2014; Eaton et al., 2002; Enneking et al., 2013; Koch et al., 2008; Matta et al., 2012; Pielage et al., 2011; Pielage et al., 2005, 2006; Stephan et al., 2015). Studies on the underlying mechanisms provided detailed insights on the regulation of synaptic function and plasticity (Enneking et al., 2013; Lepicard et al., 2014; Muller et al., 2012; Penney et al., 2012; Penney et al., 2016; Stephan et al., 2015; Wentzel et al., 2018). Despite recent progress a precise understanding of the coupling of synaptic growth, function and remodeling is still missing.

3 Myeloid leukemia factor 1 adaptor molecule (Madm) controls synapse development, maintenance and function

3.1 Abstract

The precise regulation of synaptic connectivity is essential for the establishment and function of neuronal circuitry. To identify the molecular mechanisms coupling synapse growth and maintenance we performed a large-scale RNAi-based screen targeting the Drosophila kinome. We identified the pseudo-kinase Myeloid leukemia factor-1 adapter molecule (Madm) as a novel regulator of synapse development, stability and function. Loss of Madm causes severe defects in neuromuscular junction growth and maintenance. Using tissue-specific rescue assays we demonstrate that presynaptic Madm controls synapse stability and growth while postsynaptic Madm contributes to the control of NMJ organization. Using genetic interaction assays we demonstrate that neuronal Madm acts in parallel to the mTOR pathway to regulate synapse growth at the level of the elongation factor 4E-BP. In addition, Madm is required for synaptic function and like mTOR, postsynaptic Madm is sufficient to induce synaptic potentiation. Together, our study identifies Madm as a central novel regulator of structural and functional plasticity at the NMJ.

3.2 Introduction

Synaptic plasticity is essential for the establishment and function of neural circuits. During development synaptic connections are established and later refined based on circuit activity and on information received from other neurons to develop into a mature circuit that is adjusted to the control of specific behaviors. The plastic nature of synapses provides the basis to incorporate changes into the circuit leading to adaptive behavior. Refinement of synaptic connections includes both the formation and the elimination of synapses. The molecular mechanisms that regulate formation of new synapse are relatively well understood (Goda and Davis, 2003; Lim et al., 2009; Sytnyk et al., 2017; Washbourne et al., 2004; Williams et al., 2010) whereas the mechanisms that regulate maintenance and elimination of synapses remain largely unknown (Bulat et al., 2014; Eaton et al., 2002; Enneking et al., 2013; Kasthuri and Lichtman, 2003; Keller-Peck et al., 2001; Massaro et al., 2009; Pielage et al., 2011; Pielage et al., 2008; Pielage et al., 2005, 2006). Remodeling of synapses requires mechanisms that can regulate the balance between the growth of the nerve terminal and the stabilization of the synapse. Synaptic elimination is observed in mutant animals that shows synaptic over growth (Pielage et al., 2011) and also in animals that show synaptic undergrowth (Eaton and Davis, 2005), however not all gene mutations that lead to synaptic over growth or undergrowth exhibit synaptic eliminations (Eaton and Davis, 2005). Thus, it is likely, that a specific set of molecules coordinates growth and remodeling of synapse and that these molecules may function by modulating major growth regulating factors. To gain insights on such mechanisms, we use Drosophila larval neuromuscular junction as a model, which enables simultaneous analysis of synaptic growth and stabilization parameters.

In Drosophila, forward genetic screen contributed to the identification of components of almost all growth regulating pathways in the regulation of synapse development. In addition to growth regulation, these pathways coordinate multiple other synaptic functions by regulating transcription and translation specific processes. Transcriptional mechanisms include the BMP pathway that has been reported to mediate axonal guidance (Withers et al., 2000), synaptic growth, dendritic morphology (Aberle et al., 2002; Charron and Tessier-Lavigne, 2005; Marques et al., 2002; McCabe et al., 2003; Rawson et al., 2003) and stability of synapse (Eaton and Davis, 2005). Retrograde signaling through the BMP receptors modulates the presynaptic terminal by regulating the cytoskeleton (Ball et al., 2010; Berke et al., 2013b; Heo et al., 2017; Piccioli and Littleton, 2014a) and by inducing synaptic

homeostasis (Goold and Davis, 2007a). Regulation of protein synthesis is essential for the induction of synaptic plasticity. As a translational regulator the mTOR pathway regulates growth through the regulation of protein synthesis in response to neurotrophins and other growth regulators. The mTOR pathway regulates various aspects of the nervous system from early development to functional parameters of adult stages (Garza-Lombo and Gonsebatt, 2016). During development, mTOR regulates the differentiation of pluripotent stem cells via activation of s6k (Easley et al., 2010), initiates the neuronal differentiation in vertebrate neural tube (Fishwick et al., 2010), temporally controls neurogenesis in vertebrates and Drosophila (Malagelada et al., 2011; McNeill et al., 2008) and controls the temporal differentiation of photoreceptors and chordotonal organs in Drosophila by regulating the expression of neural differentiation genes like elav, prospero, and bar proteins (Bateman and McNeill, 2004). In mature neurons, mTOR mediates the long-term and short-term synaptic plasticity through the regulation of local translation (Banko et al., 2006; Banko et al., 2005; Kelleher et al., 2004; Tang et al., 2002) to alter neuronal growth and regulates the organization of active zones (Cheng et al., 2011; Costa-Mattioli et al., 2009; Menon et al., 2004; Takei et al., 2004; Tavazoie et al., 2005). Also, the retrograde modulation of synaptic function due to the loss/blockage of AMPAR is dependent on mTOR-mediated translation in the postsynapse both in vertebrates and invertebrates (Goel et al., 2017; Henry et al., 2012; Penney et al., 2012). However, the mechanism that coordinate between synaptic growth and stabilization remains unknown. In an RNAi-based screen of the Drosophila kinome we identified Madm as a novel regulator of synapse growth and maintenance (Bulat et al., 2014).

Myeloid leukemia factor 1 adaptor molecule (Madm) is a ubiquitously expressed adaptor molecule that is highly conserved from yeast to vertebrates (Hooper et al., 2000). Madm protein contains a kinase like domain and a protein interaction domain. It also contains nuclear export and localization sequences that are proposed to regulate the transfer of Madm between nucleus and cytoplasm in a phosphorylation dependent manner (Hooper et al., 2000; Lim et al., 2002; Singh et al., 2016). Due to the lack of a conserved ATP-binding motif, Madm cannot function as a kinase. However, In vitro kinase assays performed with an immunoprecipitate from COS cells transfected with a Madm constructs showed that the precipitate can induce phosphorylation of myelin basic protein, indicating that a kinase is associated with Madm that mediates phosphorylation of potential Madm targets (Lim et al., 2002). Madm functions together with the long isoform of Bunched (BunA), interacting through its protein-binding domain to regulate the size of organs and the size of the adult

animals (Gluderer et al., 2010). Drosophila Madm and its human homolog Nuclear receptor binding protein 1 (NRBP1) were reported to function to regulate cell homeostasis and tumor suppression by functioning through multiple signaling mechanisms. These include the wnt-β catenine pathway by negative regulation of expression of downstream genes (Tan and Sansom, 2012; Wei et al., 2015), the JAK-STAT and EGFR pathway by the regulation of the expression of the EGFR ligand *vein* and Integrin (Singh et al., 2016). To date a requirement of Madm in the nervous system has not yet been described.

In this study, we demonstrate that Madm is an essential gene to regulate synapse development and maintenance with presynaptic Madm controlling synaptic growth and stability and postsynaptic Madm controlling synaptic organization. We show that Madm is essential for basal synaptic transmission and is sufficient to induce postsynaptic potentiation. Using genetic interaction analysis, we place Madm parallel to mTOR pathway converging downstream of 4E-BP, potentially regulating the elongation initiation factors during protein synthesis to regulate synapse development. Together our data identify Madm as a novel regulator of synapse development, maintenance and function.

3.3 Results

3.3.1 Madm is essential for synaptic stability

In an *in vivo* RNAi based screen performed to identify the kinases and phosphatases of Drosophila that regulate synapse development, we identified *Madm* as an important gene regulating synapse development and maintenance (Bulat et al. (2014). A stable wild-type NMJ is characterized by the precise and close apposition of the presynaptic active zone marker Bruchpilot (Brp) and postsynaptic glutamate receptor clusters (GluRIIC). Defects in synapse maintenance are characterized by the absence of Brp despite presence of GluRIIC. These events are rare (≤ 5% of all NMJs) in control animals (Figure 4C). In contrast, severe synaptic instability is observed when Madm is knocked down in the presynaptic terminal of Drosophila larval neuromuscular junction (24.5 ±4 % retractions) with varying severities from 1-2 bouton retractions to complete eliminations (Figure 4 I, J). In addition to the RNAi knockdown experiment, we tested multiple alleles of Madm: a hypomorph ($Madm^{EP3137}$), a null ($Madm^{2D2}$) and a point mutation in the protein-protein interaction domain ($Madm^{4S3}$) (Gluderer et al., 2010) (Figure 4A). All mutant alleles are homozygous lethal but survive till the 3rd instar larva as transheterozygous mutants over a Madm deficient chromosome *Df (3R) Exel728*. The expression of Madm in the nervous system of these mutants and of RNAi knockdown animals were analyzed on a western blot using a new antibody raised against Madm protein (Figure 4B). The predicted molecular weight of wild type Madm protein is 70.5 kDa. Madm is expressed in the nervous system and can be efficiently knocked down using the RNAi construct targeting the first exon. The hypomorphic mutants displayed reduced levels or complete absence of protein, the null allele displayed no protein expression and in the point mutant we observed the presence of mutant Madm with slightly reduced expression when compared to control samples. The reduced expression might be due to the analysis in trans to the deficiency. Our western blot analysis thus validated the efficiency of knockdown of Madm in the nervous system and also verified the molecular nature of the mutant alleles.

We next analyzed NMJs of these mutants for synaptic stability defects. We observed severe synaptic defects in the $Madm^{2D2/Df}$ (34.4±3.1%; Figure 4D, I, J), $Madm^{4S3/Df}$ (45.6±7.3%; Figure 4E, I, J) and $Madm^{EP3137/Df}$ (25.2±2.4%; Figure 4I, J) animals. Since we observed the strongest phenotype with $Madm^{4S3}$, we focused our analyses onto this. To determine

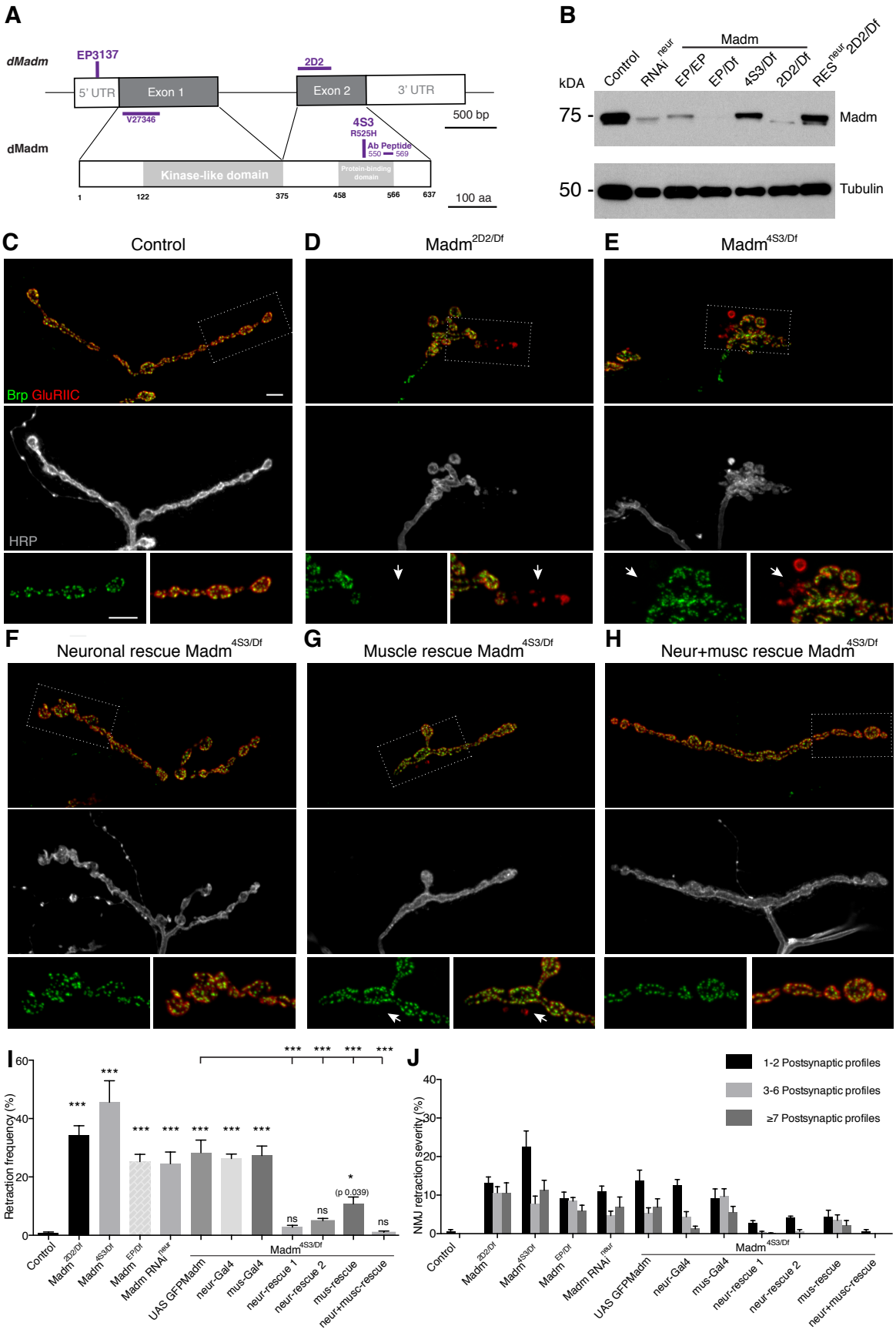

Figure 4: Presynaptic Madm is essential for synaptic Stability. (A) Schematic representation of genome locus of *Madm* on chromosome 3R, its alleles (top) and protein representing the domains, the point

mutation and the location of antigen peptide used to raise antibody (bottom). (B) Expression of Madm among different alleles and rescue. Control (w^{1118}), neuro>RNAi (*elav^{C155}-Gal4; UAS dicer/v27346*), *Madm$^{EP/EP}$ (Madm$^{EP3137/EP3137}$), Madm$^{EP/Df}$ (Madm$^{EP3137/Df(3R)\ Exel7283}$), Madm$^{4S3/Df}$ (Madm$^{4S3/Df(3R)\ Exel7283}$), Madm$^{2D2/Df}$ (Madm$^{2D2/Df(3R)\ Exel7283}$), neur- rescue Madm$^{2D2/Df}$ (elav^{C155}-Gal4; UAS Madm/+; Madm$^{2D2/Df}$)* with tubulin as control. (C-H) Analysis of synaptic stability of NMJs stained for presynaptic active zone protein Brp (green), postsynaptic glutamate receptor GluRIIC (red) and presynaptic membrane marker HRP (gray). (C) A stable control NMJ on muscle 1 with well-organized pre and post synaptic structures (*elav^{C155}-Gal4/+*). (D, E) In *Madm$^{4S3/Df}$* and *Madm$^{2D2/Df}$*, loss of function of Madm leads to severe synaptic instability. (F) Presynaptic expression of Madm in *Madm$^{4S3/Df}$* rescues synaptic stability (neuronal rescue 1: *elav^{C155}-Gal4; UAS GFP Madm/+; Madm$^{4S3/Df}$*, or neuronal rescue2: *Ok371 Gal4 / UAS GFP Madm; Madm$^{4S3/Df}$*), (G) Postsynaptic expression of Madm in *Madm$^{4S3/Df}$* partially rescues synaptic stability (*GluRIIB-Gal4/UAS GFP Madm; Madm$^{4S3/Df}$*). (H) Simultaneous pre- and postsynaptic expression of Madm in *Madm$^{4S3/Df}$* rescues synaptic stability (*elav^{C155}-Gal4; UAS GFP Madm/GluRIIB-Gal4; Madm$^{4S3/Df}$*) (I and J) Quantification of frequency of synaptic retractions (I) and severity (J) at NMJs of muscle 1/9 and 2/10 with error bar representing SEM; *, P≤0.05; **, P ≤ 0.01; ***, P ≤ 0.001; ns: not significant; ANOVA and Bonferroni multiple comparison test; n=320 NMJs; 10 animals. Scale bars represent 5µm.

whether Madm is required at pre- or postsynaptically for the regulation of synaptic stability we performed tissue specific rescue experiments. Presynpatic expression of Madm in *Madm* mutant animals using a pan-neuronal driver or a motor-neuron specific driver significantly rescued synaptic stability (2.7±0.6%; Figure 4B, F, I, J and 4.8±0.8%; Figure 4I, J respectively). This indicates that presynaptic Madm is sufficient to maintain synaptic stability. We further tested if postsynaptic Madm has any role in the regulation of synaptic stability by expressing Madm using a muscle specific driver. Interestingly, we observed a partial but significant rescue of synapse stability upon muscle expression of Madm (10.7±2.4%; Figure 4 G, I, J). Thus, Madm also has an essential role in the postsynaptic muscle during synapse development. Simultaneous expression of Madm pre- and postsynaptically perfectly restored synapse stability (0.98±0.50, %; Figure 4H, I, J), indicating that Madm regulate synaptic stability mainly from the presynapse, however, postsynaptic Madm also partially contributes.

3.3.2 Madm is essential for synaptic growth and organization

In addition to the synaptic stability defect, we observed severe morphological changes upon loss of Madm. A typical control NMJ on muscle 1 is organized into two branches and spreads on the muscle surface with its boutons organized along the main axes of the NMJ (Figure 5A). The growth of the NMJ can be characterized by the number of boutons and NMJ length and the organization of the NMJ can be characterized as NMJ area per muscle area and number

of branch points. Compared to controls, *Madm* mutant NMJs failed to grow out over the muscle surface with boutons organized compactly within small areas (Figure 5B). Mutant NMJs displayed reduced growth with a reduced number of boutons (18.6±0.6), NMJ length (66.8±2.8 µm), NMJ area per muscle area (0.4±0.03) and increased branch points (5.5±0.3) compared to that of controls (31.8±0.9 boutons), (124.2±6.2 µm NMJ length), (2.4±0.3 NMJ area/ muscle area) and (1.7±0.2 branch points) respectively (Figure 5F, G, H, I). Presynaptic expression of Madm, rescued all major morphology phenotypes with the exception of the number of branch points (3.1±0.3) (Figure 5C, F, G, H, I). Interestingly, postsynaptic expression of Madm significantly rescued the number of branch points (1.1±0.1) but failed to restore the number of boutons (17.5±0.8), NMJ length (77.7±3.6µm) or NMJ area per muscle area (0.95±0.09) (Figure 5D, F, G, H, I). These results indicate that presynaptic Madm regulates synaptic growth, while postsynaptic Madm controls synaptic organization. To support our hypothesis, we aimed to use immunohistochemical analyses to determine the localization of Madm at the pre- and postsynapse. Unfortunately, our newly generated antibody against Madm that worked well for western blots did not work for immunostainings. Therefore, we performed rescue experiments with GFP tagged Madm and analyzed the localization using an anti-GFP antibody. We observed that Madm is localized within the presynaptic terminal upon presynaptic rescue (Figure 5J) and highly enriched in the postsynaptic subsynaptic reticulum (SSR) upon postsynaptic rescue (Figure 5K). As a control, we expressed cytoplasmic EGFP in *Madm* mutants in the postsynaptic muscle and observed that cytoplasmic EGFP does not effectively localize to the SSR (Figure 5L). This suggests that the postsynaptic SSR localization is due to synaptic targeting of Madm. In support to the above results, simultaneous pre- and postsynaptic expression of Madm rescued all synaptic growth and organization phenotypes including the number of boutons (27.3±0.9), NMJ length (103.9±5.3 µm), NMJ area per muscle area (2.1±0.2) and number of branches (3.2±0.1) (Figure 5E, F, G, H, I). Together our data suggests that the coordinated function of Madm from the presynaptic motor neuron and the postsynaptic muscle is essential for NMJ development. Madm likely has a duel role during synapse development by regulating synaptic growth presynaptically and synaptic bouton organization postsynaptically.

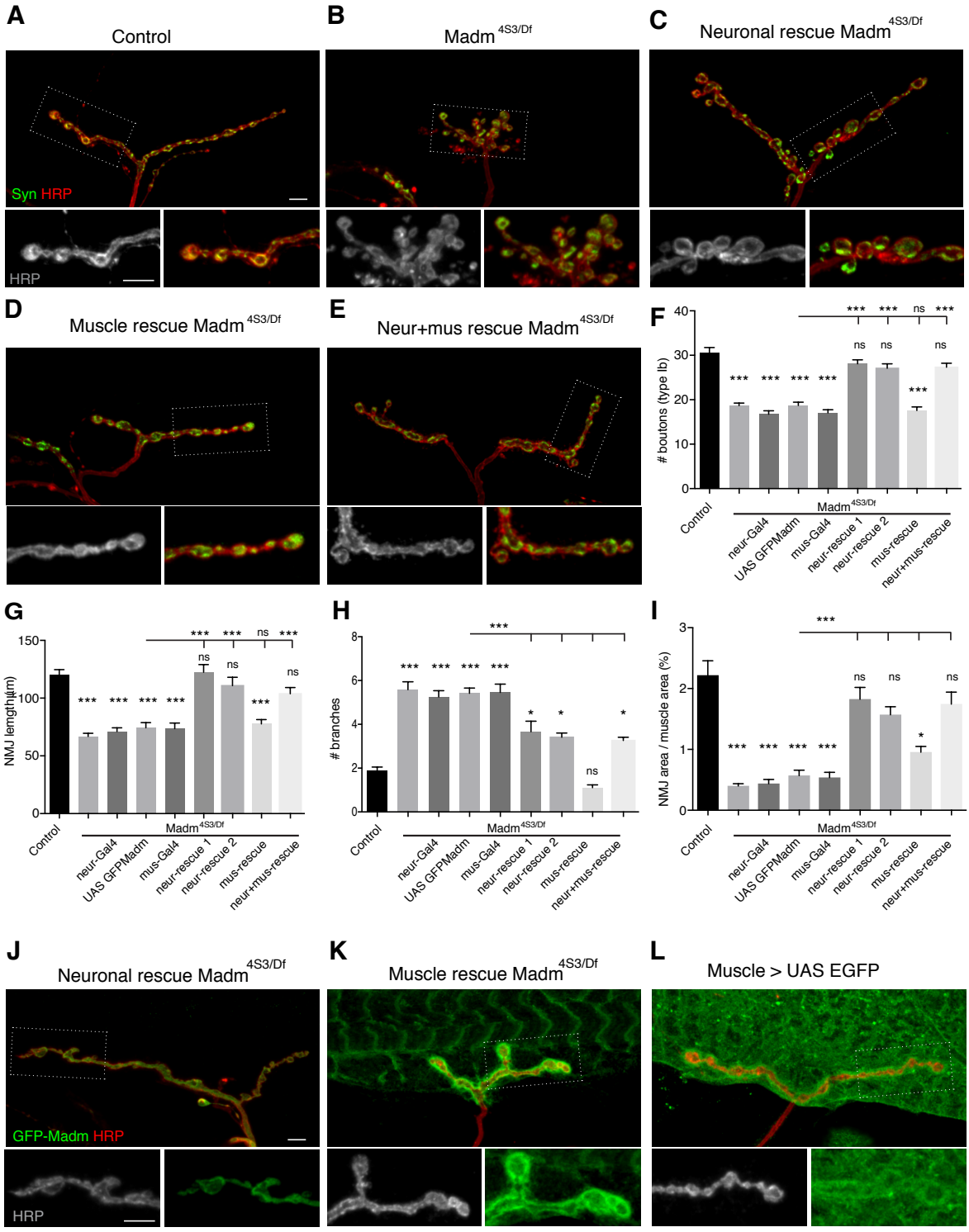

Figure 5: Madm is essential for synaptic growth and organization. (A-E) Morphological analysis of NMJs stained for the presynaptic vesicle marker Synapsin (Syn, green) and presynaptic membrane marker HRP (red). (A) A control (*elav-Gal4/+*) NMJ on muscle 1. (B) Loss of function of Madm (*Madm$^{4S3/Df}$*) results in reduced synaptic growth and clustered bouton organization. (C) Presynaptic expression of Madm in *Madm$^{4S3/Df}$* animals rescues the synaptic growth defects but doesn't restore synaptic bouton organization (neuronal rescue 1: *elav^{C155}-Gal4; UAS GFP Madm/+; Madm$^{4S3/Df}$*, or neuronal rescue2: *Ok371 Gal4 / UAS GFP Madm; Madm$^{4S3/Df}$*). (D) Postsynaptic expression of Madm in *Madm$^{4S3/Df}$* animals restores the synaptic bouton organization but

doesn't rescue synaptic growth (*GluRIIB-Gal4/UAS GFP Madm; Madm$^{4S3/Df}$*). (E) Simultaneous pre- and postsynaptic expression of Madm in *Madm$^{4S3/Df}$* animals rescues both synaptic growth and bouton organization (*elav^{C155}-Gal4; UAS GFP Madm/GluRIIB-Gal4; Madm$^{4S3/Df}$*). (F-I) Quantification of synaptic growth parameters on muscle 1 including number of boutons (F), NMJ length (G), number of branches (H) and NMJ area per muscle area (I), (*, P≤0.05; **, P ≤ 0.01; ***, P ≤ 0.001); ANOVA and Kruskal-Wallis multiple comparison test (n=20-28 NMJs from 5-7 animals). (J-L) Localization of Madm analyzed by the expression of GFP-tagged Madm and stained for GFP (green) and membrane (HRP in red). (J) Presynaptic localization of Madm after the expression of GFP-tagged Madm in *Madm$^{4S3/Df}$* mutants using a pan-neuronal driver (*elavC155-Gal4; UAS GFP Madm/+; Madm$^{4S3/Df}$*), (K) postsynaptic localization of GFP-tagged Madm in *Madm$^{4S3/Df}$* mutants using a muscle specific driver (*GluRIIB-Gal4/UAS GFP Madm; Madm$^{4S3/Df}$*) and (L) expression of cytosolic EGFP using a muscle specific driver (*GluRIIB-Gal4/UAS EGFP*). Scale bars represent 5µm.

3.3.3 Analysis of Madm requirements during synapse development

In order to determine the onset of synaptic defects in the *Madm* mutants, we analyzed second and third instar larvae for both morphology and stability defects. In controls, second instar larval NMJs are smaller in size (Figure 6A). As the animal grows to third instar larva the NMJ grows in proportion to the increasing muscle size and spreads across the muscle surface with well-organized pre and postsynaptic components and boutons (Figure 6B). Interestingly, second instar larval NMJs of *Madm* mutants appears well organized and stable but display a significant reduction in NMJ growth (number of boutons 8.3±0.4; control (11.6±4.7) (Figure 6C, E, F). However, these NMJs then fails to grow and spread along with the increased muscle and by the third instar larval stage severe organization and stability defect become apparent (45.6±7.3%) (Figure 6D, E, F). Similar to second instar larvae, third instar larvae also showed decreased NMJ growth indicating that Madm is essential for NMJ growth already during early larval development. It is interesting to note that stability is impaired only at the third instar larval stage. A minor reduction of NMJ growth is already observed in second instar larvae potentially as a consequence of a general growth defect as Madm has been identified as a growth regulator of tissues and organs (Gluderer et al., 2010).

3.3.4 Genetic interaction of Madm with Mlf1 and BunA

Loss of function of Madm leads to severe synaptic defects, but the mechanism how ´Madm regulates synapse development remains unknown. To understand the mechanism of action of Madm, we investigated potential interaction partners of Madm using genetic interaction analyses. Madm is reported to interact physically with Myeloid leukemia factor 1 (Mlf1) and

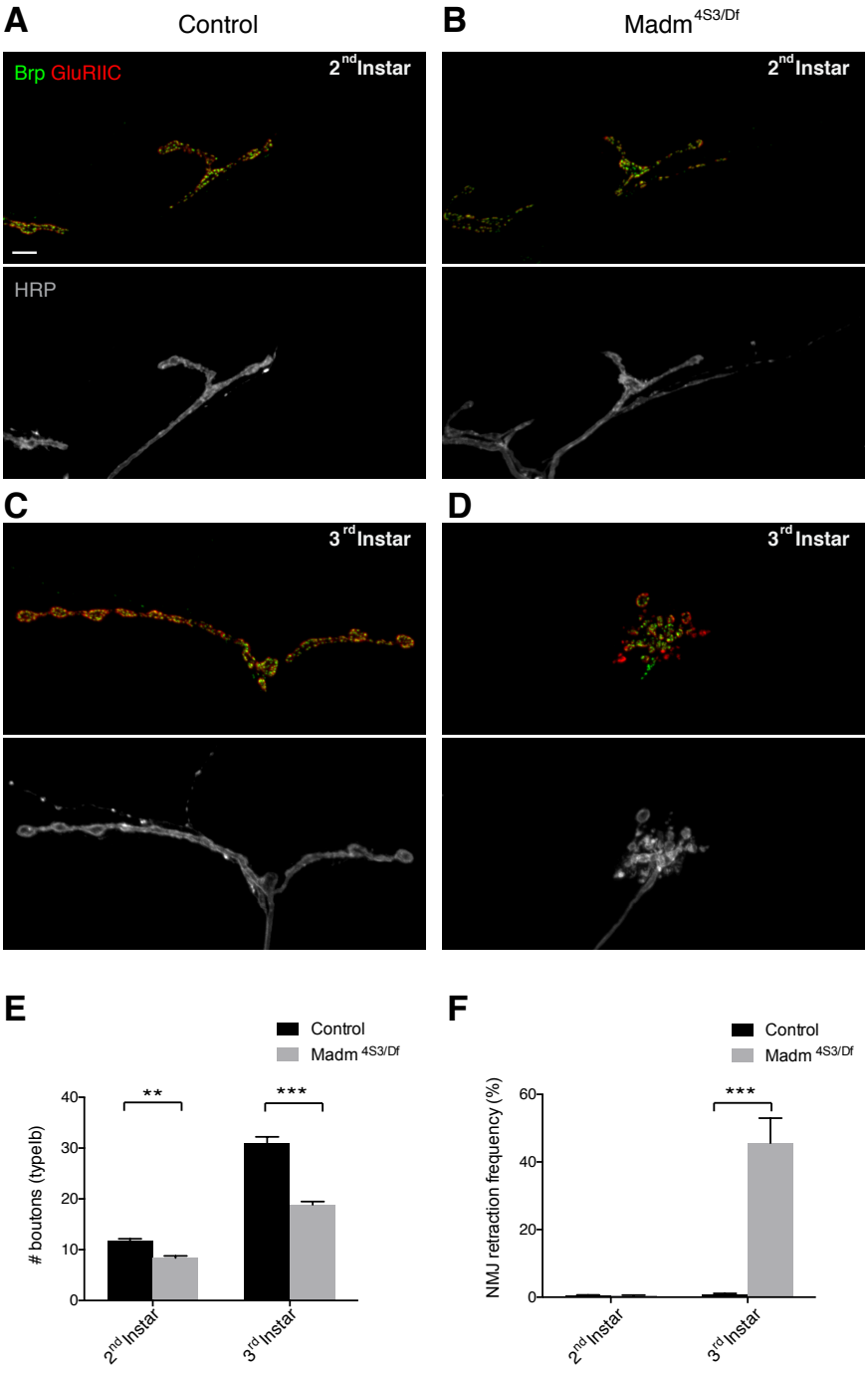

Figure 6: Madm is required for NMJ growth and stability at late larval stages. (A-D) NMJs of 2nd instar and 3rd instar larvae of control and *Madm$^{4S3/Df}$* animals analyzed on muscle 1. (A and C) A stable NMJ of a control 2nd instar (A) and a 3rd instar (C) larva. (B) A stable NMJ of a 2nd instar larva of *Madm$^{4S3/Df}$* that displays a significant reduction in size. (D) A 3rd instar larvae of Madm$^{4S3/Df}$ displays severe synaptic instability and reduced synaptic growth. (E) Quantification of NMJ growth of 2nd and 3rd instar larvae of control and *Madm$^{4S3/Df}$* animals (n=24 NMJs from 6 animals). (F) Quantification of synaptic retraction frequency in 2nd and 3rd instar larvae of control and *Madm$^{4S3/Df}$* mutant animals at NMJs of muscles 1/9 and 2/10 (n=256-320 NMJs from 8-10 animals). (*, P≤0.05; **, P ≤ 0.01; ***, P ≤ 0.001); Two-way ANOVA multiple t-test. Scale bars represent 5µm.

bunched A. Madm was reported to act as an adaptor molecule for Mlf1 to support its phosphorylation (Lim et al., 2002) and also to interact with bunched A to promote tissue and organ growth (Gluderer et al., 2010). We tested potential interactions of Madm with these known interaction partners using the alleles $Mlf^{\Delta C1}$ (Martin-Lanneree et al., 2006), Bun^{200B} and $Bun^{GE12327}$ (Gluderer et al., 2010). We first analyzed the mutants of *Mlf1* and *bunA* for synaptic defects. It has been previously reported that potential maternal contributions of Mlf partially rescue the defects of zygotic $Mlf^{\Delta C1}$ mutations (Martin-Lanneree et al., 2006). In order to analyse maternal null animals, we crossed homozygous *Mlf* mutant escapers and analysed the progeny for NMJ defects at the third instar larval stage. $Mlf^{\Delta C1}$ maternal null animals showed significant NMJ growth defects (number of boutons (16.1±0.8), NMJ length (75.3±4.2 µm) NMJ area per muscle area (1.13±0.16) (Figure 7B, G, H, I)), when compared to controls. These animals also show significant synaptic instability (12.8±2.9), indicating that Mlf1 is an essential synaptic growth-regulating component (Figure 7J, K). We also tested BunA mutants ($Bun^{200B/GE12327}$) but found no significant changes in NMJ morphology or stability (Figure 7). We further tested potential transheterozygos genetic interactions by analysing the transheterozygous mutants $Mlf^{\Delta C1/+}$; $Madm^{4S3/+}$ and $bun^{200B/+}$; $Madm^{4S3/+}$ but observed no significant changes in NMJ size (Figure 7G, H, I), indicating that the interaction of Madm with Mlf1 and bunched A might not be essential for synapse development. However, homozygous $Mlf^{\Delta C1}$ mutants showed significant synaptic growth and stability defects, but it did not display strong genetic interactions with Madm, indicating that Mlf might function independently or that 50% of the expression levels of each protein might be sufficient for their function. We also performed similar genetic interactions of Madm with Mlf1 and bunched using the *Madm* null allele $Madm^{2D2}$ (Figure 15).

3.3.5 Madm functions in parallel to mTOR pathway to regulate synapse development converging downstream of 4E-BP

We next investigated whether Madm interacts with any of the major growth regulating pathways as Madm our data and prior reports indicate that Madm acts as a growth regulator (Gluderer et al., 2010). We tested for genetic interactions of Madm with signaling components of the TGF-β/BMP and mTOR pathways (Figure 8B). We analyzed the interaction of Madm with Wit, Mad and Tkv (BMP pathway) by analyzing the following transheterozygous

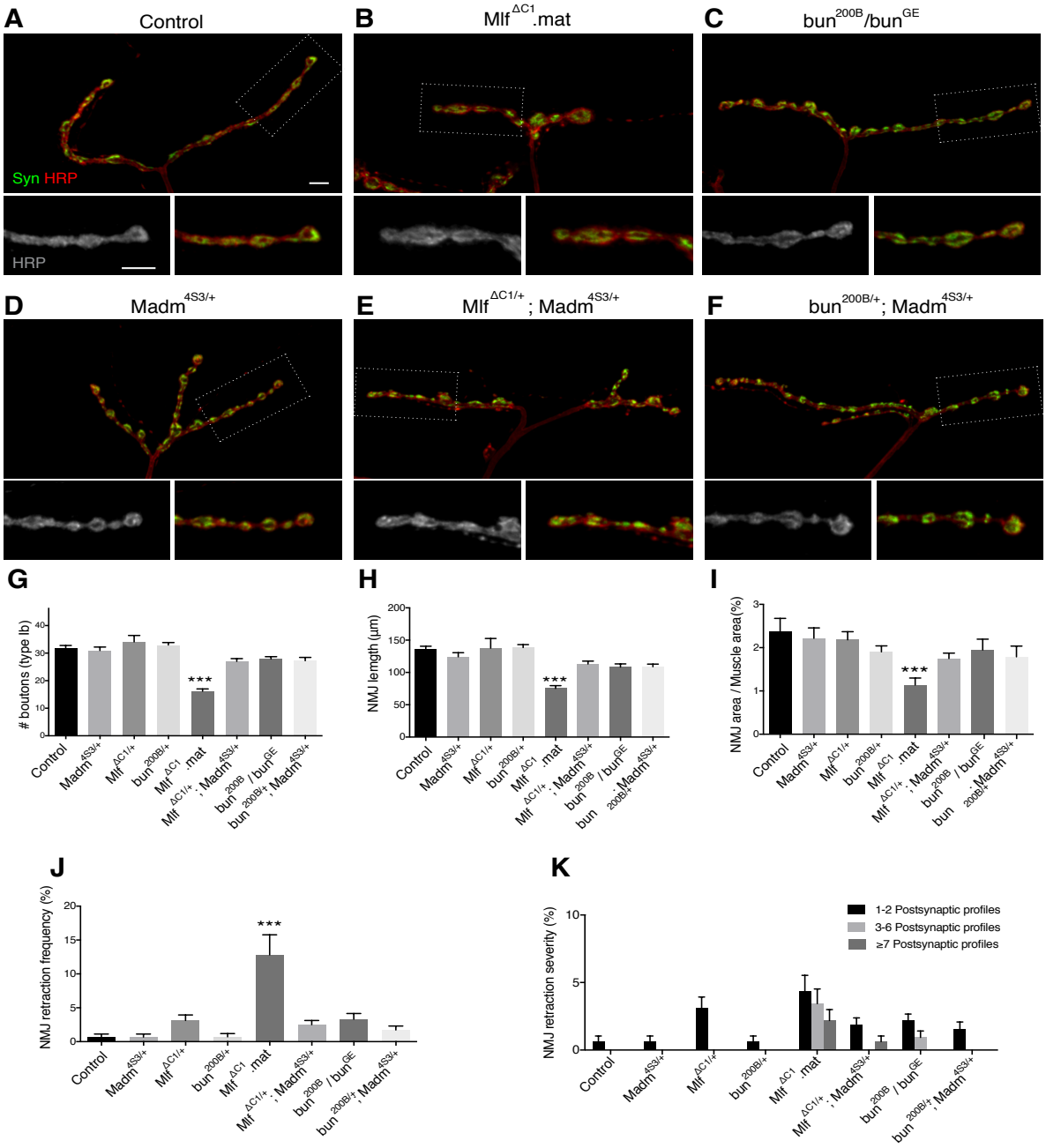

Figure 7: Genetic interaction of Madm with Mlf1 and bun. (A) NMJ of a control animal on muscle 1. (B) *Mlf$^{\Delta C1}$* maternal null animals show reduced NMJ growth. (C) NMJs of *bun$^{200B/GE}$* and (D) heterozygous *Madm$^{4S3/+}$* animals show no significant changes compared to control NMJs. (E-F) NMJs of transheterozygous animals of *Mlf$^{\Delta C1/+}$; Madm$^{4S3/+}$* and *bun$^{200B/+}$; Madm$^{4S3/+}$* do not show any significant changes when compared to controls. (G-I) Quantification of synaptic growth parameters on muscle 1 including number of boutons (G), NMJ length (H) and NMJ area per muscle area (I), One-way ANOVA with Tukey test (n=24-48 NMJs from 6-12 animals). (J) Quantification of synaptic retraction frequencies on muscles 1/9 and 2/10, error bar represents SEM. *Mlf$^{\Delta C1}$* maternal null animals show a significant increase in synaptic instability, whereas *bun$^{200B/GE}$* mutants display no increase. (K) Quantification of synaptic retraction severity. All error bars represent SEM, *, P≤0.05; **, P ≤ 0.01; ***, P ≤ 0.001; ns: not significant; ANOVA and Bonferroni multiple comparison test; n=320 NMJs from 10 animals. Scale bars represent 5µm.

mutants: *wit*^{A12}*/Madm*^{4S3}, *Mad*$^{12/+}$*; Madm*$^{4S3/+}$ and *tkv*^{1}*/Madm*^{4S3}. Homozygous *wit*, *Mad* and *tkv* mutant animals exhibit smaller NMJs with defective release properties (Aberle et al., 2002; Keshishian, 2002; Liu et al., 2014; Marques et al., 2002; Nahm et al., 2013). Transheterozygous mutants of *wit*^{A12}*/Madm*^{4S3}, *Mad*$^{12/+}$*; Madm*$^{4S3/+}$ and *tkv*^{1}*/Madm*^{4S3} didn´t exhibit any significant changes ds the NMJ morphology when compared to controls (Figure 8A). We then tested components of mTOR pathway for potential genetic interactions with Madm. We used the alleles *TSC1*^{f01910}, g*ig*^{109} and *Rheb*^{AV4}. TSC1 and TSC2 are reported to act as negative regulators and Rheb as a positive regulator of NMJ growth (Knox et al., 2007; Natarajan et al., 2013). We analyzed the following transheterozygous combinations: *TSC1*^{f01910}*/ Madm*^{4S3}, g*ig*^{109}*/ Madm*^{4S3} and *Rheb*^{AV4}*/ Madm*^{4S3}. While *TSC1*^{f01910}*/ Madm*^{4S3} didn´t show any changes in the NMJ morphology, *gig*^{109}*/ Madm*^{4S3} and *Rheb*^{Av4}*/ Madm*^{4S3} transheterozygous animals displayed a significant change in the NMJ morphology (Figure 8). Interestingly, gig control animals (*gig*$^{109/+}$) already shows a significant increase in NMJ length (161.7±8.0) and in the number of boutons (37.4±1.2) when compared to wild type NMJs (Figure 8D, I, J, K). Transheterozygous mutant *gig*^{109}*/ Madm*^{4S3} animals showed a significant reduction in number of boutons (25.5±0.8), NMJ length (105.7±3.6) and NMJ area per muscle area (1.4±0.1) (Figure 8G, I, J, K), indicating that Madm interacts with the mTOR pathway. Similarly, transheterozygous *Rheb*^{AV4}*/ Madm*^{4S3} mutants also showed a significant reduction in the number of boutons (20.5±0.7), NMJ length (78.6±2.9) and NMJ area per muscle area (1.1±0.1) when compared to controls (Figure 8H, I, J, K). These data suggest that Madm interacts with mTOR pathway components to promote synapse growth.

To further establish the site of action of Madm within the mTOR pathway, we performed a genetic overexpression analysis by increasing Rheb levels in *Madm*$^{4S3/Df}$ mutant animals. Overexpression of Rheb in neurons induces increased NMJ growth as previously published (Dimitroff et al., 2012; Natarajan et al., 2013) (Figure 9C, E, F, G, H). Interestingly, overexpressing Rheb in *Madm*$^{4S3/Df}$ mutant animals resulted in increased growth of NMJs (number of boutons (50.6±1.8), NMJ length (165.3±5.9) and NMJ area per muscle area (3.1±0.2) while bouton remained partially clustered as observed in *Madm* mutants. Thus, these NMJs exhibit both, the phenotypes due to Rheb over expression and of Madm mutants (Figure 9D, E, F, G, H). This indicates that Madm and Rheb may be acting in two parallel pathways. Within the mTOR pathway, downstream of the TOR complex, multiple

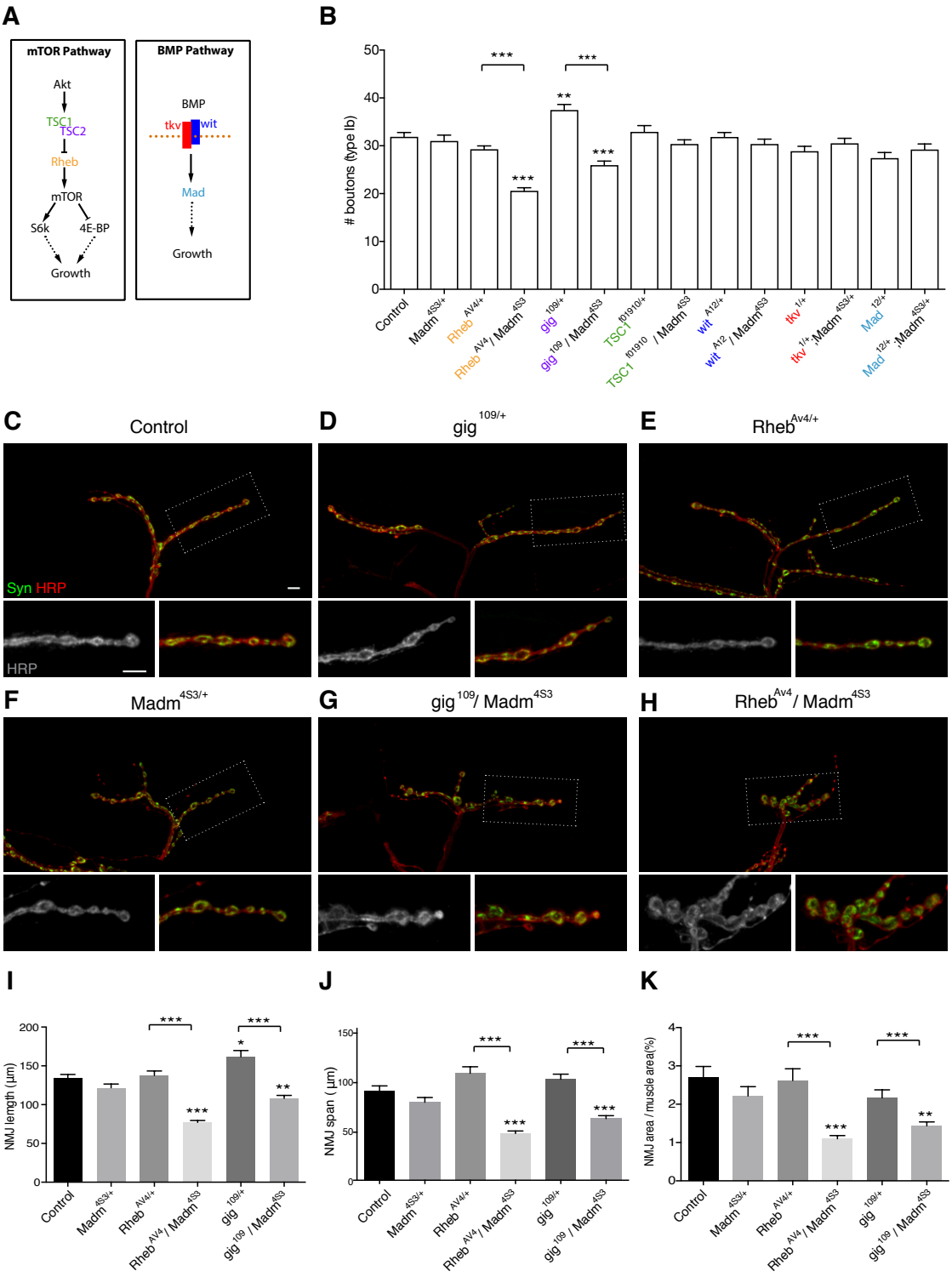

Figure 8: Genetic interaction of Madm. (A) Schematic of the mTOR and BMP pathways with their components used for genetic interaction studies highlighted in colors. (B) Transheterozygous genetic interaction analysis of Madm with components of the mTOR and BMP pathways. (C-K) Analysis of genetic interactions of Madm with gig and Rheb. (C) A NMJ of a control animal on muscle 1. (D) NMJ of a heterozygous *gig$^{109/+}$* animal displaying increased growth. (E) NMJs of heterozygous *Rheb$^{AV4/+}$* and (F) heterozygous *Madm$^{4S3/+}$* animals show no significant changes compared to control NMJs. (G) NMJs of transheterozygous *gig^{109}/Madm^{4S3}* and

Rheb^{AV4}*/Madm*^{4S3} animals show reduced synaptic growth compared to controls. (I-K) Quantification of synaptic growth parameters of NMJs on muscle 1 including number of boutons (I), NMJ length (J) and NMJ area per muscle area (K) with error bars representing SEM, (*, P≤0.05; **, P ≤ 0.01; ***, P ≤ 0.001); One-way ANOVA with Tukey test (n=24-48 NMJs from 6-12 animals).

parallel mechanisms can influence elongation initiation factors together with mTOR to regulate translation. As a consequence of Rheb overexpression, an activated mTOR complex may induce growth through one of these pathways while loss of Madm influenced the alternative arm of the pathway to induce a clustered bouton phenotype. To address this possibility, we analyzed downstream components of the mTOR pathway. We first tested a *4E-BP* (*Thor*^{2}) mutant, which represents a deletion of Thor. Interestingly *Thor* mutant animals are fertile and viable (Bernal, 2004). Third instar larvae of homozygous *Thor*^{2} animals exhibited increased NMJ growth compared to controls (number of boutons (44.5±1.0), NMJ length (174.9±7.4) and NMJ area per muscle area (4.2±0.3) (Figure 10B, H, I, J)), as predicted for a downstream mTOR pathway component. Analysis of *Thor* and *Madm* (*Thor*^{2}*; Madm*$^{4S3/Df}$) double mutants revealed decreased NMJ sizes similar to the phenotype of *Madm* single mutants but with a small increase in size (number of boutons (23.6±0.6), NMJ length (84.3±3.3) and NMJ area per muscle area (1.2±0.1) (Figure 10C, H, I, J)). This suggests that Madm functions downstream of the mTOR complex and also downstream of 4E-BP. In contrast, overexpression of Thor in the presynaptic motoneuron induced a significant decrease in NMJ size (number of boutons (22.2±1.4), NMJ length (94.7±7.6) and NMJ area per muscle area (1.2±0.1)) (Figure 10E, H, I, J) while overexpression of Madm did not change NMJ morphology (number of boutons (31.8±1.0), NMJ length (131.5±6.4) and NMJ area per muscle area (2.5±0.1) (Figure 10D, H, I, J)). Importantly, the reduced growth phenotype observed after Thor overexpression can be rescued by coexpression of Madm (number of boutons (28.1±0.6), NMJ length (120.2±3.2) and NMJ area per muscle area (2.4±0.1) (Figure 10F, H, I, J)). This supports our hypothesis that Madm functions downstream of 4E-BP to regulate synapse growth. Interestingly, we observed a partial rescue of the synaptic instability defects of *Madm* mutants after presynaptic Rheb expression in Madm$^{4S3/Df}$ mutants (15.0±2.2) and in the *Tho*^{2}*; Madm*$^{4S3/Df}$ double mutants (11.7±1.7) (Figure 10K, L, M). This data suggests that induction of ectopic growth can promote stability of the synapse. In other words, if the growth regulating function of Madm is provided by other growth promoting proteins, the synaptic stability defect can be

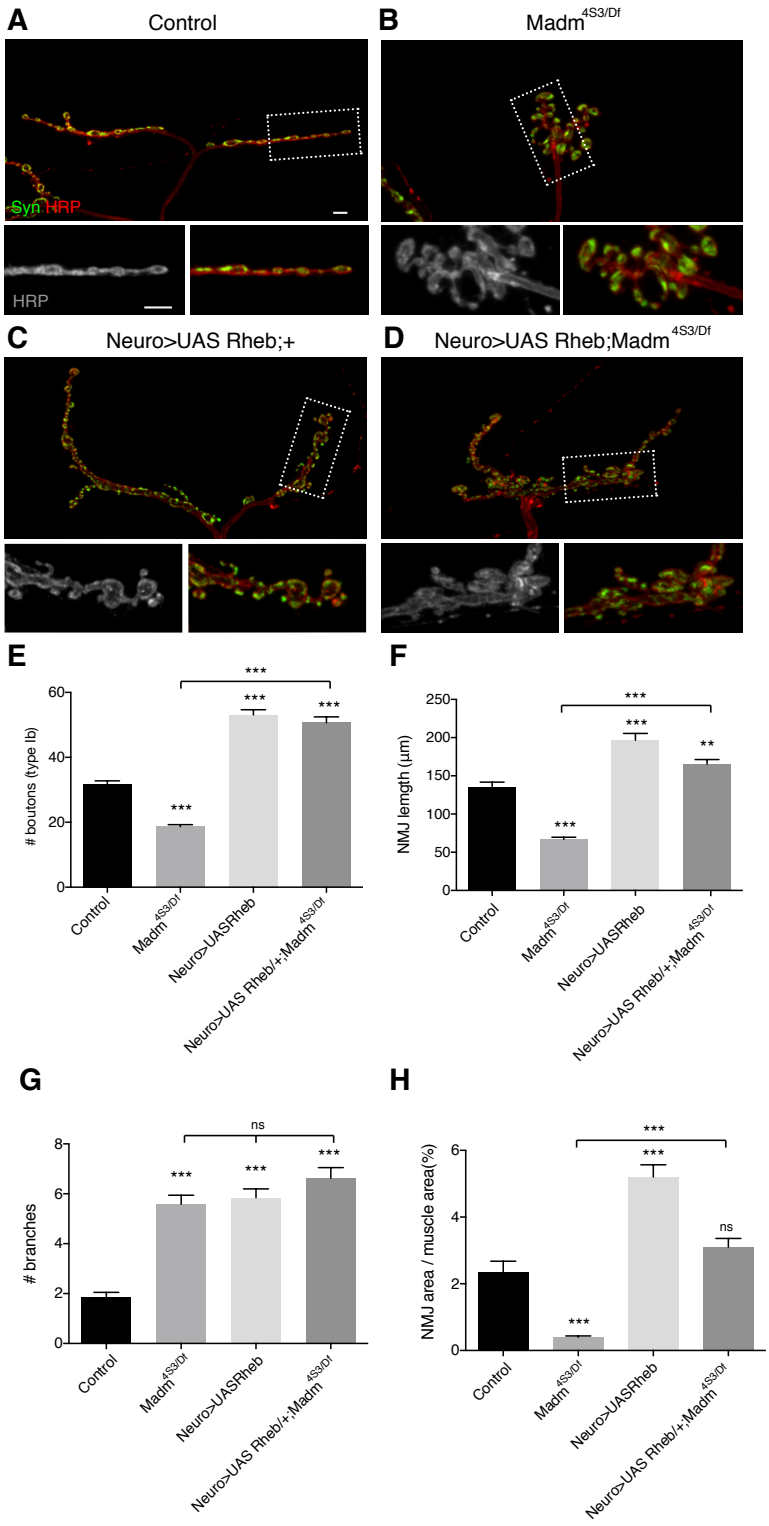

Figure 9: Madm acts downstream and/or in parallel to Rheb in the mTOR pathway.

(A) A well-grown control NMJ on muscle 1 (*elav^{C155}-Gal4/+*). (B) Loss of function of Madm in *Madm$^{4S3/Df}$* mutants led to severe synaptic growth and organization defects. (C)Presynaptic overexpression of Rheb (*elav^{C155}-Gal4; UAS-Rheb/+*) led to increase in synaptic growth. (D) Presynaptic overexpression of Rheb in the *Madm$^{4S3/Df}$* mutants (*elav^{C155}-Gal4; UAS-Rheb/+; Madm$^{4S3/Df}$*) led to increase in synaptic growth along with the organization defect of Madm mutants. (E-H) Quantification of synaptic growth defects on muscle 1 among genotypes, number of boutons (E), NMJ length (F), number of branches (G), and NMJ area per muscle area (H). Error bars

representing SEM; *, P≤0.05; **, P ≤ 0.01; ***, P ≤ 0.001; ns: not significant; ANOVA with Tukey multiple comparison test (n=24-32 NMJs and 6-8 animals).

rescued. Thus, Madm likely controls the balance between synaptic growth and stability. It is important to note that induction of growth by Rheb overexpression or loss of Thor cannot fully restore synaptic instability observed in the absence of Madm indicating that Madm is crucial for some aspects of stability that are independent of growth control. This also suggests that Madm likely acts in parallel to the mTOR pathway converging downstream of 4E-BP onto common factors to regulate synapse development. Together, our data suggests that Madm represents a novel regulator of synaptic growth and maintenance that impinges on the mTOR pathway.

3.3.6 Madm is required for basal synaptic transmission

It has been demonstrated that alterations in synaptic morphology can lead to the changes in synaptic activity (Lee et al., 2016; Wu et al., 2005; Xing et al., 2018; Zhang et al., 2017). Using intracellular electrophysiological recordings, we determined potential requirements of Madm for basal synaptic transmission. Electrophysiological analysis of *Madm* mutant NMJs showed a substantial decrease in evoked excitatory junction currents (EJCs) compared to wild type NMJs (Figure. 11 A-B). We observed a small but not significant increase in quantal size (Figure. 11B). As a result, quantal content (EJC/mEJC), which describes the number of synaptic vesicles released per action potential, was significantly decreased in *Madm* mutants (Figure. 11B). We also observed a significant increase in mEJC frequency compared to controls (Figure. 11A, 8C). As we observed unique pre- and postsynaptic requirements of Madm for morphological parameters we next tested whether Madm is required both pre and postsynaptically to maintain basal synaptic transmission (Figure 4 and Figure 5). Interestingly we could rescue the decrease in EJCs by presynaptic expression of Madm. To our surprise the EJC phenotype was also rescued by postsynaptic expression (Figure. 11A, B). In contrast, the mEJC frequency phenotype could not be significantly rescued by either pre- or postsynaptic expression of Madm (Figure 11C). Based on these results it is likely that presynaptic Madm is required to maintain basal synaptic transmission. It is interesting to speculate that alteration of postsynaptic properties as observed for the mTOR pathway that increase neurotransmitter responses may contribute to the postsynaptic rescue (see below and additional data section).

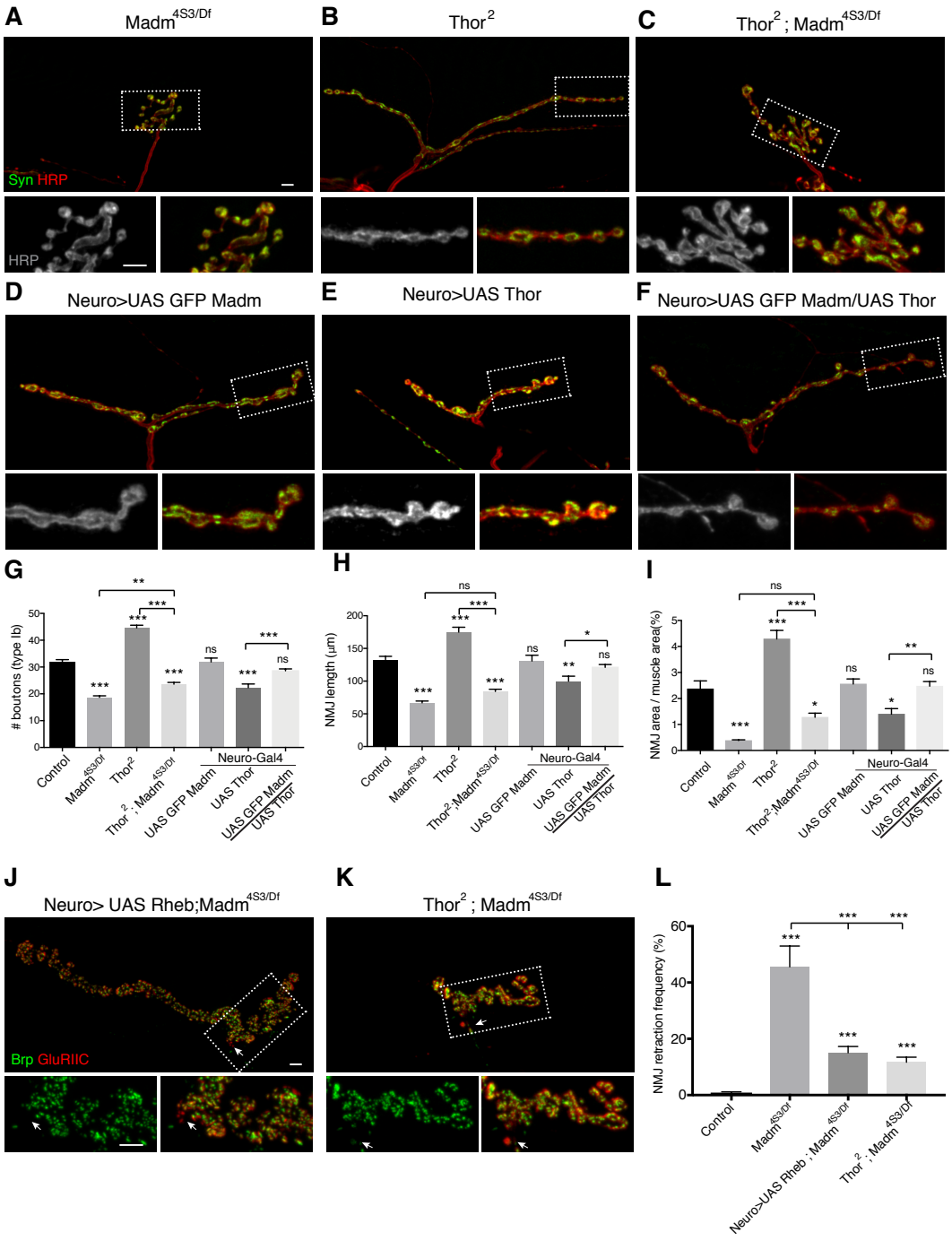

Figure 10: Madm functions downstream of 4E-BP to regulate synapse development. (A) *Madm*$^{4S3/Df}$ mutants display sever NMJ undergrowth (B) *Thor*^{2} mutants display an increase in NMJ growth (C) *Thor*^{2}*; Madm*$^{4S3/Df}$ double mutants show decrease NMJs with *Madm* like morphology. (D) Overexpression of *Madm* in the presynapse (*elav*^{C155}*; UAS-GFPMadm/+*) does not induce any changes in NMJ morphology compared to controls. (E) Overexpression of Thor in the presynapse (*elav*^{C155}*; UAS Thor/+*) reduces synaptic growth when compared to controls. (F) Co-overexpression of Madm and Thor in the presynapse (*elav*^{C155}*; UAS-GFPMadm/UAS Thor*) suppresses the effect of overexpression of just Thor (G-I) Quantification of synaptic growth parameters on muscle 1 including number of boutons (G), NMJ length (H) and NMJ area per muscle area (I),

One-way ANOVA with Tukey test (n=24-48 NMJs from 6-12 animals). (J-K) Induced growth due to the presynaptic overexpression of Rheb or loss of Thor in *Madm* mutants (*elav^{C155}; UAS Rheb/+; Madm$^{4S3/Df}$* and *Thor^{2}; Madm$^{4S3/Df}$* respectively) reduces the frequency of synaptic retractions. (L) Quantification of synaptic retractions frequencies at muscle 1/9 and 2/10. All error bars representing SEM. *, P≤0.05; **, P ≤ 0.01; ***, P ≤ 0.001; ns: not significant; ANOVA and Bonferroni multiple comparison test; n=320 NMJs; 10 animals. Scale bars represent 5µm.

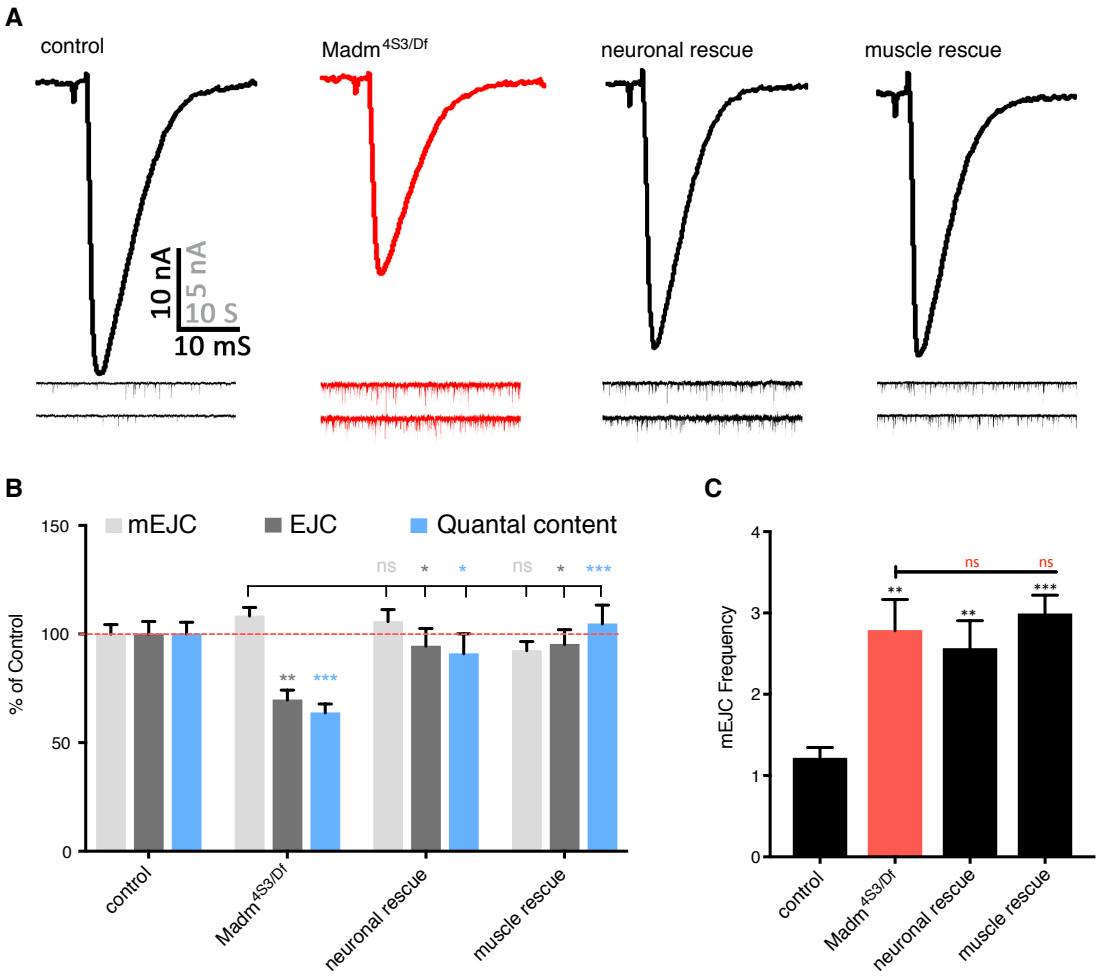

Figure 11: Madm is required for basal synaptic transmission. (A) Representative EJC and mEJC recording traces of control, *Madm$^{4S3/Df}$*, presynaptic rescue and postsynaptic rescue animals. (B) Quantification of mEJC, EJC, and QC for the indicated genotypes. (C) Quantification of mEJC frequency for the indicated genotypes, n = 12, 16, 11, 21. All error bars represent SEM, *, P≤0.05; **, P ≤ 0.01; ***, P ≤ 0.001; ns: not significant; ANOVA and Tukey multiple comparison test.

3.3.7 Madm is sufficient to induce retrograde synaptic potentiation

Our genetic interaction data indicates that Madm interacts with mTOR components (Figure. 8). In addition, we observed a postsynaptic rescue of the EJC phenotype. Therefore, we next tested whether Madm, like TOR, might be able to induce a postsynaptic potentiation of neurotransmitter release (Goel et al., 2017; Penney et al., 2012). We overexpressed Madm or TOR individually in wild type animals using a muscle driver line. Consistent with prior data by Penney et al. (2012) we observed increased neurotransmitter release in animals overexpressing TOR postsynaptically (Figure. 12J). Overexpression of TOR resulted in a significant increase in EJCs amplitude but did not alter mEJC amplitudes (Figure 12 G, I-J). Interestingly, postsynaptic overexpression of Madm resulted in a similar enhancement in synaptic strength. mEJC amplitude remains unchanged but the EJC amplitude was significantly increased compared to controls (Figure. 12 G, H, J). In contrast to Madm overexpression TOR overexpression was accompanied by a significant increase in mEJC frequency (Data not shown). These data indicate that Madm is required presynaptically for the maintenance of basal synaptic transmission, while postsynaptic overexpression of Madm is sufficient to induce retrograde synaptic potentiation at wild type NMJs. This retrograde potentiation thus restores EJC amplitudes in Madm mutants through additive mechanisms (postsynaptic potentiation – Madm release defect = control like EJC amplitude).

Penny and co-workers (2012) also demonstrated that TOR is essential for GluRIIA induced synaptic homeostasis. We therefore asked if Madm also participates in GluRIIA induced synaptic potentiation. As previously published in GluRIIA mutant animals a decreased mEJC amplitude is compensated through increased presynaptic release as reflected by a normal EJC amplitude. As a consequence, quantal content, and thus synaptic strength is increased in these animals (Figure 12C). In contrast to TOR, removal of one copy of *Madm* in the *GluRIIA* null mutants did not reduce quantal content. Similarly, postsynaptic knockdown of *Madm* in *GluRIIA* null animals or the complete absence of *Madm* in *Madm*; *GluRIIA* double mutant animals did not affect the increase in quantal content induced by the loss of GluRIIA (Figure 12C). The EJC amplitude and the quantal content of the double mutant was decreased when compared to control animals, but when compared to *Madm* mutants, the double mutants still showed a significant increase in quantal content. This suggests that the loss of Madm decrease synaptic transmission but that the induced synaptic potentiation due to the absence of GluRIIA is unaffected by the absence of Madm. Our data suggests indicate that

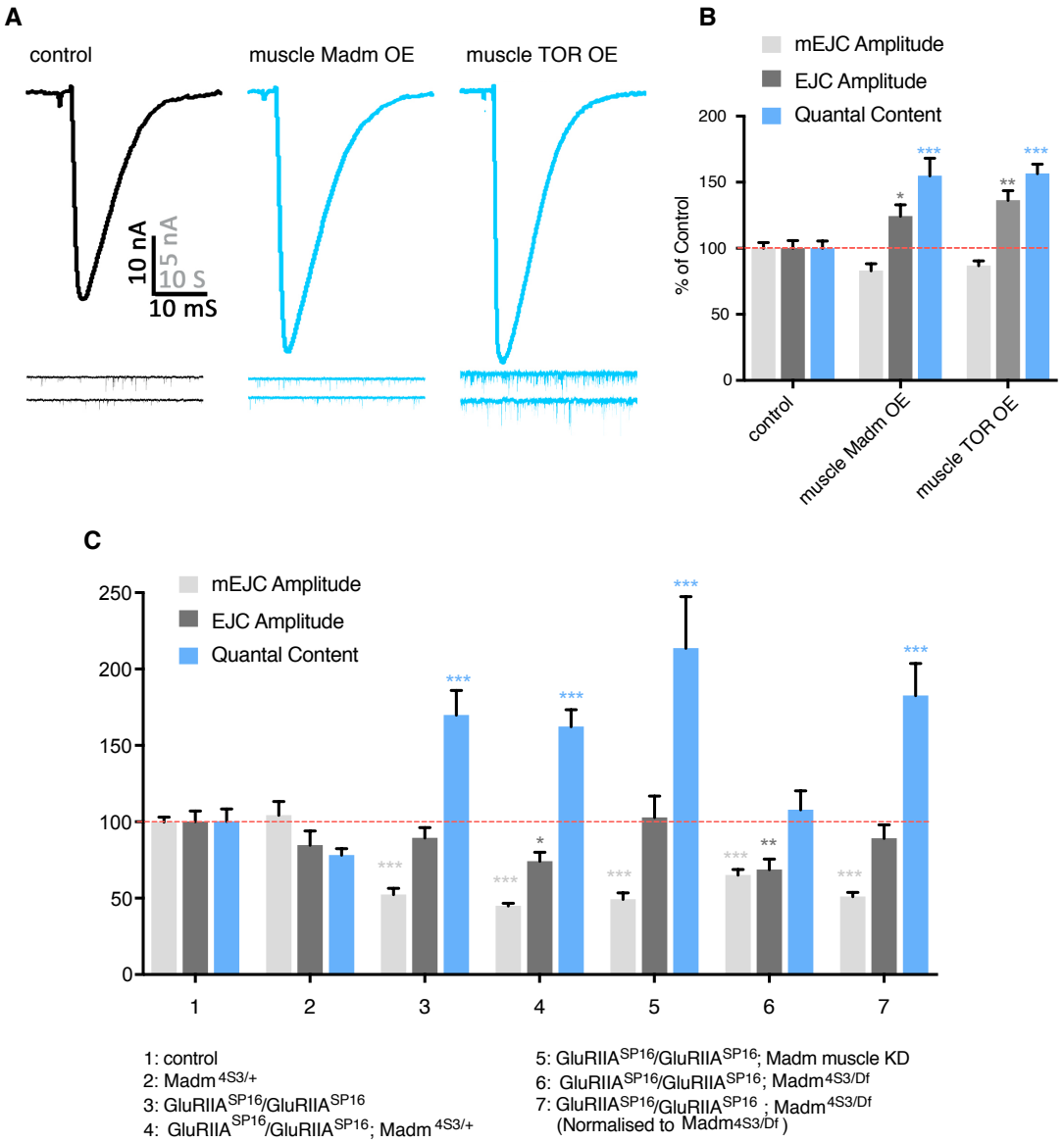

Figure 12: Madm can indice retrograde synaptic potentiation. (A) Representative EJC and mEJC recording traces of control, postsynaptic overexpression of Madm and postsynaptic overexpression of TOR (B) Quantification of mEJC, EJC, and QC for the indicated genotypes demonstrates that Madm can induce retrograde synaptic potentiation. n = 12, 16, 11, 21 (C) Quantification of mEJC, EJC, and QC of control, heterozygous *Madm*$^{4S3/+}$, *GluRIIA* null (*GluRIIA*$^{SP16/Sp16}$), loss of once copy of Madm in *GluRIIA* null (*GluRIIA*$^{SP16/Sp16}$*; Madm*$^{4S3/+}$), postsynaptic knockdown of Madm in *GluRIIA* null (*GluRIIA*$^{SP16/Sp16::VD27346}$*; BG57-Gal4/+*), double mutants of *GluRIIA* and *Madm* (*GluRIIA*$^{SP16/Sp16}$*; Madm*$^{4S3/Df}$) normalized to control and double mutants of *GluRIIA* and *Madm* (*GluRIIA*$^{SP16/Sp16}$*; Madm*$^{4S3/Df}$) normalized to *Madm*$^{4S3/Df}$, demonstrating that Madm does not impair the GluRIIA induced synaptic potentiation. n = 12, 16, 11, 21. All error bars represent SEM, *, P≤0.05; **, P ≤ 0.01; ***, P ≤ 0.001; ns: not significant; ANOVA and Tukey multiple comparison test

Madm-dependent control of synaptic morphology is essential for synaptic function. In addition, Madm has the potential to induce retrograde synaptic potentiation through a thus far unknown mechanism possibly in parallel or together with postsynaptic TOR.

3.4 Discussion

Madm has been previously identified as a ubiquitously expressed protein required to regulate body and organ size in Drosophila. In an RNAi based screen, we identified Madm as a novel regulator of synapse development, maintenance and function. Madm is expressed in the nervous system and is efficiently localized to the pre- and postsynaptic terminal. Loss of Madm leads to severe synaptic growth defect with severe synaptic instability. We observed similar phenotype among different mutant alleles with slightly variable severity. Point mutant of *Madm* (*Madm*$^{4S3/Df}$) showed the strongest effect, followed by the null allele (*Madm*$^{2D2/Df}$) and the hypomorphic allele (*Madm*$^{EP/Df}$). As the point mutant protein is expressed at almost wild type levels, a failure to interacting with its partner proteins and this defective interaction potentially contributes to the phenotypic strength of this allele. In contrast, in null mutant animals we observed no proteins. Importantly, we could rescue all synaptic defects of *Madm* mutants by pre- or postsynaptic expression of Madm.

3.4.1 Madm coordinates synapse growth and stability

Changes in the morphology of synaptic structures are observed during the development of nervous system, in response to experience-based synaptic remodeling and in many neurological disorders. The size, shape, number and organization of synapses play an important role and are tightly regulated. Regulation of cytoskeletal dynamics and protein synthesis are essential to induce changes during LTP induced synaptic remodeling (Bosch et al., 2014; Chen et al., 2007; Wosiski-Kuhn and Stranahan, 2012). This process includes the formation of new synapses and the elimination of existing synapses. To understand synaptic remodeling, it is essential to unravel the mechanisms that mediate controlled synapse formation and elimination. A number of studies have reported on the mechanism of synapse formation (growth) and synapse elimination separately. In contrast, potential interplay between synaptic growth and stability has not been addressed likely due to difficulties in experimental approaches. In this study, we identifed Madm as a potential molecule linking the regulation of synaptic growth and stability. Loss of Madm leads to instable, under grown and misorganized synapses. Using tissue specific rescue experiments we could demonstrate that presynaptic Madm regulates the growth and stability of the presynaptic terminal, while postsynaptic Madm contributes to the regulation of synaptic terminal organization. A number of molecules and pathways have been previously reported to be required both pre- and

postsynaptically to coordinate synapse development. For instance, molecules like alpha- and beta-spectrin are essential pre- and postsynapse with unique requirements on both sides of the synapse (Pielage et al., 2005, 2006). Similarly, BDNF and mTOR signaling were found to regulate synapse development pre- and postsynaptically and partially transsynaptically in a retrograde manner in both vertebrates and invertebrates (Berke et al., 2013b; Hoeffer and Klann, 2010; Kowianski et al., 2018; Tao and Poo, 2001). Here, we demonstrate that Madm is essential both pre- and postsynaptically for normal synapse development. We also show that Madm has a temporal regulatory function during synapse development, as Madm controls NMJ growth early during development and later contributes to synapse maintenance. In the absence of Madm NMJs initially grow into well-organized structures at the second instar larval stage, but then it fails to grow into the stereotypic pearls-on-a-string structure and fails to efficiently maintain synapses at the end of larval development.

Using genetic interaction assays, we then demonstrated a functional relationship of Madm with the mTOR pathway. The mTOR pathway has been extensively studied for its regulation of NMJ growth and development. Similar to other growth regulating factors, activated TOR is capable to induce synaptic growth (Kelleher et al., 2004; Knox et al., 2007; Kumar et al., 2005; Natarajan et al., 2013) synaptic function (Lenz and Avruch, 2005) and active zone organization in the presynaptic motoneuron (Cheng et al., 2011). mTOR also plays an important role in the postsynaptic compartment for the regulation of synapse development and receptor and ion channel organization and function (Niere and Raab-Graham, 2017; Sigrist et al., 2000; Sigrist et al., 2002). Here, we demonstrated that Madm acts in parallel to the mTOR pathway downstream of 4E-BP (Thor) to regulate the growth of the NMJ. Our genetic interaction data of Madm with TSC2, Rheb and Thor indicates that Madm acts in tight association with the mTOR pathway. However, the NMJ morphology phenotype of Madm mutants does not resemble the phenotype of any of the mTOR pathway mutants. The synergistic effects on NMJ growth in the transheterozygous combinations and the inhibition of Thor-dependent overgrowth by ectopic expression of Madm indicates that Madm impinges on the mTOR pathway to regulate NMJ growth. In contrast, during intestinal stem cell proliferation Nie et al. (2015) demonstrated that Madm along with bunched A, acts downstream of the mTOR complex by regulating phosphorylation of 4E-BP. In support of our working model, prior biochemical assays demonstrated a physical association of Madm with the translation initiation factor eIF-3p40, a vertebrate homolog of eIF3h (Gluderer et al., 2010), indicating that Madm acts downstream of 4E-BP. Our genetic interaction data of

Madm with Rheb and Thor also supported parallel requirements of Madm and the mTOR pathway. Overexpression of Rheb in *Madm* mutants resulted in a combined phenotype with features of loss-of-function mutations of *Madm* and of the overexpression phenotype of Rheb. Similarly, *Thor* and *Madm* double mutants displayed a *Madm* mutant morphology but showed a significant increase in the size of the NMJ compared to *Madm* mutants. Interestingly, the growth promoting features of Rheb overexpression and loss of Thor in *Madm* mutants likely contributed to the partial suppression of synaptic instability. Our data is consistent with Madm coupling the control of NMJ growth and stability. Induction of growth through alternative pathways is sufficient to supplement the growth promoting features of Madm while control of the synaptic boutons organization requires the presence of Madm.

3.4.2 Madm plays a dual role in the regulation of synaptic transmission

Severe synaptic morphology and stability defects are often accompanied by defects in synaptic efficacy (Ball et al., 2010; Eaton and Davis, 2005; Stephan et al., 2015). We demonstrated that loss of *Madm* resulted in decreased evoked synaptic transmission, which can be rescued by presynaptic expression of Madm. Interestingly, postsynaptic expression of *Madm* also restored evoked synaptic transmission. However, postsynaptic overexpression of *Madm* in control animals already resulted in a significant increase in EJC amplitude. This indicates that postsynaptic *Madm* can induce a postsynaptic potentiation that potentially masked presynaptic defects in the rescue experiments. Interestingly, such a postsynaptic potentiation mechanism has thus far only been reported as a result of the postsynaptic overexpression of TOR (Penney et al., 2012), again linking Madm to TOR signaling. However, it has also been reported that postsynaptic TOR is essential for GluRIIA-mutation dependent postsynaptic homeostatic plasticity (PHP) (Goel et al., 2017; Penney et al., 2012; Penney et al., 2016). Based on our data we can rule out a significant role of Madm in PHP as presynaptic release can still be enhanced in *GluRIIA* and *Madm* double mutant animals. Alternatively, Madm may participate in acute PHP that can be induce via pharmacological block of postsynaptic glutamate receptors. Here synaptic homeostasis is induced through CaMKII mediated mechanism (Goel et al., 2017; Hell, 2014). Computational protein sequence analysis of NRBP1, the vertebrate homolog of Madm showed that NRBP1 has potential phosphorylation sites for Casein Kinase2 (CK2) and PKC (Hooper et al., 2000). Indeed, we identified 12 potential CK2 phosphorylation motifs (S/T XX E/D) in the Drosophila Madm open reading frame (Figure 19). In hippocampal neuronal cultures, it has been shown that CK2 and

CaMKII regulate the phosphorylation of GluA1 and GluA2 and CK2 regulates the surface expression of GluA1 (Lussier et al., 2014). For mammalian cell cultures, it has been reported that CaMKII acts as an adaptor molecule to recruit CK2 to induce phosphorylation and activity dependent trafficking of NMDA receptor subunits (Hell, 2014). Postsynaptic homeostatic plasticity (synaptic scaling) has been reported to be dependent on the phosphorylation-mediated regulation of activity of the existing calcium permeable AMPA receptors at the postsynapse (Fu et al., 2011; Gilbert et al., 2016; Sanderson et al., 2018). Interestingly, immunostainings for the GluRIIA subunit in *Madm* mutants showed an increase in postsynaptic GluRIIA receptor abundance (Figure 18). Thus, it is interesting to speculate that Madm may be part of a CaMKII-CK2 dependent regulation of postsynaptic potentiation. Consistent with an involvement of CK2 in the regulation of synaptic plasticity a role of CK2 in synapse stability has recently been reported (Bulat et al., 2014). Future experiments will be required to assess and establish a role of Madm in the regulation of acute PHP.

3.5 Material and Methods

3.5.1 Fly stocks

Flies were raised at room temperature on standard fly food. All genetic crosses were performed at 25°C unless otherwise mentioned. The following fly strains were used: *w*^{1118} (as wild-type), *elav*^{C155}*-Gal4, Ok371-Gal4, UAS Madm* (lab generated), *Madm Df(3R)Exel7283*, *Madm*^{EP3137}, *Madm*^{2D2}, *Madm*^{4S3}, *UAS-GFP Madm* (Gluderer et al., 2010), *bun*^{200B}, *bun*^{GE12327} (Gluderer et al., 2008), and *Mlf*$^{\Delta C1}$ (Martin-Lanneree et al., 2006), *Rheb*^{AV4}, Rheb^{4L1},*TSC1*^{f01910}, *Gig*^{109}, *wit*^{A12}, *wit*^{B11}, *tkv*^{1}, *UAS Rheb, Thor*^{2}, *UAS Thor, GluRIIB-Gal4, GluRIIA*^{sp16}, *UAS TOR, S6k*$^{l-1}$, (Bloomington *Drosophila* Stock Center). RNAi line was obtained from the VDRC Vienna *Drosophila* RNAi Center. Madm RNAi: transformant ID 101758 with 0 off targets.

3.5.2 Generation of Madm transgenes and antibody

The full length *Madm* ORF was amplified from cDNA LD28657 obtained from the *Drosophila* Genomic Research Center (Indiana, USA) using the following primers: 5'-CACCATGTCAAATAGCCAAGCGAATG-3' and 5'-TCAATTGCTCGTCGTGCCC-3'. The ORF was cloned into pENTR using TOPO cloning protocol (Invitrogen) and shuffled into the pUASattB-10xUAS destination vector with and without N-terminal EGFP tag (Enneking et al., 2013). Constructs were verified via sequencing (FMI sequencing facility) and subsequently injected into attP40 genomic landing site (BestGene Inc, California, USA).

N-terminal 6xHis-tagged full-length Madm constructs were generated using the Gateway system (pDEST17 vector) (Invitrogen). The protein was expressed and further purification was performed under denaturing conditions using Spin-Trap Columns (GE Healthcare). Polyclonal rabbit anti-Madm antibodies were generated and purified by David's Biotechnologie (Regensburg, Germany). Pre-sera of rabbits were checked before immunization.

3.5.3 Western blot

Larval brains were dissected in HL3 Buffer containing protease inhibitor (Roche), lysed in NP40-based lysis buffer, transferred into 2X sample buffer (Invitrogen) and boiled for 10 min at 95°C. Samples were run on 8-12 % NuPage gels (Invitrogen). Subsequently, protein was transferred to Invitrolon PVDF membranes (Invitrogen) following standard procedures. Membrane was blocked in 5% milk powder solution and incubated with primary rabbit anti-

Madm (1:500; generated by David's Biotechnologie (Regensburg, Germany) & ourselves) or mouse anti-Tubulin (1:1,000; Developmental Studies Hybridoma Bank) antibody at 4°C overnight in the blocking solution. Secondary HRP-conjugated anti-rabbit or anti-mouse antibody (Jackson Immunoresearch) was used at 1:10,000 for 2 h at room temperature. Protein was detected by chemiluminescence using ECL substrate (SuperSignal West Pico Kit, Thermo Scientific) and the fluorescence signal was developed on an x-ray film (Fujifilm).

3.5.4 Immunohistochemistry

Wandering third instar larvae were dissected in cold standard dissection saline. Preparations were subsequently fixed for 5 min with Bouin's fixative (Sigma-Aldrich) and washed in PBST. Larval preparations were incubated with primary antibodies overnight at 4°C and with secondary antibodies for 2h at room temperature with sufficient washes after every step. The following antibody dilutions were used for anti-Brp (nc82) 1:250, anti-Synapsin (3c11) 1:50, rabbit anti-Dlg 1:10,000, rabbit anti-dGluRIIC 1:3,000, anti-GluRIIA (8B4D2) 1:50 and rabbit anti-GFP 1:2,000 (Invitrogen). Alexa fluor – conjugated secondary antibodies were used at 1:1,000 dilution (Invitrogen). Alexa fluor- 647 and Cy3 conjugated HRP were used at 1:500 and 1:1,000 dilutions respectively (Jackson immunoresearch laboratories). Images were acquired at LSM700 (Ziess) confocal microscope with 40X/1.3 NA and 63X/1.4 NA oil immersion objectives. Images for quantifications were acquired using same settings. Imaris (Bitplane), Fiji (ImageJ) and Photoshop (Adobe) were used for image processing and analysis.

3.5.5 Quantification of phenotypes

For the quantification of synaptic stability, postsynaptic foot-prints (representing the retraction) of NMJs were analyzed in the animals stained with presynaptic Brp and postsynaptic GluRIIC. NMJ with a one or more boutons retracted is considered as a retracted NMJ. The severity of retracted NMJs were classified based on the number of destabilized boutons as follows: 1-2 synaptic boutons, 3-6 synaptic boutons, ≥7 synaptic boutons or total elimination, scored 1, 2 and 3 respectively. Quantifications were performed on muscle 1/9 and 2/10 of segments A3, A4, A5 and A6. A minimum of 10 animals was used for each genotype.

Morphology quantifications were performed on the larval NMJs stained with presynaptic Syn, HRP and postsynaptic Dlg. NMJs were imaged using the LIC macroLib

Zen2012 (Life Imaging Center, Freiburg, Germany) at a Zeiss LSM700 confocal microscope. Muscle dimensions and different NMJ parameters were measured using a custom-written Fiji macro and MATLAB. Quantifications were performed on muscle 1 of segments A3 and A4. A minimum of 6 animals was used for each genotype.

3.5.6 Intensity Quantifications

We performed the immunostaining using specific antibodies and acquired images at LSM700 (Ziess) confocal microscope with 40X/1.3 NA and 63X/1.4 NA oil immersion objectives. Intensity measurements were performed using Fiji. All genotypes were treated alike and the images were acquired with the control acquisition settings and the results were normalized to the control.

3.5.7 Electrophysiology recordings

Two electrode voltage clamp recordings were performed on third instar wandering larvae on muscle 6 of A2 and A3 abdominal segments as described previously (Merino et.al 2009). Larval preparations were made in Ca^{2+} free HL3 (70mM NaCl, 5mM KCl, 10mM MgCl2, 10mM NaHCO3, 115mM sucrose, 5mM trehalose, 5mM HEPES) which was replaced by HL3 containing 0.45mM Ca^{2+} for current recordings. Intracellular electrodes with 15-20 MΩ resistance filled with 3M KCl were used for recordings. For current recordings muscles were clamped at -70mV for both mEJC and EJC recordings. mEJCs were collected for 60S and for EJCs segmental nerves were stimulated with suprathreshold pulses delivered by isolated pulse Stimulator (A-M systems) for at least 30 Aps. Recordings with input muscle resistance of ≥3MΩ and holding current of ≤5nA were considered for quantifications. All recordings were amplified and acquired with the help of AxoClamp 900A (Molecular Devices) and digitized by Digidata 1550b (Molecular Devices).

All recordings were analyzed with the help of Clampfit 10.7 (Molecular devices). mEJCs recorded for 60 seconds were averaged for each muscle cell. A minimum of 30 APs was recorded and averaged for each muscle cell. Quantal content was quantified by dividing average EJC amplitude with average mEJC amplitude.

3.5.8 Statistical analysis

Statistical analyses were performed using Graphpad prism 7. One-way Anova was performed to compare the phenotypes between different genotypes. Significance levels were defined as following: *** $p \leq 0.001$, ** $p \leq 0.01$, * $p \leq 0.05$ and n.s. (not significant) $p > 0.05$.

3.6 References

Aberle, H., Haghighi, A.P., Fetter, R.D., McCabe, B.D., Magalhaes, T.R., and Goodman, C.S. (2002). wishful thinking encodes a BMP type II receptor that regulates synaptic growth in Drosophila. Neuron *33*, 545-558.

Ball, R.W., Warren-Paquin, M., Tsurudome, K., Liao, E.H., Elazzouzi, F., Cavanagh, C., An, B.S., Wang, T.T., White, J.H., and Haghighi, A.P. (2010). Retrograde BMP signaling controls synaptic growth at the NMJ by regulating trio expression in motor neurons. Neuron *66*, 536-549.

Banko, J.L., Hou, L., Poulin, F., Sonenberg, N., and Klann, E. (2006). Regulation of eukaryotic initiation factor 4E by converging signaling pathways during metabotropic glutamate receptor-dependent long-term depression. The Journal of neuroscience : the official journal of the Society for Neuroscience *26*, 2167-2173.

Banko, J.L., Poulin, F., Hou, L., DeMaria, C.T., Sonenberg, N., and Klann, E. (2005). The translation repressor 4E-BP2 is critical for eIF4F complex formation, synaptic plasticity, and memory in the hippocampus. The Journal of neuroscience : the official journal of the Society for Neuroscience *25*, 9581-9590.

Bateman, J.M., and McNeill, H. (2004). Temporal control of differentiation by the insulin receptor/tor pathway in Drosophila. Cell *119*, 87-96.

Berke, B., Wittnam, J., McNeill, E., Van Vactor, D.L., and Keshishian, H. (2013). Retrograde BMP signaling at the synapse: a permissive signal for synapse maturation and activity-dependent plasticity. The Journal of neuroscience : the official journal of the Society for Neuroscience *33*, 17937-17950.

Bernal, A., Robert Schoenfeld, Kurt Kleinhesselink, Deborah A. Kimbrell (2004). Loss of Thor, the single 4E-BP gene of Drosophila, does not result in lethality. In Research Notes (http://www.ou.edu/journals/dis/DIS87/index.html: Section of Molecular and Cellular Biology, University of California, 1 Shields Avenue, Davis, California, 95616.), pp. Pages 81-84.

Bosch, M., Castro, J., Saneyoshi, T., Matsuno, H., Sur, M., and Hayashi, Y. (2014). Structural and Molecular Remodeling of Dendritic Spine Substructures during Long-Term Potentiation. Neuron *82*, 444-459.

Bulat, V., Rast, M., and Pielage, J. (2014). Presynaptic CK2 promotes synapse organization and stability by targeting Ankyrin2. The Journal of cell biology *204*, 77-94.

Charron, F., and Tessier-Lavigne, M. (2005). Novel brain wiring functions for classical morphogens: a role as graded positional cues in axon guidance. Development *132*, 2251-2262.

Chen, L.Y., Rex, C.S., Casale, M.S., Gall, C.M., and Lynch, G. (2007). Changes in synaptic morphology accompany actin signaling during LTP. Journal of Neuroscience *27*, 5363-5372.

Cheng, L., Locke, C., and Davis, G.W. (2011). S6 kinase localizes to the presynaptic active zone and functions with PDK1 to control synapse development. The Journal of cell biology *194*, 921-935.

Costa-Mattioli, M., Sossin, W.S., Klann, E., and Sonenberg, N. (2009). Translational Control of Long-Lasting Synaptic Plasticity and Memory. Neuron *61*, 10-26.

Dimitroff, B., Howe, K., Watson, A., Campion, B., Lee, H.G., Zhao, N., O'Connor, M.B., Neufeld, T.P., and Selleck, S.B. (2012). Diet and energy-sensing inputs affect TorC1-mediated axon misrouting but not TorC2-directed synapse growth in a Drosophila model of tuberous sclerosis. PloS one *7*, e30722.

Easley, C.A.t., Ben-Yehudah, A., Redinger, C.J., Oliver, S.L., Varum, S.T., Eisinger, V.M., Carlisle, D.L., Donovan, P.J., and Schatten, G.P. (2010). mTOR-mediated activation of p70 S6K induces differentiation of pluripotent human embryonic stem cells. Cellular reprogramming *12*, 263-273.

Eaton, B.A., and Davis, G.W. (2005). LIM Kinase1 controls synaptic stability downstream of the type II BMP receptor. Neuron *47*, 695-708.

Eaton, B.A., Fetter, R.D., and Davis, G.W. (2002). Dynactin is necessary for synapse stabilization. Neuron *34*, 729-741.

Enneking, E.M., Kudumala, S.R., Moreno, E., Stephan, R., Boerner, J., Godenschwege, T.A., and Pielage, J. (2013). Transsynaptic coordination of synaptic growth, function, and stability by the L1-type CAM Neuroglian. PLoS biology *11*, e1001537.

Fishwick, K.J., Li, R.A., Halley, P., Deng, P., and Storey, K.G. (2010). Initiation of neuronal differentiation requires PI3-kinase/TOR signalling in the vertebrate neural tube. Developmental biology *338*, 215-225.

Fu, A.K.Y., Hung, K.W., Fu, W.Y., Shen, C., Chen, Y., Xia, J., Lai, K.O., and Ip, N.Y. (2011). APC(Cdh1) mediates EphA4-dependent downregulation of AMPA receptors in homeostatic plasticity. Nature neuroscience *14*, 181-U263.

Garza-Lombo, C., and Gonsebatt, M.E. (2016). Mammalian Target of Rapamycin: Its Role in Early Neural Development and in Adult and Aged Brain Function. Frontiers in cellular neuroscience *10*, 157.

Gilbert, J., Shu, S., Yang, X., Lu, Y.M., Zhu, L.Q., and Man, H.Y. (2016). beta-Amyloid triggers aberrant over-scaling of homeostatic synaptic plasticity. Acta Neuropathol Com *4*.

Gluderer, S., Brunner, E., Germann, M., Jovaisaite, V., Li, C., Rentsch, C.A., Hafen, E., and Stocker, H. (2010). Madm (Mlf1 adapter molecule) cooperates with Bunched A to promote growth in Drosophila. Journal of biology *9*, 9.

Gluderer, S., Oldham, S., Rintelen, F., Sulzer, A., Schutt, C., Wu, X., Raftery, L.A., Hafen, E., and Stocker, H. (2008). Bunched, the Drosophila homolog of the mammalian tumor suppressor TSC-22, promotes cellular growth. BMC developmental biology *8*, 10.

Goda, Y., and Davis, G.W. (2003). Mechanisms of synapse assembly and disassembly. Neuron *40*, 243-264.

Goel, P., Li, X., and Dickman, D. (2017). Disparate Postsynaptic Induction Mechanisms Ultimately Converge to Drive the Retrograde Enhancement of Presynaptic Efficacy. Cell reports *21*, 2339-2347.

Goold, C.P., and Davis, G.W. (2007). The BMP ligand Gbb gates the expression of synaptic homeostasis independent of synaptic growth control. Neuron *56*, 109-123.

Hell, J.W. (2014). CaMKII: claiming center stage in postsynaptic function and organization. Neuron *81*, 249-265.

Henry, F.E., McCartney, A.J., Neely, R., Perez, A.S., Carruthers, C.J., Stuenkel, E.L., Inoki, K., and Sutton, M.A. (2012). Retrograde changes in presynaptic function driven by dendritic mTORC1. The Journal of neuroscience : the official journal of the Society for Neuroscience *32*, 17128-17142.

Heo, K., Nahm, M., Lee, M.J., Kim, Y.E., Ki, C.S., Kim, S.H., and Lee, S. (2017). The Rap activator Gef26 regulates synaptic growth and neuronal survival via inhibition of BMP signaling. Molecular brain *10*, 62.

Hoeffer, C.A., and Klann, E. (2010). mTOR signaling: At the crossroads of plasticity, memory and disease. Trends in neurosciences *33*, 67-75.

Hooper, J.D., Baker, E., Ogbourne, S.M., Sutherland, G.R., and Antalis, T.M. (2000). Cloning of the cDNA and localization of the gene encoding human NRBP, a ubiquitously expressed, multidomain putative adapter protein. Genomics *66*, 113-118.

Kasthuri, N., and Lichtman, J.W. (2003). The role of neuronal identity in synaptic competition. Nature *424*, 426-430.

Kelleher, R.J., 3rd, Govindarajan, A., and Tonegawa, S. (2004). Translational regulatory mechanisms in persistent forms of synaptic plasticity. Neuron *44*, 59-73.

Keller-Peck, C.R., Walsh, M.K., Gan, W.B., Feng, G., Sanes, J.R., and Lichtman, J.W. (2001). Asynchronous synapse elimination in neonatal motor units: studies using GFP transgenic mice. Neuron *31*, 381-394.

Keshishian, H. (2002). Is synaptic homeostasis just wishful thinking? Neuron *33*, 491-492.

Knox, S., Ge, H., Dimitroff, B.D., Ren, Y., Howe, K.A., Arsham, A.M., Easterday, M.C., Neufeld, T.P., O'Connor, M.B., and Selleck, S.B. (2007). Mechanisms of TSC-mediated control of synapse assembly and axon guidance. PloS one *2*, e375.

Kowianski, P., Lietzau, G., Czuba, E., Waskow, M., Steliga, A., and Morys, J. (2018). BDNF: A Key Factor with Multipotent Impact on Brain Signaling and Synaptic Plasticity. Cellular and molecular neurobiology *38*, 579-593.

Kumar, V., Zhang, M.X., Swank, M.W., Kunz, J., and Wu, G.Y. (2005). Regulation of dendritic morphogenesis by Ras-PI3K-Akt-mTOR and Ras-MAPK signaling pathways. The Journal of neuroscience : the official journal of the Society for Neuroscience *25*, 11288-11299.

Lee, S.H., Kim, Y.J., and Choi, S.Y. (2016). BMP signaling modulates the probability of neurotransmitter release and readily releasable pools in Drosophila neuromuscular junction synapses. Biochem Bioph Res Co *479*, 440-446.

Lenz, G., and Avruch, J. (2005). Glutamatergic regulation of the p70S6 kinase in primary mouse neurons. The Journal of biological chemistry *280*, 38121-38124.

Lim, R., Winteringham, L.N., Williams, J.H., McCulloch, R.K., Ingley, E., Tiao, J.Y., Lalonde, J.P., Tsai, S., Tilbrook, P.A., Sun, Y.*, et al.* (2002). MADM, a novel adaptor protein that mediates phosphorylation of the 14-3-3 binding site of myeloid leukemia factor 1. The Journal of biological chemistry *277*, 40997-41008.

Lim, S.H., Kwon, S.K., Lee, M.K., Moon, J., Jeong, D.G., Park, E., Kim, S.J., Park, B.C., Lee, S.C., Ryu, S.E.*, et al.* (2009). Synapse formation regulated by protein tyrosine phosphatase receptor T through interaction with cell adhesion molecules and Fyn. The EMBO journal *28*, 3564-3578.

Liu, Z., Huang, Y., Hu, W., Huang, S., Wang, Q., Han, J., and Zhang, Y.Q. (2014). dAcsl, the Drosophila ortholog of acyl-CoA synthetase long-chain family member 3 and 4, inhibits synapse growth by attenuating bone morphogenetic protein signaling via endocytic recycling. The Journal of neuroscience : the official journal of the Society for Neuroscience *34*, 2785-2796.

Lussier, M.P., Gu, X., Lu, W., and Roche, K.W. (2014). Casein kinase 2 phosphorylates GluA1 and regulates its surface expression. The European journal of neuroscience *39*, 1148-1158.

Malagelada, C., Lopez-Toledano, M.A., Willett, R.T., Jin, Z.H., Shelanski, M.L., and Greene, L.A. (2011). RTP801/REDD1 regulates the timing of cortical neurogenesis and neuron migration. The Journal of neuroscience : the official journal of the Society for Neuroscience *31*, 3186-3196.

Marques, G., Bao, H., Haerry, T.E., Shimell, M.J., Duchek, P., Zhang, B., and O'Connor, M.B. (2002). The Drosophila BMP type II receptor Wishful Thinking regulates neuromuscular synapse morphology and function. Neuron *33*, 529-543.

Martin-Lanneree, S., Lasbleiz, C., Sanial, M., Fouix, S., Besse, F., Tricoire, H., and Plessis, A. (2006). Characterization of the Drosophila myeloid leukemia factor. Genes to cells : devoted to molecular & cellular mechanisms *11*, 1317-1335.

Massaro, C.M., Pielage, J., and Davis, G.W. (2009). Molecular mechanisms that enhance synapse stability despite persistent disruption of the spectrin/ankyrin/microtubule cytoskeleton. The Journal of cell biology *187*, 101-117.

McCabe, B.D., Marques, G., Haghighi, A.P., Fetter, R.D., Crotty, M.L., Haerry, T.E., Goodman, C.S., and O'Connor, M.B. (2003). The BMP homolog Gbb provides a retrograde signal that regulates synaptic growth at the Drosophila neuromuscular junction. Neuron *39*, 241-254.

McNeill, H., Craig, G.M., and Bateman, J.M. (2008). Regulation of neurogenesis and epidermal growth factor receptor signaling by the insulin receptor/target of rapamycin pathway in Drosophila. Genetics *179*, 843-853.

Menon, K.P., Sanyal, S., Habara, Y., Sanchez, R., Wharton, R.P., Ramaswami, M., and Zinn, K. (2004). The Translational Repressor Pumilio Regulates Presynaptic Morphology and Controls Postsynaptic Accumulation of Translation Factor eIF-4E. Neuron *44*, 663-676.

Nahm, M., Lee, M.J., Parkinson, W., Lee, M., Kim, H., Kim, Y.J., Kim, S., Cho, Y.S., Min, B.M., Bae, Y.C.*, et al.* (2013). Spartin regulates synaptic growth and neuronal survival by inhibiting BMP-mediated microtubule stabilization. Neuron *77*, 680-695.

Natarajan, R., Trivedi-Vyas, D., and Wairkar, Y.P. (2013). Tuberous sclerosis complex regulates Drosophila neuromuscular junction growth via the TORC2/Akt pathway. Human molecular genetics *22*, 2010-2023.

Nie, Y., Li, Q., Amcheslavsky, A., Duhart, J.C., Veraksa, A., Stocker, H., Raftery, L.A., and Ip, Y.T. (2015). Bunched and Madm Function Downstream of Tuberous Sclerosis Complex to Regulate the Growth of Intestinal Stem Cells in Drosophila. Stem cell reviews *11*, 813-825.

Niere, F., and Raab-Graham, K.F. (2017). mTORC1 Is a Local, Postsynaptic Voltage Sensor Regulated by Positive and Negative Feedback Pathways. Frontiers in cellular neuroscience *11*, 152.

Penney, J., Tsurudome, K., Liao, E.H., Elazzouzi, F., Livingstone, M., Gonzalez, M., Sonenberg, N., and Haghighi, A.P. (2012). TOR is required for the retrograde regulation of synaptic homeostasis at the Drosophila neuromuscular junction. Neuron *74*, 166-178.

Penney, J., Tsurudome, K., Liao, E.H., Kauwe, G., Gray, L., Yanagiya, A., M, R.C., Sonenberg, N., and Haghighi, A.P. (2016). LRRK2 regulates retrograde synaptic compensation at the Drosophila neuromuscular junction. Nature communications *7*, 12188.

Piccioli, Z.D., and Littleton, J.T. (2014). Retrograde BMP signaling modulates rapid activity-dependent synaptic growth via presynaptic LIM kinase regulation of cofilin. The Journal of neuroscience : the official journal of the Society for Neuroscience *34*, 4371-4381.

Pielage, J., Bulat, V., Zuchero, J.B., Fetter, R.D., and Davis, G.W. (2011). Hts/Adducin controls synaptic elaboration and elimination. Neuron *69*, 1114-1131.

Pielage, J., Cheng, L., Fetter, R.D., Carlton, P.M., Sedat, J.W., and Davis, G.W. (2008). A presynaptic giant ankyrin stabilizes the NMJ through regulation of presynaptic microtubules and transsynaptic cell adhesion. Neuron *58*, 195-209.

Pielage, J., Fetter, R.D., and Davis, G.W. (2005). Presynaptic spectrin is essential for synapse stabilization. Current biology : CB *15*, 918-928.

Pielage, J., Fetter, R.D., and Davis, G.W. (2006). A postsynaptic spectrin scaffold defines active zone size, spacing, and efficacy at the Drosophila neuromuscular junction. The Journal of cell biology *175*, 491-503.

Rawson, J.M., Lee, M., Kennedy, E.L., and Selleck, S.B. (2003). Drosophila neuromuscular synapse assembly and function require the TGF-beta type I receptor saxophone and the transcription factor Mad. Journal of neurobiology *55*, 134-150.

Sanderson, J.L., Scott, J.D., and Dell'Acqua, M.L. (2018). Control of Homeostatic Synaptic Plasticity by AKAP-Anchored Kinase and Phosphatase Regulation of Ca2+-Permeable AMPA Receptors. Journal of Neuroscience *38*, 2863-2876.

Sigrist, S.J., Thiel, P.R., Reiff, D.F., Lachance, P.E., Lasko, P., and Schuster, C.M. (2000). Postsynaptic translation affects the efficacy and morphology of neuromuscular junctions. Nature *405*, 1062-1065.

Sigrist, S.J., Thiel, P.R., Reiff, D.F., and Schuster, C.M. (2002). The postsynaptic glutamate receptor subunit DGluR-IIA mediates long-term plasticity in Drosophila. The Journal of neuroscience : the official journal of the Society for Neuroscience *22*, 7362-7372.

Singh, S.R., Liu, Y., Zhao, J., Zeng, X., and Hou, S.X. (2016). The novel tumour suppressor Madm regulates stem cell competition in the Drosophila testis. Nature communications *7*, 10473.

Stephan, R., Goellner, B., Moreno, E., Frank, C.A., Hugenschmidt, T., Genoud, C., Aberle, H., and Pielage, J. (2015). Hierarchical microtubule organization controls axon caliber and transport and determines synaptic structure and stability. Developmental cell *33*, 5-21.

Sytnyk, V., Leshchyns'ka, I., and Schachner, M. (2017). Neural Cell Adhesion Molecules of the Immunoglobulin Superfamily Regulate Synapse Formation, Maintenance, and Function. Trends in neurosciences *40*, 295-308.

Takei, N., Inamura, N., Kawamura, M., Namba, H., Hara, K., Yonezawa, K., and Nawa, H. (2004). Brain-derived neurotrophic factor induces mammalian target of rapamycin-dependent local activation of translation machinery and protein synthesis in neuronal dendrites. The Journal of neuroscience : the official journal of the Society for Neuroscience *24*, 9760-9769.

Tan, E.H., and Sansom, O.J. (2012). A new tumour suppressor enters the network of intestinal progenitor cell homeostasis. The EMBO journal *31*, 2444-2445.

Tang, S.J., Reis, G., Kang, H., Gingras, A.C., Sonenberg, N., and Schuman, E.M. (2002). A rapamycin-sensitive signaling pathway contributes to long-term synaptic plasticity in the hippocampus. Proceedings of the National Academy of Sciences of the United States of America *99*, 467-472.

Tao, H.Z.W., and Poo, M.M. (2001). Retrograde signaling at central synapses. Proceedings of the National Academy of Sciences of the United States of America *98*, 11009-11015.

Tavazoie, S.F., Alvarez, V.A., Ridenour, D.A., Kwiatkowski, D.J., and Sabatini, B.L. (2005). Regulation of neuronal morphology and function by the tumor suppressors Tsc1 and Tsc2. Nature neuroscience *8*, 1727-1734.

Washbourne, P., Dityatev, A., Scheiffele, P., Biederer, T., Weiner, J.A., Christopherson, K.S., and El-Husseini, A. (2004). Cell adhesion molecules in synapse formation. The Journal of neuroscience : the official journal of the Society for Neuroscience *24*, 9244-9249.

Wei, H., Wang, H., Ji, Q., Sun, J., Tao, L., and Zhou, X. (2015). NRBP1 is downregulated in breast cancer and NRBP1 overexpression inhibits cancer cell proliferation through Wnt/beta-catenin signaling pathway. OncoTargets and therapy *8*, 3721-3730.

Williams, M.E., de Wit, J., and Ghosh, A. (2010). Molecular mechanisms of synaptic specificity in developing neural circuits. Neuron *68*, 9-18.

Withers, G.S., Higgins, D., Charette, M., and Banker, G. (2000). Bone morphogenetic protein-7 enhances dendritic growth and receptivity to innervation in cultured hippocampal neurons. The European journal of neuroscience *12*, 106-116.

Wosiski-Kuhn, M., and Stranahan, A.M. (2012). Transient increases in dendritic spine density contribute to dentate gyrus long-term potentiation. Synapse *66*, 661-664.

Wu, C.L., Wairkar, Y.P., Collins, C.A., and DiAntonio, A. (2005). Highwire function at the Drosophila neuromuscular junction: Spatial, structural, and temporal requirements. Journal of Neuroscience *25*, 9557-9566.

Xing, G.L., Li, M.Y., Sun, Y.C., Rui, M.L., Zhuang, Y., Lv, H.H., Han, J.H., Jia, Z.P., and Xie, W. (2018). Neurexin-Neuroligin 1 regulates synaptic morphology and functions via the WAVE regulatory complex in Drosophila neuromuscular junction. eLife *7*.

Zhang, X.W., Rui, M.L., Gan, G.M., Huang, C., Yi, J.K., Lv, H.H., and Xie, W. (2017). Neuroligin 4 regulates synaptic growth via the bone morphogenetic protein (BMP) signaling pathway at the Drosophila neuromuscular junction. Journal of Biological Chemistry *292*, 17991-18005.

3.7 Additional Data

3.7.1 Madm is essential for synapse development

Loss of *Madm* leads to sever synaptic stability, growth and morphology defects. We performed a detailed analysis by analyzing multiple alleles of *Madm* and all alleles showed similar phenotypes. $Madm^{2D2/Df}$ is a null allele due to a deletion in the second exon leading to a truncated protein. This allelic combination showed similar synaptic defects as the *Madm* point mutation (Figure 13B). The growth and stability of the NMJs of *Madm* null mutant NIMla can be rescued by presynaptic expression of Madm (Figure 13C), while postsynaptic expression rescued only the synaptic organization (Figure 13D). This suggests that Madm regulates synaptic growth and stability from the presynapse and NMJ organization from the postsynapse. Thus, the point mutant and the null allele exhibit similar phenotypes and both alleles can be rescued by a reintroduction of Madm.

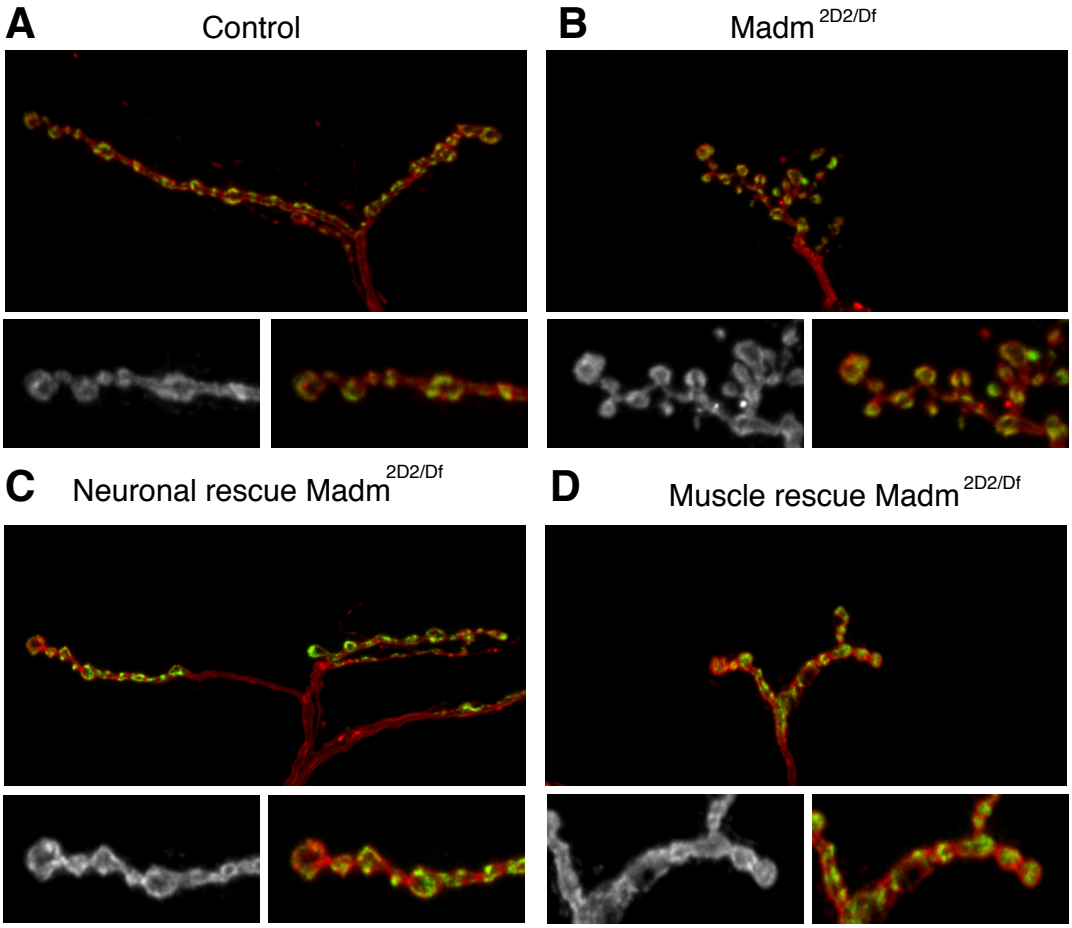

Figure 13: Madm is essential for synaptic growth and organization. (A-E) Morphological analysis of NMJs stained for presynaptic vesicle marker Syn (green) and presynaptic membrane marker HRP (red). (A) A control (*elav-Gal4/+*) NMJ on muscle 1. (B) Loss of function of Madm ($Madm^{2D2/Df}$) induces

reduced synaptic growth and a clustered synaptic bouton organization. (C) Presynaptic expression of Madm in *Madm$^{2D2/Df}$* animals rescues the synaptic growth defects (neuronal rescue 1: *elav^{C155}-Gal4; UAS GFP Madm/+; Madm$^{2D2/Df}$*, (D) Postsynaptic expression of Madm in *Madm$^{2D2/Df}$* animals rescues the synaptic bouton organization but does not rescue synaptic growth (*GluRIIB-Gal4/UAS GFP Madm; Madm$^{2D2/Df}$*).

3.7.2 Localization of Madm at the synapse

We further verified the localization of Madm at the NMJ to assess if Madm acts locally at the synapse or elsewhere in the cell to induce signaling to other molecules and thereby regulate synapse development and maintenance. We expressed GFP tagged Madm in the null mutant background (*Madm$^{2D2/Df}$*) and stained for Madm using an anti-GFP antibody. Presynaptic expression of Madm resulted in a clear and uniform localization of Madm at the synaptic terminal reflecting a cytoplasmic localization (Figure 14A). Postsynaptic expression of Madm in the null mutant showed localization at the synapse similar to postsynaptic density proteins (Figure 14B). As a control ectopically expressed cytoplasmic GFP using the same muscle driver. Unlike Madm, cytoplasmic GFP does not localize to the postsynapse (Figure 14C), indicating that the observed localization in the postsynaptic rescue condition is indeed Madm specific.

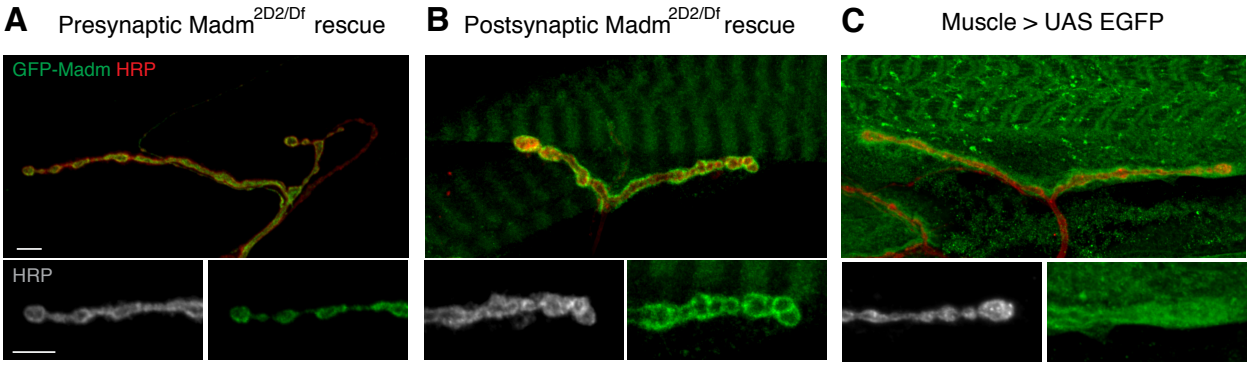

Figure 14 Localization of Madm. (A) Analysis of the presynaptic localization of Madm using GFP tagged Madm in *Madm$^{2D2/Df}$* and a pan-neuronal driver (*elavC155-Gal4; UAS GFP Madm/+; Madm$^{2D2/Df}$*). (B) Analysis of postsynaptic localization of Madm using a muscle specific driver (*GluRIIB-Gal4/UAS GFP Madm; Madm$^{2D2/Df}$*) and (C) expression of cytosolic EGFP using a muscle specific driver (*GluRIIB-Gal4/UAS EGFP*). Scale bars represent 5µm.

3.7.3 Genetic interaction of Madm with Mlf1 and bunched

In addition to the *Madm^{4S3}* allele, we also performed the genetic interaction experiments with Mlf1 and bunched with the Madm null allele (*Madm^{2D2}*). We observed similar effects as for the *Madm^{4S3}* allele (Figure 15). We observed no evidence for a genetic interaction with Mlf1 and bunched in the regulation of synapse development.

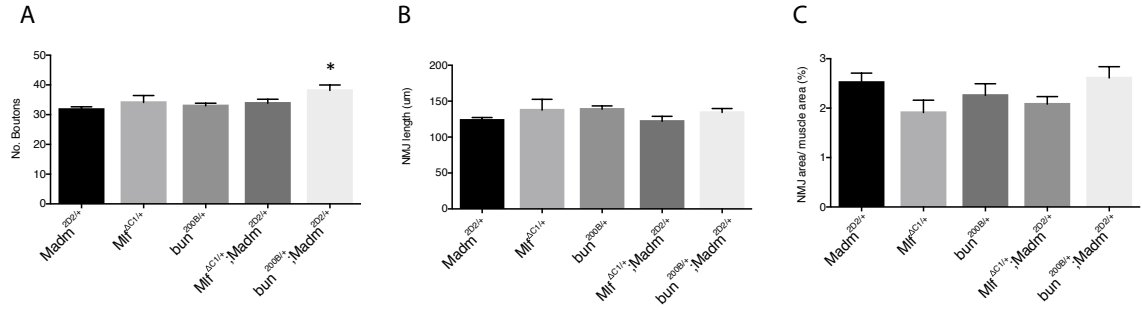

Figure 15: Genetic interaction of Madm with Mlf1 and bun. Quantification of synaptic growth parameters of NMJ on muscle 1 for the indicated genotypes, including number of boutons (A), NMJ length (B) and NMJ area per muscle area (C), One-way ANOVA with Tukey test (n=24-48 NMJs from 6-12 animals). All error bars represent SEM, *, P≤0.05; **, P ≤ 0.01; ***, P ≤ 0.001; ns: not significant.

3.7.4 Genetic interaction of Madm with components of the mTOR pathway

In order to understand the mechanism of Madm in the regulation of synapse development, we performed genetic interaction experiments of Madm with mTOR pathway components. We used multiple alleles to study the genetic interactions, including the point mutant Madm^{4S3} and the null mutant *Madm^{2D2}*. We performed genetic interactions with TSC1, TSC2, Rheb and S6k with alleles of Madm. Madm showed strong signs of genetic interactions with TSC2 and Rheb when using the *Madm^{4S3}* allele. In contrast, the allele *Madm^{2D2}* showed weaker genetic interactions with TSC2 and Rheb (Figure 16). The difference in the interaction between the alleles is likely due to the molecular nature of the alleles. In the transheterozygous point mutant animals 50% of non-functional protein is present along with 50% wild type protein while in transheterozygous null animal contains only 50% of wild type protein is present (Figure 1B). The presence of mutant protein likely uncovers the genetic interaction as signaling is perturbed at the level of Madm. However, currently we do not have any mechanistic evidence for this possibility. We also performed genetic interaction assays

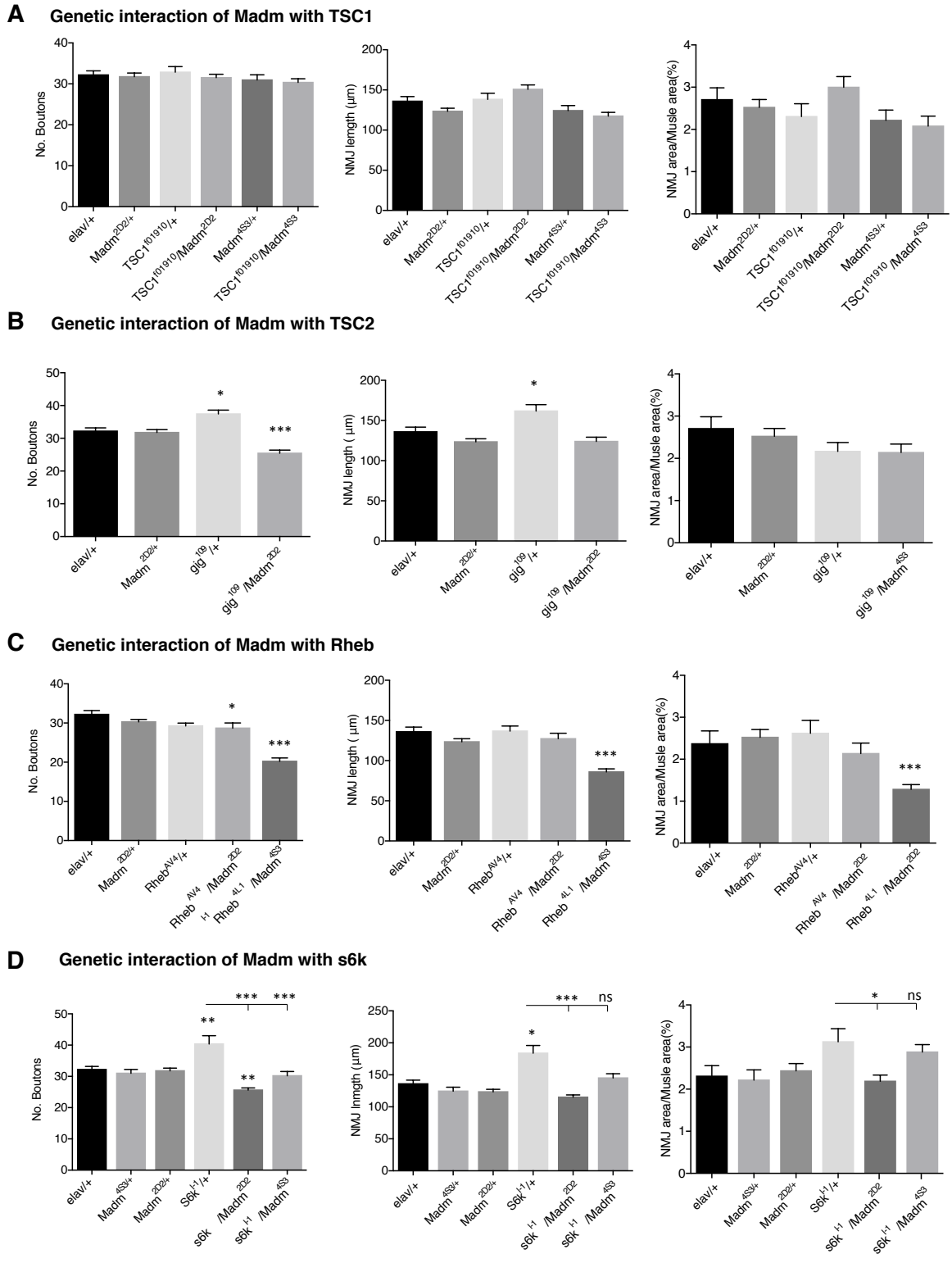

Figure 16: Genetic interaction of Madm with mTOR pathway members. Quantification of synaptic growth parameters on muscle 1 for the indicated genotypes including number of boutons, NMJ length and NMJ area per muscle area, One-way ANOVA with Tukey test (n=24-48 NMJs from 6-12 animals). All error bars represent SEM, *, P≤0.05; **, P ≤ 0.01; ***, P ≤ 0.001; ns: not significant.

with S6k using the allele *S6k*$^{l-1}$. NMJs of S6k mutant animals exhibit smaller sized boutons when compared to controls but do not show any change in the number of boutons (Cheng et al., 2011). In transheterozygous conditions of *S6k*$^{l-1/+}$, we observed an increase in NMJ size and in the number of boutons (Figure 16D), which is contradicting the published report. Nevertheless, this effect is significantly suppressed by introducing a transheterozygous Madm mutation, indicating a possible genetic interaction of Madm with S6K, further suggesting an association of Madm with the mTOR pathway during synapse development. Further verification is necessary to assess the unexpected NMJ phenotype observed in the transheterozygous *S6k*$^{l-1/+}$ animals. Interestingly, for S6k the Madm null allele showed a stronger interaction and the point mutation only a weaker interaction. Further analysis is necessary to examine the potential genetic interaction of Madm with S6k during synapse development.

3.7.5 Loss of Madm affects glutamate receptors abundance

As we observed that Madm mutants exhibit severe defects in synapse organization and stability, we further analyzed if there are any changes in active zone or glutamate receptor organization. There are reports that either pre- or postsynaptic alterations of certain molecules at the NMJ result in changes of active zones. Postsynaptic alteration of spectrin (Pielage et al., 2006) or actin (Blunk et al., 2014) leads to a change in the size and density of active zones and presynaptic loss of s6k results in a change of the size and distribution of active zones (Cheng et al., 2011). We analyzed active zone size and density by measuring the intensity of the active zone marker BRP and the number of active zones to estimate the density relative to the NMJ area (marked by HRP). We found no significant change in active zone density in *Madm* mutants. Similarly, the intensity of the BRP signal remained unchanged in mutants and also in *Madm* knockdown animals (Figure 17). In addition, we analyzed the glutamate receptor composition in the mutants and found that *Madm* mutants showed a small increase in GluRIIC intensity. Interestingly GluRIIC levels further increased in postsynaptic rescue animals. The intensity of GluRIIC was not rescued by presynaptic *Madm* expression (Figure 17I). At the moment the significance of this small increase in GluRIIC intensity remains unknown.

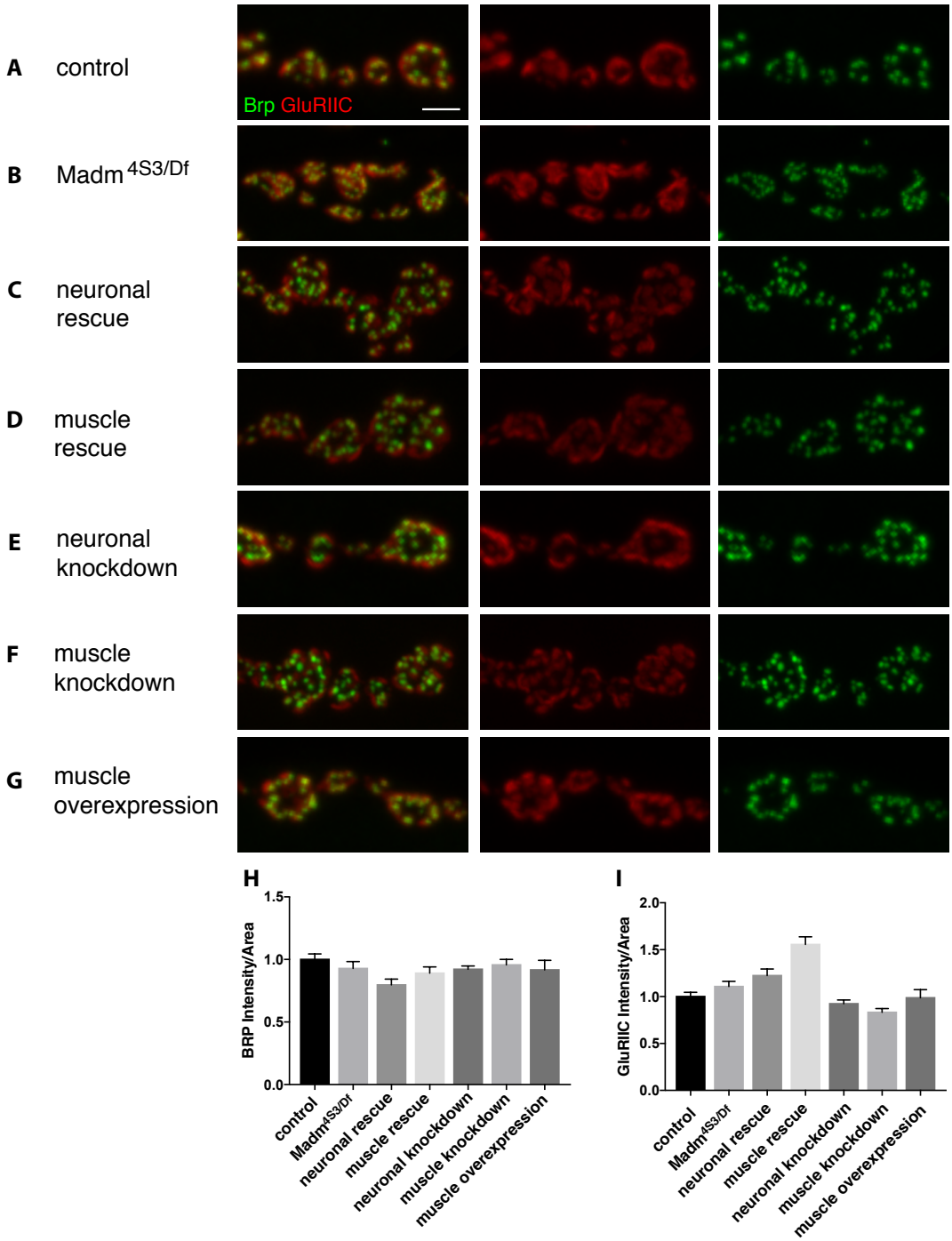

Figure 17: Levels of Brp and GluRIIC in Madm mutants. Comparison of the intensity of Brp and GluRIIC in different genotypes. (A) Control (elav^{c155}/+), (B) Madm$^{4S3/Df}$, (C) neuronal rescue (elav^{c155}; UAS-GFPMadm; Madm$^{4S3/Df}$), (D) muscle rescue (GluRIIB-Gal4/UAS-GFPMadm; Madm$^{4S3/Df}$), (E) neuronal knockdown (elav^{c155}; UAS-Dicer2/VD27346), (F) muscle knockdown (UAS-Dicer2/VD27346; BG57-Gal4/+), (G) muscle overexpression (GluRIIB-Gal4/UAS-GFPMadm. (H) Quantification of normalized intensity of Brp per HRP area. () Quantification of normalized intensity of GluRIIC per HRP area. All error bars represent SEM, *, P≤0.05; **, P ≤ 0.01; ***, P ≤ 0.001; ns: not significant; ANOVA and Tukey multiple comparison test

We also analyzed the intensity of GluRIIA levels in mutants and control and observed a strong increase in GluRIIA intensity in *Madm*$^{4S3/Df}$ and *Madm*$^{2D2/Df}$animals when compared to controls (Figure 18). Altogether, our data shows that loss of Madm does not affect active zones but results in a significant increase in glutamate receptors levels, particularly of GluRIIA. Further analysis is necessary to correlate these phenotypes with the functional data.

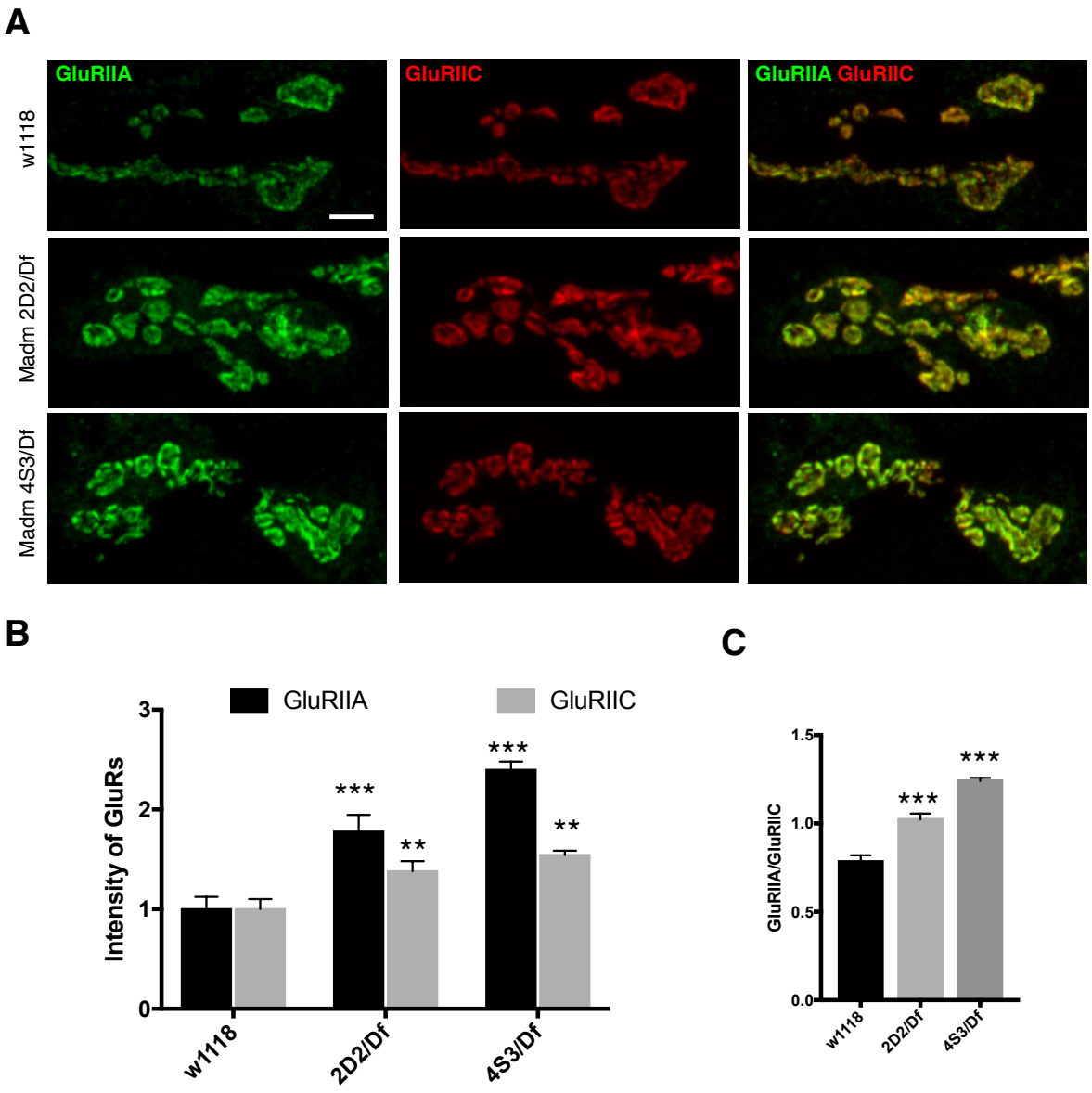

Figure 18: Levels of GluRIIA and GluRIIC in Madm mutants. (A) Comparison of the levels of GluRIIA and GluRIIC in Madm mutants and controls. Madm mutants show a strong increase of GluRIIA levels and a slight increase in GluRIIC levels when compared to controls. Madm$^{4S3/Df}$ mutants showed a stronger effect than Madm$^{2D2/Df}$. (B) Quantification of normalized levels of GluRIIA and GluRIIC per HRP area. (C) Quantification of

the levels of GluRIIA per GluRIIC. All error bars represent SEM, *, P≤0.05; **, P ≤ 0.01; ***, P ≤ 0.001; ns: not significant; ANOVA and Tukey multiple comparison test

3.7.6 Prediction of potential phosphorylation sites of the Madm protein

Madm encodes a pseudokinase and it has been reported that Madm potentially recruits other kinase, which in turn phosphorylate Madm and the target protein. Kinases that may associated with Madm are currently not known. A computational sequence analysis of NRBP1, the vertebrate homologue, has shown that NRBP1 contains phosphorylation sites for Casein kinase II (CKII) (11 sites), PKC (6 sites) and cAMP dependent protein kinase (1 Site) (Hooper et al 2000). For Madm we identified 12 potential phosphorylation sites for CKII, with 3 conserved with NRBP1 (Figure 19, 20). In addition, we identified many phosphorylation sites for multiple other kinases. CKII has been reported to regulate synaptic plasticity (Bulat et al., 2014) and is also involved in the regulation of glutamate receptors during homeostasis (Bleier and Toliver, 2017). We performed a preliminary genetic interaction analysis of Madm with CKII alpha (*CKIIα^{P1}*) but did not observe signs of genetic interaction. A detailed analysis is required to determine if CKII interacts with Madm in the regulation of synapse stability and function.

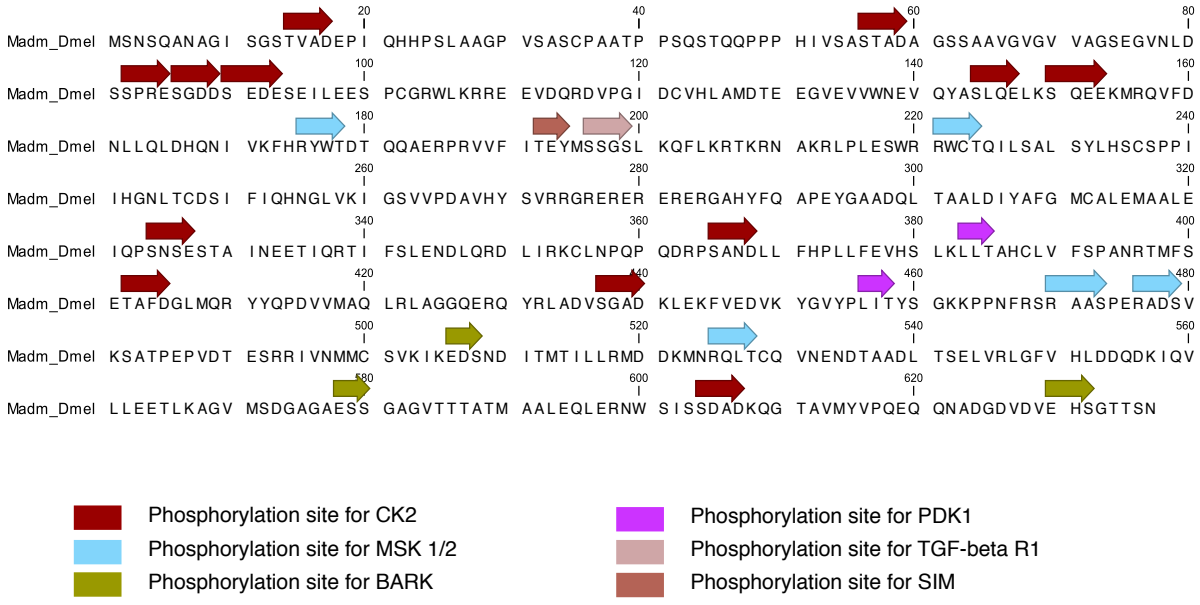

Figure 19: Sequence based prediction of potential phosphorylation site of Madm. Madm protein contains potential phosphorylation sites for many kinases. Madm contains 12 potential sites of Casein Kinase II (brown), 5 sites for Mitogen and stress associated kinase 1/2 (MSK1/2), a ribosomal protein S6k alpha 5 site (cyan), 3 sites for BARK and one for G-protein associated kinase (Olive green).

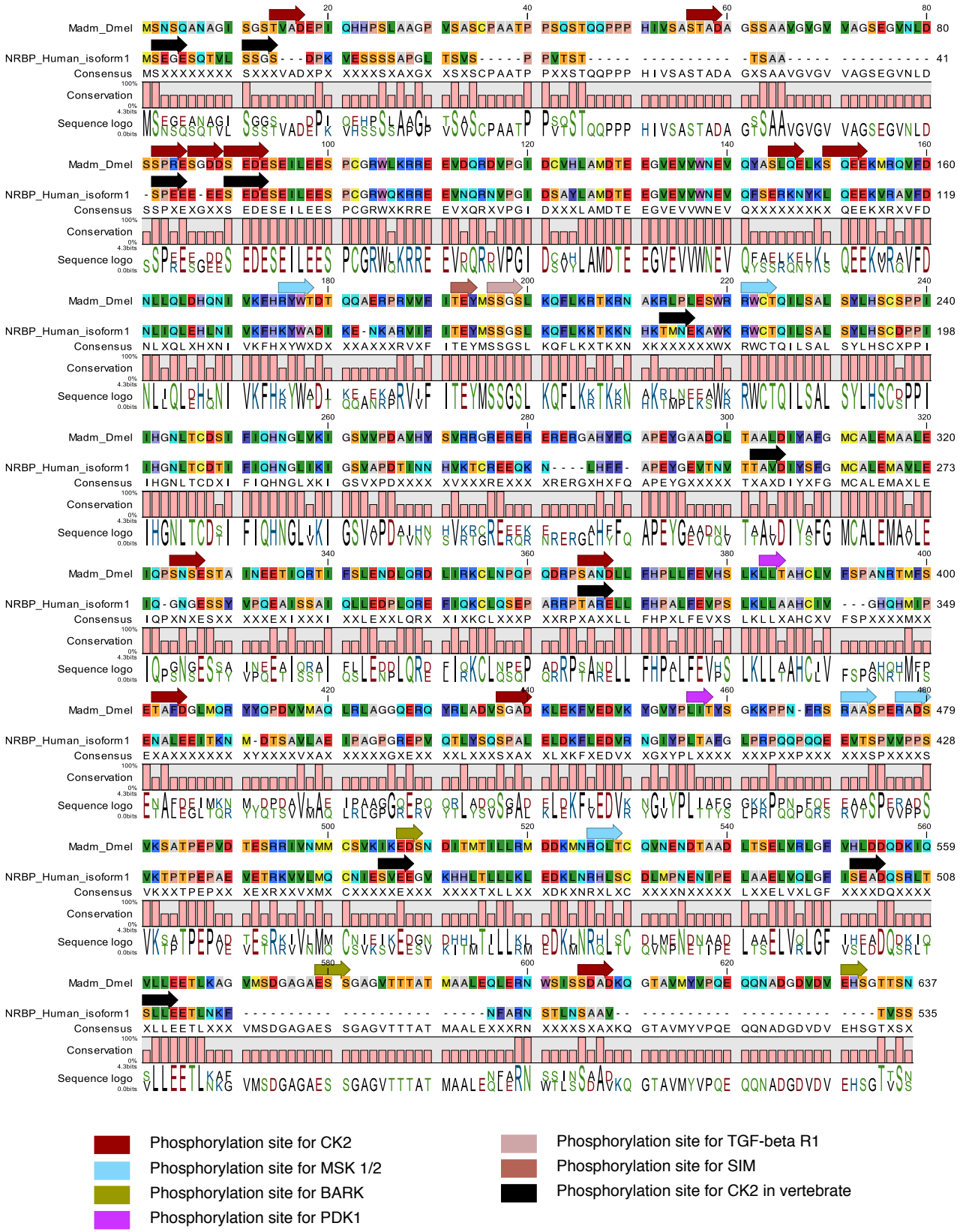

Figure 20: Comparison of the Madm protein sequence with the human homolog NRBP1.

3.8 Discussion

The ubiquitously expressed pseudokinase Madm regulates synaptic growth, maintenance and function. We could demonstrate the importance of Madm for NMJ development using multiple independent alleles. The point mutant and the null allele showed similar synaptic defects with varying intensities. In addition, the localization of Madm at the pre- and the postsynapse is not affected by the presence of non-functional protein in $Madm^{4S3}$ mutant animals. Interestingly, we observed a noticeable difference between the two alleles in our genetic interaction studies. The $Madm^{4S3}$ allele showed stronger effect compared to the $Madm^{2D2}$ allele likely due to the fact that the mutant 4S3 protein can interfere with other signaling pathway components. Despite the differences in the severity between the two alleles all data is consistent with our hypothesis of Madm acting in close association with the mTOR pathway. In addition to TSC2, Rheb and Thor we also observed a genetic interaction with S6k. We also identified multiple potential CKII phosphorylation sites in the Madm protein sequence, suggesting that CK2 may be one of the interacting kinases of Madm. Finally, we observed interesting glutamate receptor phenotypes in *Madm* mutants, indicating that *Madm* is tightly involved in the regulation of functional synaptic parameters. Further experiments are necessary to fully clarify the importance of these phenotypes.

4 Analysis of Protein phosphatase 4 in the Drosophila nervous system

4.1 Abstract

Protein phosphatase 4 (PP4) encodes a serine/threonine protein phosphatase that has been well-studied for its requirements in DNA repair and cell cycle regulation. Thus far a role of PP4 in postmitotic neuron has not been described. Here we demonstrate the importance of PP4 for nervous system development using a newly generated null mutant. Loss of PP4 results in larval lethality with an extended third instar larval life span. While the NMJs remains unchanged at late third instar larval stages, prolonged development results in severe alteration of NMJ structure. In addition, we observed significant alterations in the morphology of mitochondria and of the endoplasmic reticulum. Finally, we demonstrated that PP4 is essential for the development of adult brain structures, possibly affecting the axon pruning. Together, our data demonstrates that PP4 is essential for normal development and function of the nervous system.

4.2 Introduction

Coordinated function of protein phosphatases and kinases regulates the activity of protein by modulating their phosphorylation status. Kinases phosphorylate and phosphatases dephosphorylate target proteins. Even though these processes are equally important, the number of phosphatases encoded in the genome is far smaller than the number of kinases. It is assumed that a single phosphatase can counteract the function of many kinases. Serine/threonine phosphatases are among the best characterized types of protein phosphatases that are involved in the regulation of multiple cellular processes. They are divided into four distinct classes: PP1, PP2A, PP2B and PP2C, based on their substrates, sensitivity to certain activators and inhibitors.

Protein phosphatase 4 (PP4) belongs to the PP2A family of serine/threonine protein phosphatases and is closest related to PP2A. It is highly conserved across species and is present in almost all organisms (Hu et al., 2001). PP4C of *Drosophila melanogaster* shows 91% amino acid identity with human PP4. In humans, the gene that encodes the catalytic subunit PP4C is located on the chromosome 16p11-p12 (Bastians et al., 1997). The gene spans about 10kb with one untranslated and 8 translated exons with two transcription initiation sites 84 and 54 bp upstream of the ATG initiation codon (Huang et al., 1997). In higher animals, PP4 is ubiquitously expressed with high expression in tissues like kidney, liver, testis and lungs (Hu et al., 2001). Like other PP2A family phosphatases, PP4 also functions as a complex that includes a catalytic subunit PP4C and the regulatory subunits PP4R1, PP4R2 and PP4R3. Similarly, the PP4 complex of Drosophila contains the catalytic subunit PP4 19C and the regulatory subunits PPP4R2r and PPP4R3/falafel (flfl).

4.2.1 PP4 19C, the catalytic subunit of PP4

PP4 19C, the Drosophila catalytic subunit shows high sequence identity (94%) with mammalian PP4C (Cohen et al., 2005). *PP4 19C* is located on the X chromosome at location 19D1 in Drosophila, extending about 3kb in the genome with two untranslated and two translated exons encoding a single isoform of PP4 19C. PP4 19C is 307 amino acids in length with a molecular mass of about 35.3kDa. PP4 19C forms a complex with PPP4R2r and PPP4R3/flfl, the regulatory subunits that binds to the target molecules. PP4 19C requires reversible methyl esterification at the carboxy-terminal mediated by the Leucine Carboxyl Methyltransferase 1 (LCMT-1), to regulate the interactions with the regulatory subunits

(Hwang et al., 2016). Manganese ions acts as a cofactor for the catalytic activity of PP4 19C and it possess multiple manganese ion binding sites around the active site. The regulatory subunits mediate the interaction with the target molecules necessary for phosphorylation. The catalytic subunit shows substrate specificity similar to but not identical to that of PP2Ac. PP4 19C shows high activity towards a phosphor-threonine peptide substrate (Cohen et al., 2005). It is assumed that interaction of regulatory subunit with catalytic subunit reduces the activity of catalytic subunit, thereby acting as an auto inhibitory response.

4.2.2 Regulatory subunits

In vertebrates, the PP4 protein complex contains three regulatory subunits: PPP4R1, PPP4R2 and PPP4R3. In Drosophila, PPP4R2r and PPP4R3/flfl are the regulatory subunits for PP4 19C. PPP4R2r is about 609 amino acids long with molecular mass of 66.8kDa and is highly asymmetric. In vertebrates, R1 and R2 form core regulatory complex, which then bind to the variable regulatory subunit R3. In Drosophila, the R2 subunit forms the core complex with PP4 19C and then interacts with flfl/PPP4R3. PPP4R3 is made of 980 amino acids with a molecular mass of 109.3kDa. The activity of the PP4 complex is regulated by the phosphorylation of the regulatory subunits mediated by Cdk1 and resulting in inactivation (Voss et al., 2013). Multiple other subunits are potentially involved in the formation of PP4 complex. Gemin3 and Gemin4 are reported to form complex with PP4C in both vertebrates and in Drosophila, likely acting as additional variable regulatory subunits (Carnegie et al., 2003).

4.2.3 Functional importance of the Protein phosphatase 4 complex

PP4 regulates multiple cellular processes similar to other family members. Since the substrate specificity for PP4 is slightly different, it is assumed that PP4 might possess some special features in addition to PP2A family specific functions in the cell. PP4 was identified as an important molecule for cell cycle regulation. The formation of the mitotic spindle and the division of the centrosome is regulated by PP4 during the cell division in Drosophila, *C.elegans* and in mammals (Han et al., 2009; Helps et al., 1998; Sumiyoshi et al., 2002). Loss of PP4 results in the formation of abnormal interphase microtubules, multipolar spindles, increase in the percentage of multinuclear cells with prolonged G2/M transition and DNA repair (Falk et al., 2010; Lee et al., 2012; Liu et al., 2011a; Liu et al., 2012; Ning et al., 2006; Pfeifer, 2012). Histone H2A variant H2AX is essential for the replication mediated DNA break repair and it is dependent on the PP4 mediated activation (Chen et al., 2016; Chowdhury et al., 2008; Nakada

et al., 2008). In addition, the PP4 complex has been shown to regulate the development of the centrosome. Loss of PP4C led to an unscheduled activation of Cdk1 resulting in hyperphosphorylation of NDEL1 in the interphase, thereby disturbing the complex formation with Lis1 to form a functional spindle orientation complex (Hall et al., 2017; Toyo-oka et al., 2008b; Xie et al., 2013). The regulatory subunit 3 of Drosophila PP4, Falafel (flfl), directly interacts with the centromeric protein C (CENP-C) to bring PP4 activity to centromeres to maintain CENP-C and to attach core kinetochore proteins at chromosomes during mitosis (Lipinszki et al., 2015). PP4 also plays an essential role in the regulation of neuroblast division. The activity of the cell polarity protein Par3 is controlled by PP4 complex through its interaction with regulatory subunit smek1/PPP4R1. Interaction of Par3 with smek1 inactivates Par3 through dephosphorylation by PP4C during the induction of neuronal differentiation (Lyu et al., 2013). PP4 mediated dephosphorylation of Mira through its interaction with Flfl is a crucial process in the cortical association/asymmetric localization of Mira (Sousa-Nunes et al., 2009). PP4C and R2 mediate the localization of small nuclear RNPs through its interaction with survival of motor neuron complex proteins gemin3 and gemin4 (Carnegie et al., 2003).

In addition, PP4 has been reported to function in multiple other pathways, which have been reported to be involved the development and function of nervous system. Loss of PP4 leads to a disruption of Notch Signaling. PP4 regulates the activity of JNK1, as an increase in PP4 activity resulted in an increase in the JNK1 activity (Inostroza et al., 2005). PP4 suppresses the expression and activity of insulin receptor subunit IRS-1 and IRS-4 by promoting JNK induced phosphorylation and controls hepatic insulin resistance (Dou et al., 2017; Mihindukulasuriya et al., 2004; Zhao et al., 2015; Zhou et al., 2002). PP4 controls Hh signaling by inhibiting the activity of smoother (Smo) by its phosphatase activity. Loss of PP4 was found to result in the high levels of phosphorylated Smo resulting in the hyperactivation of Hh signaling (Jia et al., 2009). PPP4R1 has been shown to interact with NF-kappa B to perform PP4C mediated dephophorylation induced inactivation of NF-kappa B signaling in T cell lymphocytes (Abdul-Sada et al., 2017; Brechmann et al., 2012; Hadweh et al., 2014; Yeh et al., 2004). However, a requirement of PP4 in post-mitotic neurons has not yet been demonstrated. Here we address the potential importance of PP4 in the nervous system.

4.3 Results

4.3.1 Generation of PP4 19C null alleles

PP4 19C, the catalytic subunit of PP4 is a ubiquitously expressed protein. It is highly conserved form yeast to human and has been reported to be essential during early embryonic development in mice. Loss of PP4 resulted in embryonic lethality as early as embryonic day 9.5 (Shui et al., 2007). In Drosophila hypomorphic mutants of *PP4 19C* (*PP4 19C*^{G11307} and *PP4 19C*^{cmm}) were reported to exhibit semi-lethality due to reduced levels of PP4 (Helps et al., 1998). Along with the hypomorphic allele *PP4 19C*^{G11307}, we used various other transgenic RNAi lines from both VDRC and BDSC to study the importance of PP4 in synapse development

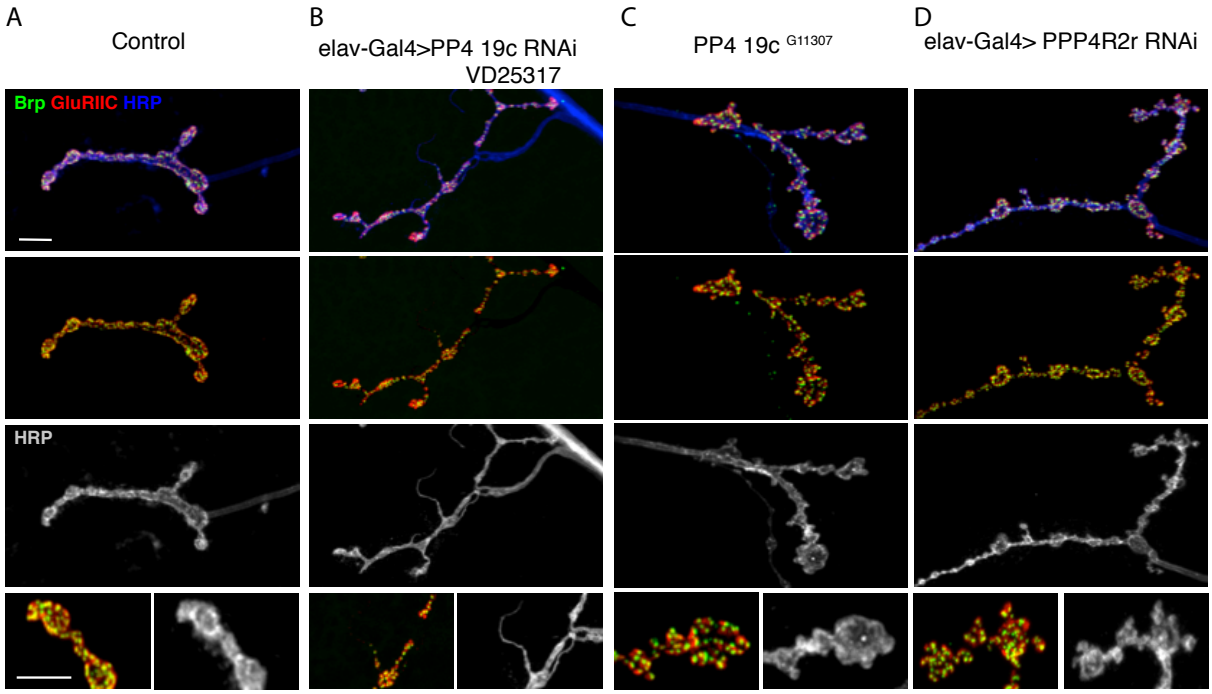

Figure 21 Analysis of the effect of loss of function of PP4 at the NMJ

Analysis of the effect of loss of function mutations of PP4 using different transgenic lines targeting the catalytic subunit and the regulatory subunit. NMJs were stained with the presynaptic active zone marker Brp (green), postsynaptic glutamate receptor subunit GluRIIC (red) and the motoneuron membrane (Hrp, blue/grey). (A) A stable NMJ of a control animal on muscle 4 with well-formed boutons. (B) NMJ of an animal after presynaptic knockdown of PP4 19C, the catalytic subunit of PP4 using the RNAi line VD25317. The NMJ displays filopodia-like protrusions with developing release sites as an indication of the formation of new boutons. (C) NMJ of the hypomorphic mutant of *PP4 19C* (*PP4 19C*^{G11037}). The NMJ shows normal growth with many satellite boutons particularly at the terminal boutons. (D) NMJ of an animal after presynaptic knockdown of PPP4R2r, the regulatory subunit of PP4. The NMJ exhibits normal growth but has many satellite boutons. Scale bar represents 5µm.

and maintenance. Presynaptic knockdown of PP4 19C by BDSC transgenic RNAi lines didn't show significant changes at the NMJ and animals were healthy and viable upon knockdown using a ubiquitous driver. Knockdown of PP4 19C using the VDRC transgenic RNAi (*VD25317*) line induced significant changes in NMJ morphology. Presynaptic knockdown of PP4 19C was lethal between early larvae to late third instar stages. Knockdown of PP4 19C using VD25317 led to NMJs with an increased number of filopodia-like membrane protrusions. At these sites new active zones developed along the length of the protrusion (Figure 21B). However, hypomorphic mutant animals showed NMJs with many satellite boutons but no protrusions (Figure 21C). Similarly, presynaptic knockdown of regulatory subunit PPP4R2r also led to an increased number of satellite boutons at the NMJ but no protrusions (Figure 21D). Based on these phenotypic variations we asked whether the protrusion phenotype was indeed due to a loss of function of PP4. To address this, we decided to generate a complete null allele of *PP4*. We took advantage of CRISPR/Cas9 genome editing to generate a null mutant for *PP4*, using the tools and protocols from Gratz et al. (2014) and http://flycrispr.molbio.wisc.edu. (Described in detail in the materials and methods).

The gene *PP4 19C* is located on the X chromosome at chromosomal location 19D1. We designed CRISPR targets, guide RNAs and the dsRed donor vector in order to create a minimal deletion on the chromosome, so that the entire PP4 open reading frame is deleted without disturbing neighboring genes. Microinjections were performed in embryos that express the enzyme Cas9 under the germ line promoter of *vasa*. A plasmid DNA cocktail containing guide RNA expressing vectors and donor vector was injected at the posterior region of the embryo. *gRNA*s identify the target location in the genome and recruit Cas9 to induce DNA breaks at the desired target sites. The donor vector that carries the homologous sequence around the cut sites facilitates homology-mediated repair, thereby leading to an insertion of the dsRed cassette into the location of *PP4 19C* (Figure 22B, C). The injected embryos were carefully raised and adults were crossed to w^{1118} animals and progeny was screened for dsRed expression under the *3xP3* promotor. Since it was expected that homozygous or hemizygous animals were lethal, we established the stocks with first chromosome balancers marked by GFP (*FM6GFP*). The insertion was verified by PCR. The size difference between the *PP4* gene region and the inserted dsRed cassette between homology arms allowed us to verify the deletion using PCR (Figure 22C, D). In the progeny from heterozygous population, we

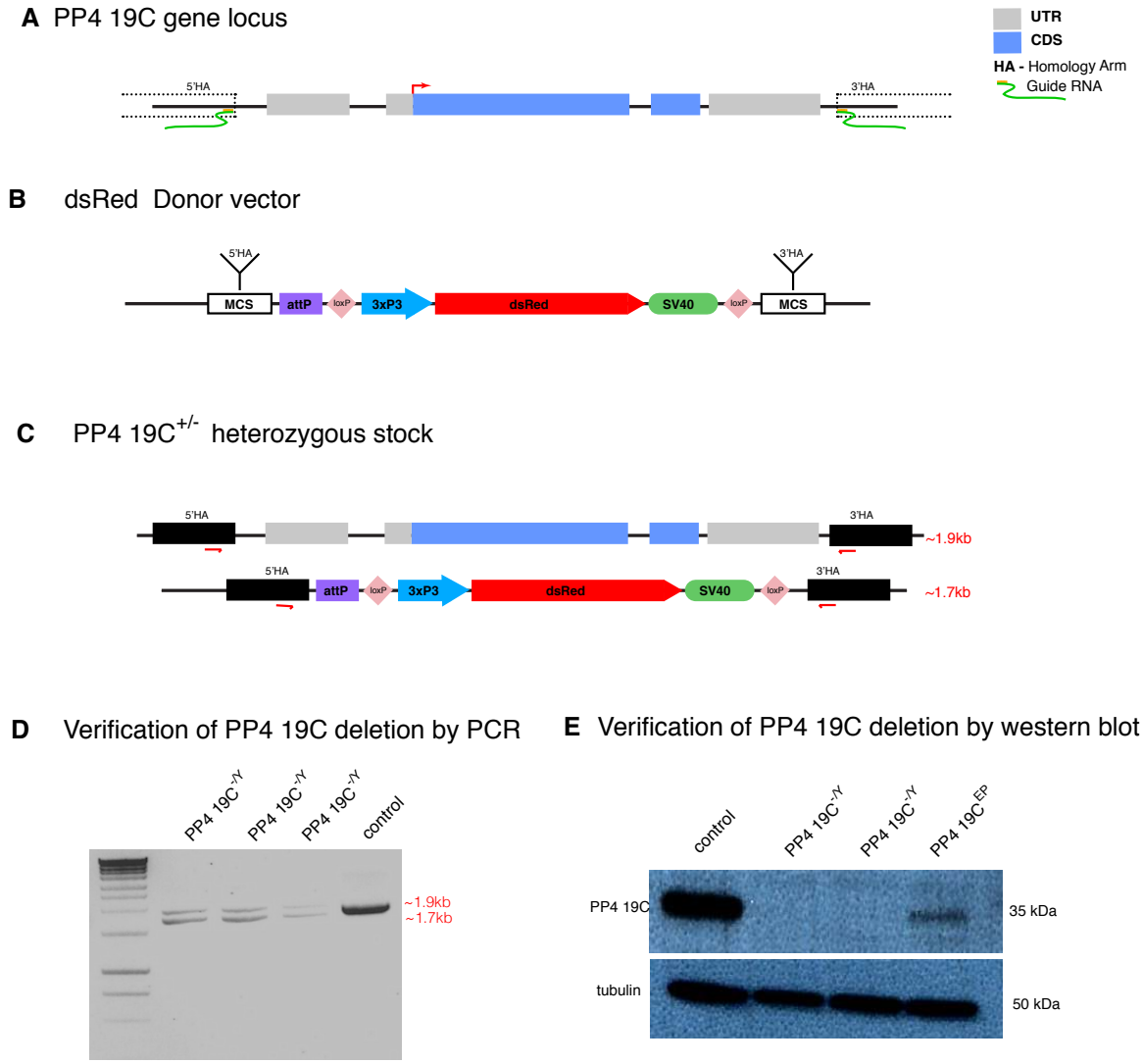

Figure 22 Generation of a PP4 19C null mutation

(A) Schematic representation of the *PP4* gene locus with gRNA targeting sites for CRISPR mediated DNA breaks. (B) Schematic of the dsRed Donor vector cassette with multiple cloning sites (MCS), dsRed under the control of *3xP3* promoter and *loxP* on either side of dsRed. (C) Representation of the heterozygous chromosomal locus of *PP4* null over a balancer chromosome. (D) Verification of the *PP4 19C* deletion in three independent mutant lines by PCR using the primers designed in the homology arms covering the *PP4* gene locus. The difference in the size due to the replacement of *PP4 19C* locus with dsRed cassette on one of the chromosomes produces PCR product of ~1.9kb (corresponding to *PP4 19C*) and ~1.7kb (corresponding to dsRed cassette insertion). (E) Verification of *PP4* null in two independent mutants and the hypomorph using the antibody generated against PP4 19C and tubulin as a loading control.

identified viable, dsRed positive male larvae, which were supposed to be null alleles of *PP4 19C* (hemizygous). Genomic DNA was isolated from these males and the deletion was confirmed by PCR. In addition, we generated an antibody against PP4 19C. We verified the expression of PP4 in the brain using Western blots and could demonstrate a complete elimination of PP4 in mutant males (dsred positive hemizygous males). We also verified the nature of the hypomorphic mutants (*PP4 19C*^{G11307}) (Figure 22E). Thus, we successfully generated a null mutant of *PP4 19C*. Loss of PP4 is not embryonic lethal in Drosophila. In order to delete the dsRed marker, we crossed females to cre expressing males and removed the dsRed with the help of the *loxP* sites that are present on both sides of dsRed and re-established the stock with the balancer.

4.3.2 Developmental analysis of *PP4* null animals

Using PCR, sequencing and western blot, we could confirm the deletion of *PP4*. Multiple reports showed that loss of *PP4* is embryonic lethal both in mice and Drosophila. To address this, we staged *PP4 19C* null larvae and could show that mutants survive until the 3rd instar stage but fail to pupate. Mutant larvae exhibited a slight delay in growth compared to controls. At 25°C, wild type larvae take 5 days to reach the late 3rd instar larval stage and then develop into prepupa. *PP4 19C* mutant animals displayed a slight delay in growth with a smaller body size on day 3, day 4 and day 5 when compared to wild type. *PP4 19C* mutant larvae reached the size of 5-day old wild type larva on the 6th day at 25°C (Figure 23). Surprisingly, these mutant larvae remained in the 3rd instar stage for up to 10 days and then fail to pupate and die as larva. After day 6, *PP4 19C* mutant larvae grow slightly bigger than the 5 days old wild type larvae. In addition, we observed an absence of appropriately developed imaginal discs in these larvae. Viability and the development of imaginal discs could be rescued by ubiquitous expression of wild type PP4 19C. Expression of PP4 19C using either a neuronal driver or a muscle driver did not rescue the lethality. However, expression of PP4 19C under a neuronal driver promoted the formation of prepupa but did not restore growth of imaginal discs. We observed similar characteristics when analyzing the hypomorphic mutant animals however with less severe phenotypes. All hypomorphic mutants develop into pupae and died as late pupae.

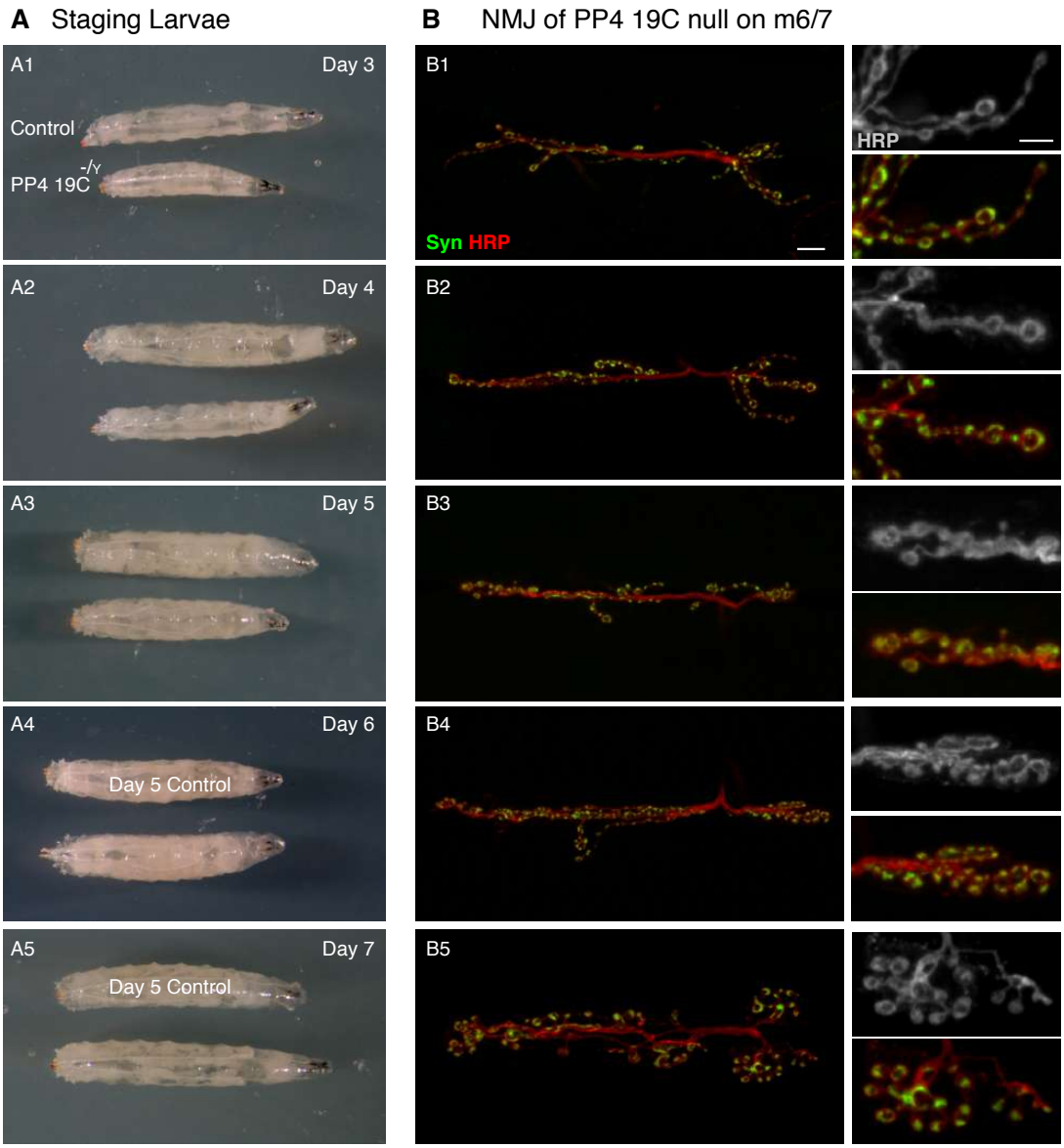

Figure 23 Developmental analysis of *PP4 19C* null larvae

(A) Staging of *PP4 19C* null larva in comparison with wild type (w^{1118}) larvae on day 3 (A1), da y4 (A2), day 5 (A3), day 6 (A4), day 7 (A5). (B) NMJ of *PP4 19C* null larva on muscle 6/7 on day 3 (B1), day 4 (B2), day 5 (B3), day 6 (B4), day 7 (B5), stained with Synapsin (green) and HRP (red). Scale bar represent 10µm and 5µm.

4.3.3 Abnormalities in NMJ development in the absence of PP4

In an RNAi based screen, PP4 was identified as an essential regulator of synapse development and maintenance (Bulat et al., 2014). Presynaptic knockdown of PP4 19C using transgenic RNAi (VD25317) resulted in formation of long protrusions at the NMJ, particularly at terminal boutons in contrast to control NMJs. In the control animals, terminal boutons were round and large in size, but knockdown of *PP4* in motoneurons resulted in change in the shape of boutons in the NMJs. Long filopodia like protrusions were observed with

postsynaptic receptors beginning to be establish along the protrusions. The insertion of postsynaptic receptors might be an indication of developing NMJ structures as demonstrated using live imaging (Rasse et al., 2005). In contrast, NMJs of *PP4* hypomorphs showed an increase in satellite boutons at terminal boutons (Figure 21C). Formation of satellite bouton is proposed to be an initiation step in the formation of a new bouton (Zito et al., 1999). To further confirm the phenotype, we analyzed the NMJs of the newly generated *PP4 19C* null animals. As the *PP4 19C* null animals exhibited a delay in the development, we analyzed the NMJs of larvae from 3 days to 8 days old. Until the day 5, NMJs of *PP4 19C* mutants developed with normal bouton shape and size (Figure 23B3). The NMJs of day 6 larvae displayed small bud like structures at terminal boutons. At this stage NMJs were smaller compared to controls (Figure 23B4). NMJs of *PP4* mutants on day 7 displayed a severe increase in satellite bouton number and also in the size of satellite boutons (Figure 23B5). In addition, the NMJs displayed small boutons throughout the entire NMJ. Due to the lack of a proper control for the extended life span of the larvae, it was difficult to interpret the NMJ phenotype of *PP4 19C* mutants. Comparing the NMJs to extended third instar (ETI) larvae obtained via a knockdown of torso in the ring gland (*phm-Gal4>UAS-torso-RNAi)* (Miller et al., 2012b) would be potential solution. It has been reported that the NMJs of the ETI larvae increase in size matching the increased body size. In contrast to this, the NMJs of *PP4* mutants did not increased in size, but rather developed into numerous small boutons, indicating that the phenotype is not due to prolonged larval development. Unfortunately, thus far we were not able to rescue only the extended larval development without expression of PP4 in the nervous system to address neuronal specific requirements of PP4. We further verified the efficiency of all RNAi lines (including the VDRC line) using the generated antibody and found that the recently generated line BL#57823 showed the most efficient knockdown. In contrast the RNAi line VD25317 could only mediate a partial knockdown and all other stocks didn't show significant knockdown (Figure 24A). Importantly, the RNAi line BL#57823 showed similar features as the *PP4 19C* null allele. Knockdown of PP4 19C using the RNAi line BL#57823 with a ubiquitous driver (*da-Gal4*) resulted in larvae with extended 3rd instar stages that failed to pupate and did not contain any imaginal discs. When the knockdown was performed using the pan-neuronal driver (*elav^{C155}-Gal4*), most of the animals died as late pupa and very few turned into adults. In contrast, knockdown of PP4 19C using the RNAi line VD25317 with a ubiquitous driver (*da-Gal4*) or a pan-neuronal driver (*elav^{C155}-Gal4*) resulted in embryonic to early 3rd instar larval lethality indicating possible off-target effects. Thus, it is likely that the NMJ phenotype

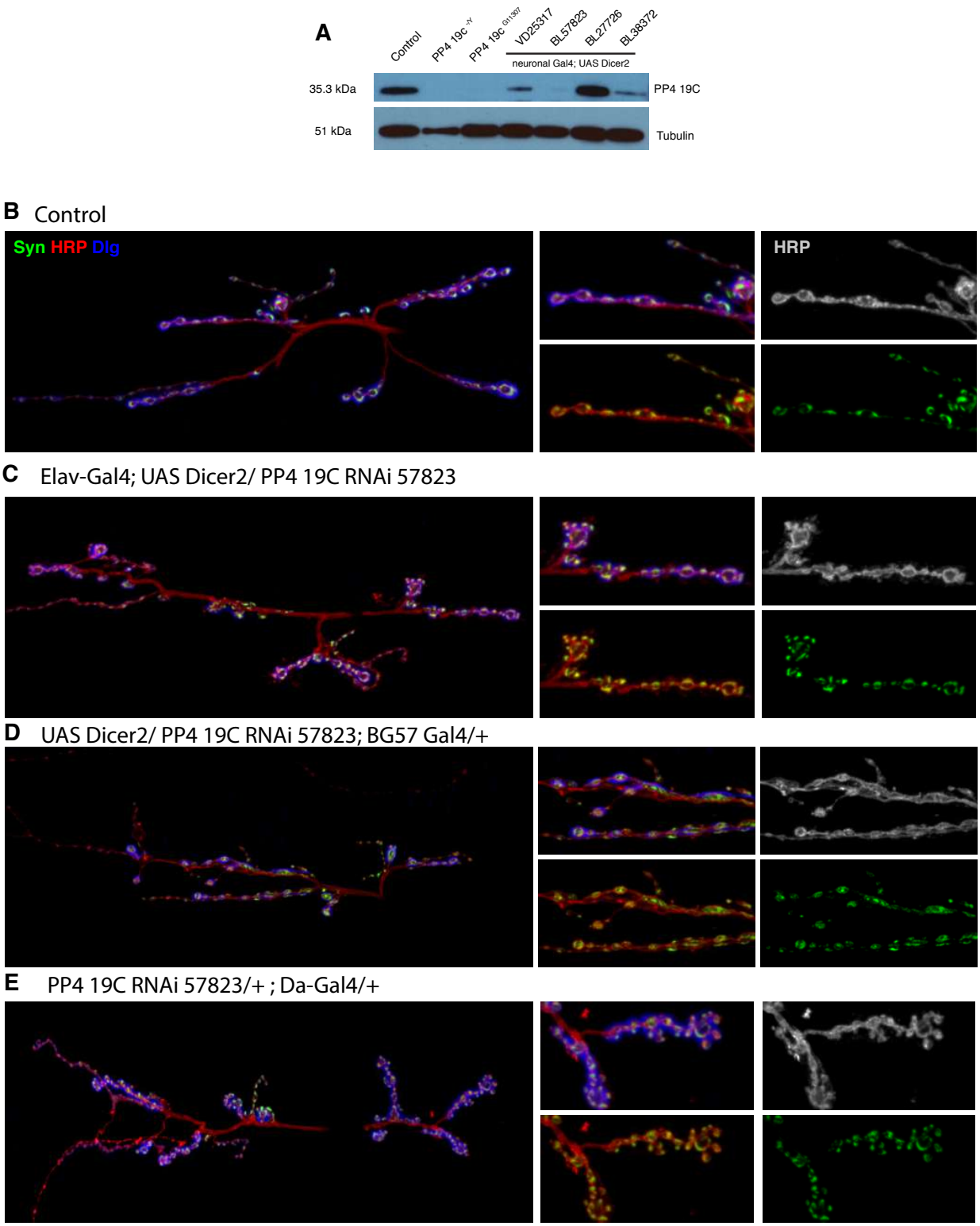

Figure 24 Analysis of NMJs upon tissue specific knockdown of PP4 19C. (A) Western blot demonstrating the expression of PP4 19C in different genotypes. Knockdown includes the transgenic RNAi lines from both VDRC and BDSC, where the BDSC stock BL57823 showed a significant knockdown of PP4 19C, while VD25317 achieved only a partial knockdown. (B) A control NMJ on the muscle 6/7 stained with anti Synapsin (green), membrane marked by anti HRP (red) and anti Dlg (blue) antibodies. Control NMJ shows well-grown and spread NMJ on the muscle. (C) Presynaptic knockdown of PP4 resulted in the formation of satellite boutons on

the larger boutons. (D) Postsynaptic knockdown of PP4 19C didn't show any significant change at the NMJ (E) Ubiquitous knockdown of PP4 19C resulted in increased numbers of satellite boutons similar to that of PP4 19C null animals.

observed after VD25317-mediated knockdown was due to off-target effects in addition to the partial knockdown of PP4.

We then analyzed potential NMJ phenotypes resulting from specific knockdown of PP4 using the RNAi line BL#57823. Similar to the null mutant, ubiquitous knockdown of PP4 resulted in a strong morphology phenotype with small boutons at late larval stage and with some satellite boutons at early 3rd instar stages (Figure 24 and additional data). We did not observe any defects in synapse stability (Figure 30).

4.3.4 Loss of PP4 leads to defective adult brain development

When we induced a neuronal knockdown of PP4 (*elav-Gal4*), we observed that most of the progeny died as late pupa, however we could also isolate a few adult escapers. These adult escaper animals displayed severe motor defects. Animals showed weak motor strength and displayed difficulties in hatching and walking. Analysis of the adult brain using anti-FasII and anti-Brp antibodies revealed severe impairments of brain development including poorly developed mushroom bodies and antennal lobes. Almost all brains displayed defective mushroom bodies with a near complete loss of α/α' and β/β' lobes. The glomeruli structures in the antennal lobes were severely perturbed (Figure 25). In order to better understand the role of PP4 in the brain development, we performed a mushroom body specific knockdown using the driver lines *c739- Gal4* and *OK107-Gal4*. *c739-Gal4* mediated knockdown resulted in normal γ lobes but defective αβ lobes (Figure 26 and 27). These animals displayed a decrease in the number of mushroom body neurons. Similarly, we observed defective mushroom body structures after *OK107-Gal4* mediated knockdown of PP4 19C. In addition, these animals showed defective eye development, as *OK107-Gal4* also drives Gal4-expression in the eye. We then analyzed larvae of PP4 knockdown under *OK107-Gal4* and found no abnormalities in the mushroom body structures when compared to controls (Figure 28). This indicates that PP4 is essential for the formation of mushroom body development by regulating neuronal division and potentially for axonal pruning.

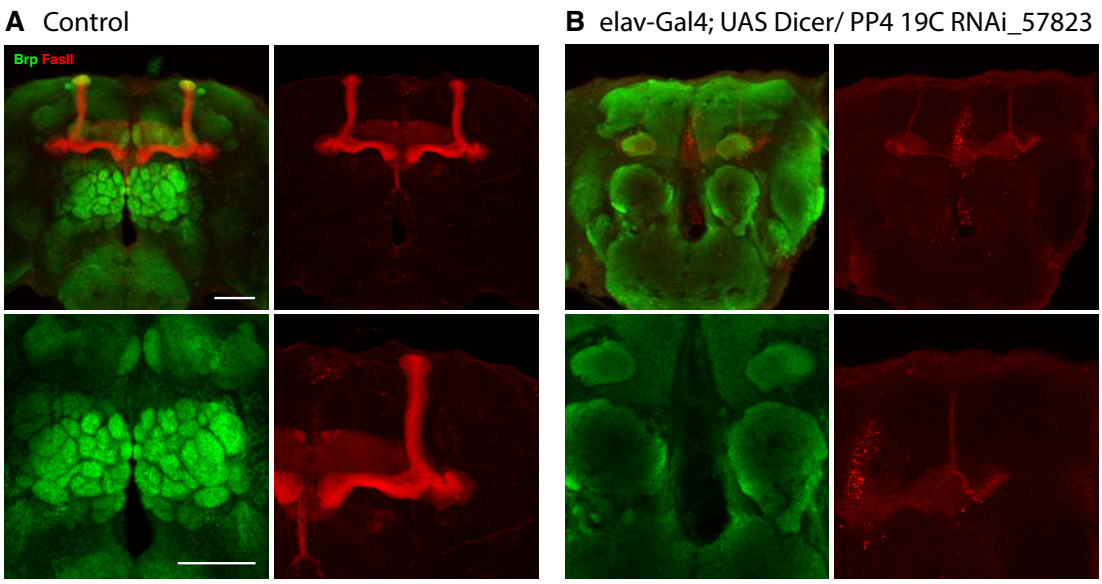

Figure 25 Effect of loss of PP4 on the adult brain

(A) Control adult brain with stained for mushroom bodies using Brp (green) and FasII (red) antibodies. Antennal lobe glomeruli structures (bottom left in green) and well-developed mushroom bodies are present (bottom right in red). (B) Knockdown of PP4 19C using a pan-neuronal driver (*elav^{C155}-Gal4; UAS dicer2/ PP4 19C RNAi_BL#57823*) resulted in sever developmental defects in the adult brain. Antennal lobes lose the glomeruli structures and resemble a smooth brain disorder in humans (bottom left in green) and have poorly developed mushroom body structures (bottom right in red). Scale bar represents 50µm.

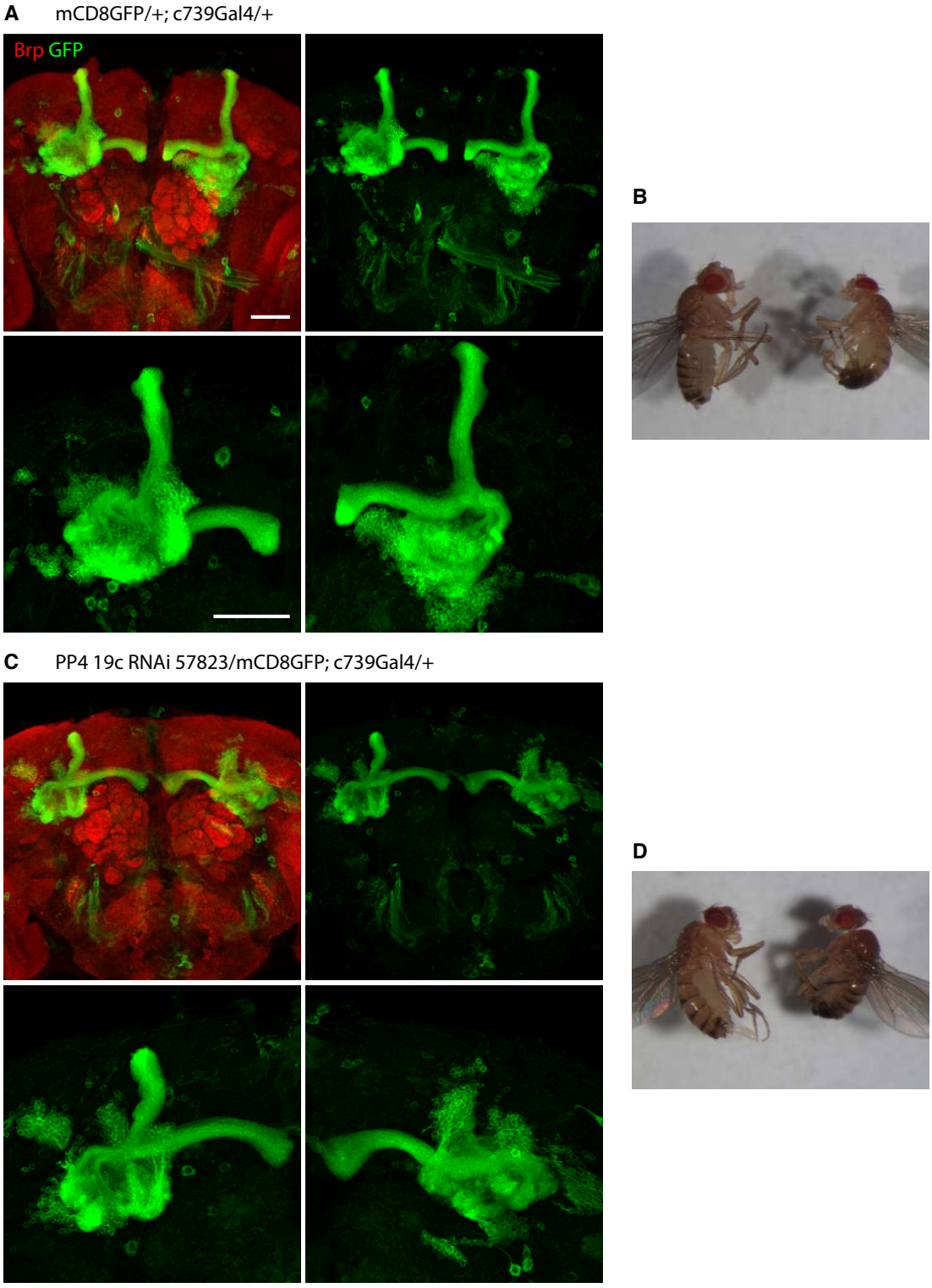

Figure 26 Effect of loss of PP4 in the adult brain (A) Control adult brain expressing mCD8GFP in mushroom body neurons using c739 Gal4 (*mCD8GFP/+; c739 Gal4/+*), stained with anti-Brp (red) and anti-GFP (green) antibodies. (B) Well-grown control adult flies without any abnormalities. (C) Adult brain showing defective α/α' lobe in the mushroom body with a reduced population of mushroom body neurons due to the knockdown of PP4 using c739 Gal4 (*mCD8GFP/BL#57823_PP4 19C RNAi; c739 Gal4/+*). (D) Well-grown adult flies without any abnormalities upon the knockdown of PP4 19C. Scale bar represents 50µm.

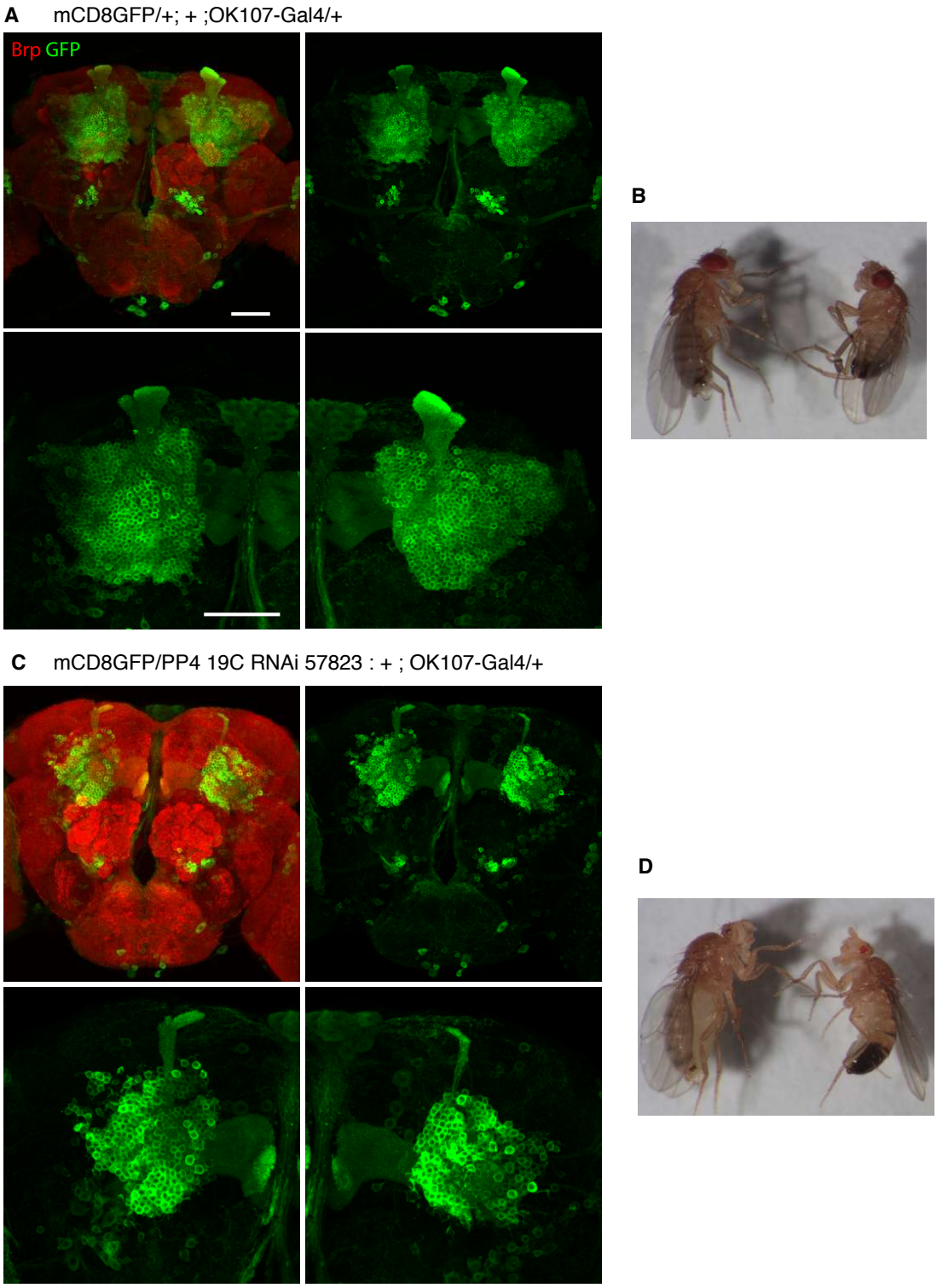

Figure 27 Effect of loss of PP4 in the adult brain

(A) Control adult brain expressing mCD8GFP in the mushroom body neuron using OK107 Gal4 (*mCD8GFP/+; +; OK107 Gal4/+*), stained with anti-Brp (red) and anti-GFP (green) antibodies. (B) Well-grown control adult flies without any abnormalities. (C) Adult brain showing defective α/α' lobe in the mushroom body with a reduced population of mushroom body neurons due to the knockdown of PP4 using OK107 Gal4 (*mCD8GFP/BL#57823_PP4 19C RNAi; +; OK107 Gal4/+*). (D) Adult flies with defective eyes due to the knockdown of PP4 19C. Scale bar represents 50µm.

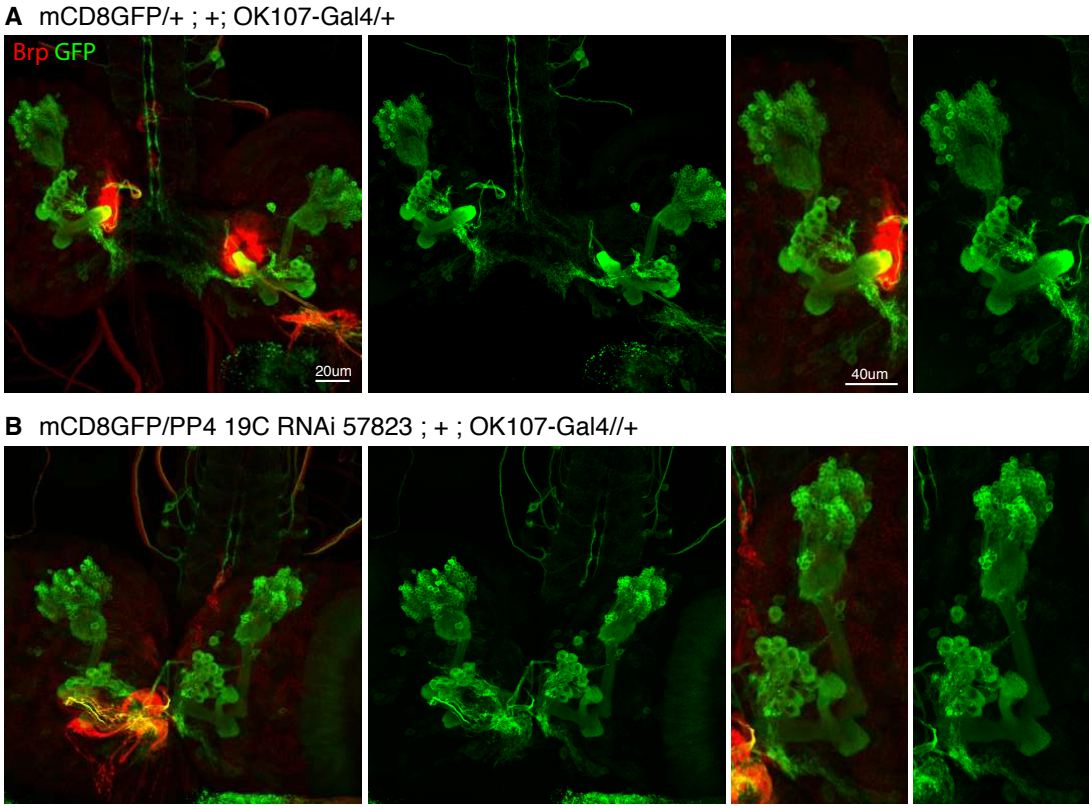

Figure 28 Effect of loss of PP4 in the larval brain

(A) Control 3rd instar larval brain expressing mCD8GFP in the mushroom body neuron under the OK107 Gal4 (*mCD8GFP/+; +; OK107 Gal4/+*), stained with Brp (red) and GFP (green) antibodies. (B) Larval brain showing well developed lobes in the mushroom body and population of mushroom body neurons even after the knockdown of PP4 using OK107 Gal4 (*mCD8GFP/BL#57823_PP4 19C RNAi; +; OK107 Gal4/+*). Scale bar represents 20µm and 40µm.

4.3.5 *PP4 19C* mutants showed abnormal mitochondria and endoplasmic reticulum

Also, next analyzed potential subcellular alterations caused by the absence of PP4 19C. Mitochondria and the endoplasmic reticulum are essential for the development and function of the nervous system. We used a single motor neuron driver (5053-Gal4) to analyze organelle organization in individual motor neurons. Using mito-GFP, we observed that absence of *PP4 19C* results in an increase in mitochondrial size while the number of mitochondria remained unchanged (Figure 29B, E). In a preliminary experiment, we also observed that mitochondria display impaired mobility (data not shown). Over expression of a phosphatase dead version of PP4 19C (UAS PP4 19C $^{[D85N, H115N]}$) also showed an increase mitochondria size (Figure 29B, E) indicating that PP4 19C is required for the establishment or maintenance of mitochondrial

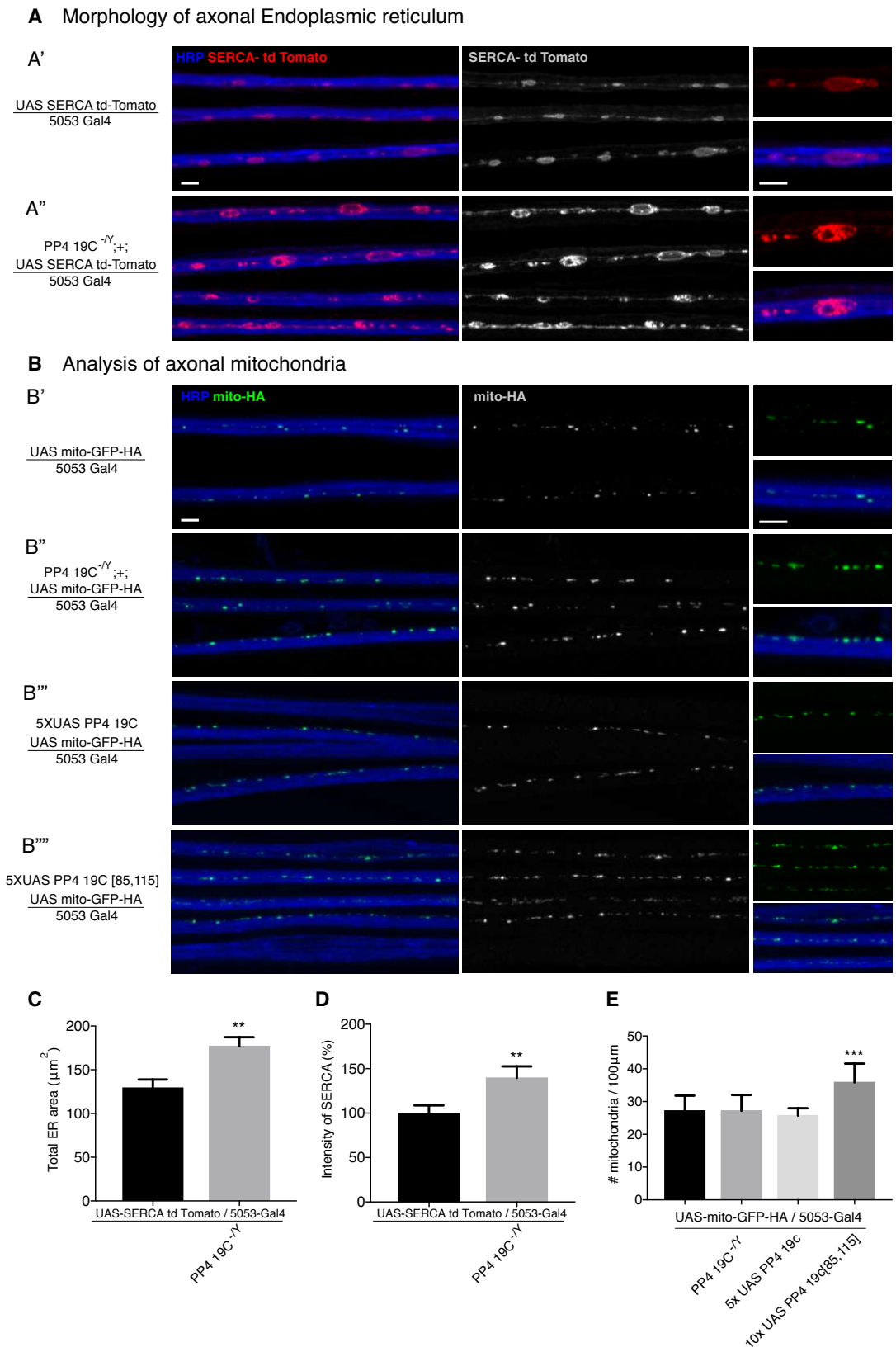

Figure 29 Effect of loss of PP4 on endoplasmic reticulum and mitochondria

Analysis of the morphology of the endoplasmic reticulum and mitochondria in axons. (A) Endoplasmic reticulum in the single axon is labeled by the expression of td-tomato tagged SERCA channel using the single motor neuron driver (*5053-Gal4*) and stained with anti td-tomato antibody. Control animals show a continuous endoplasmic

reticulum with small and smooth vacuolar structures along the length of the axon (A"), whereas loss of PP4 19C leads to a significant increase in the size of the vacuolar structures and with increased roughness in the structure (A"). Expression of SERCA in the ER is significantly increased in the absence of PP4 19C (D). All images were acquired using identical acquisition settings. (B) Mitochondria in the single axon is labeled by the expression of mito-GFP-HA using the single motor neuron driver (5053-Gal4) and stained with anti HA antibody. Control animals show small but occasionally slightly larger mitochondria along the length of the axon (B'). Loss of PP4 19C resulted in increase in the number of large mitochondria, however the number didn't show a significant change (B"). Overexpression of PP4 19C didn't show any significant changes in the mitochondria size and number (B"'). But, overexpression of a phosphatase dead version of PP4 19C resulted in an increase in the number of larger mitochondria (B""). (C) Quantification of total ER per 100µm length of axon, (D) quantification of intensity of SERCA channel (E) quantification of number of mitochondria per 100µm of axon among the genotypes. Error bars representing SEM; *, P≤0.05; **, P ≤ 0.01; ***, P ≤ 0.001; ns: not significant; ANOVA and Tukey multiple comparison test; n=15 axons. Scale bars represent 5µm.

morphology. It might be possible that these mitochondria might fail to undergo fusion-fission processes in the absence of PP4. It has been reported that defective mitochondria are kept less mobile in order to undergo mitochondrial recycling (Dahlmans et al., 2016; Mishra and Chan, 2016; Wai and Langer, 2016). Thus, mitochondria of *PP4 19C* mutants might be functionally defective. Prior studies showed that phosphorylation of Cdk1 and Cdk5 regulates mitochondrial fusion and fission (Strack et al., 2013) and that Cdk1 activity is controlled by PP4 (Toyo-oka et al., 2008b; Voss et al., 2013). It will be interesting to determine the precise molecular mechanisms underlying the mitochondrial abnormalities.

Finally, we analyzed the morphology of endoplasmic reticulum by expressing the td-tomato tagged SERCA (Sarco/Endoplasmic Reticulum Ca^{2+} ATPase) channel that localizes to the ER and is commonly used as a marker to label ER both in vertebrates and invertebrates. SERCA is an ER Ca^{2+} pump that regulates calcium homeostasis in the cell. When the td-tomato tagged SERCA is expressed under the single motor neuron driver in *PP4 19C* mutants, we observed changes in ER morphology compared to controls. The ER of *PP4 19C* mutants appeared bigger in size with increased roughness in vacuolar structures, while the ER of control animals was smaller and with a smooth vacuolar structure (Figure 29A, C). In addition, *PP4 19C* mutants showed an increase in the intensity of the SERCA channel (Figure 29D). It will be of the importance to elucidate the precise function of PP4 in the regulation of endoplasmic reticulum morphology and function in the future.

4.4 Discussion

Regulation of cellular mechanisms requires controlled and timely activity of kinases and phosphatases mediate on-off processes. In a screen focused on the identification of essential kinases and phosphatases in the regulation of synaptic plasticity (Bulat et al., 2014) identified PP4 as a potential regulator of synaptic plasticity. PP4, a serine/threonine phosphatase of the PP2A family of phosphatases is ubiquitously expressed and is conserved across all species. It has been reported that loss of function of PP4 is embryonic lethal. However, our clean deletion mutant of *PP4 19C* survived until the late 3rd instar stage. *PP4 19C* mutant larvae exhibit a small developmental delay in growth but survive as 3rd instar larvae for more than 10 days before they die. These larvae do not contain any developed imaginal discs, likely due to the importance of PP4 in the regulation of cell division. PP4 is essential for centrosome-mediated cell division, chromosomal segregation during cell division and also plays an essential role in cell cycle regulation (Helps et al., 1998; Lee et al., 2012; Liu et al., 2011a; Liu et al., 2012; Pfeifer, 2012; Sumiyoshi et al., 2002; Toyo-oka et al., 2008b; Voss et al., 2013). A potential reason for the extended 3rd instar stage arrest could be an impairment of neuronal cells involved in the regulation of the ecdysone-dependent molting system.

Preliminary RNAi based analysis of PP4 knockdown using line VD25317 pointed towards a role in the regulation of synaptic stability and morphology (Bulat et al., 2014). The observed phenotypes resembled the phenotype due to loss of function mutations of adducin, an actin-capping molecule (Pielage et al., 2011). Our analysis using the newly generated and molecularly defined *PP4* null allele demonstrated that PP4 19C is not required for the regulation of synapse stability. Our western blot analysis revealed that the knockdown of PP4 19C by VD25317 is not fully effective indicating that the RNAi line VD25317 might exhibit off-target effects. Analysis of the null mutation clearly showed that loss of PP4 19C does not affect NMJ morphology until day 6 (late 3rd instar), but then led to a dramatic increase in satellite boutons. The prolonged pupation process and thus the extended larval stage might be the underlying reason for the defective NMJ morphology. However, as NMJs of other extended 3rd instar larvae mutations (knockdown of torso in the ring gland) did not show such phenotypes (Miller et al., 2012a), it may indicate a novel requirement of PP4 in the regulation of NMJ development. Future analysis of neuron-specific PP4 mutations will be necessary to determine the precise role of PP4 in nervous system development.

We observed various other defects due to the loss of function of PP4 in neurons. Loss of PP4 resulted in abnormal mitochondrial and endoplasmic reticulum morphology. Cdk1 and Cdk5 have been reported to regulate the mitochondrial dynamics and PP4 has been demonstrated to regulate the activity of Cdk1 (Strack et al., 2013; Toyo-Oka et al., 2008a). In addition Cdk1 is important for the remodeling of cell organelles during mitosis (Lowe and Barr, 2007). The observed ER and mitochondrial phenotypes in the absence of PP4 19C reveals an interesting novel requirement of PP4 in post mitotic cells.

Finally, we could demonstrate that PP4 is essential for the development of the brain. In the absence of PP4 19C brain size is dramatically reduced with defective mushroom bodies and antennal lobes. PP4 has been demonstrated to regulate neuroblast division. Loss of PP4 19C thus likely impairs neurogenesis during metamorphosis, resulting in underdeveloped brain structures. *PP4* mutant animals also showed phenotypes consistent with defective axonal pruning. A recent study in Drosophila has demonstrated that loss of PP4 induces defects in axonal pruning in the central brain though RNAi analysis using the VD25317 transgenic line (Winfree et al., 2017). As we demonstrated potential off-target effects for this line, the reported results may be misleading. However, as this RNAi line achieves a knockdown efficiency of about 50% the reported phenotype might still be right. As Cdk5 has been reported to play essential role in the development of brain and mushroom body in Drosophila, by regulating microtubule dynamics in the central brain (Hayashi et al., 2006; Shah and Lahiri, 2017; Smith-Trunova et al., 2015), it may be possible that PP4 controls this process through Cdk1/Cdk5. A detailed analysis using the newly generated RNAi line (BL57823), our null mutant and selective drivers that are active during neurogenesis is essential to understand the function of PP4 in neurogenesis and axon pruning. In summary, our data clearly demonstrate essential functions of PP4 for the development and function of the nervous system.

4.5 Materials and methods

4.5.1 Generation of PP4 19C mutant and transgenic flies

We aimed to delete the *PP4 19C* gene locus without perturbing neighboring genes. We used CRISPR/Cas9 mediated genome editing to create a *PP4 19C* null allele. CRISPR targets were designed using CRISPR target finder from FLYCRISPR and were cloned into pBbsI-U6-gRNA vector. A donor vector was designed by cloning approximately 1kb sequence upstream from the 5' cut site and 1kb sequence downstream to the 3' cut site, which serves as the homology sequence during the homology mediated repair at the cut sites thereby resulting in the replacement of *PP4 19C* with the sequence between the homology arm. The dsRed cassette with the 3xP3 promotor facilitates the identification of the *PP4 19C* deletion. These vectors were injected into *vasa* Cas9 flies and mutants were identified by the dsRed expression in the F1 generation (see general materials and methods (6.7 & 6.8) for the detailed protocol).

We generated additional transgenic flies for *PP4 19C* (to express wild type PP4 19C untagged, tagged, phosphatase dead forms with and without tag). The cDNA for *PP4 19C* was obtained from the DGRC gold cDNA library. The p^{FLC-I} PP4 19C vector clone was obtained from the library, cultured, isolated the plasmid and sequenced with T7 primers to confirm the clone and the sequence for any polymorphisms. The cDNA was amplified with the primers designed for PP4 19C with added 5' CACC on the forward primer, which is essential for its cloning into the entry vector. Two reverse primers were made one with STOP codon and the other without to generate the p^{ENTRY}-*PP4 19C* with and without stop codons. The topo cloning reaction was set with the purified PCR product (phusion DNA polymerase was used) and the p^{ENTRY} vector as per the recommended protocol. The vectors were sequenced to verify the insertion. A LR clonase reaction was set using the entry vector and a destination vector using the recommended protocol. Multiple destination vectors were used in this study; p-10xUAST-rfa, p-10xUAST-rfa-EGFP, p-10xUAST-EGFP-rfa, p-5xUAST-rfa, p-5xUAST- EGFP-rfa, pDEST 15. In order to generate the transgenic animal to express the phosphatase dead version of PP4 19C, entry vectors PP4 $19C^{D85N,H115N}$ and PP4 $19C^{D85N}$ were obtained as a kind gift from Dr. Marcin R. Przewloka (Lipinszki et al., 2015). All vectors were sequenced to confirm the sequence. The vectors were sent to BestGene for injections to generate transgenic animals.

4.5.2 Generation of a PP4 antibody

The expression of PP4 19C protein was carried out using the pDEST-15 vector. A p^{Entry}

vector baring the PP4 19C$^{1-50}$ amino acid coding sequence was obtained as a kind gift from Dr. Marcin R. Przewloka (Lipinszki et al., 2015). Using LR clonase reaction, the sequence PP4 19C$^{1-50}$ was cloned into the pDEST-15 vector. The protein was expressed and purified by affinity purification column. GST- PP4 19C$^{1-50}$ was purified and sent as an antigen to Davis biotechnology ltd to raise an anti-rabbit antibody against PP4 19C. The generated antibody was further purified against the antigen and verified on a Western blot.

4.5.3 Immunostaining and Western blot

Wandering third instar larvae were selected for the staining the NMJ for different synaptic components. The larvae were washed in PBS, dissected in ice-cold HL3 dissection saline without calcium. The dissected larvae were fixed using Bouin's fixative for 5 minutes, washed thoroughly with PBST until the fixative is washed out completely. The washed larvae were then incubated with a variety of primary antibodies over night at 4°C. The larvae were washed 4 times 15 minutes in PBST to remove excess primary antibodies. The washed larvae were then incubated with the corresponding secondary antibodies labeled with Alexa fluorophores for 2 hours at room temperature. The larvae were washed and then cleared using 70% glycerol in PBS for 45minutes and mounted on the slide using prolong gold antifade reagent (Invitrogen). The following antibodies were used in the study: mouse anti-BRP (nc82; 1:250), mouse anti-syn (3C11; 1:50), mouse anti futsch (22c10; 1:500), mouse anti-FasII (1DF; 1:50), mouse anti-GluRIIA (8B4D2; 1:50), rabbit anti-Dlg (1:10,000), rabbit anti-GluRIIC (1:3000), rabbit anti-GFP (invitrogen;1:2000), rabbit anti-dsRed (Invitrogen; 1:2000), mouse anti-HA (1:100), HRP (cy3 or Alexa fluorophore; Jackson Immunoresearch laboratories).

Larval brains of wandering third instar larvae were isolated carefully and crushed on ice in NP-40 buffer with protease inhibitor. A minimum of 10-15 brains of each genotype were isolated. The crushed brain sample was incubated on ice for 30 minutes for further lysis. The sample was spun at 10,000g for 10 minutes and the supernatant was transferred to a fresh Eppendorf tube. Concentration of the protein was estimated using Bradford's method and the sample was denatured at 90°C for 10 minutes using sample denaturation buffer (Invitrogen). Equal concentrations or 3 brain equivalents of protein were loaded from each genotype. Protein electrophoresis was performed on 4-12% Bis-Tris NuPage gels (Invitrogen) according to the recommended protocol. Using a Western blot transfer protocol, the protein was transferred onto a PVDF membrane, blocked with 5% skimmed milk solution and treated

with primary and secondary antibodies in the blocking solution. The following antibody dilutions were used: rabbit anti-PP4 19C (1:500), mouse anti-β-tubulin (E7; 1:1000), goat anti-mouse-IgG-HRP (1:4000), goat anti-rabbit-IgG-HRP (1:4000). The blot was washed for 3 times 5 minutes after each antibody treatment and equal volume of chemiluminol and substrate was added, incubated for 15 minutes and developed using fuji X-ray films.

4.5.4 Statistical analysis

Statistical analyses were performed using Graphpad prism 7. One-way Anova was performed to compare the phenotypes between different genotypes. Significance levels were defined as following: *** $p \leq 0.001$, ** $p \leq 0.01$, * $p \leq 0.05$ and n.s. (not significant) $p > 0.05$.

4.6 Additional data

Analysis of synaptic stability upon conditional loss of PP4 19C

In the RNAi screen performed in the lab, loss of PP4 19C was reported to lead to synaptic instability. To confirm this, we performed detailed analysis of potential synaptic stability defects under different conditions. Using the null mutant, hypomorph and the RNAi line, we analyzed the condition of presynaptic, postsynaptic and ubiquitous knockdown of PP4 19C and found no synaptic instability defects including in the null mutants (Figure 30). In addition, loss of PP4 19C did not influence active zone or postsynaptic receptor components (Figure 31).

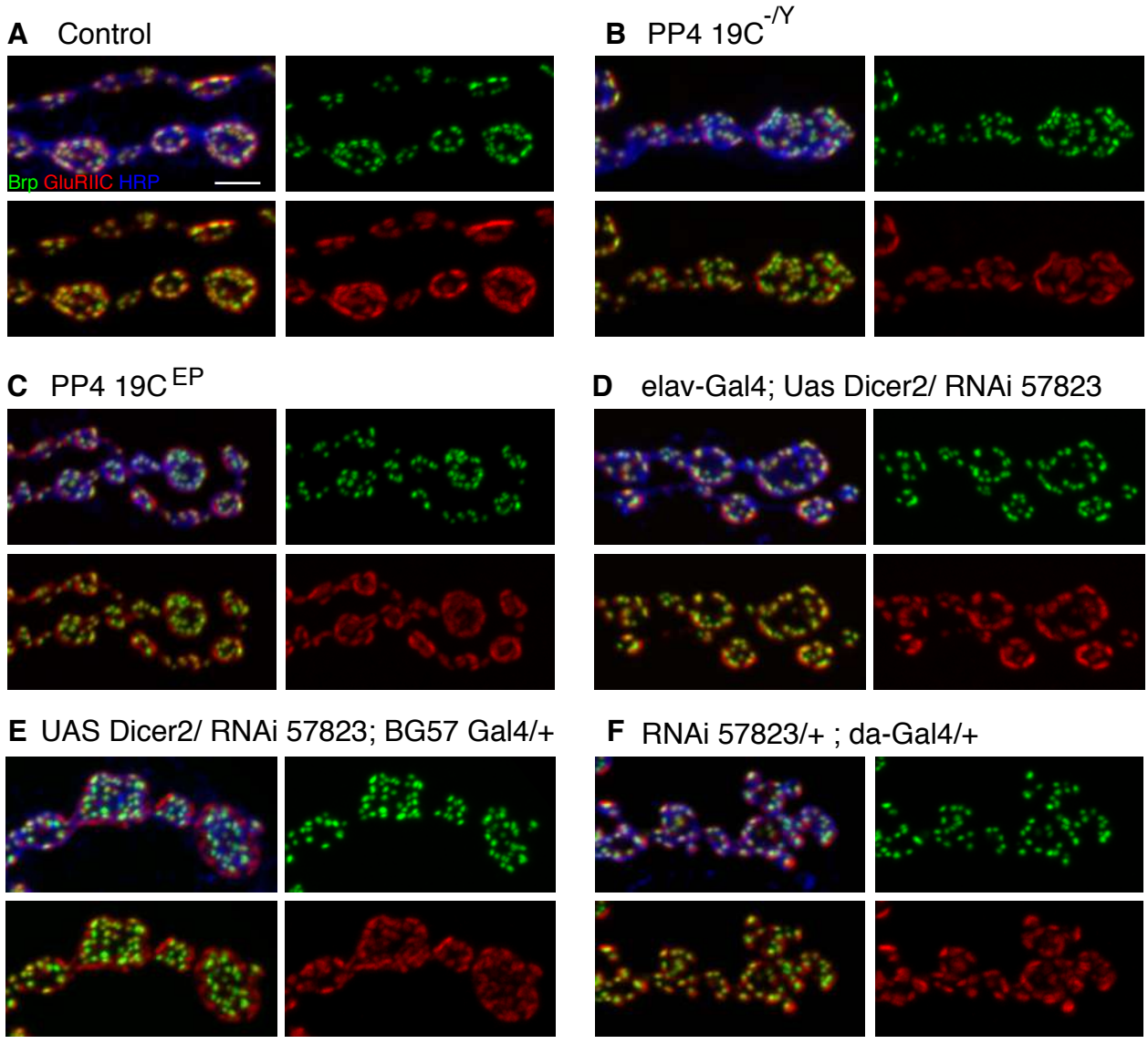

Figure 30: Analysis of synaptic stability. (A) Control NMJ with well-organized Brp (green), GluRIIC (red) and membrane labeled by HRP (blue). (B-D) *PP4 19C* null males (*PP4 19C*$^{-/Y}$) (B) hypomorphic male (*PP4 19C*$^{CG11307/Y}$) (C) and presynaptic knockdown of PP4 (D) did not show any changes in the organization of Brp and GluRIIC. (E) Knockdown of PP4 19C in the muscle appears to induce an increase in the density of active zones.

(F) Knockdown of PP4 19C using a ubiquitous driver did not alter the organization of Brp and GluRIIC. Scale bar represents 2µm.

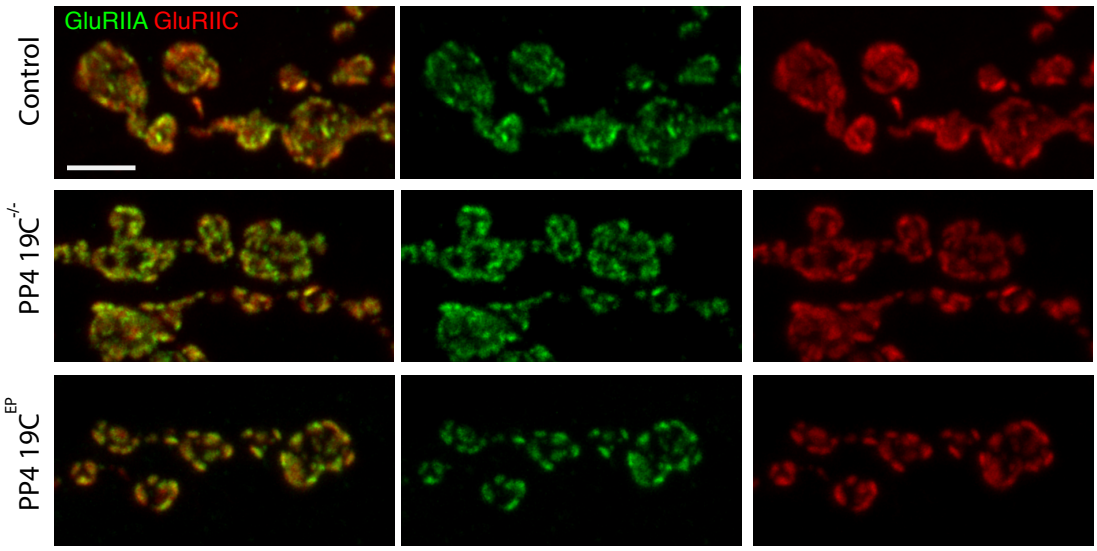

Figure 31: Analysis of GluRIIA and GluRIIC in *PP4* mutants. NMJ stained for GluRIIA (green), GluRIIC (red) for the following genotypes: control (*w1118*), *PP4 19C* $^{-/-}$ (*PP4 19C*$^{-/Y}$) and *PP4 19C*^{EP} (*PP4 19C*$^{G11307/Y}$). Scale bar represents 2µm.

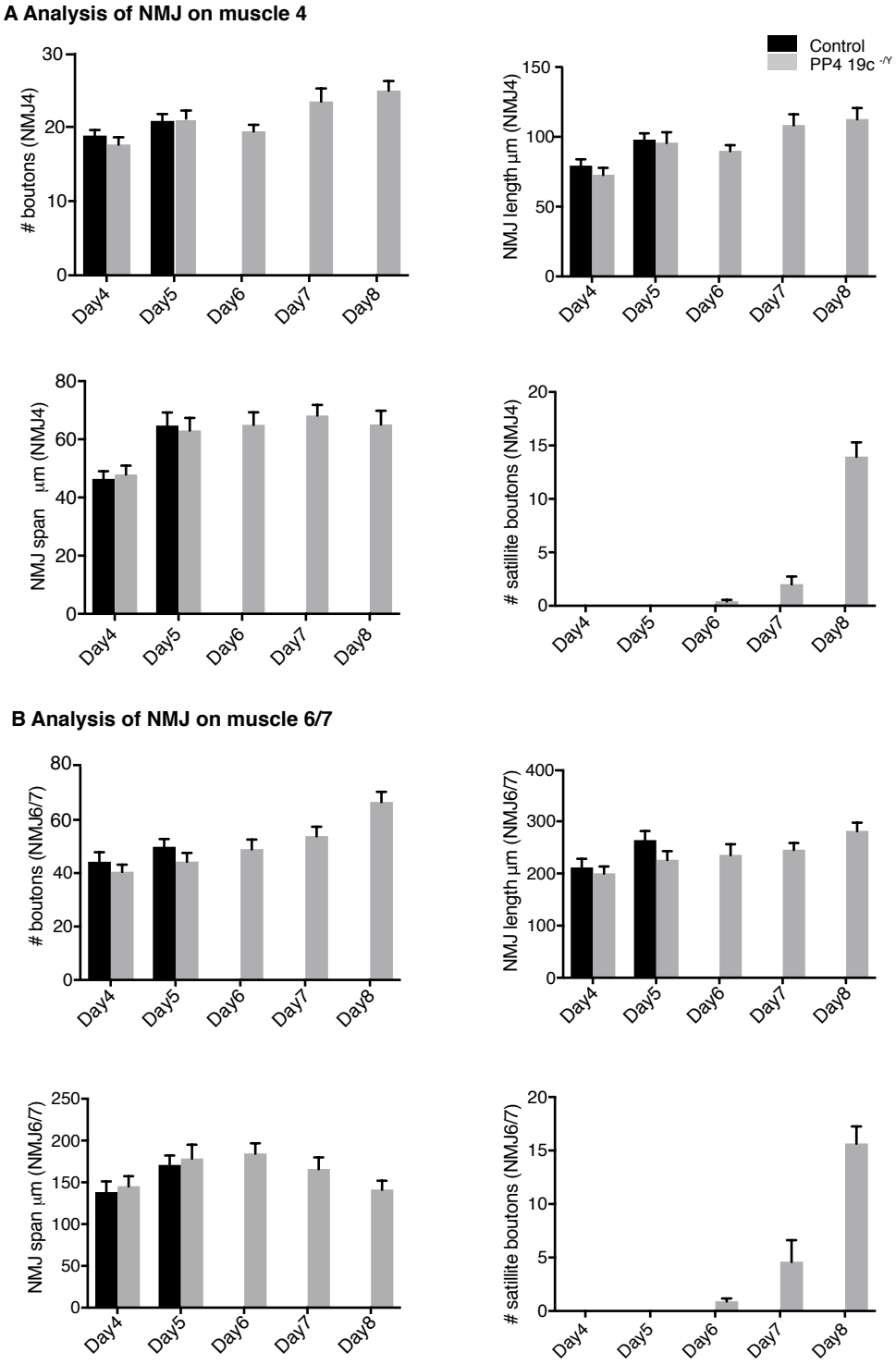

Figure 32: Quantification of NMJ phenotypes of *PP4 19C* null mutant larvae. Quantification of NMJ growth parameters on muscle 4(A) and muscle 6/7 (B) for control and *PP4 19C* null mutant animals. Number of boutons, NMJ length, NMJ span and number of satellite boutons.

5 Extended discussion

Protein kinases and phosphatases modulate the majority of cell signaling pathways in all cell types by controlling the activity of pathway components. Coordinated regulation of protein phosphorylation and dephosphorylation by kinases and phosphatases keeps the system balanced through homeostasic and adaptation mechanisms. In this study, we identified the pseudokinase Madm and the protein phosphatase PP4 as regulators of synaptic plasticity and function. Synaptic plasticity requires a coordinated regulation of pre- and postsynaptic mechanisms including the regulation of growth, cytoskeleton remodeling and recycling and activation of postsynaptic receptors. Many of these mechanisms dependent on each other during synaptic development and function and all depend on kinases and phosphatases.

5.1 Kinases and phosphatases in the regulation of the presynaptic terminal

Action potential that reach the presynaptic nerve terminal are transferred to the postsynapse through the release of neurotransmitters at the specialized structures called active zones. Synapses undergo structural changes depending on activity patterns in neuronal circuits. A series of kinases and phosphatases participates in these processes. Increased calcium concentrations due to the action potential at the presynapse can activate PP2A by inhibiting AMPK-dependent inhibition of PP2A (Park et al., 2013). Activated PP2A regulates the organization of active zone and synaptic morphology by controlling microtubule dynamics (Viquez et al., 2009; Viquez et al., 2006). In addition, activated PP2A controls CaMKII mediated synaptic plasticity by inducing activity dependent structural changes and functional changes at the synapse (Colbran, 2004). Multiple such mechanisms work in combination to make the circuit flexible to respond to different kinds of stimuli. Here, we identified the pseudo-kinase Madm as a regulator of synaptic structure, dynamics and function acting in parallel with the mTOR pathway. We also demonstrated that PP4 affects neuronal mitochondria and the endoplasmic reticulum, thereby likely affecting calcium dynamics at the presynapse.

5.2 Kinases and phosphatases in the regulation of postsynapse

Regulation of postsynaptic processes during synaptic plasticity is well studied in vertebrates. Change in dendritic morphology and receptor composition are mediated by a number of kinases including CaMKII, CaMKIV, PKC, Cdk5, PKA, and LIMK1. Only very few

phosphatases like CaN, PP1 and PP2A have been demonstrated to participate in postsynaptic processes by regulating phosphoproteins including e.g. neurabin1 or spinophilin. mTOR signaling in the postsynapse has been demonstrated to be essential for the regulation of receptor assembly (Sigrist et al., 2000; Sigrist et al., 2002) and synaptic homeostasis (Penney et al., 2012; Penney et al., 2016). Interestingly, the phosphatase PP1 has been demonstrated to be essential for the regulation of synaptic homeostasis by downscaling synaptic parameters (Siddoway et al., 2013). Similarly, we could demonstrate that Madm is an essential regulator of synaptic plasticity by regulating synaptic homeostasis and also by affecting GluRIIA receptor expression. In the future it will be essential to identify the entire set of kinases and phosphatases contributing to synapse development and function.

6 General Materials and Methods

6.1 Genomic DNA preparation

Reagents required:

Stock solution:

1M Tris HCl, pH7.5; 500mM EDTA, pH8.0; 5M NaCl; 10% SDS; 5M Potassium acetate (KAc); 6M LiCl

Buffer A

100mM Tris HCl, pH7.5; 100mM EDTA pH8.0; 100mM NaCl; 0.5% SDS

LiCl/KAc Solution

1.44M KAc; 4.3M LiCl

RNAse A (1mg/mL)

- Dissolve 10mg RNAse A in 1ml of 15mM NaCl, 10mM Tris, pH7.5 in an Eppendorf tube
- Boil for 15 min on the heat block
- Allow the sample to cool down slowly at room temperature
- Aliquot in 10 Eppendorf tubes
- Use 10 µL and dilute with 990 µL ddH_2O to get 1 µg/mL concentration

Protocol:

- Collect the samples of about 15 flies per Eppendorf tube
- On ice, add 200 µL of Buffer A to each sample
- Homogenize the flies using a disposal tissue grinder aand add 200 µL of Buffer A
- Incubate at 65°C for 30 minutes
- Add 800 µL of freshly prepared LiCl/KAc solution and invert several times to mix and incubate on ice for 10 minutes
- Spin at 14000 rpm for 15 minutes at room temperature
- Transfer the supernatant to a fresh Eppendorf tube (care is taken to exclude the floating solids)
- Supernatant is spun again to remove the floating solids if any present
- Add 800 µL of isopropanol and mixed well by inverting several times
- Spin at 14000 rpm for 10 minutes at room temperature
- Aspirate and discard the supernatant, quick spin and aspirate
- Wash the pellet with 500 µL ice cold 70% EtOH
- Spin 5min at 14000 rpm in a microfuge at room temperature

- Aspirate and discard supernatant, quick spin, aspirate again
- Air dry the pellet for about 2 hours
- Resuspend the pellet in about 70µL ddH2O with RNAse (20 µg/mL) over night at room temperature, store at -20°C

6.2 PCR reaction

DNA	1µL
Forward Primer	1µL
Reverse Primer	1µL
PCR Buffer	5µL
$MgCl_2$	1.5µL
*dNTP*s	1µL
Taq Polymarase	0.2µL
H_2O	37.3µL (make up to 50 µL)

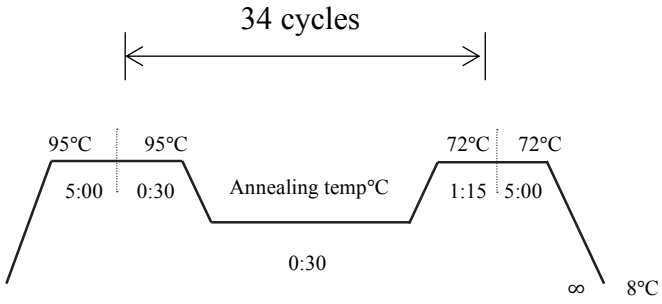

6.3 Restriction Digestion reaction

DNA	1µg
Restriction enzyme	1µL
10X Buffer	5µL
H_2O	make it to 50 µL

Incubate at 37°C for 1hour

6.4 Ligation reaction

Insert DNA	150ng
Vector DNA	200ng
Ligation buffer	2 µL
T4 DNA ligase	1 µL
H_2O	make it to 20 µL

Incubate at room temperature for 3 hours

6.5 p^{ENTRY} cloning reaction

Entry vector	1 µL

Salt solution	1 µL
DNA (PCR purified)	2 µL
H_2O	make up to 5 µL

Incubate at room temperature for 30 minutes and transform

6.6 LR clonase reaction

Entry clone	100ng
Destination vector	150ng
LR clonase II enzyme mix	1 µL
TE buffer pH8.0	to 8 µL

Incubate the reaction at 25°C for 1hour

Add 1 µL of Proteinase K to each sample and incubate it at 37°C for 10 minutes

1 µL of each LR reaction was transformed into 50 µL of OneShot phage resistant cells using the recommended protocol.

6.7 CRISPR Cloning

Genome editing using CRISPR/Cas9 requires the presence of DNA nuclease Cas9 enzyme and a chimeric guide RNA (gRNA) sequence in the cell. Cas9 enzyme induces a site-specific double stranded break with the help of gRNA. gRNA is the key for the site specificity as the gRNA hold the target sequence and recruits the Cas9 to the target. Cas9 recognizes the protospacer adjacent motif (PAM) in the target, usually (-NGG) and cleaves the DNA 3 nucleotides upstream of the PAM sequence. A 20-nucleotide sequence upstream to PAM sequence can act as a potential target. The probability of availability of similar sequences at multiple locations in the genome is high and the appreciable tolerance of CRISPR system towards the mismatch in the target demands the identification of unique target sequences. Guide RNA expression vectors are generated using the unique target sequences and injected into the cell. Once the gRNA is expressed/injected into the Cas9 expressing cells, a site-specific double stranded break is induced through the interaction of Cas9-gRNA with the DNA. The induced double stranded break triggers the DNA repair mechanism in the cell. Cell follows two major DNA repair mechanism; (1) non-homologous end joining (NHEJ) that repairs the broken DNA by ligating the ends which includes addition or deletion of some sequence at the

broken ends resulting in changes in the genome, (2) homology directed repair (HDR), where the DNA repair mechanism uses the homologous sequence as a template and repairs the DNA break by synthesizing the DNA between the breaks. Taking the advantage of these mechanisms, one can edit the genome by designing the appropriate gRNAs to induce site-specific cleavage by Cas9 and the vectors that carry the homologous sequence around the target sites.

6.7.1 Identification of CRISPR targets

To design the CRISPR targets, genomic sequence of PP4 19C was obtained from flybase and annotated. The gene is located on the first chromosome at 19D1; spans about 3 kb with two untranslated and two translated exons coding single protein PP4 19C. The genomic sequence from 3 kb upstream to 3 kb downstream of PP4 19C was fed to the CRISPR optimal target finder tool developed by FLYCRISPR. All possible CRISPR targets with zero off-targets were identified and assembled to the annotated gene sequence to identify the target locations on the gene. All possible targets were chosen to perform a minimal deletion covering all exons. Priority was given to the targets with 5'G and a 5'G was added to the targets which lacks 5'G (as per the CRISPR protocol). Finally, two pairs of targets were chosen to perform two independent deletions by generating DNA break upstream and downstream of PP4 19C. These target sequences were used to generate the gRNAs and the homologous sequence for the donor vector is designed around these sequences ie, up to approximately 1kb upstream or downstream from the cut site.

6.7.2 Generation of U6-gRNA (chiRNA) vectors

U6-gRNA vector was obtained from addgene (p-U6-BbsI-chiRNA; cat# 45946). The sense and anti-sense sequences for the chosen targets were obtained without the PAM (NGG) sequence. BbsI restriction site (sense oligos: 5' – **CTTCG** (19 nt) – 3' and anti-sense oligos: 3' – C (19 nt) **CAAA** – 5') was added to the targets, which are complementary to the overhangs generated by the digestion of U6-gRNA with BbsI restriction enzyme. The sense and anti-sense target oligos were synthesized with 5' phosphorylation. Oligos were diluted to 100 µM in H_2O and the following reaction was set up and run on a thermocycler as per the program below to anneal the sense and anti-sens oligos.

1µL sense oligos

1µL anti-sense oligos

1µL 10x T4 ligation buffer

7µL water

Thermocycler program:

95˚C for 5 min followed by ramp to 25˚C at a rate of -0.1˚C/sec.

1µg of U6-gRNA was digested with BbsI restriction enzyme (NEB) as per the protocol recommended. 1µL of Calf Intestinal Alkaline Phosphatase (NEB) was added to dephosphorylate the cut ends of the vector. The digested vector was run on 1% agarose gel and purified using the Qiagen gel purification kit. The concentration of the purified product was determined using a Nanodrop. The annealed oligos and the purified digested U6-gRNA vector were ligated by the following reaction:

50ng BbsI digested pU6-BbsI-gRNA

1µL annealed oligo insert

1µL 10x T4 ligation buffer

1µL T4 DNA ligase (NEB)

H_2O to 10µL

Reaction was incubated at 25˚C for one hour and transformed into DH5α cells and plated on LB agar plates with ampicillin. Insert was confirmed by sequencing the vectors with T7 forward and reverse primers. The quality of the vector was analyzed by restriction digestion using multiple cutter enzymes. The product was run on 1% agarose gel and sharp clear bands with no smear were confirmed.

6.7.3 Construction of pHD-DsRed-attP dsDNA donor vector

The pHD-DsRed-attP dsDNA donor vector was obtained from addgene (cat# 51019). The vector is designed to replace the genomic DNA or introduce a new sequence into the genome at the cut sites using homology directed repair (HDR). The vector contains a cassette with multiple cloning site (MCS), 50-bp attp phage recombination site, loxP, 3XP3-DsRed-SV40, loxP, multiple cloning site. MCS on either side is built with unique restriction enzymes to facilitate easy cloning of homology arm into the MCS.

6.7.4 Homology arm Design and cloning

Cas9 cleaves the DNA at 3 nucleotides upstream to the PAM sequence of the target. The homology arm is designed upstream and downstream from the point of cleavage or deletion with a minimum size of 1kb. First, the sequence upstream and downstream of the cut sites were sequenced and verified for the polymorphism in the genome of the stocks in which the deletions are to be made (vas-Cas9 stocks; BL#51324). Homologous arms upstream and downstream of the desired deletion site were selected; primers were designed to clone the homology arm and selected restriction sites were added on the 5' end of the primers as shown below. Precautions were taken during the selection of restriction enzymes to avoid a second cut in the vector and in the selected homology arms.

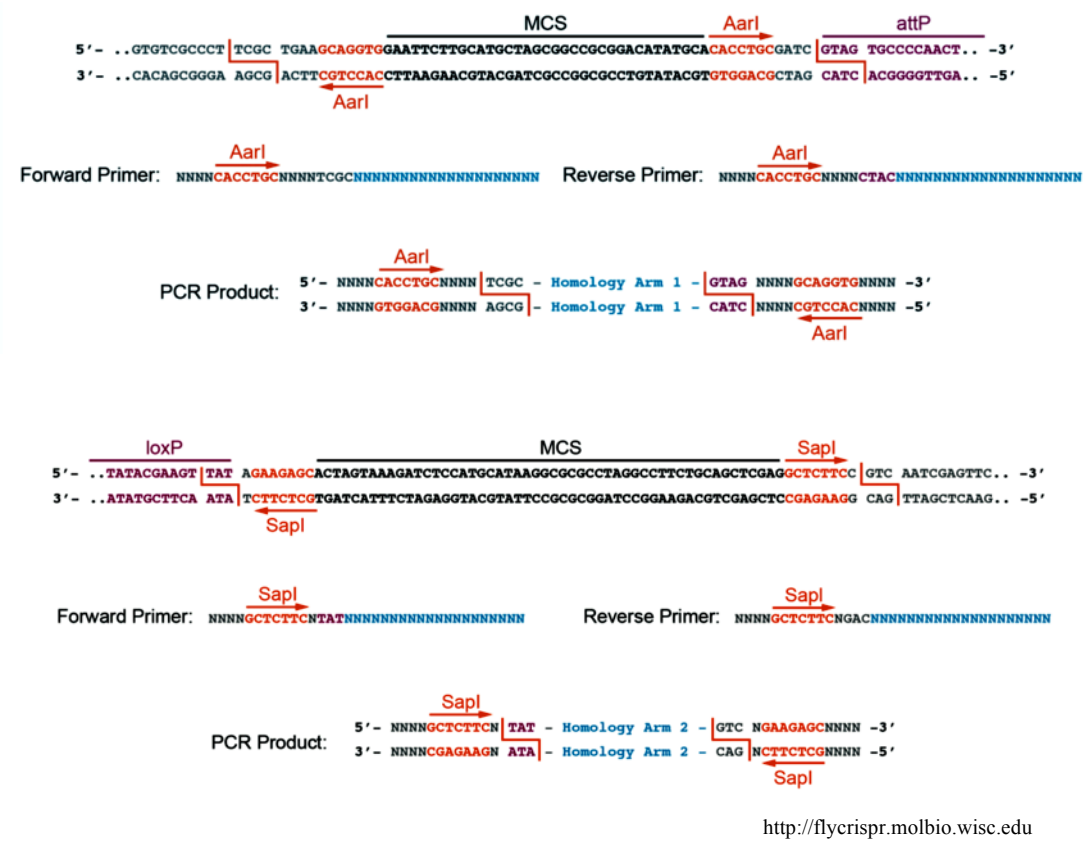

http://flycrispr.molbio.wisc.edu

The pHD-DsRed-attP dsDNA donor vector was first digested with AarI restriction enzyme following the protocol recommended, purified and concentration was estimated as mentioned above. Meanwhile, a PCR reaction was performed with the primers containing the added AarI restriction site using the genomic DNA from the flies that were selected for injections. The product was purified with the PCR purification kit as per the protocol recommended (Qiagen). The purified PCR product was digested with the AarI restriction enzyme and purified to avoid the self-ligation of cut ends. The purified pHD-DsRed-attP dsDNA donor vector digest was ligated with the purified homology arm digest using the

ligation protocol. The ligated product was transformed into DH5-α competent cells and plated on LB agar plates with ampicillin. The positive colonies were verified by a PCR reaction with the primers used to clone the inserted homology arm. The plasmid DNA was isolated from at least 3 positive clones and sequence was verified. The primers used for sequencing the homology arms were designed in a way that these primers could sequence at least 200bp on either side of the ligation sites. Similarly, the second homology arm is cloned into the pHD-**Homology_arm1**-DsRed-attP dsDNA donor vector using SapI restriction enzyme and sequenced. The quality of the vector was estimated using restriction digestion as mentioned above. Now, the vector pHD-**Homology_arm1**-DsRed-attP- **Homology_arm2** is ready for injection.

6.8 Microinjection

6.8.1 Materials required

Injection needles, DNA loading tips, Glass slides Glued-Cover slips, Voltolef oil – 10S, Brushes, Moderately sharp metal needles, Humid chamber, 50% Bleach, PBST, Dechorinating chamber, Timers (2 in number), Clean cages, Apple Juice agar plates (embryo collection medium), Yeast paste, Blade, DNA mix, Distilled Water

6.8.2 Embryo collection

The flies were raised at 25°C in large vials to collect enough number of age matched flies

Day 1:

- Clean cages were prepared with a little yeast paste spread on the apple juice plates.
- 3-5 day old flies were collected to make 3-4 cages (approx. 150-200 flies per cage to collect enough embryos).
- Flies were kept in the cages for at least 18h-20hrs at 25°C with changing the apple juice agar plates every 4hrs.
- Glued coverslips were prepared by applying glue for 3/4th of the area from one margin.

Day 2: (On the day of injection)

- The apple juice plates in the cages were changed every 2hr with a fresh plate (for at least 3 times)
- And again, at every 30 minutes for at least 3 times before embryo collection (to reduce the collection of unfertilized eggs); the cages are now ready to collect embryos

- Embryos were collected at every 20-25 minutes by replacing a fresh apple juice plate (use this time to mount the needle)
- The apple juice plate with freshly collected embryos were washed gently with PBST using a brush to collect the embryos
- Embryos were transferred into the bleaching chamber and washed with water to remove the excess yeast
- Embryos were dipped in 50% bleach for 30 seconds for dechorination (time and concentration can be adjusted according to the efficiency and concentration of bleach)
- Dechorinated embryos were washed with water and the chamber containing dechorinated embryos was placed in the fresh water to avoid drying of embryos
- A small piece of cold (stored at 4°C) apple juice agar was cut and placed it on a glass slide
- A straight line is marked using a blade on the agar and the embryos (20-50) were aligned along the straight line with their anterior pole towards the line using the moderately sharp metal needle under a stereo microscope with less possible light in order to avoid drying of dechorionated embryos (avoid embryos touching each other to facilitate even drying)
- The whole process of collection to alignment should not take more than 20 minutes
- Aligned embryos were transferred to the glued coverslips by gently touching the glued surface of the coverslip on to the aligned embryos. The embryos were transferred in a way that the posterior pole (side of injection) is towards the edge of the glued slide
- The embryos holding cover slip was transferred on to a glass slide exposing the embryos. A drop of voltalef 10S oil is used to stick the cover slip on the glass slide
- Embryos were allowed to air dry for 1-2 minutes depend upon the room humidity and temperature conditions. Drying of embryos was verified by a gentle poke on the embryo using a sharp needle. A properly dried embryo will show a depression with folding surrounding the poke and regains the membrane structure once the needle is taken back. Proper drying is necessary to facilitate better injection. Less dried embryos will break on injection and more dried embryos will die
- After proper drying, the embryos were covered with Voltalef10S oil and taken for injection.

6.8.3 Injection

- Good sharp needles with proper opening were selected
- Empty needle was plugged and the injection conditions were adjusted (injection pressure (P_i) and compensation pressure (P_c)), following the femtoJet operating manual
- Injection parameters were adjusted by injection pressure pulse with the needle immersed in a drop of Voltalef 10S oil
- The injection pressure was adjusted based on the size of the air bubble formed upon the injection. The pressure was adjusted such that the size of the air bubble formed due to single injection doesn't exceed the approximate $1/4^{th}$ width of the embryo at the center
- The DNA mix (5-10µL) was loaded into the needle and the compensation pressure was adjusted (compensation pressure was adjusted such that a little DNA mix is pushed out of the needle without the injection pressure pulse)
- The needle is adjusted at an angle of 5-10° between the slide and the tip of the needle
- Embryos were injected by moving the embryos towards the needle
- Care was taken to maintain the sharpness of the needle and the needle is changed for every 100 embryos
- Embryos were injected before blastoderm cellularization, a developmental stage that begins 45-50 minutes after eggs were laid at 22°C. Cellularization can be identified under the microscope and were destroyed by piercing the injection needle through the embryos to the other end. Injections were performed with in the first 45 minutes after egg laying
- The coverslip with injected embryos was transferred on to the apple juice plate with little yeast paste. Embryos were covered with voltalef 10S oil and the plates were left in a humidified chamber at 18° or 22°C
- The plates with injected embryos were regularly monitored to collect the larvae from the injected embryos (No force/push should be applied on the larvae to get out of the embryonic membranes even if it is half out)
- Completely developed and free moving larvae were collected into a fresh food vial (normal fly food) with maximum of 50 larvae in one vial

- The larvae were raised at 22°C and the adult flies were collected.
- Every individual fly was crossed with balancer flies (F0). FM6-GFP/Nrg^{14} flies were used to screen the PP4 19C deletion mutants
- The larvae from the F1 generation were screened under the fluorescent binocular and dsRed positive larvae were selected and transferred into a fresh vial
- Adults from the screened larvae were collected and stock was established using the balancer males
- The generated mutants contain vasa-Cas9 in the genome. Few females from the stock was crossed with wild type males, screened for non cas9 expressing (green florescence in the eye due to the artificial promoter expressing GFP used in the cas9 insertion and screening) dsRed positive flies and stock was established

6.9 Buffers and media

Dissecting saline 1x (1 L, no calcium)

4.08 g NaCl

4.08 g MgCl2 6H2O

0.36 g KCl

1.2 g HEPES

0.84 g NaHCO3

39.2 g Sucrose

40 ml EGTA (0.5M)

Adjust to pH 7.0 with NaOH

PBS 10x (1 L)

75.97 g NaCl

9.94 g Na2HPO4

4.14 g NaH2PO4

Adjust to pH 7.0 autoclave

Apple juice plates (2 L)

24 g Sucrose

60 g agar agar

Autoclave and cool down

40 ml 100% ethanol

20 ml 100% acetic acid

Standard fly food (30 L)

130 g Fadenagar

80 g USB agar

Dissolve in 10 l hot water

1070 g corn meal (in 2.5 l warm water)

1070 g malt

600 g treache (in 1.5 l warm water)

270 g soy meal (in 2 l warm water)

480 g try yeast

Mix all ingredients and cook for 10 min, cool down to 72 °C

64 g methyl hydroxyl benzoate (solved in 350 ml ethanol

NP-40 lysis buffer

150 mM NaCl,

1% NP-40,

50 mM Tris-HCl (pH7.5 - 8)

Before use, 1 tablet protease inhibitor (EDTA-free, Roche) was added to 10 ml of buffer. Stored at 4°C

7 Bibliography

Abdul-Sada, H., Muller, M., Mehta, R., Toth, R., Arthur, J.S.C., Whitehouse, A., and Macdonald, A. (2017). The PP4R1 sub-unit of protein phosphatase PP4 is essential for inhibition of NF-kappa B by merkel polyomavirus small tumour antigen. Oncotarget *8*, 25418-25432.

Aberle, H., Haghighi, A.P., Fetter, R.D., McCabe, B.D., Magalhaes, T.R., and Goodman, C.S. (2002). wishful thinking encodes a BMP type II receptor that regulates synaptic growth in Drosophila. Neuron *33*, 545-558.

Arellano, J.I., Espinosa, A., Fairen, A., Yuste, R., and DeFelipe, J. (2007). Non-synaptic dendritic spines in neocortex. Neuroscience *145*, 464-469.

Ataman, B., Ashley, J., Gorczyca, M., Ramachandran, P., Fouquet, W., Sigrist, S.J., and Budnik, V. (2008). Rapid activity-dependent modifications in synaptic structure and function require bidirectional Wnt signaling. Neuron *57*, 705-718.

Baines, R.A. (2004). Synaptic strengthening mediated by bone morphogenetic protein-dependent retrograde signaling in the Drosophila CNS. Journal of Neuroscience *24*, 6904-6911.

Baliki, M.N., Petre, B., Torbey, S., Herrmann, K.M., Huang, L., Schnitzer, T.J., Fields, H.L., and Apkarian, A.V. (2012). Corticostriatal functional connectivity predicts transition to chronic back pain. Nature neuroscience *15*, 1117-1119.

Ball, R.W., Warren-Paquin, M., Tsurudome, K., Liao, E.H., Elazzouzi, F., Cavanagh, C., An, B.S., Wang, T.T., White, J.H., and Haghighi, A.P. (2010). Retrograde BMP signaling controls synaptic growth at the NMJ by regulating trio expression in motor neurons. Neuron *66*, 536-549.

Ballard, S.L., Miller, D.L., and Ganetzky, B. (2014). Retrograde neurotrophin signaling through Tollo regulates synaptic growth in Drosophila. Journal of Cell Biology *204*, 1157-1172.

Bamburg, J.R. (1999). Proteins of the ADF/cofilin family: essential regulators of actin dynamics. Annu Rev Cell Dev Biol *15*, 185-230.

Banko, J.L., Hou, L., Poulin, F., Sonenberg, N., and Klann, E. (2006). Regulation of eukaryotic initiation factor 4E by converging signaling pathways during metabotropic glutamate receptor-dependent long-term depression. The Journal of neuroscience : the official journal of the Society for Neuroscience *26*, 2167-2173.

Banko, J.L., Poulin, F., Hou, L., DeMaria, C.T., Sonenberg, N., and Klann, E. (2005). The translation repressor 4E-BP2 is critical for eIF4F complex formation, synaptic plasticity, and memory in the hippocampus. The Journal of neuroscience : the official journal of the Society for Neuroscience *25*, 9581-9590.

Barnes, S.J., Sammons, R.P., Jacobsen, R.I., Mackie, J., Keller, G.B., and Keck, T. (2015). Subnetwork-Specific Homeostatic Plasticity in Mouse Visual Cortex In Vivo. Neuron *86*, 1290-1303.

Bastians, H., Krebber, H., Hoheisel, J., Ohl, S., Lichter, P., Ponstingl, H., and Joos, S. (1997). Assignment of the human serine/threonine protein phosphatase 4 gene (PPP4C) to chromosome 16p11-p12 by fluorescence in situ hybridization. Genomics *42*, 181-182.

Bateman, J.M., and McNeill, H. (2004). Temporal control of differentiation by the insulin receptor/tor pathway in Drosophila. Cell *119*, 87-96.

Bednarek, E., and Caroni, P. (2011). beta-Adducin is required for stable assembly of new synapses and improved memory upon environmental enrichment. Neuron *69*, 1132-1146.

Benzer, S. (1967). Behavioral Mutants of Drosophila Isolated by Countercurrent Distribution. Proceedings of the National Academy of Sciences of the United States of America *58*, 1112-&.

Berke, B., Wittnam, J., McNeill, E., Van Vactor, D.L., and Keshishian, H. (2013a). Retrograde BMP Signaling at the Synapse: A Permissive Signal for Synapse Maturation and Activity-Dependent Plasticity. Journal of Neuroscience *33*, 17937-17950.

Berke, B., Wittnam, J., McNeill, E., Van Vactor, D.L., and Keshishian, H. (2013b). Retrograde BMP signaling at the synapse: a permissive signal for synapse maturation and activity-dependent plasticity. The Journal of neuroscience : the official journal of the Society for Neuroscience *33*, 17937-17950.

Bernal, A., Robert Schoenfeld, Kurt Kleinhesselink, Deborah A. Kimbrell (2004). Loss of Thor, the single 4E-BP gene of Drosophila, does not result in lethality. In Research Notes (http://www.ou.edu/journals/dis/DIS87/index.html: Section of Molecular and Cellular Biology, University of California, 1 Shields Avenue, Davis, California, 95616.), pp. Pages 81-84.

Biggi, S., Buccarello, L., Sclip, A., Lippiello, P., Tonna, N., Rumio, C., Di Marino, D., Miniaci, M.C., and Borsello, T. (2017). Evidence of Presynaptic Localization and Function of the c-Jun N-Terminal Kinase. Neural Plast.

Bishop, D.L., Misgeld, T., Walsh, M.K., Gan, W.B., and Lichtman, J.W. (2004). Axon branch removal at developing synapses by axosome shedding. Neuron *44*, 651-661.

Bleier, J., and Toliver, A. (2017). Exploring the Role of CaMKIV in Homeostatic Plasticity. Journal of Neuroscience *37*, 11520-11522.

Blunk, A.D., Akbergenova, Y., Cho, R.W., Lee, J., Walldorf, U., Xu, K., Zhong, G., Zhuang, X., and Littleton, J.T. (2014). Postsynaptic actin regulates active zone spacing and glutamate receptor apposition at the Drosophila neuromuscular junction. Molecular and cellular neurosciences *61*, 241-254.

Borlikova, G.G., Trejo, M., Mably, A.J., Mc Donald, J.M., Sala Frigerio, C., Regan, C.M., Murphy, K.J., Masliah, E., and Walsh, D.M. (2013). Alzheimer brain-derived amyloid beta-protein impairs synaptic remodeling and memory consolidation. Neurobiology of aging *34*, 1315-1327.

Bosch, M., Castro, J., Saneyoshi, T., Matsuno, H., Sur, M., and Hayashi, Y. (2014). Structural and Molecular Remodeling of Dendritic Spine Substructures during Long-Term Potentiation. Neuron *82*, 444-459.

Bramham, C.R. (2008). Local protein synthesis, actin dynamics, and LTP consolidation. Curr Opin Neurobiol *18*, 524-531.

Brechmann, M., Mock, T., Nickles, D., Kiessling, M., Weit, N., Breuer, R., Muller, W., Wabnitz, G., Frey, F., Nicolay, J.P.*, et al.* (2012). A PP4 Holoenzyme Balances Physiological and Oncogenic Nuclear Factor-Kappa B Signaling in T Lymphocytes. Immunity *37*, 697-708.

Bulat, V., Rast, M., and Pielage, J. (2014). Presynaptic CK2 promotes synapse organization and stability by targeting Ankyrin2. The Journal of cell biology *204*, 77-94.

Butz, M., Worgotter, F., and van Ooyen, A. (2009). Activity-dependent structural plasticity. Brain research reviews *60*, 287-305.

Campanac, E., and Debanne, D. (2008). Spike timing-dependent plasticity: a learning rule for dendritic integration in rat CA1 pyramidal neurons. The Journal of physiology *586*, 779-793.

Campbell, D.S., and Holt, C.E. (2001). Chemotropic responses of retinal growth cones mediated by rapid local protein synthesis and degradation. Neuron *32*, 1013-1026.

Carnegie, G.K., Sleeman, J.E., Morrice, N., Hastie, C.J., Peggie, M.W., Philp, A., Lamond, A.I., and Cohen, P.T.W. (2003). Protein phosphatase 4 interacts with the Survival of Motor Neurons complex and enhances the temporal localisation of snRNPs. Journal of cell science *116*, 1905-1913.

Caroni, P., Donato, F., and Muller, D. (2012). Structural plasticity upon learning: regulation and functions. Nature reviews Neuroscience *13*, 478-490.

Chang, R.C.C., Suen, K.C., Ma, C.H., Elyaman, W., Ng, H.K., and Hugon, J. (2002). Involvement of double-stranded RNA-dependent protein kinase and phosphorylation of eukaryotic initiation factor-2 alpha in neuronal degeneration. J Neurochem *83*, 1215-1225.

Charron, F., and Tessier-Lavigne, M. (2005). Novel brain wiring functions for classical morphogens: a role as graded positional cues in axon guidance. Development *132*, 2251-2262.

Chen, C.K., Bregere, C., Paluch, J., Lu, J.F., Dickman, D.K., and Chang, K.T. (2014). Activity-dependent facilitation of Synaptojanin and synaptic vesicle recycling by the Minibrain kinase. Nature communications *5*, 4246.

Chen, L.Y., Rex, C.S., Casale, M.S., Gall, C.M., and Lynch, G. (2007). Changes in synaptic morphology accompany actin signaling during LTP. Journal of Neuroscience *27*, 5363-5372.

Chen, M.Y., Chen, Y.P., Tan, T.H., and Su, Y.W. (2016). Serine/threonine phosphatase PP4 is required for class switch recombination through recruitment of gammaH2AX. Eur J Immunol *46*, 62-62.

Cheng, L., Locke, C., and Davis, G.W. (2011). S6 kinase localizes to the presynaptic active zone and functions with PDK1 to control synapse development. The Journal of cell biology *194*, 921-935.

Cho, R.W., Buhl, L.K., Volfson, D., Tran, A., Li, F., Akbergenova, Y., and Littleton, J.T. (2015). Phosphorylation of Complexin by PKA Regulates Activity-Dependent Spontaneous Neurotransmitter Release and Structural Synaptic Plasticity. Neuron *88*, 749-761.

Chowdhury, D., Xu, X.Z., Zhong, X.Y., Ahmed, F., Zhong, J.N., Liao, J., Dykxhoorn, D.M., Weinstock, D.M., Pfeifer, G.P., and Lieberman, J. (2008). A PP4-phosphatase complex dephosphorylates gamma-H2AX generated during DNA replication. Mol Cell *31*, 33-46.

Ciani, L., Boyle, K.A., Dickins, E., Sahores, M., Anane, D., Lopes, D.M., Gibb, A.J., and Salinas, P.C. (2011). Wnt7a signaling promotes dendritic spine growth and synaptic strength through Ca2+/Calmodulin-dependent protein kinase II. Proceedings of the National Academy of Sciences of the United States of America *108*, 10732-10737.

Cingolani, L.A., and Goda, Y. (2008). Actin in action: the interplay between the actin cytoskeleton and synaptic efficacy. Nature Reviews Neuroscience *9*, 344-356.

Cohen, P.T.W., Philp, A., and Vazquez-Martin, C. (2005). Protein phosphatase 4 - from obscurity to vital functions. FEBS letters *579*, 3278-3286.

Colbran, R.J. (2004). Protein phosphatases and calcium/calmodulin-dependent protein kinase II-dependent synaptic plasticity. Journal of Neuroscience *24*, 8404-8409.

Collins, C.A., Wairkar, Y.P., Johnson, S.L., and DiAntonio, A. (2006). Highwire restrains synaptic growth by attenuating a MAP kinase signal. Neuron *51*, 57-69.

Costa-Mattioli, M., Sossin, W.S., Klann, E., and Sonenberg, N. (2009). Translational Control of Long-Lasting Synaptic Plasticity and Memory. Neuron *61*, 10-26.

Coyle, I.P., Koh, Y.H., Lee, W.C.M., Slind, J., Fergestad, T., Littleton, J.T., and Ganetzky, B. (2004). Nervous wreck, an SH3 adaptor protein that interacts with Wsp, regulates synaptic growth in Drosophila. Neuron *41*, 521-534.

Coyle, J.T., Tsai, G., and Goff, D. (2003). Converging evidence of NMDA receptor hypofunction in the pathophysiology of schizophrenia. Annals of the New York Academy of Sciences *1003*, 318-327.

Cramer, S.C. (2008). Repairing the human brain after stroke: I. Mechanisms of spontaneous recovery. Annals of neurology *63*, 272-287.

Crino, P.B. (2009). Focal brain malformations: Seizures, signaling, sequencing. Epilepsia *50*, 3-8.

Crino, P.B. (2010). The pathophysiology of tuberous sclerosis complex. Epilepsia *51*, 27-29.

Crino, P.B. (2011). mTOR: A pathogenic signaling pathway in developmental brain malformations. Trends Mol Med *17*, 734-742.

Crino, P.B., Nathanson, K.L., and Henske, E.P. (2006). The tuberous sclerosis complex. New Engl J Med *355*, 1345-1356.

Dahlmans, D., Houzelle, A., Schrauwen, P., and Hoeks, J. (2016). Mitochondrial dynamics, quality control and miRNA regulation in skeletal muscle: implications for obesity and related metabolic disease. Clinical science *130*, 843-852.

Davis, M.J., Wu, X., Nurkiewicz, T.R., Kawasaki, J., Gui, P., Hill, M.A., and Wilson, E. (2001). Regulation of ion channels by protein tyrosine phosphorylation. American journal of physiology Heart and circulatory physiology *281*, H1835-1862.

Day, M., Wang, Z.F., Ding, J., An, X.H., Ingham, C.A., Shering, A.F., Wokosin, D., Ilijic, E., Sun, Z.X., Sampson, A.R*., et al.* (2006). Selective elimination of glutamatergic synapses on striatopallidal neurons in Parkinson disease models. Nature neuroscience *9*, 251-259.

Dickman, D.K., and Davis, G.W. (2009). The schizophrenia susceptibility gene dysbindin controls synaptic homeostasis. Science *326*, 1127-1130.

Diering, G.H., Gustina, A.S., and Huganir, R.L. (2014). PKA-GluA1 Coupling via AKAP5 Controls AMPA Receptor Phosphorylation and Cell-Surface Targeting during Bidirectional Homeostatic Plasticity. Neuron *84*, 790-805.

Dimitroff, B., Howe, K., Watson, A., Campion, B., Lee, H.G., Zhao, N., O'Connor, M.B., Neufeld, T.P., and Selleck, S.B. (2012). Diet and energy-sensing inputs affect TorC1-mediated axon misrouting but not TorC2-directed synapse growth in a Drosophila model of tuberous sclerosis. PloS one *7*, e30722.

Dou, L., Wang, S.Y., Sun, L.B., Huang, X.Q., Zhang, Y., Shen, T., Guo, J., Man, Y., Tang, W.Q., and Li, J. (2017). Mir-338-3p Mediates Tnf-A-Induced Hepatic Insulin Resistance by Targeting PP4r1 to Regulate PP4 Expression. Cell Physiol Biochem *41*, 2419-2431.

Easley, C.A.t., Ben-Yehudah, A., Redinger, C.J., Oliver, S.L., Varum, S.T., Eisinger, V.M., Carlisle, D.L., Donovan, P.J., and Schatten, G.P. (2010). mTOR-mediated activation of p70 S6K induces differentiation of pluripotent human embryonic stem cells. Cellular reprogramming *12*, 263-273.

Eaton, B.A., and Davis, G.W. (2005). LIM Kinase1 controls synaptic stability downstream of the type II BMP receptor. Neuron *47*, 695-708.

Eaton, B.A., Fetter, R.D., and Davis, G.W. (2002). Dynactin is necessary for synapse stabilization. Neuron *34*, 729-741.

Ehrlich, I., Klein, M., Rumpel, S., and Malinow, R. (2007). PSD-95 is required for activity-driven synapse stabilization. Proceedings of the National Academy of Sciences of the United States of America *104*, 4176-4181.

Enneking, E.M., Kudumala, S.R., Moreno, E., Stephan, R., Boerner, J., Godenschwege, T.A., and Pielage, J. (2013). Transsynaptic coordination of synaptic growth, function, and stability by the L1-type CAM Neuroglian. PLoS biology *11*, e1001537.

Espinosa, J.S., and Stryker, M.P. (2012). Development and plasticity of the primary visual cortex. Neuron *75*, 230-249.

Falk, J.E., Chan, A.C.H., Hoffmann, E., and Hochwagen, A. (2010). A Mec1-and PP4-Dependent Checkpoint Couples Centromere Pairing to Meiotic Recombination. Developmental cell *19*, 599-611.

Fernandez, E., Rajan, N., and Bagni, C. (2013). The FMRP regulon: from targets to disease convergence. Front Neurosci-Switz *7*.

Fishwick, K.J., Li, R.A., Halley, P., Deng, P., and Storey, K.G. (2010). Initiation of neuronal differentiation requires PI3-kinase/TOR signalling in the vertebrate neural tube. Developmental biology *338*, 215-225.

Frank, C.A. (2014a). Homeostatic plasticity at the Drosophila neuromuscular junction. Neuropharmacology *78*, 63-74.

Frank, C.A. (2014b). How voltage-gated calcium channels gate forms of homeostatic synaptic plasticity. Frontiers in cellular neuroscience *8*.
Frank, C.A., Kennedy, M.J., Goold, C.P., Marek, K.W., and Davis, G.W. (2006). Mechanisms underlying the rapid induction and sustained expression of synaptic homeostasis. Neuron *52*, 663-677.
Fu, A.K.Y., Hung, K.W., Fu, W.Y., Shen, C., Chen, Y., Xia, J., Lai, K.O., and Ip, N.Y. (2011). APC(Cdh1) mediates EphA4-dependent downregulation of AMPA receptors in homeostatic plasticity. Nature neuroscience *14*, 181-U263.
Fuentes-Medel, Y., Ashley, J., Barria, R., Maloney, R., Freeman, M., and Budnik, V. (2012). Integration of a Retrograde Signal during Synapse Formation by Glia-Secreted TGF-beta Ligand. Current Biology *22*, 1831-1838.
Garza-Lombo, C., and Gonsebatt, M.E. (2016). Mammalian Target of Rapamycin: Its Role in Early Neural Development and in Adult and Aged Brain Function. Frontiers in cellular neuroscience *10*, 157.
Geng, J., Wang, L., Lee, J.Y., and Chen, C.K. (2016). Phosphorylation of Synaptojanin Differentially Regulates Endocytosis of Functionally Distinct Synaptic Vesicle Pools. *36*, 8882-8894.
Ghogha, A., Bruun, D.A., and Lein, P.J. (2012). Inducing Dendritic Growth in Cultured Sympathetic Neurons. Jove-J Vis Exp.
Gilbert, J., Shu, S., Yang, X., Lu, Y.M., Zhu, L.Q., and Man, H.Y. (2016). beta-Amyloid triggers aberrant over-scaling of homeostatic synaptic plasticity. Acta Neuropathol Com *4*.
Gluderer, S., Brunner, E., Germann, M., Jovaisaite, V., Li, C., Rentsch, C.A., Hafen, E., and Stocker, H. (2010). Madm (Mlf1 adapter molecule) cooperates with Bunched A to promote growth in Drosophila. Journal of biology *9*, 9.
Gluderer, S., Oldham, S., Rintelen, F., Sulzer, A., Schutt, C., Wu, X., Raftery, L.A., Hafen, E., and Stocker, H. (2008). Bunched, the Drosophila homolog of the mammalian tumor suppressor TSC-22, promotes cellular growth. BMC developmental biology *8*, 10.
Goda, Y., and Davis, G.W. (2003). Mechanisms of synapse assembly and disassembly. Neuron *40*, 243-264.
Goel, A., and Lee, H.K. (2007). Persistence of experience-induced homeostatic synaptic plasticity through adulthood in superficial layers of mouse visual cortex. Journal of Neuroscience *27*, 6692-6700.
Goel, P., Li, X., and Dickman, D. (2017). Disparate Postsynaptic Induction Mechanisms Ultimately Converge to Drive the Retrograde Enhancement of Presynaptic Efficacy. Cell reports *21*, 2339-2347.
Gong, L.W., and De Camilli, P. (2008). Regulation of postsynaptic AMPA responses by synaptojanin 1. Proceedings of the National Academy of Sciences of the United States of America *105*, 17561-17566.
Goold, C.P., and Davis, G.W. (2007a). The BMP ligand Gbb gates the expression of synaptic homeostasis independent of synaptic growth control. Neuron *56*, 109-123.
Goold, C.P., and Davis, G.W. (2007b). The BMP ligand Gbb gates the expression of synaptic horneostasis independent of synaptic growth control. Neuron *56*, 109-123.
Gratz, S.J., Ukken, F.P., Rubinstein, C.D., Thiede, G., Donohue, L.K., Cummings, A.M., and O'Connor-Giles, K.M. (2014). Highly specific and efficient CRISPR/Cas9-catalyzed homology-directed repair in Drosophila. Genetics *196*, 961-971.
Grefkes, C., and Fink, G.R. (2012). Disruption of motor network connectivity post-stroke and its noninvasive neuromodulation. Current opinion in neurology *25*, 670-675.
Hadweh, P., Habelhah, H., Kieff, E., Mosialos, G., and Hatzivassiliou, E. (2014). The PP4R1 subunit of protein phosphatase PP4 targets TRAF2 and TRAF6 to mediate inhibition of NF-kappa B activation. Cell Signal *26*, 2730-2737.

Haghighi, A.P., McCabe, B.D., Fetter, R.D., Palmer, J.E., Hom, S., and Goodman, C.S. (2003). Retrograde control of synaptic transmission by postsynaptic CaMKII at Drosophila neuromuscular. Neuron *39*, 255-267.

Hall, E.T., Pradhan-Sundd, T., Samnani, F., and Verheyen, E.M. (2017). The protein phosphatase 4 complex promotes the Notch pathway and wingless transcription. Biol Open *6*, 1165-1173.

Han, X., Gomes, J.E., Birmingham, C.L., Pintard, L., Sugimoto, A., and Mains, P.E. (2009). The Role of Protein Phosphatase 4 in Regulating Microtubule Severing in the Caenorhabditis elegans Embryo. Genetics *181*, 933-943.

Hayashi, K., Pan, Y., Shu, H., Ohshima, T., Kansy, J.W., White, C.L., Tamminga, C.A., Sobel, A., Curmi, P.A., Mikoshiba, K.*, et al.* (2006). Phosphorylation of the tubulin-binding protein, stathmin, by Cdk5 and MAP kinases in the brain. J Neurochem *99*, 237-250.

Heinemann, U. (2009). Homeostatic Plasticity and Generation of Epilepsy. Epilepsia *50*, 40-40.

Hell, J.W. (2014). CaMKII: claiming center stage in postsynaptic function and organization. Neuron *81*, 249-265.

Helps, N.R., Brewis, N.D., Lineruth, K., Davis, T., Kaiser, K., and Cohen, P.T. (1998). Protein phosphatase 4 is an essential enzyme required for organisation of microtubules at centrosomes in Drosophila embryos. Journal of cell science *111 (Pt 10)*, 1331-1340.

Henry, F.E., McCartney, A.J., Neely, R., Perez, A.S., Carruthers, C.J., Stuenkel, E.L., Inoki, K., and Sutton, M.A. (2012). Retrograde changes in presynaptic function driven by dendritic mTORC1. The Journal of neuroscience : the official journal of the Society for Neuroscience *32*, 17128-17142.

Heo, K., Nahm, M., Lee, M.J., Kim, Y.E., Ki, C.S., Kim, S.H., and Lee, S. (2017). The Rap activator Gef26 regulates synaptic growth and neuronal survival via inhibition of BMP signaling. Molecular brain *10*, 62.

Hoeffer, C.A., and Klann, E. (2010). mTOR signaling: At the crossroads of plasticity, memory and disease. Trends in neurosciences *33*, 67-75.

Hoeffer, C.A., Tang, W., Wong, H., Santillan, A., Patterson, R.J., Martinez, L.A., Tejada-Simon, M.V., Paylor, R., Hamilton, S.L., and Klann, E. (2008). Removal of FKBP12 Enhances mTOR-Raptor Interactions, LTP, Memory, and Perseverative/Repetitive Behavior. Neuron *60*, 832-845.

Hofer, S.B., Mrsic-Flogel, T.D., Bonhoeffer, T., and Hubener, M. (2009). Experience leaves a lasting structural trace in cortical circuits. Nature *457*, 313-317.

Holtmaat, A., and Svoboda, K. (2009). Experience-dependent structural synaptic plasticity in the mammalian brain. Nature Reviews Neuroscience *10*, 647-658.

Holtmaat, A.J.G.D., Trachtenberg, J.T., Wilbrecht, L., Shepherd, G.M., Zhang, X.Q., Knott, G.W., and Svoboda, K. (2005). Transient and persistent dendritic spines in the neocortex in vivo. Neuron *45*, 279-291.

Hooper, J.D., Baker, E., Ogbourne, S.M., Sutherland, G.R., and Antalis, T.M. (2000). Cloning of the cDNA and localization of the gene encoding human NRBP, a ubiquitously expressed, multidomain putative adapter protein. Genomics *66*, 113-118.

Horiuchi, D., Barkus, R.V., Pilling, A.D., Gassman, A., and Saxton, W.M. (2005). APLIP1, a Kinesin binding JIP-1/JNK scaffold protein, influences the axonal transport of both vesicles and mitochondria in Drosophila. Current Biology *15*, 2137-2141.

Hou, L.F., and Klann, E. (2004). Activation of the phosphoinositide 3-kinase-akt-mammalian target of rapamycin signaling pathway is required for metabotropic glutamate receptor-dependent long-term depression. Journal of Neuroscience *24*, 6352-6361.

Hou, Q.M., Ruan, H.Y., Gilbert, J., Wang, G., Ma, Q., Yao, W.D., and Man, H.Y. (2015). MicroRNA miR124 is required for the expression of homeostatic synaptic plasticity. Nature communications *6*.

Houweling, A.R., Bazhenov, M., Timofeev, I., Steriade, M., and Sejnowski, T.J. (2005). Homeostatic synaptic plasticity can explain post-traumatic epileptogenesis in chronically isolated neocortex. Cereb Cortex *15*, 834-845.

Hu, M.C.T., Shui, J.W., Mihindukulasuriya, K.A., and Tan, T.H. (2001). Genomic structure of the mouse PP4 gene: a developmentally regulated protein phosphatase. Gene *278*, 89-99.

Huang, X.Z., Cheng, A.Y., and Honkanen, R.E. (1997). Genomic organization of the human PP4 gene encoding a serine/threonine protein phosphatase (PP4) suggests a common ancestry with PP2A. Genomics *44*, 336-343.

Hubener, M., and Bonhoeffer, T. (2010). Searching for engrams. Neuron *67*, 363-371.

Hutchins, B.I., and Kalil, K. (2008). Differential outgrowth of axons and their branches is regulated by localized calcium transients. The Journal of neuroscience : the official journal of the Society for Neuroscience *28*, 143-153.

Hwang, J., Lee, J.A., and Pallas, D.C. (2016). Leucine Carboxyl Methyltransferase 1(LCMT-1) Methylates Protein Phosphatase 4(PP4) and Protein Phosphatase 6(PP6) and Differentially Regulates the Stable Formation of Different PP4 Holoenzymes. Journal of Biological Chemistry *291*, 21008-21019.

Inestrosa, N.C., and Varela-Nallar, L. (2014). Wnt signaling in the nervous system and in Alzheimers disease. J Mol Cell Biol *6*, 64-74.

Inostroza, J., Saenz, L., Calaf, G., Cabello, G., and Parra, E. (2005). Role of the phosphatase PP4 in the activation of JNK-1 in prostate carcinoma cell lines PC-3 and LNCaP resulting in increased AP-1 and EGR-1 activity. Biol Res *38*, 163-178.

Irwin, S.A., Patel, B., Idupulapati, M., Harris, J.B., Crisostomo, R.A., Larsen, B.P., Kooy, F., Willems, P.J., Cras, P., Kozlowski, P.B.*, et al.* (2001). Abnormal dendritic spine characteristics in the temporal and visual cortices of patients with fragile-X syndrome: A quantitative examination. Am J Med Genet *98*, 161-167.

Jakawich, S.K., Neely, R.M., Djakovic, S.N., Patrick, G.N., and Sutton, M.A. (2010). An Essential Postsynaptic Role for the Ubiquitin Proteasome System in Slow Homeostatic Synaptic Plasticity in Cultured Hippocampal Neurons. Neuroscience *171*, 1016-1031.

Jang, S.S., Royston, S.E., Xu, J., Cavaretta, J.P., Vest, M.O., Lee, K.Y., Lee, S., Jeong, H.G., Lombroso, P.J., and Chung, H.J. (2015). Regulation of STEP61 and tyrosine-phosphorylation of NMDA and AMPA receptors during homeostatic synaptic plasticity. Molecular brain *8*.

Jaworski, J., and Sheng, M. (2006). The growing role of mTOR in neuronal development and plasticity. Mol Neurobiol *34*, 205-219.

Jeans, A.F., van Heusden, F.C., Al-Mubarak, B., Padamsey, Z., and Emptage, N.J. (2017). Homeostatic Presynaptic Plasticity Is Specifically Regulated by P/Q-type Ca2+ Channels at Mammalian Hippocampal Synapses. Cell reports *21*, 341-350.

Jensen, T.P., Buckby, L.E., and Empson, R.M. (2009). Reduced expression of the "fast" calcium transporter PMCA2a during homeostatic plasticity. Molecular and Cellular Neuroscience *41*, 364-372.

Jia, H., Liu, Y., Yan, W., and Jia, J. (2009). PP4 and PP2A regulate Hedgehog signaling by controlling Smo and Ci phosphorylation. Development *136*, 307-316.

Jiang, M.H., Lee, C.L., Smith, K.L., and Swann, J.W. (1998). Spine loss and other persistent alterations of hippocampal pyramidal cell dendrites in a model of early-onset epilepsy. Journal of Neuroscience *18*, 8356-8368.

Johnson, E.L., Fetter, R.D., and Davis, G.W. (2009). Negative Regulation of Active Zone Assembly by a Newly Identified SR Protein Kinase. PLoS biology *7*.

Johnson, R.E., Tien, N.W., Shen, N., Pearson, J.T., Soto, F., and Kerschensteiner, D. (2017). Homeostatic plasticity shapes the visual system's first synapse. Nature communications *8*.

Jourdain, P., Fukunaga, K., and Muller, D. (2003). Calcium/calmodulin-dependent protein kinase II contributes to activity-dependent filopodia growth and spine formation. The

Journal of neuroscience : the official journal of the Society for Neuroscience *23*, 10645-10649.
Kasthuri, N., and Lichtman, J.W. (2003). The role of neuronal identity in synaptic competition. Nature *424*, 426-430.
Kelleher, R.J., 3rd, Govindarajan, A., and Tonegawa, S. (2004). Translational regulatory mechanisms in persistent forms of synaptic plasticity. Neuron *44*, 59-73.
Keller-Peck, C.R., Walsh, M.K., Gan, W.B., Feng, G., Sanes, J.R., and Lichtman, J.W. (2001). Asynchronous synapse elimination in neonatal motor units: studies using GFP transgenic mice. Neuron *31*, 381-394.
Kerr, K.S., Fuentes-Medel, Y., Brewer, C., Barria, R., Ashley, J., Abruzzi, K.C., Sheehan, A., Tasdemir-Yilmaz, O.E., Freeman, M.R., and Budnik, V. (2014). Glial Wingless/Wnt Regulates Glutamate Receptor Clustering and Synaptic Physiology at the Drosophila Neuromuscular Junction. Journal of Neuroscience *34*, 2910-2920.
Keshishian, H. (2002). Is synaptic homeostasis just wishful thinking? Neuron *33*, 491-492.
Kim, J., Jung, S.C., Clemens, A.M., Petralia, R.S., and Hoffman, D.A. (2007). Regulation of dendritic excitability by activity-dependent trafficking of the A-type K+ channel subunit Kv4.2 in hippocampal neurons. Neuron *54*, 933-947.
Kirov, S.A., and Harris, K.M. (2000). Dendrites are more spiny on mature hippocampal neurons when synapses are inactivated (vol 2, pg 878, 1999). Nature neuroscience *3*, 409-409.
Knafo, S., Alonso-Nanclares, L., Gonzalez-Soriano, J., Merino-Serrais, P., Fernaud-Espinosa, I., Ferrer, I., and DeFelipe, J. (2009). Widespread Changes in Dendritic Spines in a Model of Alzheimer's Disease. Cereb Cortex *19*, 586-592.
Knox, S., Ge, H., Dimitroff, B.D., Ren, Y., Howe, K.A., Arsham, A.M., Easterday, M.C., Neufeld, T.P., O'Connor, M.B., and Selleck, S.B. (2007). Mechanisms of TSC-mediated control of synapse assembly and axon guidance. PloS one *2*, e375.
Koch, I., Schwarz, H., Beuchle, D., Goellner, B., Langegger, M., and Aberle, H. (2008). Drosophila ankyrin 2 is required for synaptic stability. Neuron *58*, 210-222.
Kowianski, P., Lietzau, G., Czuba, E., Waskow, M., Steliga, A., and Morys, J. (2018). BDNF: A Key Factor with Multipotent Impact on Brain Signaling and Synaptic Plasticity. Cellular and molecular neurobiology *38*, 579-593.
Kumar, V., Zhang, M.X., Swank, M.W., Kunz, J., and Wu, G.Y. (2005). Regulation of dendritic morphogenesis by Ras-PI3K-Akt-mTOR and Ras-MAPK signaling pathways. The Journal of neuroscience : the official journal of the Society for Neuroscience *25*, 11288-11299.
Lang, S.B., Bonhoeffer, T., and Lohmann, C. (2006). Simultaneous imaging of morphological plasticity and calcium dynamics in dendrites. Nature protocols *1*, 1859-1864.
LaSarge, C.L., and Danzer, S.C. (2014). Mechanisms regulating neuronal excitability and seizure development following mTOR pathway hyperactivation. Front Mol Neurosci *7*.
Laugks, U., Hieke, M., and Wagner, N. (2017). MAN1 Restricts BMP Signaling During Synaptic Growth in Drosophila. Cellular and molecular neurobiology *37*, 1077-1093.
Le Be, J.V., and Markram, H. (2006). Spontaneous and evoked synaptic rewiring in the neonatal neocortex. Proceedings of the National Academy of Sciences of the United States of America *103*, 13214-13219.
Lee, D.H., Goodarzi, A.A., Adelmant, G.O., Pan, Y.F., Jeggo, P.A., Marto, J.A., and Chowdhury, D. (2012). Phosphoproteomic analysis reveals that PP4 dephosphorylates KAP-1 impacting the DNA damage response. Embo Journal *31*, 2403-2415.
Lee, S.H., Kim, Y.J., and Choi, S.Y. (2016). BMP signaling modulates the probability of neurotransmitter release and readily releasable pools in Drosophila neuromuscular junction synapses. Biochem Bioph Res Co *479*, 440-446.
Lenz, G., and Avruch, J. (2005). Glutamatergic regulation of the p70S6 kinase in primary mouse neurons. The Journal of biological chemistry *280*, 38121-38124.

Lepicard, S., Franco, B., de Bock, F., and Parmentier, M.L. (2014). A Presynaptic Role of Microtubule-Associated Protein 1/Futsch in Drosophila: Regulation of Active Zone Number and Neurotransmitter Release. Journal of Neuroscience *34*, 6759-6771.

Liao, D., Grigoriants, O.O., Wang, W., Wiens, K., Loh, H.H., and Law, P.Y. (2007). Distinct effects of individual opioids on the morphology of spines depend upon the internalization of mu opioid receptors. Molecular and Cellular Neuroscience *35*, 456-469.

Lichtman, J.W., and Sanes, J.R. (2003). Watching the neuromuscular junction. Journal of neurocytology *32*, 767-775.

Lim, R., Winteringham, L.N., Williams, J.H., McCulloch, R.K., Ingley, E., Tiao, J.Y., Lalonde, J.P., Tsai, S., Tilbrook, P.A., Sun, Y.*, et al.* (2002). MADM, a novel adaptor protein that mediates phosphorylation of the 14-3-3 binding site of myeloid leukemia factor 1. The Journal of biological chemistry *277*, 40997-41008.

Lim, S.H., Kwon, S.K., Lee, M.K., Moon, J., Jeong, D.G., Park, E., Kim, S.J., Park, B.C., Lee, S.C., Ryu, S.E.*, et al.* (2009). Synapse formation regulated by protein tyrosine phosphatase receptor T through interaction with cell adhesion molecules and Fyn. The EMBO journal *28*, 3564-3578.

Lin, P.T., and Hallett, M. (2009). The pathophysiology of focal hand dystonia. Journal of hand therapy : official journal of the American Society of Hand Therapists *22*, 109-113; quiz 114.

Lipinszki, Z., Lefevre, S., Matthew, S.S.W., Singleton, M.R., Glover, D.M., and Przewloka, M.R. (2015). Centromeric binding and activity of Protein Phosphatase 4. Nature communications *6*.

Lisman, J., Yasuda, R., and Raghavachari, S. (2012). Mechanisms of CaMKII action in long-term potentiation. Nature Reviews Neuroscience *13*, 169-182.

Liu, J., Xu, L., and Xu, X. (2011a). PP4 is required for NHEJ-mediated repair of DNA double strand breaks. Mol Biol Cell *22*.

Liu, J.P., Xu, L.L., Zhong, J.N., Liao, J., Li, J., and Xu, X.Z. (2012). Protein phosphatase PP4 is involved in NHEJ-mediated repair of DNA double-strand breaks. Cell cycle (Georgetown, Tex) *11*, 2643-2649.

Liu, K.S.Y., Siebert, M., Mertel, S., Knoche, E., Wegener, S., Wichmann, C., Matkovic, T., Muhammad, K., Depner, H., Mettke, C.*, et al.* (2011b). RIM-Binding Protein, a Central Part of the Active Zone, Is Essential for Neurotransmitter Release. Science *334*, 1565-1569.

Liu, Z., Huang, Y., Hu, W., Huang, S., Wang, Q., Han, J., and Zhang, Y.Q. (2014). dAcsl, the Drosophila ortholog of acyl-CoA synthetase long-chain family member 3 and 4, inhibits synapse growth by attenuating bone morphogenetic protein signaling via endocytic recycling. The Journal of neuroscience : the official journal of the Society for Neuroscience *34*, 2785-2796.

Liu, Z.H., Huang, Y., Zhang, Y., Chen, D., and Zhang, Y.Q. (2011c). Drosophila Acyl-CoA Synthetase Long-Chain Family Member 4 Regulates Axonal Transport of Synaptic Vesicles and Is Required for Synaptic Development and Transmission. Journal of Neuroscience *31*, 2052-2063.

Lowe, M., and Barr, F.A. (2007). Inheritance and biogenesis of organelles in the secretory pathway. Nat Rev Mol Cell Bio *8*, 429-439.

Lu, C.S., Hodge, J.J., Mehren, J., Sun, X.X., and Griffith, L.C. (2003). Regulation of the Ca2+/CaM-responsive pool of CaMKII by scaffold-dependent autophosphorylation. Neuron *40*, 1185-1197.

Lund, I.V., Hu, Y.H., Raol, Y.H., Benham, R.S., Faris, R., Russek, S.J., and Brooks-Kayal, A.R. (2008). BDNF Selectively Regulates GABA(A) Receptor Transcription by Activation of the JAK/STAT Pathway. Sci Signal *1*.

Lussier, M.P., Gu, X., Lu, W., and Roche, K.W. (2014). Casein kinase 2 phosphorylates GluA1 and regulates its surface expression. The European journal of neuroscience *39*, 1148-1158.

Lyu, J., Kim, H.R., Yamamoto, V., Choi, S.H., Wei, Z., Joo, C.K., and Lu, W. (2013). Protein Phosphatase 4 and Smek Complex Negatively Regulate Par3 and Promote Neuronal Differentiation of Neural Stem/Progenitor Cells. Cell reports *5*, 593-600.

Ma, T., Hoeffer, C.A., Capetillo-Zarate, E., Yu, F.M., Wong, H., Lin, M.T., Tampellini, D., Klann, E., Blitzer, R.D., and Gouras, G.K. (2010). Dysregulation of the mTOR Pathway Mediates Impairment of Synaptic Plasticity in a Mouse Model of Alzheimer's Disease. PloS one *5*.

Malagelada, C., Lopez-Toledano, M.A., Willett, R.T., Jin, Z.H., Shelanski, M.L., and Greene, L.A. (2011). RTP801/REDD1 regulates the timing of cortical neurogenesis and neuron migration. The Journal of neuroscience : the official journal of the Society for Neuroscience *31*, 3186-3196.

Marques, G., Bao, H., Haerry, T.E., Shimell, M.J., Duchek, P., Zhang, B., and O'Connor, M.B. (2002). The Drosophila BMP type II receptor Wishful Thinking regulates neuromuscular synapse morphology and function. Neuron *33*, 529-543.

Martin-Lanneree, S., Lasbleiz, C., Sanial, M., Fouix, S., Besse, F., Tricoire, H., and Plessis, A. (2006). Characterization of the Drosophila myeloid leukemia factor. Genes to cells : devoted to molecular & cellular mechanisms *11*, 1317-1335.

Massaro, C.M., Pielage, J., and Davis, G.W. (2009). Molecular mechanisms that enhance synapse stability despite persistent disruption of the spectrin/ankyrin/microtubule cytoskeleton. The Journal of cell biology *187*, 101-117.

Matta, S., Van Kolen, K., da Cunha, R., van den Bogaart, G., Mandemakers, W., Miskiewicz, K., De Bock, P.J., Morais, V.A., Vilain, S., Haddad, D.*, et al.* (2012). LRRK2 controls an EndoA phosphorylation cycle in synaptic endocytosis. Neuron *75*, 1008-1021.

McCabe, B.D., Marques, G., Haghighi, A.P., Fetter, R.D., Crotty, M.L., Haerry, T.E., Goodman, C.S., and O'Connor, M.B. (2003). The BMP homolog Gbb provides a retrograde signal that regulates synaptic growth at the Drosophila neuromuscular junction. Neuron *39*, 241-254.

McKinney, R.A., Capogna, M., Durr, R., Gahwiler, B.H., and Thompson, S.M. (1999). Miniature synaptic events maintain dendritic spines via AMPA receptor activation. Nature neuroscience *2*, 44-49.

McNeill, H., Craig, G.M., and Bateman, J.M. (2008). Regulation of neurogenesis and epidermal growth factor receptor signaling by the insulin receptor/target of rapamycin pathway in Drosophila. Genetics *179*, 843-853.

Mendez, P., Stefanelli, T., Flores, C.E., Muller, D., and Luscher, C. (2018). Homeostatic Plasticity in the Hippocampus Facilitates Memory Extinction. Cell reports *22*, 1451-1461.

Menon, K.P., Sanyal, S., Habara, Y., Sanchez, R., Wharton, R.P., Ramaswami, M., and Zinn, K. (2004). The Translational Repressor Pumilio Regulates Presynaptic Morphology and Controls Postsynaptic Accumulation of Translation Factor eIF-4E. Neuron *44*, 663-676.

Merino, C., Penney, J., Gonzalez, M., Tsurudome, K., Moujahidine, M., O'Connor, M.B., Verheyen, E.M., and Haghighi, P. (2009). Nemo kinase interacts with Mad to coordinate synaptic growth at the Drosophila neuromuscular junction. Journal of Cell Biology *185*, 713-725.

Mihindukulasuriya, K.A., Zhou, G.S., Qin, J., and Tan, T.H. (2004). Protein phosphatase 4 interacts with and down-regulates insulin receptor substrate 4 following tumor necrosis factor-alpha stimulation. Journal of Biological Chemistry *279*, 46588-46594.

Miller, D.L., Ballard, S.L., and Ganetzky, B. (2012a). Analysis of Synaptic Growth and Function in Drosophila with an Extended Larval Stage. Journal of Neuroscience *32*, 13776-13786.

Miller, D.L., Ballard, S.L., and Ganetzky, B. (2012b). Analysis of synaptic growth and function in Drosophila with an extended larval stage. The Journal of neuroscience : the official journal of the Society for Neuroscience *32*, 13776-13786.

Mishra, P., and Chan, D.C. (2016). Metabolic regulation of mitochondrial dynamics. The Journal of cell biology *212*, 379-387.

Miskiewicz, K., Jose, L.E., Bento-Abreu, A., Fislage, M., Taes, I., Kasprowicz, J., Swerts, J., Sigrist, S., Versees, W., Robberecht, W.*, et al.* (2011). ELP3 Controls Active Zone Morphology by Acetylating the ELKS Family Member Bruchpilot. Neuron *72*, 776-788.

Morrison, D.K., Murakami, M.S., and Cleghon, V. (2000). Protein kinases and phosphatases in the Drosophila genome. Journal of Cell Biology *150*, F57-F62.

Muller, M., Liu, K.S.Y., Sigrist, S.J., and Davis, G.W. (2012). RIM Controls Homeostatic Plasticity through Modulation of the Readily-Releasable Vesicle Pool. Journal of Neuroscience *32*, 16574-16585.

Nagerl, U.V., Eberhorn, N., Cambridge, S.B., and Bonhoeffer, T. (2004). Bidirectional activity-dependent morphological plasticity in hippocampal neurons. Neuron *44*, 759-767.

Nahm, M., Lee, M.J., Parkinson, W., Lee, M., Kim, H., Kim, Y.J., Kim, S., Cho, Y.S., Min, B.M., Bae, Y.C.*, et al.* (2013). Spartin regulates synaptic growth and neuronal survival by inhibiting BMP-mediated microtubule stabilization. Neuron *77*, 680-695.

Nakada, S., Chen, G.I., Gingras, A.C., and Durocher, D. (2008). PP4 is gamma H2AX phosphatase required for recovery from the DNA damage checkpoint (vol 9, pg 1019, 2008). Embo Rep *9*, 1251-1251.

Natarajan, R., Trivedi-Vyas, D., and Wairkar, Y.P. (2013). Tuberous sclerosis complex regulates Drosophila neuromuscular junction growth via the TORC2/Akt pathway. Human molecular genetics *22*, 2010-2023.

Newman, Z.L., Hoagland, A., Aghi, K., Worden, K., Levy, S.L., Son, J.H., Lee, L.P., and Isacoff, E.Y. (2017). Input-Specific Plasticity and Homeostasis at the Drosophila Larval Neuromuscular Junction. Neuron *93*, 1388-1404.e1310.

Nie, D., Di Nardo, A., Han, J.M., Baharanyi, H., Kramvis, I., Huynh, T., Dabora, S., Codeluppi, S., Pandolfi, P.P., Pasquale, E.B.*, et al.* (2010). Tsc2-Rheb signaling regulates EphA-mediated axon guidance. Nature neuroscience *13*, 163-172.

Nie, Y., Li, Q., Amcheslavsky, A., Duhart, J.C., Veraksa, A., Stocker, H., Raftery, L.A., and Ip, Y.T. (2015). Bunched and Madm Function Downstream of Tuberous Sclerosis Complex to Regulate the Growth of Intestinal Stem Cells in Drosophila. Stem cell reviews *11*, 813-825.

Niere, F., and Raab-Graham, K.F. (2017). mTORC1 Is a Local, Postsynaptic Voltage Sensor Regulated by Positive and Negative Feedback Pathways. Frontiers in cellular neuroscience *11*, 152.

Ning, L.F., Long, Z.T., Huang, X.Q., Sun, L.L., and Sang, J.L. (2006). Effects of PP4 suppression on the proliferation of MCF7 cells. Chinese Sci Bull *51*, 2335-2341.

O'Connor-Giles, K.M., Ho, L.L., and Ganetzky, B. (2008). Nervous wreck interacts with thickveins and the endocytic machinery to attenuate retrograde BMP signaling during synaptic growth. Neuron *58*, 507-518.

O'Connor, A.B., Schwid, S.R., Herrmann, D.N., Markman, J.D., and Dworkin, R.H. (2008). Pain associated with multiple sclerosis: Systematic review and proposed classification. Pain *137*, 96-111.

Okamoto, K.I., Nagai, T., Miyawaki, A., and Hayashi, Y. (2004). Rapid and persistent modulation of actin dynamics regulates postsynaptic reorganization underlying bidirectional plasticity. Nature neuroscience *7*, 1104-1112.

Owald, D., Fouquet, W., Schmidt, M., Wichmann, C., Mertel, S., Depner, H., Christiansen, F., Zube, C., Quentin, C., Korner, J.*, et al.* (2010). A Syd-1 homologue regulates pre- and postsynaptic maturation in Drosophila. Journal of Cell Biology *188*, 565-579.

Owald, D., Khorramshahi, O., Gupta, V.K., Banovic, D., Depner, H., Fouquet, W., Wichmann, C., Mertel, S., Eimer, S., Reynolds, E.*, et al.* (2012). Cooperation of Syd-1 with Neurexin synchronizes pre- with postsynaptic assembly. Nature neuroscience *15*, 1219-U1274.

Packard, M., Koo, E.S., Gorczyca, M., Sharpe, J., Cumberledge, S., and Budnik, V. (2002). The drosophila wnt, wingless, provides an essential signal for pre- and postsynaptic differentiation. Cell *111*, 319-330.

Page, G., Bilan, A.R., Ingrand, S., Lafay-Chebassier, C., Pain, S., Pochat, M.C.P., Bouras, C., Bayer, T., and Hugon, J. (2006). Activated double-stranded RNA-dependent protein kinase and neuronal death in models of Alzheimer's disease. Neuroscience *139*, 1343-1354.

Park, S., Scheffler, T.L., Rossie, S.S., and Gerrard, D.E. (2013). AMPK activity is regulated by calcium-mediated protein phosphatase 2A activity. Cell calcium *53*, 217-223.

Penney, J., Tsurudome, K., Liao, E.H., Elazzouzi, F., Livingstone, M., Gonzalez, M., Sonenberg, N., and Haghighi, A.P. (2012). TOR is required for the retrograde regulation of synaptic homeostasis at the Drosophila neuromuscular junction. Neuron *74*, 166-178.

Penney, J., Tsurudome, K., Liao, E.H., Kauwe, G., Gray, L., Yanagiya, A., M, R.C., Sonenberg, N., and Haghighi, A.P. (2016). LRRK2 regulates retrograde synaptic compensation at the Drosophila neuromuscular junction. Nature communications *7*, 12188.

Perry, S., Han, Y.F., Das, A., and Dickman, D. (2017). Homeostatic plasticity can be induced and expressed to restore synaptic strength at neuromuscular junctions undergoing ALS-related degeneration. Human molecular genetics *26*, 4153-4167.

Pfeifer, G.P. (2012). Protein phosphatase PP4: Role in dephosphorylation of KAP1 and DNA strand break repair. Cell cycle (Georgetown, Tex) *11*, 2590-2591.

Piccioli, Z.D., and Littleton, J.T. (2014a). Retrograde BMP signaling modulates rapid activity-dependent synaptic growth via presynaptic LIM kinase regulation of cofilin. The Journal of neuroscience : the official journal of the Society for Neuroscience *34*, 4371-4381.

Piccioli, Z.D., and Littleton, J.T. (2014b). Retrograde BMP Signaling Modulates Rapid Activity-Dependent Synaptic Growth via Presynaptic LIM Kinase Regulation of Cofilin. Journal of Neuroscience *34*, 4371-4381.

Pielage, J., Bulat, V., Zuchero, J.B., Fetter, R.D., and Davis, G.W. (2011). Hts/Adducin controls synaptic elaboration and elimination. Neuron *69*, 1114-1131.

Pielage, J., Cheng, L., Fetter, R.D., Carlton, P.M., Sedat, J.W., and Davis, G.W. (2008). A presynaptic giant ankyrin stabilizes the NMJ through regulation of presynaptic microtubules and transsynaptic cell adhesion. Neuron *58*, 195-209.

Pielage, J., Fetter, R.D., and Davis, G.W. (2005). Presynaptic spectrin is essential for synapse stabilization. Current biology : CB *15*, 918-928.

Pielage, J., Fetter, R.D., and Davis, G.W. (2006). A postsynaptic spectrin scaffold defines active zone size, spacing, and efficacy at the Drosophila neuromuscular junction. The Journal of cell biology *175*, 491-503.

Portera-Cailliau, C., Weimer, R.M., De Paola, V., Caroni, P., and Svoboda, K. (2005). Diverse modes of axon elaboration in the developing neocortex. PLoS biology *3*, e272.

Ranson, A., Cheetham, C.E.J., Fox, K., and Sengpiel, F. (2012). Homeostatic plasticity mechanisms are required for juvenile, but not adult, ocular dominance plasticity. Proceedings of the National Academy of Sciences of the United States of America *109*, 1311-1316.

Rasse, T.M., Fouquet, W., Schmid, A., Kittel, R.J., Mertel, S., Sigrist, C.B., Schmidt, M., Guzman, A., Merino, C., Qin, G.*, et al.* (2005). Glutamate receptor dynamics organizing synapse formation in vivo. Nature neuroscience *8*, 898-905.

Rawson, J.M., Lee, M., Kennedy, E.L., and Selleck, S.B. (2003). Drosophila neuromuscular synapse assembly and function require the TGF-beta type I receptor saxophone and the transcription factor Mad. Journal of neurobiology *55*, 134-150.

Riffault, B., Medina, I., Dumon, C., Thalman, C., Ferrand, N., Friedel, P., Gaiarsa, J.L., and Porcher, C. (2014). Pro-Brain-Derived Neurotrophic Factor Inhibits GABAergic Neurotransmission by Activating Endocytosis and Repression of GABA(A) Receptors. Journal of Neuroscience *34*, 13516-13534.

Ripley, B., Otto, S., Tiglio, K., Williams, M.E., and Ghosh, A. (2011). Regulation of synaptic stability by AMPA receptor reverse signaling. Proceedings of the National Academy of Sciences of the United States of America *108*, 367-372.

Rocha, M., and Sur, M. (1995). Rapid Acquisition of Dendritic Spines by Visual Thalamic Neurons after Blockade of N-Methyl-D-Aspartate Receptors. Proceedings of the National Academy of Sciences of the United States of America *92*, 8026-8030.

Rollenhagen, A., and Lubke, J.H. (2006). The morphology of excitatory central synapses: from structure to function. Cell and tissue research *326*, 221-237.

Saab, C.Y. (2012). Pain-related changes in the brain: diagnostic and therapeutic potentials. Trends in neurosciences *35*, 629-637.

Sacktor, T.C. (2011). How does PKMzeta maintain long-term memory? Nature reviews Neuroscience *12*, 9-15.

Sadigh-Eteghad, S., Askari-Nejad, M.S., Mahmoudi, J., and Majdi, A. (2016). Cargo trafficking in Alzheimer's disease: the possible role of retromer. Neurol Sci *37*, 17-22.

Sanderson, J.L., Scott, J.D., and Dell'Acqua, M.L. (2018). Control of Homeostatic Synaptic Plasticity by AKAP-Anchored Kinase and Phosphatase Regulation of Ca2+-Permeable AMPA Receptors. Journal of Neuroscience *38*, 2863-2876.

Schulz, D.J., and Lane, B.J. (2017). Homeostatic plasticity of excitability in crustacean central pattern generator networks. Curr Opin Neurobiol *43*, 7-14.

Seeburg, D.P., Feliu-Mojer, M., Gaiottino, J., Pak, D.T.S., and Sheng, M. (2008). Critical role of CDK5 and Polo-like kinase 2 in homeostatic synaptic plasticity during elevated activity. Neuron *58*, 571-583.

Seeburg, D.P., and Sheng, M. (2008). Activity-induced polo-like kinase 2 is required for homeostatic plasticity of hippocampal neurons during epileptiform activity. Journal of Neuroscience *28*, 6583-6591.

Shah, K., and Lahiri, D.K. (2017). A Tale of the Good and Bad: Remodeling of the Microtubule Network in the Brain by Cdk5. Mol Neurobiol *54*, 2255-2268.

Shi, W.W., Chen, Y., Gan, G.M., Wang, D., Ren, J.Q., Wang, Q.F., Xu, Z.H., Xie, W., and Zhang, Y.Q. (2013). Brain Tumor Regulates Neuromuscular Synapse Growth and Endocytosis in Drosophila by Suppressing Mad Expression. Journal of Neuroscience *33*, 12352-12363.

Shui, J.W., Hu, M.C., and Tan, T.H. (2007). Conditional knockout mice reveal an essential role of protein phosphatase 4 in thymocyte development and pre-T-cell receptor signaling. Molecular and cellular biology *27*, 79-91.

Siddoway, B.A., Altimimi, H.F., Hou, H.L., Petralia, R.S., Xu, B., Stellwagen, D., and Xia, H.H. (2013). An Essential Role for Inhibitor-2 Regulation of Protein Phosphatase-1 in Synaptic Scaling. Journal of Neuroscience *33*, 11206-11211.

Sigrist, S.J., Thiel, P.R., Reiff, D.F., Lachance, P.E., Lasko, P., and Schuster, C.M. (2000). Postsynaptic translation affects the efficacy and morphology of neuromuscular junctions. Nature *405*, 1062-1065.

Sigrist, S.J., Thiel, P.R., Reiff, D.F., and Schuster, C.M. (2002). The postsynaptic glutamate receptor subunit DGluR-IIA mediates long-term plasticity in Drosophila. The Journal of neuroscience : the official journal of the Society for Neuroscience *22*, 7362-7372.

Singh, S.R., Liu, Y., Zhao, J., Zeng, X., and Hou, S.X. (2016). The novel tumour suppressor Madm regulates stem cell competition in the Drosophila testis. Nature communications *7*, 10473.

Smith-Trunova, S., Prithviraj, R., Spurrier, J., Kuzina, I., Gu, Q., and Giniger, E. (2015). Cdk5 Regulates Developmental Remodeling of Mushroom Body Neurons in Drosophila. Dev Dynam *244*, 1550-1563.

Soares, C., Lee, K.F.H., Nassrallah, W., and Beique, J.C. (2013). Differential Subcellular Targeting of Glutamate Receptor Subtypes during Homeostatic Synaptic Plasticity. Journal of Neuroscience *33*, 13547-13559.

Sousa-Nunes, R., Chia, W., and Somers, W.G. (2009). Protein Phosphatase 4 mediates localization of the Miranda complex during Drosophila neuroblast asymmetric divisions. Gene Dev *23*, 359-372.

Spring, A.M., Brusich, D.J., and Frank, C.A. (2016). C-terminal Src Kinase Gates Homeostatic Synaptic Plasticity and Regulates Fasciclin II Expression at the Drosophila Neuromuscular Junction. PLoS genetics *12*.

Stephan, K.E., Baldeweg, T., and Friston, K.J. (2006). Synaptic plasticity and dysconnection in schizophrenia. Biological psychiatry *59*, 929-939.

Stephan, R., Goellner, B., Moreno, E., Frank, C.A., Hugenschmidt, T., Genoud, C., Aberle, H., and Pielage, J. (2015). Hierarchical microtubule organization controls axon caliber and transport and determines synaptic structure and stability. Developmental cell *33*, 5-21.

Strack, S., Wilson, T.J., and Cribbs, J.T. (2013). Cyclin-dependent kinases regulate splice-specific targeting of dynamin-related protein 1 to microtubules. The Journal of cell biology *201*, 1037-1051.

Sugie, A., Hakeda-Suzuki, S., Suzuki, E., Silies, M., Shimozono, M., Mohl, C., Suzuki, T., and Tavosanis, G. (2015). Molecular Remodeling of the Presynaptic Active Zone of Drosophila Photoreceptors via Activity-Dependent Feedback. Neuron *86*, 711-725.

Sumiyoshi, E., Sugimoto, A., and Yamamoto, M. (2002). Protein phosphatase 4 is required for centrosome maturation in mitosis and sperm meiosis in C-elegans. Journal of cell science *115*, 1403-1410.

Sutton, M.A. (2010). Homeostatic Plasticity: Single Hippocampal Neurons See the Light. Neuron *68*, 326-328.

Swann, J.W., and Rho, J.M. (2014). How Is Homeostatic Plasticity Important in Epilepsy? Issues in Clinical Epileptology: A View from the Bench *813*, 123-131.

Swiech, L., Perycz, M., Malik, A., and Jaworski, J. (2008). Role of mTOR in physiology and pathology of the nervous system. Biochimica et biophysica acta *1784*, 116-132.

Sytnyk, V., Leshchyns'ka, I., and Schachner, M. (2017). Neural Cell Adhesion Molecules of the Immunoglobulin Superfamily Regulate Synapse Formation, Maintenance, and Function. Trends in neurosciences *40*, 295-308.

Takei, N., Inamura, N., Kawamura, M., Namba, H., Hara, K., Yonezawa, K., and Nawa, H. (2004). Brain-derived neurotrophic factor induces mammalian target of rapamycin-dependent local activation of translation machinery and protein synthesis in neuronal dendrites. The Journal of neuroscience : the official journal of the Society for Neuroscience *24*, 9760-9769.

Tan, E.H., and Sansom, O.J. (2012). A new tumour suppressor enters the network of intestinal progenitor cell homeostasis. The EMBO journal *31*, 2444-2445.

Tanaka, J.I., Horiike, Y., Matsuzaki, M., Miyazaki, T., Ellis-Davies, G.C.R., and Kasai, H. (2008). Protein synthesis and neurotrophin-dependent structural plasticity of single dendritic spines. Science *319*, 1683-1687.

Tang, S.J., Reis, G., Kang, H., Gingras, A.C., Sonenberg, N., and Schuman, E.M. (2002). A rapamycin-sensitive signaling pathway contributes to long-term synaptic plasticity in the hippocampus. Proceedings of the National Academy of Sciences of the United States of America *99*, 467-472.

Tao, H.Z.W., and Poo, M.M. (2001). Retrograde signaling at central synapses. Proceedings of the National Academy of Sciences of the United States of America *98*, 11009-11015.

Tavazoie, S.F., Alvarez, V.A., Ridenour, D.A., Kwiatkowski, D.J., and Sabatini, B.L. (2005). Regulation of neuronal morphology and function by the tumor suppressors Tsc1 and Tsc2. Nature neuroscience *8*, 1727-1734.

Teichert, M., Liebmann, L., Hubner, C.A., and Bolz, J. (2017). Homeostatic plasticity and synaptic scaling in the adult mouse auditory cortex. Sci Rep-Uk *7*.

Thiagarajan, T.C., Lindskog, M., Malgaroli, A., and Tsien, R.W. (2007). LTP and adaptation to inactivity: overlapping mechanisms and implications for metaplasticity. Neuropharmacology *52*, 156-175.

Thomas, U., and Sigrist, S.J. (2012). Glutamate Receptors in Synaptic Assembly and Plasticity: Case Studies on Fly NMJs. Synaptic Plasticity: Dynamics, Development and Disease *970*, 3-28.

Tien, N.W., Soto, F., and Kerschensteiner, D. (2017). Homeostatic Plasticity Shapes Cell-Type-Specific Wiring in the Retina. Neuron *94*, 656-+.

Tiwari, S.K., Seth, B., Agarwal, S., Yadav, A., Karmakar, M., Gupta, S.K., Choubey, V., Sharma, A., and Chaturvedi, R.K. (2015). Ethosuximide Induces Hippocampal Neurogenesis and Reverses Cognitive Deficits in an Amyloid-beta Toxin-induced Alzheimer Rat Model via the Phosphatidylinositol 3-Kinase (PI3K)/Akt/Wnt/beta-Catenin Pathway. Journal of Biological Chemistry *290*, 28540-28558.

Toyo-Oka, K., Mori, D., Yano, Y., Shiota, M., Iwao, H., Goto, H., Inagaki, M., Hiraiwa, N., Muramatsu, M., Wynshaw-Boris, A*., et al.* (2008a). Protein phosphatase 4 catalytic subunit regulates Cdk1 activity and microtubule organization via NDEL1 dephosphorylation. Journal of Cell Biology *180*, 1133-1147.

Toyo-oka, K., Mori, D., Yano, Y., Shiota, M., Iwao, H., Goto, H., Inagaki, M., Hiraiwa, N., Muramatsu, M., Wynshaw-Boris, A*., et al.* (2008b). Protein phosphatase 4 catalytic subunit regulates Cdk1 activity and microtubule organization via NDEL1 dephosphorylation. The Journal of cell biology *180*, 1133-1147.

Turrigiano, G.G., Leslie, K.R., Desai, N.S., Rutherford, L.C., and Nelson, S.B. (1998). Activity-dependent scaling of quantal amplitude in neocortical neurons. Nature *391*, 892-896.

Turrigiano, G.G., and Nelson, S.B. (2004). Homeostatic plasticity in the developing nervous system. Nature Reviews Neuroscience *5*, 97-107.

Uylings, H.B.M., and de Brabander, J.M. (2002). Neuronal changes in normal human aging and Alzheimer's disease. Brain Cognition *49*, 268-276.

Vagnoni, A., and Bullock, S.L. (2018). A cAMP/PKA/Kinesin-1 Axis Promotes the Axonal Transport of Mitochondria in Aging Drosophila Neurons. Current Biology *28*, 1265-+.

Viquez, N.M., Fuger, P., Valakh, V., Daniels, R.W., Rasse, T.M., and DiAntonio, A. (2009). PP2A and GSK-3 beta Act Antagonistically to Regulate Active Zone Development. Journal of Neuroscience *29*, 11484-11494.

Viquez, N.M., Li, C.R., Wairkar, Y.P., and DiAntonio, A. (2006). The B ' protein phosphatase 2A regulatory subunit well-rounded regulates synaptic growth and cytoskeletal stability at the Drosophila neuromuscular junction. Journal of Neuroscience *26*, 9293-9303.

Voss, M., Campbell, K., Saranzewa, N., Campbell, D.G., Hastie, C.J., Peggie, M.W., Martin-Granados, C., Prescott, A.R., and Cohen, P.T. (2013). Protein phosphatase 4 is phosphorylated and inactivated by Cdk in response to spindle toxins and interacts with gamma-tubulin. Cell cycle (Georgetown, Tex) *12*, 2876-2887.

Wai, T., and Langer, T. (2016). Mitochondrial Dynamics and Metabolic Regulation. Trends in endocrinology and metabolism: TEM *27*, 105-117.

Wang, H.L., Zhang, Z.J., Hintze, M., and Chen, L. (2011). Decrease in Calcium Concentration Triggers Neuronal Retinoic Acid Synthesis during Homeostatic Synaptic Plasticity. Journal of Neuroscience *31*, 17764-17771.

Wang, T.T., Hauswirth, A.G., Tong, A., Dickman, D.K., and Davis, G.W. (2014). Endostatin Is a Trans-Synaptic Signal for Homeostatic Synaptic Plasticity. Neuron *83*, 616-629.

Washbourne, P., Dityatev, A., Scheiffele, P., Biederer, T., Weiner, J.A., Christopherson, K.S., and El-Husseini, A. (2004). Cell adhesion molecules in synapse formation. The Journal of neuroscience : the official journal of the Society for Neuroscience *24*, 9244-9249.

Wei, H., Wang, H., Ji, Q., Sun, J., Tao, L., and Zhou, X. (2015). NRBP1 is downregulated in breast cancer and NRBP1 overexpression inhibits cancer cell proliferation through Wnt/beta-catenin signaling pathway. OncoTargets and therapy *8*, 3721-3730.

Wentzel, C., Delvendahl, I., Sydlik, S., Georgiev, O., and Muller, M. (2018). Dysbindin links presynaptic proteasome function to homeostatic recruitment of low release probability vesicles. Nature communications *9*, 267.

Wierenga, C.J., Ibata, K., and Turrigiano, G.G. (2005). Postsynaptic expression of homeostatic plasticity at neocortical synapses. Journal of Neuroscience *25*, 2895-2905.

Wierenga, C.J., Walsh, M.F., and Turrigiano, G.G. (2006). Temporal regulation of the expression locus of homeostatic plasticity. J Neurophysiol *96*, 2127-2133.

Williams, M.E., de Wit, J., and Ghosh, A. (2010). Molecular mechanisms of synaptic specificity in developing neural circuits. Neuron *68*, 9-18.

Winfree, L.M., Speese, S.D., and Logan, M.A. (2017). Protein phosphatase 4 coordinates glial membrane recruitment and phagocytic clearance of degenerating axons in Drosophila. Cell Death Dis *8*, e2623.

Withers, G.S., Higgins, D., Charette, M., and Banker, G. (2000). Bone morphogenetic protein-7 enhances dendritic growth and receptivity to innervation in cultured hippocampal neurons. The European journal of neuroscience *12*, 106-116.

Wondolowski, J., and Dickman, D. (2013). Emerging links between homeostatic synaptic plasticity and neurological disease. Frontiers in cellular neuroscience *7*.

Wosiski-Kuhn, M., and Stranahan, A.M. (2012). Transient increases in dendritic spine density contribute to dentate gyrus long-term potentiation. Synapse *66*, 661-664.

Wu, C.L., Wairkar, Y.P., Collins, C.A., and DiAntonio, A. (2005). Highwire function at the Drosophila neuromuscular junction: Spatial, structural, and temporal requirements. Journal of Neuroscience *25*, 9557-9566.

Xie, Y.L., Juschke, C., Esk, C., Hirotsune, S., and Knoblich, J.A. (2013). The Phosphatase PP4c Controls Spindle Orientation to Maintain Proliferative Symmetric Divisions in the Developing Neocortex. Neuron *79*, 254-265.

Xing, G.L., Li, M.Y., Sun, Y.C., Rui, M.L., Zhuang, Y., Lv, H.H., Han, J.H., Jia, Z.P., and Xie, W. (2018). Neurexin-Neuroligin 1 regulates synaptic morphology and functions via the WAVE regulatory complex in Drosophila neuromuscular junction. eLife *7*.

Xu, J., Kang, N., Jiang, L., Nedergaard, M., and Kang, J. (2005). Activity-dependent long-term potentiation of intrinsic excitability in hippocampal CA1 pyramidal neurons. The Journal of neuroscience : the official journal of the Society for Neuroscience *25*, 1750-1760.

Xu, T., Yu, X., Perlik, A.J., Tobin, W.F., Zweig, J.A., Tennant, K., Jones, T., and Zuo, Y. (2009). Rapid formation and selective stabilization of synapses for enduring motor memories. Nature *462*, 915-919.

Yamagata, Y., Kobayashi, S., Umeda, T., Inoue, A., Sakagami, H., Fukaya, M., Watanabe, M., Hatanaka, N., Totsuka, M., Yagi, T.*, et al.* (2009). Kinase-dead knock-in mouse reveals an essential role of kinase activity of Ca2+/calmodulin-dependent protein kinase IIalpha in dendritic spine enlargement, long-term potentiation, and learning. The Journal of neuroscience : the official journal of the Society for Neuroscience *29*, 7607-7618.

Yeh, P.Y., Yeh, K.H., Chuang, S.E., Song, Y.C., and Cheng, A.L. (2004). Suppression of MEK/ERK signaling pathway enhances cisplatin-induced NF-kappa B activation by protein phosphatase 4-mediated NF-kappa B p65 Thr dephosphorylation. Journal of Biological Chemistry *279*, 26143-26148.

Zhang, X.W., Rui, M.L., Gan, G.M., Huang, C., Yi, J.K., Lv, H.H., and Xie, W. (2017). Neuroligin 4 regulates synaptic growth via the bone morphogenetic protein (BMP)

signaling pathway at the Drosophila neuromuscular junction. Journal of Biological Chemistry *292*, 17991-18005.

Zhao, C.J., Dreosti, E., and Lagnado, L. (2011). Homeostatic Synaptic Plasticity through Changes in Presynaptic Calcium Influx. Journal of Neuroscience *31*, 7492-7496.

Zhao, H.Y., Huang, X.Q., Jiao, J., Zhang, H.X., Liu, J., Qin, W.W., Meng, X.Y., Shen, T., Lin, Y.J., Chu, J.J*., et al.* (2015). Protein phosphatase 4 (PP4) functions as a critical regulator in tumor necrosis factor (TNF)-alpha-induced hepatic insulin resistance. Sci Rep-Uk *5*.

Zhou, G.S., Mihindukulasuriya, K.A., MacCorkle-Chosnek, R.A., Van Hooser, A., Hu, M.C.T., Brinkley, B.R., and Tan, T.H. (2002). Protein phosphatase 4 is involved in tumor necrosis factor-alpha-induced activation of c-Jun N-terminal kinase. Journal of Biological Chemistry *277*, 6391-6398.

Zhou, Q., Homma, K.J., and Poo, M.M. (2004). Shrinkage of dendritic spines associated with long-term depression of hippocampal synapses. Neuron *44*, 749-757.

Zito, K., Parnas, D., Fetter, R.D., Isacoff, E.Y., and Goodman, C.S. (1999). Watching a synapse grow: noninvasive confocal imaging of synaptic growth in Drosophila. Neuron *22*, 719-729.

8 Supplemental Information

8.1 Supplemental information for Madm

Madm is essential for synaptic stability (Figure 4)

Table 1 Frequency of synaptic retractions

Genotype	Retraction frequency ± SEM (%)	p value	n
Control	0.67±0.4479		10
Madm $^{4S3/Df}$	45.6±7.381	<0.0001	10
Madm$^{2D2/Df}$	34.38±3.16	<0.0001	10
Madm $^{EP/Df}$	25.26±2.479	<0.0001	10
neur$^{elav;\ dcr2}$ >Madm ^{RNAi}	24.54±4.008	<0.0001	10
rescue construct; Madm$^{4S3/Df}$	28.33±4.276	<0.0001	10
neur >;; Madm$^{4S3/Df}$	26.32±1.549	<0.0001	10
musc >; Madm$^{4S3/Df}$	27.32±3.249	<0.0001	10
neur 1> rescue; Madm$^{4S3/Df}$	2.742±0.6687	0.651	10
neur 2> rescue; Madm$^{4S3/Df}$	4.986±0.8113	0.3468	8
musc> rescue; Madm$^{4S3/Df}$	10.75±2.391	0.0295	10
neur + musc> rescue; Madm$^{4S3/Df}$	0.983±0.5019	0.9455	10

Retraction frequency of mentioned genotypes on muscle group m1/9 & m2&10. p value is calculated relative to control. n equals to number of animals analyzed.

Table 1a Statistical comparisons between genotypes

Statistical comparison between genotypes		p value
rescue construct; Madm$^{4S3/Df}$	*neur 1> rescue; Madm$^{4S3/Df}$*	<0.0001
rescue construct; Madm$^{4S3/Df}$	*neur 2> rescue; Madm$^{4S3/Df}$*	<0.0001
rescue construct; Madm$^{4S3/Df}$	*neur + musc> rescue; Madm$^{4S3/Df}$*	<0.0001
musc > Madm$^{4S3/Df}$	*musc> rescue; Madm$^{4S3/Df}$*	0.0004

Madm is essential for synaptic growth and organization (Figure 5)

Table 2 Number of boutons

Genotype	# boutons ± SEM (%)	p value	n
Control	30.54±1.195		24
Madm $^{4S3/Df}$	18.68±0.5843	0.0001	28
neur >; ; Madm$^{4S3/Df}$	16.75±0.7761	0.0001	24
rescue construct; Madm$^{4S3/Df}$	18.71±0.7398	0.0001	28
musc >; Madm$^{4S3/Df}$	17.05±0.6884	0.0001	22
neur 1> rescue; Madm$^{4S3/Df}$	28.08±0.9147	0.2408	24
neur 2> rescue; Madm$^{4S3/Df}$	27.09±1.004	0.041	22
musc> rescue; Madm$^{4S3/Df}$	17.57±0.8123	0.0001	28
neur + musc> rescue; Madm$^{4S3/Df}$	27.3±0.9208	0.0952	20

Number of boutons among genotypes on muscle1. p value is calculated relative to control.

n equals to number of NMJs analyzed

Table 2a Statistical comparisons between genotypes

Statistical comparison between genotypes		p value
rescue construct; Madm$^{4S3/Df}$	*neur 1> rescue; Madm$^{4S3/Df}$*	0.0001
rescue construct; Madm$^{4S3/Df}$	*neur 2> rescue; Madm$^{4S3/Df}$*	0.0001
rescue construct; Madm$^{4S3/Df}$	*neur + musc> rescue; Madm$^{4S3/Df}$*	0.0001
musc > Madm$^{4S3/Df}$	*musc> rescue; Madm$^{4S3/Df}$*	0.9993

Table 3 NMJ length (µm)

Genotype	NMJ length (µm) ± SEM	p value	n
Control	119.9±4.772		24
Madm $^{4S3/Df}$	66.8±2.817	0.0001	28
neur >; ; Madm$^{4S3/Df}$	71.02±3.24	0.0001	24
rescue construct; Madm$^{4S3/Df}$	74.28±4.555	0.0001	28
musc >; Madm$^{4S3/Df}$	73.56±4.878	0.0001	22

neur 1> rescue; Madm$^{4S3/Df}$	122.5±6.616	0.9994	24
neur 2> rescue; Madm$^{4S3/Df}$	110.8±7.363	0.7044	22
musc> rescue; Madm$^{4S3/Df}$	77.71±3.673	0.0001	28
neur + musc> rescue; Madm$^{4S3/Df}$	103.9±5.361	0.1579	20

Number of boutons among genotypes on muscle1. p value is calculated relative to control.

n equals to number of NMJs analyzed

Table 3a Statistical comparisons between genotypes

Statistical comparison between genotypes		**p value**
rescue construct; Madm$^{4S3/Df}$	*neur 1> rescue; Madm$^{4S3/Df}$*	0.0001
rescue construct; Madm$^{4S3/Df}$	*neur 2> rescue; Madm$^{4S3/Df}$*	0.0001
rescue construct; Madm$^{4S3/Df}$	*neur + musc> rescue; Madm$^{4S3/Df}$*	0.0003
musc > Madm$^{4S3/Df}$	*musc> rescue; Madm$^{4S3/Df}$*	0.9993

Table 4 Number of branches

Genotype	**# branches ± SEM**	**p value**	**n**
Control	1.875±0.1735		24
Madm $^{4S3/Df}$	5.586±0.3562	0.0001	28
neur >;; Madm$^{4S3/Df}$	5.25±0.2839	0.0001	24
rescue construct; Madm$^{4S3/Df}$	5.417±0.2401	0.0001	28
musc >; Madm$^{4S3/Df}$	5.458±0.3806	0.0001	22
neur 1> rescue; Madm$^{4S3/Df}$	3.667±0.4765	0.0007	24
neur 2> rescue; Madm$^{4S3/Df}$	3.409±0.1936	0.0071	22
musc> rescue; Madm$^{4S3/Df}$	1.107±0.1295	0.3728	28
neur + musc> rescue; Madm$^{4S3/Df}$	3.263±0.1499	0.0276	20

Number of branches among genotypes on muscle1. p value is calculated relative to control.

n equals to number of NMJs analyzed

Table 4a Statistical comparisons between genotypes

Statistical comparison between genotypes		**p value**
rescue construct; Madm$^{4S3/Df}$	*neur 1> rescue; Madm$^{4S3/Df}$*	0.001
rescue construct; Madm$^{4S3/Df}$	*neur 2> rescue; Madm$^{4S3/Df}$*	0.0002
rescue construct; Madm$^{4S3/Df}$	*neur + musc> rescue; Madm$^{4S3/Df}$*	0.0001
musc > Madm$^{4S3/Df}$	*musc> rescue; Madm$^{4S3/Df}$*	0.0001

Table 5 NMJ area per muscle area

Genotype	**NMJ area/ muscle area ± SEM**	**p value**	**n**
Control	2.217±0.2403		24
Madm $^{4S3/Df}$	0.3996±0.0355	<0.0001	28
neur >;; Madm$^{4S3/Df}$	0.4367±0.07042	<0.0001	24
rescue construct; Madm$^{4S3/Df}$	0.5699±0.089	<0.0001	28
musc >; Madm$^{4S3/Df}$	0.5355±0.08905	<0.0001	22
neur 1> rescue; Madm$^{4S3/Df}$	1.823±0.1952	>0.9999	24
neur 2> rescue; Madm$^{4S3/Df}$	1.568±0.1326	>0.9999	22
musc> rescue; Madm$^{4S3/Df}$	0.9535±0.09419	0.0060	28
neur + musc> rescue; Madm$^{4S3/Df}$	1.744±0.1982	>0.9999	20

NMJ area per muscle area among genotypes on muscle1. p value is calculated relative to control. n equals to number of NMJs analyzed

Table 5a Statistical comparisons among genotypes

Statistical comparison between genotypes		**p value**
rescue construct; Madm$^{4S3/Df}$	*neur 1> rescue; Madm$^{4S3/Df}$*	<0.0001
rescue construct; Madm$^{4S3/Df}$	*neur 2> rescue; Madm$^{4S3/Df}$*	<0.0001
rescue construct; Madm$^{4S3/Df}$	*neur + musc> rescue; Madm$^{4S3/Df}$*	<0.0001
musc > Madm$^{4S3/Df}$	*musc> rescue; Madm$^{4S3/Df}$*	0.0498

Madm is essential at the later stages of synapse development (Figure 6)

Table 6 Morphology comparisons of 2nd and 3rd instar larvae of comtrol and Madm mutant

Genotype	2nd Instar	3rd Instar	n
Control	11.666±0.476	8.375±0.411	24
Madm $^{4S3/Df}$	30.958±1.266	18.833±0.658	24
p Value	0.003642	<0.000001	

Number of boutons among genotypes on muscle1. p value is calculated relative to control. n equals to number of NMJs analyzed.

Table 7 Frequency of retraction of NMJs among 2nd and 3rd instar larvae of control and Madm mutant

Genotype	2nd Instar	3rd Instar	n
Control	0.331±0.331	0.313±0.313	10
Madm $^{4S3/Df}$	0.67±0.447	45.595±7.381	10
P Value	0.997277	<0.000001	

Retraction frequency of mentioned genotypes on muscle group m1/9 & m2&10. p value is calculated relative to control. n equals to number of animals analyzed.

Genetic interaction of Madm with Mlf1 and bun (Figure 7)

Table 8 Number of boutons

Genotype	# boutons ± SEM	p value	n
Control	31.83±0.9415		24
Madm$^{4S3/+}$	30.96±1.266	>0.9999	24
Mlf$^{\Delta C1/+}$	34.09±2.33	0.9454	22
bun$^{200B/+}$	32.96±0.9018	0.9996	24
Mlf$^{\Delta C1}$/Mlf$^{\Delta C1}$.mat	16.17±0.8527	<0.0001	24
Mlf$^{\Delta C1}$/+; Madm$^{4S3/+}$	27±1.022	0.0664	31
bun^{200B}/bun^{GE}	27.88±0.8455	0.3139	26
bun$^{200B/+}$; Madm$^{4S3/+}$	27.26±1.189	0.1298	27

Number of boutons among genotypes on muscle1. p value is calculated relative to control. n equals to number of NMJs analyzed.

Table 9 NMJ length

Genotype	NMJ length ± SEM (μm)	p value	n
Control	135.2±5.376		24
$Madm^{4S3/+}$	124.2±6.271	>0.9999	24
$Mlf^{\Delta C1/+}$	137.5±15.14	>0.9999	22
$bun^{200B/+}$	138.4±4.475	>0.9999	24
$Mlf^{\Delta C1}/Mlf^{\Delta C1}$.mat	75.31±4.272	<0.0001	24
$Mlf^{\Delta C1}$/+; $Madm^{4S3/+}$	113±4.638	0.4871	31
bun^{200B}/bun^{GE}	108.5±4.836	0.0886	26
$bun^{200B/+}$; $Madm^{4S3/+}$	108.8±4.149	0.1094	27

NMJ length among genotypes on muscle1. p value is calculated relative to control. n equals to number of NMJs analyzed.

Table 10 NMJ area per muscle area

Genotype	NMJ area per muscle area ± SEM	p value	n
Control	2.368±0.3081		24
$Madm^{4S3/+}$	2.217±0.2403	0.9993	24
$Mlf^{\Delta C1/+}$	2.18±0.1898	0.9965	22
$bun^{200B/+}$	1.905±0.1365	0.6123	24
$Mlf^{\Delta C1}/Mlf^{\Delta C1}$.mat	1.137±0.1604	0.0011	24
$Mlf^{\Delta C1}$/+; $Madm^{4S3/+}$	1.748±0.1257	0.2339	31
bun^{200B}/bun^{GE}	1.947±0.2488	0.7214	26
$bun^{200B/+}$; $Madm^{4S3/+}$	1.789±0.2466	0.3018	27

NMJ area per muscle area among genotypes on muscle1. p value is calculated relative to control. n equals to number of NMJs analyzed.

Table 11 Frequency of synaptic retractions

Genotype	Retraction frequency ± SEM (%)	p value	n
Control	0.67±0.4479		10
Madm$^{4S3/+}$	0.67±0.4479	>0.9999	10
Mlf$^{C1/+}$	3.127±0.8069	0.6007	10
bun$^{200B/+}$	0.714±0.476	>0.9999	10
Mlf^{C1}/Mlf^{C1}.mat	12.8±2.969	<0.0001	10
Mlf^{C1}/+; Madm$^{4S3/+}$	2.503±0.6253	>0.9999	10
bun^{200B}/bun^{GE}	3.314±0.8498	0.2298	10
bun$^{200B/+}$; Madm$^{4S3/+}$	1.728±0.581	>0.9999	10

Retraction frequency of mentioned genotypes on muscle group m1/9 & m2&10. p value is calculated relative to control. n equals to number of animals analyzed.

Genetic interaction of Madm with BMP and mTOR pathway components (Figure 8)

Table 12 Number of boutons

Genotype	# boutons ± SEM	p value	n
Control	31.83±0.9415		24
Madm^{4S3}/+	30.96±1.266	>0.9999	24
Rheb^{AV4}/+	29.24±0.7287	0.9932	25
Rheb^{AV4}/Madm^{4S3}	20.53±0.6986	<0.0001	36
gig^{109}/+	37.43±1.204	0.0197	47
gig^{109}/Madm^{4S3}	25.92±0.8987	0.0077	49
TSC1/+	32.86±1.354	>0.9999	22
TSC1^{f01910}/Madm^{4S3}	30.33±0.9042	>0.9999	27
wit^{A12}/+	31.8±0.9747	>0.9999	25
wit^{A12}/Madm^{4S3}	30.33±1.059	>0.9999	24
tkv^{1}/Madm^{4S3}	30.48±1.081	>0.9999	21
tkv^{1}/+	28.82±1.072	0.953	28
Mad^{12}/+	27.37±1.214	0.5948	19
Mad^{12}/Madm^{4S3}	29.16±1.212	0.9959	19

Number of boutons among genotypes on muscle1. p value is calculated relative to control. n equals to number of NMJs analyzed

Table 12a Statistical comparisons between genotypes

Statistical comparison between genotypes		**p value**
Madm^{4S3}/+	*Rheb^{AV4}/+*	0.4122
Rheb^{AV4}/+	*Rheb^{AV4}/Madm^{4S3}*	<0.0001
Madm^{4S3}/+	*Rheb^{AV4}/Madm^{4S3}*	<0.0001
Madm^{4S3}/+	*gig^{109}/+*	0.0012
gig^{109}/+	*gig^{109}/Madm^{4S3}*	<0.0001
Madm^{4S3}/+	*gig^{109}/Madm^{4S3}*	0.0144

Table 13 NMJ length

Genotype	**NMJ length (µm) ± SEM**	**p value**	**n**
Control	134±4.95		24
Madm$^{4S3/+}$	121.7±4.904	0.8164	24
Rheb^{AV4}/+	137.6±5.841	0.999	25
Rheb^{AV4}/Madm^{4S3}	77.03±2.514	<0.0001	35
gig^{109}/+	161.7±8.071	0.0173	48
gig^{109}/Madm^{4S3}	105.7±3.662	0.0143	48

NMJ length among genotypes on muscle1. p value is calculated relative to control. n equals to number of NMJs analyzed

Table 13a Statistical comparisons between genotypes

Statistical comparison between genotypes		**p value**
Madm^{4S3}/+	*Rheb^{AV4}/+*	0.0414
Rheb^{AV4}/+	*Rheb^{AV4}/Madm^{4S3}*	<0.0001
Madm^{4S3}/+	*Rheb^{AV4}/Madm^{4S3}*	<0.0001
Madm^{4S3}/+	*gig^{109}/+*	0.0004
gig^{109}/+	*gig^{109}/Madm^{4S3}*	<0.0001

Madm^{4S3}/+	*gig^{109}/Madm^{4S3}*	0.2557

Table 14 NMJ span

Genotype	NMJ span (µm) ± SEM	p value	n
Control	91.7±5.125		24
Madm$^{4S3/+}$	80.28±4.823	0.663	24
Rheb^{AV4}/+	109.4±6.552	0.1785	25
Rheb^{AV4}/Madm^{4S3}	48.71±2.585	<0.0001	35
gig^{109}/+	103.5±5.033	0.469	48
gig^{109}/Madm^{4S3}	63.8±2.92	0.0005	48

NMJ span among genotypes on muscle1. p value is calculated relative to control. n equals to number of NMJs analyzed

Table 14a Statistical comparisons between genotypes

Statistical comparison between genotypes		p value
Madm^{4S3}/+	*Rheb^{AV4}/+*	0.0002
Rheb^{AV4}/+	*Rheb^{AV4}/Madm^{4S3}*	<0.0001
Madm^{4S3}/+	*Rheb^{AV4}/Madm^{4S3}*	<0.0001
Madm^{4S3}/+	*gig^{109}/+*	0.0029
gig^{109}/+	*gig^{109}/Madm^{4S3}*	<0.0001
Madm^{4S3}/+	*gig^{109}/Madm^{4S3}*	0.0475

Table 15 NMJ length

Genotype	NMJ length (um)	p value	n
Control	2.409±0.2969		24
Madm$^{4S3/+}$	2.217±0.2403	0.9907	24
Rheb^{AV4}/+	2.617±0.3084	0.9888	25
Rheb^{AV4}/Madm^{4S3}	1.156±0.09653	0.0005	35
gig^{109}/+	2.267±0.2067	0.996	48
gig^{109}/Madm^{4S3}	1.436±0.1016	0.0077	48

NMJ area per muscle area among genotypes on muscle1. p value is calculated relative to control. n equals to number of NMJs analyzed

Table 15a Statistical comparisons between genotypes

Statistical comparisons between genotypes		**p value**
Madm^{4S3}/+	*Rheb^{AV4}/+*	0.4082
Rheb^{AV4}/+	*Rheb^{AV4}/Madm^{4S3}*	0.0009
Madm^{4S3}/+	*Rheb^{AV4}/Madm^{4S3}*	<0.0001
Madm^{4S3}/+	*gig^{109}/+*	0.9817
gig^{109}/+	*gig^{109}/Madm^{4S3}*	0.0134
Madm^{4S3}/+	*gig^{109}/Madm^{4S3}*	0.0013

Genetic interaction of Madm with Rheb (Figure 9)

Table 16 Number of boutons

Genotype	**# boutons ± SEM**	**p value**	**n**
Control	31.83±0.9415		24
Madm$^{4S3/Df}$	18.68±0.5843	<0.0001	28
Neuro>UAS Rheb/+; Madm$^{4S3/Df}$	50.66±1.84	<0.0001	32
Neuro>UASRheb	53.09±1.603	<0.0001	32

Number of boutons among genotypes on muscle1. p value is calculated relative to control. n equals to number of NMJs analyzed

Table 16a Statistical comparisons among genotypes

Statistical comparison between genotypes		**p value**
Madm$^{4S3/Df}$	*Neuro>UAS Rheb/+; Madm$^{4S3/Df}$*	<0.0001

Table 17 NMJ length

Genotype	**NMJ length(µm) ± SEM**	**p value**	**n**
Control	31.83±0.9415		24
Madm$^{4S3/Df}$	18.68±0.5843	<0.0001	28
Neuro>UAS Rheb/+; Madm$^{4S3/Df}$	50.66±1.84	0.014	32
Neuro>UASRheb	53.09±1.603	<0.0001	32

NMJ length among genotypes on muscle1. p value is calculated relative to control. n equals to number of NMJs analyzed

Table 17a Statistical comparisons between genotypes

Statistical comparison between genotypes		**p value**
Madm$^{4S3/Df}$	*Neuro>UAS Rheb/+; Madm$^{4S3/Df}$*	<0.0001

Table 18 Number of branches

Genotype	**# branches ± SEM**	**p value**	**n**
Control	1.875±0.1735		24
Madm$^{4S3/Df}$	5.586±0.3562	<0.0001	28
Neuro>UAS Rheb/+; Madm$^{4S3/Df}$	6.625±0.423	<0.0001	32
Neuro>UASRheb	5.844±0.3539	<0.0001	32

Number of branches among genotypes on muscle1. P value is calculated relative to control. n equals to number of NMJs analyzed

Table 18a Statistical comparisons between genotypes

Statistical comparison between genotypes		**p value**
Madm$^{4S3/Df}$	*Neuro>UAS Rheb/+; Madm$^{4S3/Df}$*	<0.0001

Table 19 NMJ area per muscle area

Genotype	**NMJ area per muscle area ± SEM (%)**	**p value**	**n**
Control	2.368±0.3081		24
Madm$^{4S3/Df}$	0.3996±0.0355	<0.0001	28
Neuro>UAS Rheb/+; Madm$^{4S3/Df}$	3.09±0.26	0.2704	32
Neuro>UASRheb	5.204±0.3634	<0.0001	32

NMJ area per muscle area among genotypes on muscle1. p value is calculated relative to control. n equals to number of NMJs analyzed

Table 19a Statistical comparisons between genotypes

Statistical comparison between genotypes		p value
Madm$^{4S3/Df}$	*Neuro>UAS Rheb/+; Madm$^{4S3/Df}$*	<0.0001

Genetic interaction of Madm with Thor (Figure 10)

Table 20 Number of boutons

Genotype	# boutons ± SEM	p value	n
Control	31.83±0.9415		24
Madm$^{4S3/Df}$	18.68±0.5843	<0.0001	28
Thor^{2}	44.58±1.032	<0.0001	24
Thor^{2}; Madm$^{4S3/Df}$	23.61±0.683	<0.0001	28
neuro>UASThor	22.25±1.425	<0.0001	20
neuro>UAS GFP Madm	31.84±1.089	>0.9999	44
neuro>UASThor/UAS GFP Madm	28.15±0.653	0.0737	48

Number of boutons among genotypes on muscle1. p value is calculated relative to control. n equals to number of NMJs analyzed

Table 20a Statistical comparisons between genotypes

Statistical comparison between genotypes		p value
Madm$^{4S3/Df}$	*Thor^{2}; Madm$^{4S3/Df}$*	0.0087
Thor^{2}	*Thor^{2}; Madm$^{4S3/Df}$*	<0.0001
neuro>UASThor	*neuro>UASThor/UAS GFP Madm*	0.0006
neuro>UAS GFP Madm	*neuro>UASThor/UAS GFP Madm*	0.0139

Table 21 NMJ length

Genotype	NMJ length (μm) ± SEM	p value	n
Control	132.8±5.031		23
Madm$^{4S3/Df}$	66.8±2.817	<0.0001	28
Thor^{2}	174.9±7.445	<0.0001	24

Thor^{2}; Madm$^{4S3/Df}$	84.33±3.304	<0.0001	28
neuro>UASThor	94.77±7.624	0.0011	18
neuro>UAS GFP Madm	131.5±6.449	>0.9999	44
neuro>UASThor/UAS GFP Madm	120.2±3.25	0.6209	48

NMJ length among genotypes on muscle1. p value is calculated relative to control. n equals to number of NMJs analyzed

Table 21a Statistical comparison between genotypes

Statistical comparison between genotypes		**p value**
Madm$^{4S3/Df}$	*Thor^{2}; Madm$^{4S3/Df}$*	0.2833
Thor^{2}	*Thor^{2}; Madm$^{4S3/Df}$*	<0.0001
neuro>UASThor	*neuro>UASThor/UAS GFP Madm*	0.0321
neuro>UAS GFP Madm	*neuro>UASThor/UAS GFP Madm*	0.518

Table 22 NMJ area per muscle area

Genotype	**NMJ area per muscle area ± SEM**	**p value**	**n**
Control	2.368±0.3081		24
Madm$^{4S3/Df}$	0.381±0.03141	<0.0001	28
Thor^{2}	4.29±0.3299	<0.0001	24
Thor^{2}; Madm$^{4S3/Df}$	1.277±0.1595	0.0166	28
neuro>UASThor	1.271±0.1758	0.0137	20
neuro>UAS GFP Madm	2.556±0.1957	0.9956	44
neuro>UASThor/UAS GFP Madm	2.473±0.1787	0.9998	48

NMJ area per muscle area among genotypes on muscle1. P value is calculated relative to control. n equals to number of NMJs analyzed

Table 22a Statistical comparisons between genotypes

Statistical comparison between genotypes		**p value**
Madm$^{4S3/Df}$	*Thor^{2}; Madm$^{4S3/Df}$*	0.0737
Thor^{2}	*Thor^{2}; Madm$^{4S3/Df}$*	<0.0001

neuro>UASThor	*neuro>UASThor/UAS GFP Madm*	0.0041
neuro>UAS GFP Madm	*neuro>UASThor/UAS GFP Madm*	0.9999

Table 23 NMJ retraction frequency

Genotype	Retraction frequency ± SEM (%)	p value	n
Control	0.67±0.4479		10
$Madm^{4S3/Df}$	45.6±7.381	<0.0001	10
Neur>UAS Rheb; $Madm^{4S3/Df}$	15±2.273	<0.0001	10
$Thor^{2}$; $Madm^{4S3/Df}$	11.7±1.769	<0.0001	12

NMJ retraction frequency among genotypes on muscle1/2 and 2/10 groups. p value is calculated relative to control. n equals to number of animals analyzed

Table 23a Statistical comparisons between genotypes

Statistical comparison between genotypes		p value
$Madm^{4S3/Df}$	*Neur>UAS Rheb; $Madm^{4S3/Df}$*	<0.0001
$Madm^{4S3/Df}$	*$Thor^{2}$; $Madm^{4S3/Df}$*	<0.0001

<u>Madm is essential for basal synaptic transmission (Figure 11)</u>

Table 24 Normalized mEJC Amplitude

Genotype	mEJC Amplitude ± SEM	p value	n
control	99.94±4.41		17
$Madm^{4S3/Df}$	108.33±3.88	0.8103	12
neuronal rescue	105.71±5.51	0.911	16
muscle rescue	92.32±4.22	0.8185	16

p value is calculated relative to control. n equals to number of NMJs analyzed

Table 24a Statistical comparison between genotypes

Statistical comparison between genotypes		p value
$Madm^{4S3/Df}$	*neuronal rescue*	0.9928
	muscle rescue	0.3401

Table 25 Normalized EJC Amplitude

Genotype	EJC Amplitude ± SEM	p value	n
control	99.99±5.76		17
Madm$^{4S3/Df}$	69.6±4.62	0.0083	12
neuronal rescue	94.42±8.16	0.9193	16
muscle rescue	95.21±6.83	0.9468	16

p value is calculated relative to control. n equals to number of NMJs analyzed

Table 25a Statistical comparison between genotypes

Statistical comparison between genotypes		p value
Madm$^{4S3/Df}$	*neuronal rescue*	0.0497
	muscle rescue	0.0401

Table 26 Normalized Quantal content

Genotype	QC ± SEM	p value	n
control	100±5.46		17
Madm$^{4S3/Df}$	63.73±4.04	0.001	12
neuronal rescue	90.84±9.25	0.72	16
muscle rescue	104.58±8.75	0.953	16

p value is calculated relative to control. n equals to number of NMJs analyzed

Table 26a Statistical comparison between genotypes

Statistical comparison between genotypes		p value
Madm$^{4S3/Df}$	*neuronal rescue*	0.0261
	muscle rescue	0.0002

Table 27 mEJC frequency

Genotype	Frequency ± SEM	p value to control	n

W1118	1.211 ± 0.1354		17
Madm$^{4S3/Df}$	2.78 ± 0.3863	0.0017	12
neuronal rescue	2.559 ± 0.3462	0.0039	16
muscle rescue	2.986 ± 0.2329	0.0003	16

p value is calculated relative to control. n equals to number of NMJs analyzed

Table 27a Statistical comparisons between genotypes

Statistical comparison between genotypes		**p value**
Madm$^{4S3/Df}$	neuronal rescue	0.9953
	muscle rescue	0.9978

Madm plas dual role in the regulation of synaptic transmission (Figure 12)

Table 28 Normalized mEJC amplitude

Genotype	**mEJC Amplitude ± SEM**	**p value**	**n**
Control	99.65±11.85		14
Madm$^{4S3/+}$	104.21±32.5	0.6269	13
GluRIIA$^{SP16/SP16}$	52.2±14.76	<0.0001	13
GluRIIA$^{SP16/SP16}$; Madm$^{4S3/+}$	44.82±6.89	<0.0001	14
GluRIIA$^{SP16/SP16}$; muscle Madm KD	49.23±11.86	<0.0001	8
GluRIIA$^{SP16/SP16}$; Madm$^{4S3/Df}$	65.087±13.77	<0.0001	14
GluRIIA$^{SP16/SP16}$; Madm$^{4S3/Df}$ normalized to Madm$^{4S3/Df}$	50.93±10.78		14
muscle> UAS GFP Madm	82.96+5.33	0.2225	16
muscle> UAS TOR	86.73+3.745	0.4002	16

p value is calculated relative to control. n equals to number of NMJs analyzed

Table 29 Normalized EJC Amplitude

Genotype	EJC Amplitude ± SEM	p value	n
Control	99.98±25.8		14
$Madm^{4S3/+}$	84.68±33.57	0.1943	13
$GluRIIA^{SP16/SP16}$	89.28±25.29	0.2781	14
$GluRIIA^{SP16/SP16}$; $Madm^{4S3/+}$	74.16±21.76	0.0082	14
$GluRIIA^{SP16/SP16}$; muscle Madm KD	102.8±39.81	0.8416	8
$GluRIIA^{SP16/SP16}$; $Madm^{4S3/Df}$	68.66±25.77	0.0034	14
$GluRIIA^{SP16/SP16}$; $Madm^{4S3/Df}$ normalized to $Madm^{4S3/Df}$	89.062±33.42	<0.0001	14
muscle> UAS GFP Madm	124.288.64	0.0485	16
muscle> UAS TOR	136.22+7.37	0.0015	16

p value is calculated relative to control. n equals to number of NMJs analyzed

Table 30 Quantal content

Genotype	QC ± SEM	p value	n
Control	100.01±30.87		14
$Madm^{4S3/+}$	78.18±15.37	0.0303	13
$GluRIIA^{SP16/SP16}$	169.61±58.33	0.0006	13
$GluRIIA^{SP16/SP16}$; $Madm^{4S3/+}$	162.18±41.94	0.0001	14
$GluRIIA^{SP16/SP16}$; muscle Madm KD	213.59±95.54	0.0004	8
$GluRIIA^{SP16/SP16}$; $Madm^{4S3/Df}$	107.73±46.57	0.6094	14
$GluRIIA^{SP16/SP16}$; $Madm^{4S3/Df}$ normalized to $Madm^{4S3/Df}$	182.52±78.91	0.0011	14
muscle> UAS GFP Madm	154.83+13.26	<0.0001	16
muscle> UAS TOR	156.47+7.2	<0.0001	16

p value is calculated relative to control. n equals to number of NMJs analyzed

Genetic interaction of Madm with Mlf and bun (Figure 15)

Table 31 Number of boutons

Genotypes	# boutons ± SEM	p value	n
Madm$^{2D2/+}$	31.75±0.8933		28
Mlf$^{\Delta C1/+}$	34.09±2.33	0.8089	22
bun$^{200B/+}$	32.96±0.9018	0.978	24
Mlf$^{\Delta C1/+}$; Madm$^{2D2/+}$	33.86±1.342	0.8311	28
bun$^{200B/+}$; Madm$^{2D2/+}$	38.13±1.852	0.0229	24

Number of boutons among genotypes on muscle1. p value is calculated relative to control. n equals to number of NMJs analyzed.

Table 32 NMJ length

Genotypes	NMJ length (µm) ± SEM	p value	n
Madm$^{2D2/+}$	123.4±3.905		28
Mlf$^{\Delta C1/+}$	137.5±15.14	>0.9999	22
bun$^{200B/+}$	138.8±4.644	0.6298	24
Mlf$^{\Delta C1/+}$; Madm$^{2D2/+}$	121.9±7.096	>0.9999	28
bun$^{200B/+}$; Madm$^{2D2/+}$	134.2±5.561	>0.9999	24

NMJ length among genotypes on muscle1. p value is calculated relative to control. n equals to number of NMJs analyzed

Table 33 NMJ area per muscle area

Genotypes	NMJ area/ muscle area ± SEM	p value	n
Madm$^{2D2/+}$	2.521±0.1893		28
Mlf$^{\Delta C1/+}$	1.911±0.2492	0.3425	22
bun$^{200B/+}$	2.081±0.1523	>0.9999	24
Mlf$^{\Delta C1/+}$; Madm$^{2D2/+}$	2.258±0.2358	>0.9999	28
bun$^{200B/+}$; Madm$^{2D2/+}$	2.61±0.2293	>0.9999	24

Number of branches among genotypes on muscle1. p value is calculated relative to control. n equals to number of NMJs analyzed

Genetic interaction of Madm with mTOR pathway components (Figure 16)

Table 34 Number of boutons

Genotypes	# boutons ± SEM	p value	n
elav/+	32.18±0.9949		22
$Madm^{2D2/+}$	31.75±0.8933	0.9954	28
$gig^{109}/+$	37.44±1.178	0.0104	48
$gig^{109}/Madm^{2D2}$	25.44±0.9384	0.0007	41

Number of boutons among genotypes on muscle1. p value is calculated relative to control. n equals to number of NMJs analyzed

Table 35 NMJ length

Genotypes	NMJ length (µm) ± SEM	p value	n
elav/+	136±5.746		22
$Madm^{2D2/+}$	123.4±3.905	0.5436	28
$gig^{109}/+$	161.7±8.071	0.0318	48
$gig^{109}/Madm^{2D2}$	123.9±5.307	0.5109	41

NMJ length among genotypes on muscle1. p value is calculated relative to control. n equals to number of NMJs analyzed

Table 36 NMJ area per muscle area

Genotypes	NMJ area/ muscle area ± SEM	p value	n
elav/+	2.703±0.2823		22
$Madm^{2D2/+}$	2.521±0.1893	0.9577	28
$gig^{109}/+$	2.166±0.2096	0.373	48
$gig^{109}/Madm^{2D2}$	2.137±0.1996	0.3489	41

NMJ area per muscle area among genotypes on muscle1. p value is calculated relative to control. n equals to number of NMJs analyzed

Table 37 Number of boutons

Genotypes	# boutons ± SEM	p value	n
elav/+	32.18±0.9949		22
$Madm^{2D2/+}$	30.29±0.6412	0.4165	24
$Rheb^{AV4}/+$	29.24±0.7287	0.0874	25
$Rheb^{AV4}/Madm^{2D2}$	28.67±1.344	0.0396	21
$Rheb^{4L1}/Madm^{4S3}$	20.21±0.855	0.0001	28

Number of boutons among genotypes on muscle1. p value is calculated relative to control. n equals to number of NMJs analyzed

Table 38 NMJ length

Genotypes	NMJ length (μm) ± SEM	p value	n
elav/+	136±5.746		24
$Madm^{2D2/+}$	123.4±3.905	0.2454	28
$Rheb^{AV4}/+$	136.6±6.309	0.9999	23
$Rheb^{AV4}/Madm^{2D2}$	127.3±6.696	0.626	21
$Rheb^{4L1}/Madm^{4S3}$	85.97±3.79	0.0001	28

NMJ length among genotypes on muscle1. p value is calculated relative to control. n equals to number of NMJs analyzed

Table 39 NMJ area per muscle area

Genotypes	NMJ area/ muscle area ± SEM	p value	n
elav/+	2.368±0.3081		24
$Madm^{2D2/+}$	2.521±0.1893	0.9705	28
$Rheb^{AV4}/+$	2.617±0.3084	0.8819	23
$Rheb^{AV4}/Madm^{2D2}$	2.135±0.25	0.9006	21
$Rheb^{4L1}/Madm^{4S3}$	1.281±0.1127	0.0037	28

NMJ area per muscle area among genotypes on muscle1. p value is calculated relative to control. n equals to number of NMJs analyzed

Table 40 Number of boutons

Genotypes	# boutons ± SEM	p value	n
elav/+	32.18±0.9949		22
$Madm^{4S3/+}$	30.96±1.266	0.9657	24
$Madm^{2D2/+}$	31.75±0.8933	0.9657	28
$s6k^{l-1}$/+	40.35±2.686	0.004	32
$S6k^{l-1}/Madm^{2D2}$	25.62±0.7111	0.0054	47
$S6k^{l-1}/Madm^{4S3}$	30.18±1.397	0.876	44

Number of boutons among genotypes on muscle1. p value is calculated relative to control. n equals to number of NMJs analyzed

Table 40a Statistical comparisons between genotypes

Statistical comparison between genotypes		p value
$S6k^{l-1}$/+	*$S6k^{l-1}/Madm^{2D2}$*	<0.0001
	$S6k^{l-1}/Madm^{4S3}$	<0.0001

Table 41 NMJ length

Genotypes	NMJ length (µm) ± SEM	p value	n
elav/+	136±5.746		22
$Madm^{4S3/+}$	124.2±6.271	>0.9999	24
$Madm^{2D2/+}$	123.4±3.905	>0.9999	28
$S6k^{l-1}$/+	183.9±12.14	0.0283	32
$S6k^{l-1}/Madm^{2D2}$	115.1±3.665	0.1328	47
$S6k^{l-1}/Madm^{4S3}$	145.1±6.562	>0.9999	44

NMJ length among genotypes on muscle1. p value is calculated relative to control. n equals to number of NMJs analyzed

Table 41a Statistical comparisons between genotypes

Statistical comparison between genotypes		p value
$S6k^{l-1}$/+	$S6k^{l-1}/Madm^{2D2}$	<0.0001

	$S6k^{l-1}/Madm^{4S3}$	0.0513

Table 42 NMJ area per muscle area

Genotypes	NMJ area/ muscle area ± SEM	p value	n
elav/+	2.308±0.2502		22
$Madm^{4S3/+}$	2.217±0.2403	0.9998	24
$Madm^{2D2/+}$	2.434±0.175	0.9987	28
$s6k^{l-1}/+$	3.126±0.3107	0.2004	32
$S6k^{l-1}/Madm^{2D2}$	2.189±0.1454	0.9985	47
$S6k^{l-1}/Madm^{4S3}$	2.883±0.1754	0.3773	44

NMJ area per muscle area among genotypes on muscle1. p value is calculated relative to control. n equals to number of NMJs analyzed

Table 42a Statistical comparisons between genotypes

Statistical comparison between genotypes		p value
$S6k^{l-1}/+$	$S6k^{l-1}/Madm^{2D2}$	0.0304
	$S6k^{l-1}/Madm^{4S3}$	0.9711

Table 43 Number of boutons

Genotypes	# boutons ± SEM	p value	n
elav/+	32.18±0.9949		22
$Madm^{4S3/+}$	30.96±1.266	0.9666	24
$Madm^{2D2/+}$	31.75±0.8933	0.9997	28
$TSC1^{f01910}/+$	32.86±1.354	0.9979	22
$TSC1^{f01910}/Madm^{4S3}$	30.33±0.9042	0.8132	27
$TSC1^{f01910}/Madm^{2D2}$	31.5±0.8598	0.9979	22

Number of boutons among genotypes on muscle1.p value is calculated relative to control. n equals to number of NMJs analyzed

Table 44 NMJ length

Genotypes	NMJ length (µm) ± SEM	p value	n
elav/+	136±5.746		22
$Madm^{4S3/+}$	124.2±6.271	0.9666	24
$Madm^{2D2/+}$	123.4±3.905	0.9997	28
$TSC1^{f01910}/+$	138.2±7.66	0.9979	22
$TSC1^{f01910}/Madm^{4S3}$	117.4±4.718	0.8132	27
$TSC1^{f01910}/Madm^{2D2}$	150.8±5.5	0.9979	22

NMJ length among genotypes on muscle1. p value is calculated relative to control. n equals to number of NMJs analyzed

Table 45 NMJ area per muscle area

Genotypes	NMJ area/ muscle area ± SEM	p value	n
elav/+	2.703±0.2823		22
$Madm^{4S3/+}$	2.217±0.2403	0.7607	24
$Madm^{2D2/+}$	2.521±0.1893	0.9952	28
$TSC1^{f01910}/+$	2.305±0.3032	0.8849	22
$TSC1^{f01910}/Madm^{4S3}$	2.078±0.2388	0.5066	27
$TSC1^{f01910}/Madm^{2D2}$	2.997±0.2537	0.9699	22

NMJ area per muscle area among genotypes on muscle1. p value is calculated relative to control. n equals to number of NMJs analyzed

Analysis of BRP and GluRs in Madm mutants. (Figure 17)

Table 46 Intensity of BRP per HRP area (Normalized)

Genotype	BRP Intensity ±SEM (Normalized)	n	p value
Control	1±0.04487	32	
$Madm^{4S3/Df}$	0.9279±0.05496	32	0.6866

Neuronal rescue	0.7973±0.0459	19	0.0212
Muscle rescue	0.8907±0.05046	27	0.3197
Neuronal Madm KD	0.9213±0.02638	30	0.6208
Muscle Madm KD	0.9574±0.04367	16	0.9827
Muscle Madm OE	0.9167±0.07583	12	0.8071

p value is calculated relative to control. n equals to number of NMJs analyzed

Table 47 Normalized intensity of GluRIIC per HRP area

Genotype	GluRIIC Intensity ± SEM	n	p value
Control	1±0.04525	32	
Madm$^{4S3/Df}$	1.199±0.04809	30	0.0363
Neuronal rescue	1.224±0.06965	19	0.0387
Muscle rescue	1.556±0.0813	27	0.0001
Neuronal Madm KD	0.9235±0.04027	30	0.7916
Muscle Madm KD	0.8323±0.04083	16	0.2366
Muscle Madm OE	0.9871±0.0875	12	0.9998

p value is calculated relative to control. n equals to number of NMJs analyze

Analysis of GluRIIA and GluRIIC in Madm mutants. (Figure 18)

Table 48 Normalized intensity of GluRIIA and GluRIIC per HRP area in Madm mutants

Genotype	GluRIIA Intensity ±SEM	p value	GluRIIC Intensity ±SEM	p value	n
w1118	1.0±0.12		1.0±0.1		8
Madm$^{2D2/Df}$	1.77±0.16	<0.0001	1.38±0.1	0.0489	8
Madm$^{4S3/Df}$	2.39±0.08	<0.0001	1.54±0.04	0.0005	17

Table 49 Ratio of GluRIIA and GluRIIC receptors in Madm mutants

Genotype	GluRIIA / GluRIIC ± SEM	P Value to control	n
w1118	0.78±0.03		8

Madm$^{2D2/Df}$	1.02±0.03	<0.0001	8
Madm$^{4S3/Df}$	1.24±0.01	<0.0001	17

p value is calculated relative to control. n equals to number of NMJs analyzed

8.2 Supplemental information for PP4

Table 1 Selected targets for CRISPR mediated PP4 19C deletion

3' Target (5'-3')	5' Target (5'-3')
+CTTCGTACCTGGGTTTCTCCAGG	+CTTCTTTTAGCTGTTTTAGATGG
-GCGACGGGGAAGCGGTGAATCGG	+ACGAAACGTGTATTTGACAGTGG
-CTAAGCTAGGACATATTTAGGGG	-TCATGGACTATCTCAACAAGTGG
+AGTAGCTAGATGAGGTGCACAGG	+ACTTGTTGAGATAGTCCATGAGG
+CACAGGTAGAGGTAAACAGATGG	-TTCATTGCGAAATAGCCTCATGG

Design of Homology arm primers with appropriate restriction sites:

AarI(4/8) **5'nnnnCACCTGCnnnn nnnn-NNNNNNNNNNN'3**

5' Homologous arm_3.29 target

Arm Size: 1097bp

5'HA_ct3.29_fw: 5'tgcaCACCTGCgatc ctac -ATGAGGCTATTTCGCAATG'3

5'HA_ct3.29_rv: 5'attcCACCTGCtgaa tcgc - CCTTGTCTCTGTGATCTC'3

5' Homologous arm_3.34 target

Arm Size: 1076bp

5'HA_ct3.34_fw: 5' tgcaCACCTGC gatc ctac - CAGTGGATAGGGTTGGAT'3

5'HA_ct34_rv: 5' attcCACCTGC tgaa tcgc- CTGGACGTCGAACTCGACGG'3

SapI(1/4) **5'nnnnGCTCTTCn nnn-NNNNNNNNNNN'3**

3' Homologous arm_1.5 target

Arm Size: 1167bp

Fwd: 5' cgagGCTCTTCa gac -TAGCTCCTATAAAACGCC'3

Rev: 5' tagtGCTCTTCa tat-GAAACCCAGGTACGAAGA'3

3' Homologous arm_1.35 target

Arm Size: 1112bp

Fwd: 5' cgagGCTCTTCa gac -TGCAGAGAAGGAAGACGC'3

Rev: 5' tagtGCTCTTCa tat- TGCAAAAGCGAAGCGAAC'3

Primers to verify the deletion of PP4 19C

PP43.29HA_1217Rv: 5' AGCTGGACGTCGAACTCGACG '3

PP43.29HA_894Rv: 5' AATGCTAGCGTTGCCAGATGG '3

PP41.35HA_1329Fw: 5' AGCTGATGAGCCACGACCTGC '3

PP41.35HA_941Fw: 5' AGCAAATGAAGGAGCATGGACTCG '3

Primers for sequencing of CRISPR Target site:

3'HA Target 1.5

Name: Pp4-CT.seq1.5

Fwd Primer: 5'CTCGGGACCCATAATTTAC'3

Rev Primer: 5'CTTGGGCAGCATACTATAC'3

3'HA Target 1.35

Pp4-CT.seq1.35 fw: 5'GGTAGAGGTAAACAGATGG'3

Pp4-CT.seq1.35 rv: 5'GCGGACTACTTTCTCTAAG'3

5'HA Target 3.29

Name: Pp4- CT.seq3.29

Fwd Primer: 5' GGCCATAAAGTGCATCTG'3

Rev Primer: 5' CAGGCGAACTCAAAAACCG'3

Oligos for guide RNA construction with BbsI site:

5'phosphorylated oligos (added G at the 5' end as per the CRISPR protocol)

Pp4_CT_1.5 sens: 5`CTTCGCTTCGTACCTGGGTTTCTCC`3

Pp4_CT_1.5anti: 5`AAACGGAGAAACCCAGGTACGAAGC`3

Pp4_CT_1.35sens: 5`CTTCGTTCGCTTCGCTTTTGCAGGC`3

Pp4_CT_1.35anti: 5`AAACGCCTGCAAAAGCGAAGCGAAC`3

Pp4_CT_3.29sens: 5`CTTCGACTTGTTGAGATAGTCCATG`3

Pp4_CT_3.29anti: 5`AAACCATGGACTATCTCAACAAGTC`3

Pp4_CT_3.34sens: 5`CTTCGACGAAACGTGTATTTGACAG`3

Pp4_CT_3.34anti: 5`AAACCTGTCAAATACACGTTTCGTC`3

P^{ENTRY} cloning primers for generation of transgenic lines:

Pp4_cDNA_Fw: 5`CACCATGTCCGACTACAGCGAC`3

Pp4_cDNA_Rv: 5`TTAGAGAAAGTAGTCCGCCTG`3

Pp4_cDNA_Nostop_Rv: 5`GAGAAAGTAGTCCGCCTGAG`3

P^{ENTRY} cloning primers for antibody generation:

PP4_Abpep2_fw: 5'CACCATGGGCGATTTCGTGGACC '3

PP4_Abpep2_rv: 5' CCAAAGCAGGTCGCACATG '3

PP4_Abpep3_fw: 5' CACCATGTGCGACCTGCTTTGGAGC '3

PP4_Abpep1_rv: 5' GCTGCACGTTGCCCTCCTCC '3

PP4_Abpep4_fw: 5'CACCATGGAGGGCTTCAAGTGG '3

PP4_Abpep5_rv: 5'ACCGTGGATGTCGCCGCACACG'3

PP4_Abpep6_rv: 5'CTGCACGTTGCCCTCCTCC'3

PP4_Abpep1-50_rv: 5'TTAGGTCACTGGCGAGTCCACAC'3

PP4_Abpep80-197rv 5'TTACCAAAGCAGGTCGCACATG'3

9 Abbreviations

4E-BP	Eukaryotic initiation factor 4E (eIF-4E) binding protein-1
ALS	Amyloid lateral sclerosis
AMPA	α-Amino-3hydroxy-5-methyl-4-isoxazolepropionic acid
Aβ	Amyloid β
Ank2	Ankyrin2
BMP	Bone morphogenic protein
Brp	Bruchpilot
BunA	Bunched A
CA1	cornu ammonis 1
CaMKII	Ca^{2+} /calmodulin-dependent protein kinase II
CaMKIV	Ca^{2+} /calmodulin-dependent protein kinase IV
cAMP	cyclic adenosine monophosphate
Cdk1	Cyclin dependent kinase 1
Cdk5	Cyclin dependent kinase 5
CENP-C	Centromere protein C
CK2α	Casein kinase 2α
CREB	cAMP response element binding protein
CRISPR	Clustered Regularly Interspaced Short Palindromic Repeats
Df	deficiency
Dlg	Discs large
dpp	Decapentaplagic
dVGluT	Drosophila vesicular glutamate transporter
EGFP	Enhanced green fluorescent protein
EGFR	Epidermal growth factor receptor
EMS	Ethyl methanesulfonate
ER	Endoplasmic reticulum
FasII	Fasciclin II
Flfl	Falafel
FMRP	Fragile X Mental Retardation Protein
GABA	γ-Aminobutyric acid
Gbb	Glass bottom boat

Gig	Gigas
GluR	Glutamate receptor
GluRIIA	Glutamate receptor subunit IIA
GluRIIB	Glutamate receptor subunit IIB
GluRIIc	Glutamate receptor subunit IIC
gRNA	guide RNA
GSK3-β	Glycogen synthase kinase 3-β
Hh	Hedgehog
HRP	Horseradish peroxidase
HSP	Homeostatic synaptic plasticity
JAK-STAT	Janus kinase & signal transducer and activators of transcription
JNK	c-Jun N-terminal kinase
LCMT1	Leucine carboxyl methyltransferase 1
LTP	Long-term potentiation
LTD	Long-term depression
LRRK2	Leucine rich repeat kinase 2
Mad	Mothers against dpp
Madm	Mlf1 adaptor molecule
MAPK	Mitogen activated protein kinase
Mav	Maverick
Mira	Miranda
Mlf1	Myeloid leukemia factor 1
mTOR	mammalian target of rapamycin
NDEL1	Nuclear distribution protein nudE-like 1
NF-κB	Nuclear factor kappa-light-chain-enhancer of activated B-cells
NMJ	Neuromuscular junction
NMDA	N-Methyl-D-aspartic acid
NRBP1	Nuclear receptor binding protein 1
Nwk	Nervous wreck
PP2A	Protein phosphatase 2A
PP4	Protein phosphatase 4
PP4C	Protein phosphatase 4 catalytic subunit
PP4R1	Protein phosphatase 4 regulatory subunit 1

PP4R2r	Protein phosphatase 4 regulatory subunit 2r
PP4R3	Protein phosphatase 4 regulatory subunit 3
PHP	Presynaptic homeostatic potentiation
PKA	Protein kinase A
PKC	Protein kinase C
PSD-95	Postsynaptic density protein-95
PTEN	Phosphatase and tensin homolog
Rab11	Ras-related protein 11
Rab5	Ras-related protein 5
Ras	Rat sarcoma
Rheb	Ras homolog enriched in brain
Rho-GTPase	Ras homolog GTPase
RNAi	Ribonucleic acid interference
S6k	S6kinase
SEM	Standard error of mean
SERCA	Sarco/endoplasmic reticulum Ca^{2+} ATPase
SMA	Spinal muscular atrophy
SMN	Survival of motor neuron
Smo	smoother
SNARE	Soluble N-ethylmaleimide-sensitive factor activating protein receptor
Spz3	Spaetzle3
SSR	Sub synaptic reticulum
Syn	Synapsin
Synj	Synaptojanin
TGF-β	Transforming growth factor-β
Tkv	Thick vein
TLRs	Tollo like receptors
TOR	Target of rapamycin
TSC 1	Tuberous sclerosis complex 1
TSC 2	Tuberous sclerosis complex 2
UAS	Upstream activation sequence
Wit	Wishful thinking
Wnt	Wingless & int-1

10 Curriculum vitae

Kumar Aavula

Address	Gotleib Daimler strasse 68/A315, 67663 Kaiserslautern, Germany.
Email	kumar.aavula@biologie.uni-kl.de

Education

05.2014 - 08.2018	**PhD in Neurobiology**, Technical University Kaiserslautern, Kaiserslautern, Germany and Friedrich Miescher Institute for biomedical research, Basel, Switzerland
06.2011 – 05.2013	**Master of Technology in Biotechnology**, Vellore Institute of Technology, India
07. 2007 - 05.2011	**Bachelor of Engineering in Biotechnology**, Vinayaka Missions University, India

Research Experience:

05.2014 - 08.2018	**PhD Thesis** Under Prof. Dr. Jan Pielage, Technical University Kaiserslautern and FMI, Basel. 'Study on the role of pseudokinase Madm and protein phosphatase PP4 in synaptic plasticity.'
06. 2012 – 02.2014	**Masters Thesis** Under Prof. Dr. Upendra Nongthomba, Indian Institute of Science, India. 'Identified the role of Beadex in cellular immunity of Drosophila.'
08-2011 – 05.2012	**Internship** Under Prof. Dr. Anil Kumar Gopinathan, Vellore Institute of Technology, India. 'Identification of *XRCC1* gene polymorphism in Schizophrenia patients.'

11 Acknowledgement

This work was performed in the laboratory of Prof. Dr. Jan Pielage at Technical University Kaiserslautern, Germany and Friedrich Miescher Institute for biomedical research, Basel. I am deeply grateful to Prof. Dr. Jan Pielage for introducing me to Neurobiology research and for his continuous support and encouragement during my time in the lab. Thank you very much Jan.

I would like to thank Technical University Kaiserslautern and Friedrich Miescher Institute for biomedical research for the provided research facility.

I would like to thank my thesis committee, especially Prof. Dr. Martin Müller who agreed to be co-referent for my thesis.

I express my thanks to Dr. Ingrid Kieweg for initiating the Madm project, where she identified, characterized the Madm mutant phenotypes and generated transgenic rescue lines and antibody. I express my thanks to Raiko Stephan for training me on microinjections to generate transgenic animals, Zeeshan Mushtaq for training me on electrophysiology and for his kindness to record on my mutants (where I performed the genetics and supplied the larvae for recordings), Dominique Siegenthaler for his help on adult brain dissections, discussions and German translations and Benjamin Escribano for his kind help in and outside the lab in Basel and Kaiserslautern.

I would like to thank the whole Pielage lab members (present and past) for a nice and friendly atmosphere with many productive discussions and coffee breaks in the lab.

I thank Deepti Bapat and Ruchi Jhonsa for their time and kindness to check my thesis.

My heartfelt thanks to my parents *Venkataswamy* and *Rathnamma* for their unconditional love and support. I thank my siblings Thulasi, Jyothibabu, my brother-in-law Jagannatham and my dear friends Chakri and Harshitha for their moral support, without whom my journey wouldn't be possible.

And I thank all other people who supported and made this journey pleasant and memorable. Thank you.